Measurement and modelling of the vapour-liquid equilibria of binary mixtures of water and alkanols

Sonja Almi Milé Smith

Thesis presented in partial fulfilment of the requirements for the degree

MASTER OF ENGINEERING

(Chemical Engineering)

in the Faculty of Engineering
at Stellenbosch University

Supervisor
Prof. C.E. Schwarz

Co-Supervisor
Prof. A.J. Burger

March 2017

Declaration

By submitting this thesis electronically, I declare that the entirety of the work contained therein is my own, original work, that I am the sole author thereof (save to the extent explicitly otherwise stated), that reproduction and publication thereof by Stellenbosch University will not infringe any third party rights and that I have not previously in its entirety or in part submitted it for obtaining any qualification.

Date: March 2017

Abstract

Aqueous mixtures of (C_1–C_5) alkanols are found in the petrochemical and biofuel industries, amongst others. Molecular interactions, of which hydrogen bonding (association) and polar effects are large contributors, render these mixtures complex and separation becomes a difficult task. For efficient design of separation processes, mixture phase behaviour needs to be understood, and a suitable equation of state is required to represent this behaviour mathematically.

Equations of state with sound theoretical foundations have been developed, amongst others the *Statistical Associating Fluid Theory* (SAFT). Two SAFT variants were considered in this investigation: simplified Perturbed-Chain SAFT (sPC-SAFT) and SAFT with Variable Range Mie-potential (SAFT-VR Mie). In these models, association schemes are used to describe the amount and type of association sites on a molecule. To explicitly account for polarity, two polar terms, those of Gross and Vrabec (GV), and Jog and Chapman (JC), were considered in this work. While each polar term has a parameter that describes a molecule's degree of polarity, the polar functional group's location is not specified. It is therefore questioned whether the SAFT framework has the ability to account for structural isomerism, in lieu of a positional specifier. Structural isomers of linear (C_1–C_5) alkanols provide a suitable homologous series for investigation, and their aqueous mixtures are of interest to this study.

The overarching aim of this project was to evaluate how a shifting hydroxyl group influences water + alkanol phase behaviour, and whether the SAFT models are able to predict this phase behaviour. This aim was met by the following objectives: (1) Generate vapour-liquid equilibrium (VLE) data for binary water + alkanol mixtures and analyse the observed phase behaviour; (2) Generate model parameters and evaluate their performance; (3) Compare the performance of sPC-SAFT to that of SAFT-VR Mie, evaluate whether a polar term is necessary to model water + alkanol mixtures, determine whether a superior association scheme for primary and secondary alkanols exists, and whether the SAFT framework can distinguish between structural isomers of linear alkanols; (4) Lastly, evaluate whether the model parameters are able to predict thermodynamic properties other than VLE.

The first objective was met by measuring VLE of four binary aqueous mixtures of 1-butanol, 1-pentanol, 2-pentanol, and 3-pentanol at p = 0.1013 MPa. Temperature and pressure were measured within an accuracy of 0.05 K and 2×10^{-4} MPa, respectively. Together with analytic errors this resulted in compositional measurements accurate within 0.023 mole fraction. Experimental difficulties resulted in scattered data for the water + 2-pentanol and water + 3-pentanol mixtures that were not consolidated, even after repeated measurements. All data were determined to be thermodynamically consistent by the McDermott-Ellis and Wisniak L/W tests.

Comparison between mixtures of water + (C_2–C_5) linear alkanol highlighted how molecular structure influences phase behaviour: Firstly, shifting the polar hydroxyl group away from the terminal methyl group results in higher saturated vapour pressures, and influences the binary phase envelope by reducing the azeotropic temperature and resulting in an azeotropic vapour composition richer in alkanol. Secondly, primary C_x- and secondary $C_{(x+1)}$-alkanols exhibit similar saturated vapour pressures, and similar phase behaviour in binary mixtures with water.

Thermodynamic modelling was conducted in an in-house developed simulation software and model parameters were regressed for water and nine (C_1–C_5) linear alkanols, using a single regression procedure. No parameters could be determined for SAFT-VR Mie-JC, because the polar parameter was driven to zero during regression, regardless of the initial guess value. Therefore, the performance of this model could not be evaluated. sPC-SAFT, sPC-SAFT-GV, sPC-SAFT-JC, SAFT-VR Mie, and SAFT-VR Mie-GV performed equally well for pure component property predictions, independent of the association scheme. However, compared to the sPC-SAFT models, the SAFT-VR Mie models show superiority for speed of sound predictions.

To evaluate the description of mixture properties, alkane + alkanol mixtures were also considered. In these mixtures, all polar and associating behaviour can be isolated to the alkanol alone, since alkanes do not exhibit any functionality over and above dispersion. sPC-SAFT and SAFT-VR Mie gave similar qualitative descriptions of alkane + alkanol VLE. Polar terms improved predictions significantly and excellent descriptions were obtained. This indicated that it is necessary to explicitly account for polarity in alkane + alkanol mixtures. For water + alkanol VLE, sPC-SAFT provided better predictions than SAFT-VR Mie. The polar terms did not provide significant improvement, indicating that, compared to hydrogen bonding, polar forces are negligible in mixtures of associating compounds.

The 4C association scheme was used for water in all predictions. The most suitable association scheme for alkanols, however, is system and model dependent. In binary mixtures with alkanes, the 2C association scheme delivered the best description of VLE, using the nonpolar models. However, with the polar models, the three association schemes provide indistinguishable predictions for alkane + alkanol VLE, rendering the choice of association scheme in the

polar models arbitrary. In water + alkanol mixtures, primary and secondary alkanols were best described by the 2C and 3B association schemes, respectively.

In both mixture types, excess property description is troublesome, indicating that the flaw in thermodynamic description is a result of the SAFT framework as a whole, and not restricted to a single form of the model. This suggests that the SAFT framework as a whole requires further refinement in order to simultaneously predict all thermodynamic properties accurately.

Lastly, the description of both primary and secondary alkanols in mixture of alkanes and in mixtures of water are of similar quality, indicating that the SAFT framework is sufficiently flexible to accommodate structural isomers.

Opsomming

Mengsels van water en (C_1–C_5)-alkanole word in verskeie industrieë aangetref, onder andere die petrochemiese- en biobrandstof-industrieë. Molekulêre interaksies, waarvan waterstofbindings (assosiasie) en polêre invloede die grootste bydrae maak, veroorsaak dat hierdie mengsels kompleks is en skeidingsprosesse bemoeilik. Vir die effektiewe ontwerp van skeidingsprosesse, word 'n goeie begrip van die mengsel se fasegedrag vereis, terwyl 'n gepaste toestandsvergelyking benodig word om hierdie gedrag wiskundig te verteenwoordig.

Toestandsvergelykings met grondige teoretiese beginsels is oor die jare ontwikkel, onder andere die *Statistical Associating Fluid Theory* (SAFT). Twee SAFT-variante is in hierdie ondersoek gebruik: *simplified Perturbed-Chain*-SAFT (sPC-SAFT), en SAFT met 'n reëlbare rekwydte Mie-potensiaal (SAFT-VR Mie). In hierdie modelle word assosiasieskemas gebruik om die aantal en tipe assosiasieliggings op 'n molekule te beskryf. Om polariteit eksplisiet in bereking te bring, is twee polêre terme, dié van Gross en Vrabec (GV), en Jog en Chapman (JC), in hierdie ondersoek gebruik. Beide hierdie terme neem die grootte van die molekuul se polariteit in ag, maar die ligging van die polêre groep word nie gespesifiseer nie. Dit word dus bevraagteken of die SAFT-raamwerk strukturele isomere van mekaar kan onderskei. Strukturele isomere van lineêre (C_1–C_5) alkanole dien as die gepaste homoloë reeks om dié vraagstuk te ondersoek. Mengsels van hierdie alkanole met water is in hierdie studie van belang.

Die oorkoepelende doel van hierdie projek was om die invloed van die hidroksielgroep-posisie op die fasegedrag van water + alkanol mengsels te evalueer, en te bepaal of SAFT-modelle hierdie gedrag kan voorspel. Die volgende doelwitte is derhalwe gestel: (1) Genereer damp-vloeistof-ewewigsdata (VLE-data) vir binêre water + alkanol mengsels en analiseer die waargenome fasegedrag; (2) Genereer modelparameters en evalueer hul werkverrigting; (3) Vergelyk die werkverrigting van sPC-SAFT met dié van SAFT-VR Mie, bepaal of 'n polêre term benodig word om water + alkanol mengsels te modelleer, bepaal of daar 'n meer gepaste assosiasieskema vir primêre en sekondêre alkanole is, en bepaal of die SAFT-raamwerk onderskeid maak tussen strukturele isomere van lineêre alkanole; (4) Laastens, evalueer die modelparameters se geskiktheid vir die voorspelling van termodinamiese eienskappe, bo en behalwe VLE.

Die eerste doelwit is behaal deur die VLE van vier binêre mengsels, water + 1-butanol, + 1-pentanol, + 2-pentanol, en + 3-pentanol, by p = 0.1013 MPa te meet. Temperatuur- en druklesings is binne 'n akkuraatheid van 0.05 K en 2×10^{-4} MPa onderskeidelik geneem. Tesame met analitiese foute is samestellings binne 'n akkuraatheid van 0.023 molfraksie bepaal. Eksperimentele struikelblokke het daartoe gelei dat die data vir die water + 2-pentanol, en water + 3-pentanol mengsels verspreid was, en selfs na herhaalde metings nie verenig kon word nie. Alle data is as termodinamies konsekwent bepaal deur die McDermott-Elllis en Wisniak L/W toetse.

Die effek van molekulêre struktuur is waargeneem deur water + (C_2–C_5)-alkanol mengsels met mekaar te vergelyk: Ten eerste word 'n hoër dampdruk veroorsaak deur die polêre hidroksielgroep weg van die terminale metielgroep te skuif. Hierdie skuif het ook 'n direkte effek op die binêre fasegedrag, waar die aseotrooptemperatuur verlaag word, en die samestelling van die aseotroop-dampfase ryker in alkanol word. Ten tweede vertoon primêre C_x- en sekondêre $C_{(x+1)}$-alkanole soortgelyke dampdrukke, en soortgelyke fasegedrag in binêre watermengsels.

Termodinamiese modellering is uitgevoer in 'n in-huis ontwikkelde simulasie sagteware. Modelparameters is vir water en nege (C_1–C_5) lineêre alkanole deur regressie bepaal, deur 'n enkele regressieprosedure te gebruik. Geen parameters is vir SAFT-VR Mie-JC bepaal nie, en die model kon dus nie evalueer word nie. Die polêre parameter het tydens regressie onafhanklik van die begin soekwaarde na nul gestreef het. sPC-SAFT, sPC-SAFT-GV, sPC-SAFT-JC, SAFT-VR Mie, en SAFT-VR Mie-GV lewer soortgelyke resultate wanneer suiwer komponentdata voorspel word, onafhanklik van die assosiasieskema-keuse. Die SAFT-VR Mie-modelle se spoed-van-klank voorspellings is superieur in vergelyking met dié van die sPC-SAFT-modelle.

Om die beskrywing van mengseleienskappe te evalueer, is alkaan + alkanol mengsels ook ondersoek. Omdat alkane geen ander energiebydrae, bo en behalwe die dispersie-energie, toon nie, kan alle assosiasie- en polêre gedrag aan die alkanol toegeëien word. sPC-SAFT en SAFT-VR Mie voorspellings van alkaan + alkanol VLE is kwalitatief in ooreenstemming. Die polêre terme verbeter voorspellings noemenswaardig en lewer uitstekende resultate. Polariteit moet dus eksplisiet in berekening gebring word vir alkaan + alkanol mengsels. sPC-SAFT lewer beter voorspellings van water + alkanol VLE as SAFT-VR Mie. Vir hierdie mengsels is die verbetering wat die polêre modelle bied nie noemenswaardig nie, wat daarop dui dat polêre interaksies, in vergelyking met sterk assosiasie, weglaatbaar is in mengsels van assosiërende komponente.

Die 4C-assosiasieskema is deurgaans vir water gebruik. Die meer gepaste assosiasieskema vir alkanole is egter afhanklik van beide die sisteem en die model. In binêre mengsels met alkane, bied die 2C-assosiasieskema die beste beskrywing van VLE wanneer die nie-polêre modelle gebruik word. Die keuse van assosiasieskema raak irrelevant binne die polêre modelle, aangesien

die verskillende skemas ononderskeidbare voorspellings lewer. In watermengsels lewer die 2C-skema en die 3B-skema die beste beskrywings vir primêre en sekondêre alkanole, onderskeidelik.

Die beskrywing van oormaateienskappe is in beide mengseltipes moeilik. Dit dui daarop dat die fout in termodinamiese beskrywing nie binne die omskrywing van 'n enkele model lê nie, maar eerder 'n fout in die SAFT-raamwerk in die geheel is. Die SAFT-raamwerk benodig dus verfyning sodat alle termodinamiese eienskappe gelyktydig, en met dieselfde akkuraatheid, beskryf kan word.

Laastens is die kwaliteit van die beskrywing van primêre en sekondêre alkanole in beide alkaan- en watermengsels soortgelyk, wat daarop dui dat die SAFT-raamwerk buigsaam genoeg is om strukturele isomere te akkomodeer.

Acknowledgements

The following people assisted, great and small, in keeping me sane for the duration of my project:

- Prof. C.E. Schwarz. Exiting your meetings always left me with a sense of direction and clarity about where my project was headed.
- Prof. A.J. Burger. For seeing the bigger picture, challenging and forming my ideas, and catch-up meetings in the departmental kitchen.
- Dr Jamie Cripwell. You were basically my third supervisor and I don't think a mere "thank you" suffices, but here I go: for the training, guidance, quick chats, your patience with my tons of small questions, insight into troubles, cheering up when bad data got me down, pictures of Yoda, and basic Chinese. Xièxiè.
- Dr Riaan de Villiers. For setting aside time to write emails the size of books to help me with modelling related work.
- Mrs Hanlie Botha. For your assistance with the GC and all other analysis related questions.
- The inhabitants of C416. I baked for stress relief and you helped me to not get fat by myself. Thank you for the shared jokes, obligatory Monday morning social coffees, pub lunches, board games, Friday rituals, sun sessions, Speckled Eggs, and Lemon Creams.
- My parents, Alec and Salomi. Julle het my tot op hierdie plek gebring en ek sou dit nie sonder julle onvoorwaardelike ondersteuning en liefde kon vermag nie.
- My brother, André. Jy's die coolste.
- The Wilhelm Frank Trust. Thank you for the financial support during my master's studies.

Contents

Nomenclature

List of Roman Symbols

Symbol	Definition	Symbol	Definition
a_1, a_2, a_3	dispersion perturbation term	N	number of chemical species
A	Helmholtz energy	p	pressure
A_i	Antoine constant	r	radial distance
A_2, A_3	polar second- and third order terms	$r^{\mathrm{c}}_{A_iB_j}$	association range
B_i	Antoine constant	$r^{\mathrm{d}}_{A_iB_j}$	association distance
c_p	isobaric heat capacity	R_f	response factor
C_i	Antoine constant	S	entropy
C_{ij}	Mie potential parameter	s_1	MSW potential constant
D	deviation parameter	t, T	temperature
$\hat{f}$	fugacity	T_L	lower critical solution temperature
F	reduced residual Helmholtz energy state function	T_{n}	normal boiling temperature
g	radial distribution function	T_U	upper critical solution temperature
G	Gibbs free energy	T^{az}, T^*	azeotropic temperature
h	molar enthalpy	u	potential energy function
$I^{A_iB_j}$	association integral	u^{liq}	speed of sound
$K^{A_iB_j}$	association volume	V	molar volume, vapour phase
L	liquid phase, Wisniak L/W integral	w	Wisniak L/W parameter
m	segment number	W	Wisniak L/W integral
M	extensive thermodynamic property	x	liquid mole fraction
$\bar{M}$	partial molar property	x_{p}	fraction of polar segments
M_W	molecular weight	X_{A_i}	monomer fraction
n	mole number	y	vapour mole fraction
n_{p}	number of polar segments	Z	compressibility factor

List of Greek Symbols

Symbol	Definition
β_T	isothermal compressibility
γ	activity coefficient
$\Delta^{A_iB_j}$	association strength
ε	potential well depth, segment energy
$\varepsilon^{A_iB_j}$	energy of association
λ	well width, variable range parameter
μ	chemical potential, dipole moment
ρ	density
σ	segment diameter
$\hat{\phi}$	fugacity coefficient
ω	regression weight

Subscripts

Symbol	Description
a	alkanol-rich phase
a, b, j	experimental points
i, j, k	component indices
max	maximum
r	reduced property
w	water-rich phase
$1, 2$	phase indices

Physical Constants

Symbol	Description	Value
k	Boltzmann constant	1.380×10^{-23} J·K^{-1}
R	universal gas constant	8.314 J·(mol·K)$^{-1}$

Abbreviations

Abbreviation	Description
DIPPR	Design Institute for Physical Properties
EoS	equation of state
GC	gas chromotography
GV	Gross and Vrabec (polar term)
JC	Jog and Chapman (polar term)
LCST	lower critical solution temperature
LJ	Lennard-Jones
LLE	liquid-liquid equilibrium
MSW	modified square-well
OF	objective function
PC-SAFT	Perturbed-Chain SAFT
RDF	radial distribution function
SAFT	statistical associating fluid theory
SAFT-HR	SAFT of Huang and Radosz
SAFT-VR	SAFT variable range
SAFT-VR Mie	SAFT-VR with Mie-potential
sPC-SAFT	simplified PC-SAFT
SW	square-well
TPT1	first-order thermodynamic perturbation theory
UCST	upper critical solution temperature
VLE	vapour-liquid equilibrium
VLLE	vapour-liquid-liquid equilibrium
%AAD	percentage absolute average deviation

Superscripts

Symbol	Description
a	attractive parameter
A, B, C, D	association sites
A_iB_j	association between two sites
assoc	association
calc	calculated
chain	chain
comp	compressed
disp	dispersion
E	excess molar property
exp	experimental
hc	hard-chain
hs	hard-sphere
liq	liquid
Mie	Mie-potential
mix	mixture
polar	polar
r	residual molar property, repulsive parameter
sat	saturation property
seg	segment
SW	square-well potential
vap	vaporisation property
α, β, π	phase indices

Chapter 1

Introduction

In various industrial sectors, amongst others the chemical and biochemical fields, separation processes are required to purify products from product streams [1]. The mixtures in these streams often exhibit complex molecular interactions which complicate separation. To design a large scale separation unit, a firm understanding of the mixture's phase behaviour and its thermodynamic properties is required. This is gained through experimental work. Phase behaviour, or more specifically phase equilibrium, and other thermodynamic properties are intertwined at a molecular level and can be expressed mathematically in the form of an equation of state (EoS). These mathematical models are ultimately used in the design and optimisation of separation processes. If models can accurately predict phase behaviour, experimental time can be reduced. However, the necessity of experimental work lies therein to generate data through which the accuracy and predictive capability of EoSs can be measured.

1.1 Thermodynamics and Thermodynamic Modelling

Thermodynamics is a mathematical tool that is used to describe the relationship that holds between the heat and work of any physical process. A schematic representation of the application of thermodynamics is shown in Fig. 1.1. Thermodynamics can be applied to the real world phase equilibrium problem. The phase equilibrium problem seeks to relate the state of the equilibrium system to the intensive variables that define this state, amongst others temperature, pressure, density, and composition. Step 1 realises that this problem can be described in terms of abstract mathematics and is ultimately solved in Step 2 with the equality of chemical potential for each component in each of the coexisting phases α, β, and π [3]:

$$\mu_i^{\alpha} = \mu_i^{\beta} = ... = \mu_i^{\pi} \tag{1.1}$$

1. INTRODUCTION

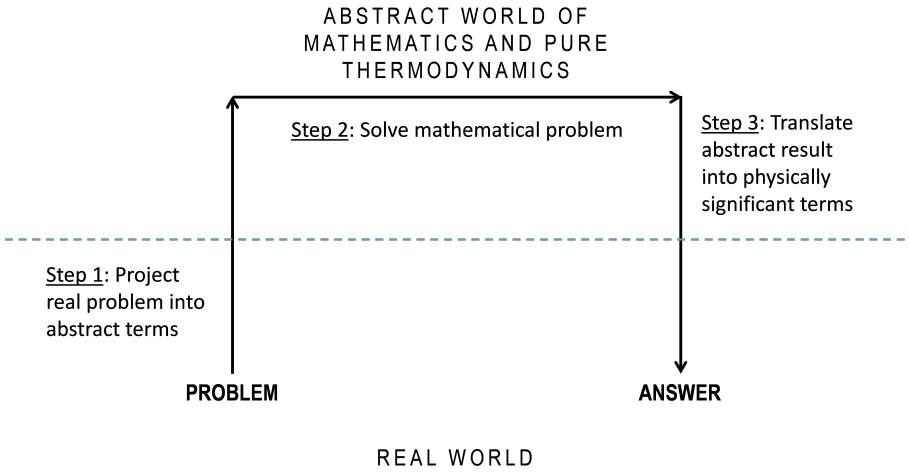

Figure 1.1: Three-step application of thermodynamics to the phase equilibrium problem. Figure adapted and redrawn from Prausnitz, et al. [2].

Since $\mu_i = \Gamma_i + RT \ln \hat{f}_i$, the equality of fugacity for each component in the coexisting phases is obtained [3]:

$$\hat{f}_i^{\alpha} = \hat{f}_i^{\beta} = \ldots = \hat{f}_i^{\pi} \tag{1.2}$$

The phase equilibrium problem now has a mathematical solution, but has no physical meaning in terms of the intensive variables. The first step toward a real world solution is to introduce the concept of a fugacity coefficient, $\hat{\phi}_i$. Suppose phase α is a liquid phase and phase β a vapour phase, then it can be proven:

$$\hat{\phi}_i^{\mathrm{L}} x_i = \hat{\phi}_i^{\mathrm{V}} y_i \tag{1.3}$$

$\hat{\phi}_i$ can further be expressed as [1]:

$$RT \ln \hat{\phi}_i = \int_V^{\infty} \left[\left(\frac{\partial p}{\partial n_i} \right)_{T,V,n_j} - \frac{RT}{V} \right] \mathrm{d}V - RT \ln Z \tag{1.4}$$

The fugacity coefficient is therefore described with reference to the ideal gas state, represented by the last term in Eq. 1.4. The integral in Eq. 1.4 describes all nonidealities in the system that cause deviation from the ideal gas state. However, an abstract, mathematical solution to the phase equilibrium problem remains and is transformed through Step 3 in Fig. 1.1. From the fundamentals of molecular physics and statistical mechanics, equations of state are developed in the attempt to describe, from a molecular level, the macroscopic behaviour of systems. This allows the translation of abstract results into terms of physical significance, such as temperature, pressure, and volume, which can be interpreted in the real world [2].

1.1.1 Equations of State

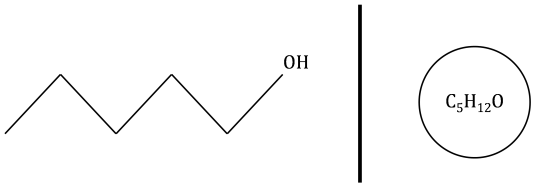

Figure 1.2: Representation of a 1-pentanol molecule using the hard-sphere reference model.

From thermodynamics it has been attempted to describe the state of phase coexistence, with varying degrees of success. The van der Waals EoS [4] was the first of the so-called classic cubic EoSs. Quantitatively the equation delivered poor results. However, the equation was the first EoS to give a qualitative description of vapour-liquid equilibrium [5] and serves as a useful stepping stone to the modelling of phase behaviour.

Numerous modifications to the van der Waals equation have been made and are used to model various mixtures of components successfully. Most notably are the improvements by Redlich and Kwong [6], Soave [7], and Peng and Robinson [8]. These models find extensive use in the petrochemical industry [1, 9].

The application of cubic EoSs is limited since the reference fluid in the original van der Waals equation is one that assumes all molecules are spherical and interact with one another according to the hard-sphere potential. From Fig. 1.2 it is clear that a spherical reference fluid overestimates molecular volume for larger molecules. Furthermore, the nonideal behaviour that exists between molecules can often be ascribed to the presence of intermolecular forces, amongst others the association, solvation, and polar interactions, which cannot be described by the hard-sphere potential.

To account for the flaws of the cubic EoS and to move toward a more fundamental model, much research has been aimed at the development of association theories. These theories attempt to account for chain length as well as intermolecular forces, because it has been found that these two characteristics significantly affect fluid behaviour [10]. The association theories are grouped into 3 main categories: chemical theories (PHCT [11], APACT [12–14]), lattice-fluid theories (NRHB [15]), and perturbation theories (SAFT[16, 17], CPA [18]).

The most successful of the EoSs to be born from the association theories is the *Statistical Associating Fluid Theory*, or SAFT, family of equations, and it is this EoS family that is the focus of this investigation.

1.1.2 Introduction to SAFT

The SAFT EoS has a sound theoretical foundation as it is derived from statistical mechanical principles. The original SAFT, developed by Chapman and co-workers [16, 19–21], finds its roots in the first-order thermodynamic perturbation theory of Wertheim [22–27]. Within this theory, chemical species are represented by a reference fluid which consists of spherical segments. Dispersion, dipolar, and association interactions are treated through perturbation. SAFT is derived in terms of the residual Helmholtz energy, $A^{\mathrm{r}}(T, V)$, by summing various intermolecular interactions, with the assumption that these interactions are independent of one another [16, 21]:

$$\frac{A^{\mathrm{r}}}{RT} = \left(\frac{A^{\mathrm{hs}}}{RT} + \frac{A^{\mathrm{disp}}}{RT} \right)^{\mathrm{seg}} + \frac{A^{\mathrm{chain}}}{RT} + \frac{A^{\mathrm{assoc}}}{RT} \tag{1.5}$$

The three terms on the right hand side of Eq. 1.5 each represent a contribution to A^{r} due to repulsive and dispersive forces between segments, A^{seg}, the formation of chains, A^{chain}, and the association of segments, A^{assoc} [16, 17].

1.2 Problem Identification

Mixtures of water and alkanols are found in various industries, amongst others the textile, pharmaceutical, and petrochemical industries. In most cases, the alkanols need to be separated from water. These mixtures exhibit large deviations from ideal behaviour due to the presence of association through hydrogen bonding, bond-cooperativity [28, 29], and polar forces. In addition, the alkyl part of the alkanol is responsible for the low solubility of alkanols in the water-rich composition range [30]. An EoS that is used to model these mixtures needs to account for the complex molecular interactions to obtain good predictions of mixture properties.

Different versions of SAFT have previously been used to model water + alkanol mixtures: perturbed-chain SAFT (PC-SAFT) [31, 32], simplified PC-SAFT (sPC-SAFT) [30, 33], SAFT with variable range (SAFT-VR) [34], as well as a few polar-SAFT variants [35], to mention but a few. In many cases, a binary interaction parameter is required to obtain a good model fit to experimental data. The models also struggle to predict both VLE and LLE of the same mixture using the same binary interaction parameter [30, 33].

In answer to some of the limitations of SAFT modelling, de Villiers [36] developed a new association scheme for alkanols, the 2C association scheme, in an attempt to improve the description of cross-association in water + alkanol mixtures. Also, following the work of Al-Saifi, et al. [35], de Villiers [36] included the Jog and Chapman (JC) [37, 38], and Gross and Vrabec (GV) [39] polar terms to the sPC-SAFT framework, resulting in sPC-SAFT-JC and sPC-SAFT-GV, respectively. De Villiers investigated the modelling of, amongst others, water + 1-alkanol

mixtures with sPC-SAFT, sPC-SAFT-GV, and sPC-SAFT-JC, using the 2B, 2C, and 3B association schemes for the alkanols, and found the prediction of vapour-liquid equilibrium to be excellent, with large deviations observed in predicting liquid-liquid behaviour [36]. Moreover, de Villiers found that excess properties are very poorly described and attributed the apparent flaw in the sPC-SAFT framework to an incorrect temperature dependence of the EoS [36].

In a subsequent study, Cripwell [40] investigated alkane + heptanone mixtures, with the particular focus on structural isomers of heptanones in order to (1) observe the effect of a shifting polar functional group on phase equilibrium, and (2) evaluate the ability of sPC-SAFT-GV and sPC-SAFT-JC to predict this phase behaviour in lieu of a parameter that specifies the position of the polar functional group. No similar study was found that systematically evaluated SAFT's performance when predicting secondary alkanols, i.e. structural isomers of linear alkanols.

Considering water + alkanol mixtures, a few research questions arise:

- Association forces are generally an order of magnitude larger than polar interactions. Is the polar term addition required for alkanols?
- Does the SAFT framework perform equally well for both primary and secondary alkanols? Given that the polar terms do not have a positional specifier, can the SAFT framework distinguish between different structural isomers of linear alkanols?
- Is the inability of sPC-SAFT models in predicting excess properties bound to the specific form of the SAFT model, i.e. sPC-SAFT, or to the foundation of the model, i.e. Wertheim's perturbation theory?

1.3 Study Objectives

The aim of this investigation is to observe the effect of a shifting hydroxyl group on the vapour-liquid equilibrium behaviour of water + alkanol mixtures, and subsequently, to evaluate the performance of SAFT-type models to predict this phase behaviour. Binary aqueous mixtures containing (C_1–C_5) alkanols are investigated. The VLE property of many of these aqueous mixtures have been thoroughly investigated; however, no isobaric VLE data for the water + 2-pentanol, and water + 3-pentanol mixtures exist.

A novel version of SAFT, the SAFT with variable range Mie-potential, or SAFT-VR Mie, was presented in 2006 [41] and was later improved in 2013 [42]. The preliminary results for SAFT-VR Mie [42] are promising and show improved performance over previous versions of SAFT, especially for the prediction of second-order derivative properties [42, 43]. To evaluate

the SAFT framework as a whole, SAFT-VR Mie is included in this investigation. To evaluate the value of the polar addition, the GV- and JC-polar terms are added to the SAFT-VR Mie framework in this investigation.

The thermodynamic modelling of alkane + alkanol mixtures are considered in addition to the water + alkanol mixtures to evaluate the description of self-association and polar effects in mixtures where the second component (i.e. alkanes) does not have any functionality beyond dispersion forces.

The objectives of this investigation are thus to:

1. Generate isobaric VLE data for binary water + alkanol mixtures, in particular 2-pentanol and 3-pentanol, and test the thermodynamic consistency of the generated data. Subsequently, compare the phase behaviour of water + (C_2–C_5) alkanol mixtures, and evaluate how shifting the hydroxyl group affects phase behaviour.

2. Where required, generate pure component parameters for sPC-SAFT and SAFT-VR Mie, and their polar versions.

3. Predict the experimental phase equilibrium data with a thermodynamic model, in particular nonpolar and polar sPC-SAFT and SAFT-VR Mie and evaluate the following:

   (a) The performance of sPC-SAFT compared to SAFT-VR Mie.

   (b) The necessity of including a polar term to the Helmholtz reduced energy expansion for modelling alkanols and their mixtures, and which polar term has the better performance.

   (c) The choice of association scheme for alkanol molecules.

   (d) The quality of predictions obtained for secondary alkanols and their mixtures, and how this compares to those of primary alkanols.

4. Evaluate the performance of the models in predicting mixture excess properties.

1.4 Thesis Overview

Chapter 2 presents an overview of the development of SAFT, focussing on sPC-SAFT and SAFT-VR Mie, as well as the Jog and Chapman, and Gross and Vrabec polar terms. In Chapter 3, the fundamentals of low pressure phase equilibrium, the development of vapour-liquid equilibrium measurement techniques, and how vapour-liquid equilibrium data can be tested for thermodynamic consistency are discussed. The experimental method used in this investigation, a dynamic isobaric method, is detailed in Chapter 4. Verification of the experimental method

is presented in Chapter 5, followed by the vapour-liquid equilibrium data generated for this investigation. In Chapter 6, a discussion of the regression procedure used to determine pure component parameters is presented, and a short analysis of the regressed parameters is given. Thereafter, the modelling of alkane + alkanol mixtures is assessed, followed by that of water + alkanol mixtures. The conclusions of this study and recommendations for future work are presented in Chapter 7.

Chapter 2

The Statistical Associating Fluid Theory

In this chapter, the development of SAFT is discussed briefly, with particular attention given to the sPC-SAFT and SAFT-VR Mie equations of state, as well as the Jog and Chapman, and Gross and Vrabec polar terms.

However, since thermodynamics is ultimately the study of a system's energy, it is important to understand how intermolecular forces affect the system's energy and how these forces can be expressed mathematically.

2.1 Intermolecular Forces and Potentials

Before it can be attempted to develop a fundamentally sound thermodynamic model, it is necessary to understand the behaviour of individual molecules on a molecular level [44]. It is from the intermolecular forces between molecules that macroscopic behaviour, and subsequently thermodynamic properties, are determined [2, 3]. The current understanding of the nature of intermolecular forces is incomplete and analytical expressions that attempt a description thereof are limited to very simple cases [2].

The internal energy of a molecule can be attributed to the molecular kinetic energy, and the molecular potential energy. Kinetic energy is a result of the rotational, vibrational, and translational motion of a molecule and can therefore be observed in a molecule's velocity, which is in turn related to temperature. The relative position of one molecule to another results in the potential energy of the molecules and is directly related to pressure. Molecular potential energy can be further subdivided into intra- and intermolecular potential energies. Intramolecular potential energy is mainly due to the chemical bonds that keep the atoms of a molecule together. Intermolecular potential energy is due to the interaction between different molecules and is a

function of both the attractive and repulsive forces between molecules [44]. In a very generalised sense, it is attraction forces that cause gases to condense, and repulsive forces that cause the incompressibility of liquids [2].

The repulsive force is mainly due to the short range repulsion of electron clouds. The attractive forces, also known as van der Waals forces, are due to a number of different types of forces [2, 44]. Some of the more important forces are listed here:

- *Dispersion forces*, or *London dispersion forces*, which describe the instantaneous dipole moment of seemingly nonpolar molecules, such as oxygen or nitrogen, and is common to all components;
- *Electrostatic forces*, also known as *polar forces*, are a result of the net charges on molecules (point charges), or the charge distribution on molecules with a net neutral charge (electric dipoles), which result in permanent dipoles, quadrupoles, and higher multipoles;
- *Induction forces*, which result when the dipole of one molecule influences the electric structure of a neighbouring molecule;
- *Specific chemical forces*, that lead to the formation of so-called "loose chemical bonds", such as self- and cross-association.

Intermolecular forces are expressed in terms of potential energy functions, which describe the intermolecular potential energy as a function of the distance between molecules, and includes both the attractive and repulsive forces that exist between molecules. In general, potential functions are restricted to two-body, or pair interactions, since it is difficult to represent higher order interactions. A number of potential functions have been developed and range from primitive functions (e.g. hard-sphere, square-well) to functions of moderate complexity (e.g. Lennard-Jones, Yukawa).

2.2 Introduction to SAFT

The SAFT EoS has a sound theoretical foundation as it is derived from statistical mechanical principles. In statistical mechanics, bulk phase properties are determined by the collective interactions between the molecules of the system [9]. One of the approaches used in statistical mechanics to reduce complexity is called perturbation theory. For the potential function, $u(r)$, this becomes [9]:

$$u(r) = u^0(r) + u^1(r) \tag{2.1}$$

$u^0(r)$ is the potential of the reference system, while $u^1(r)$ represents perturbations to the reference system. The first term is relatively simple to calculate, while the more complex second term relies on perturbation theory [9]. Central to the SAFT framework is the first-order thermodynamic perturbation theory (TPT1) of Wertheim [22–27]. In this theory, the reference fluid is one of hard-spheres, while dispersion and association contributions are treated as perturbations [9].

The research group of Chapman [16, 19–21] first incorporated Wertheim's TPT1 in the original SAFT EoS, using the Lennard-Jones (LJ) potential function as reference fluid (Fig. 2.1). The authors formulated their EoS in terms of a Helmholtz energy expansion [16, 21]:

$$\frac{A^{\mathrm{r}}}{RT} = \left(\frac{A^{\mathrm{hs}}}{RT} + \frac{A^{\mathrm{disp}}}{RT}\right)^{\mathrm{seg}} + \frac{A^{\mathrm{chain}}}{RT} + \frac{A^{\mathrm{assoc}}}{RT} \tag{2.2}$$

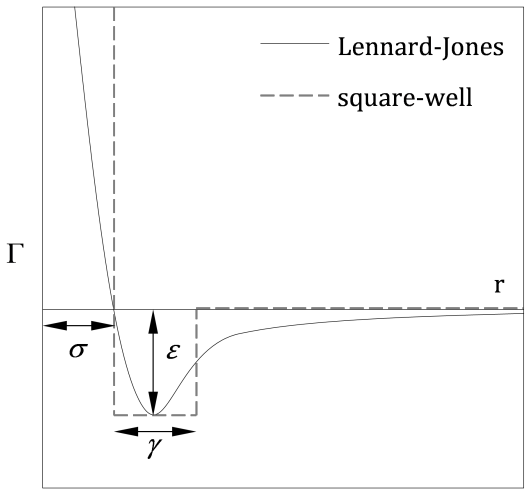

Figure 2.1: Schematic representation of the Lennard-Jones and square-well potentials (σ, segment diameter; ε, potential well depth; λ, potential well width).

The Helmholtz energy, A^{r}, serves as a useful starting point to develop molecular based EoSs, since all thermodynamic properties can be obtained from A^{r} by performing the appropriate integration [45, 46]. A convenient expression for A^{r} is shown in Eq. 2.3 [46]:

$$A^{\mathrm{r}}(T,V,n) = \int_V^\infty \left(P - \frac{nRT}{V}\right) \mathrm{d}V \tag{2.3}$$

In the SAFT framework, a molecule is formed following the diagram in Fig. 2.2: (a) The system consists of a reference fluid of segments, represented by hard spheres; (b) Dispersion forces, indicated by the thicker border, are added to each segment; (c) The segments form chains; (d) Association sites, represented by grey circles, are added to each chain.

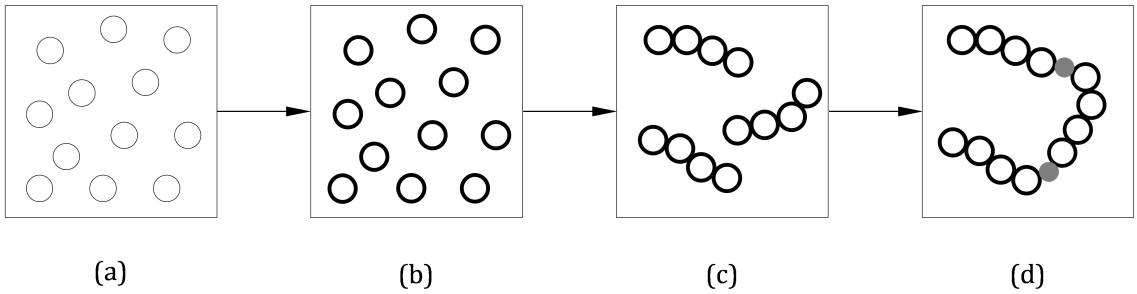

Figure 2.2: Formation of a molecule in the SAFT framework [1].

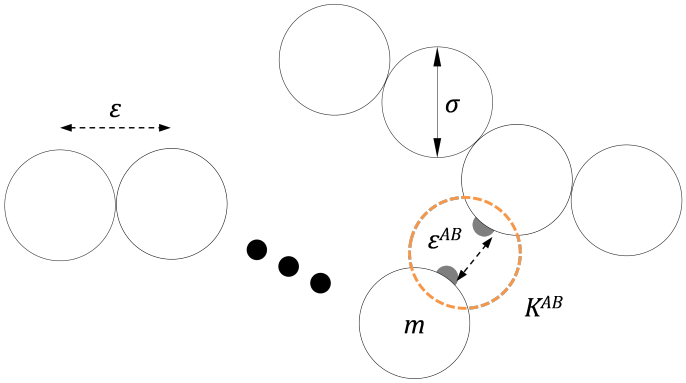

Figure 2.3: Diagram to illustrate the five pure component parameters: σ, segment diameter; m, segment number; ε, dispersion energy; ε^{AB}, association energy; K^{AB}, association volume [16, 21].

Each component is described by three parameters, namely the segment diameter, σ, the number of hard-sphere segments, m, and the segment energy parameter, ε, that describes the dispersion energy between two segments (Fig. 2.3). For associating molecules, two additional parameters are defined, namely the association energy, $\varepsilon^{A_iB_j}$, and the association volume, $K^{A_iB_j}$.

The main difference between different versions of SAFT, is the definition of the reference fluid, and the potential function used to describe this reference fluid. One of the first modifications made by Huang and Radosz (SAFT-HR) [17, 47], using a square-well (SW) reference fluid, rather than the LJ-reference used in the original formulation (Fig. 2.1).

Since its inception, SAFT has developed rapidly. The best known versions of the EoS are: SAFT-VR [48, 49] and later SAFT-VR Mie [41–43], soft-SAFT [50, 51], PC-SAFT [52–54], and its simplified version, sPC-SAFT [45, 55]. There are a number of good reviews [9, 10, 56–59] which describe the development of SAFT and the successes and limitations of the different versions.

In the following sections two very different versions of SAFT will be discussed, namely the simplified Perturbed-Chain SAFT (sPC-SAFT), and the SAFT with Variable Range Mie-potential (SAFT-VR Mie).

2.3 Simplified Perturbed-Chain SAFT

2.3.1 Derivation

The Perturbed-Chain SAFT (PC-SAFT) equation was developed by Gross and Sadowski [52–54]. The fundamental difference introduced by PC-SAFT is that a reference fluid of chains, rather than segments, is considered. This means that the formation of molecules now follows a path different than the one depicted in Fig. 2.2. Molecules are thus formed following the scheme in Fig. 2.4: (a) The system contains individual hard sphere monomers; (b) Chains form; (c) Dispersive forces, indicated by the thicker border, are applied to each chain; (d) Association sites, represented by grey circles, are added to each chain.

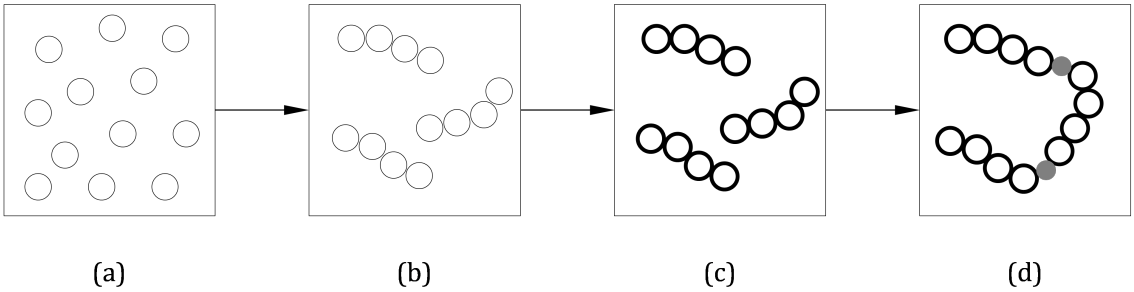

Figure 2.4: Formation of a molecule in the PC-SAFT framework [1].

The hard-chain reference results in a rearrangement of Eq. 1.5:

$$\frac{A^{\mathrm{r}}}{RT} = \left(\frac{A^{\mathrm{hs}}}{RT} + \frac{A^{\mathrm{chain}}}{RT}\right)^{\mathrm{hc}} + \frac{A^{\mathrm{disp}}}{RT} + \frac{A^{\mathrm{assoc}}}{RT} \tag{2.4}$$

Molecules interact with the modified square-well (MSW) potential function proposed by Chen and Kreglewski [60] (Eq. 2.5), presented graphically in Fig. 2.5.

$$u^{\mathrm{MSW}}(r) = \begin{cases} \infty & \text{for } r < (\sigma - s_1) \\ 3\varepsilon & \text{for } (\sigma - s_1) \leq r < \sigma \\ -\varepsilon & \text{for } \sigma < r < \lambda\sigma \\ 0 & \text{for } r \geq \lambda\sigma \end{cases} \tag{2.5}$$

The hard-chain reference term in Eq. 2.4 is comprised of two contributions: the hard-sphere contribution and the chain contribution. The hard-sphere contribution is given by the expression of Boublík [61] and Mansoori, et al. [62], which reduces to the expression proposed by Carnahan and Starling [63] for pure fluids. The formation of chains is obtained by assuming that segments

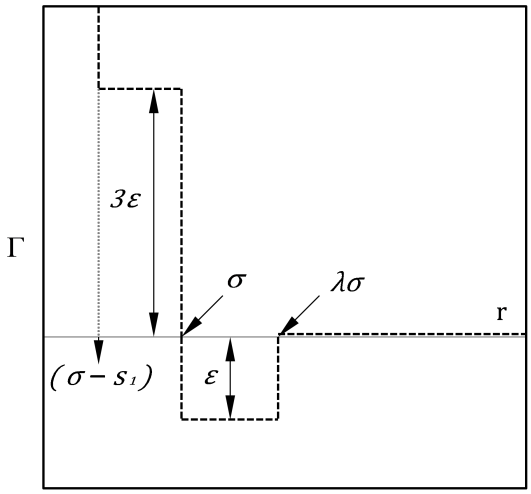

Figure 2.5: Schematic representation of the modified square-well potential.

are bonded tangentially at $r = \sigma$ [20], and results in:

$$\frac{A^{\text{chain}}}{RT} = \sum_i n_i (1 - m_i) \left[\ln g^{\text{M}}(\sigma_{ii}) \right] \tag{2.6}$$

where the summation is over all molecules i in the mixture. g^{M} is the radial distribution function (RDF), and describes how the density of a system of particles varies as a function of distance from a reference particle [2]. Through perturbation theory it follows that [48]:

$$g^{\text{M}}(r) = g^{\text{hs}}(r) + \frac{\varepsilon}{kT} g_1(r) + \left(\frac{\varepsilon}{kT}\right)^2 g_2(r) + \ldots \tag{2.7}$$

PC-SAFT incorporates only the zeroth-order RDF, such that $g^{\text{M}} = g^{\text{hs}}$, determined by the expression of Boublík [61] and Mansoori, et al. [62].

The dispersion term in Eq. 2.4 is treated with the second-order high-temperature perturbation theory of Barker and Henderson [64–66], resulting in a second-order expansion of the dispersion contribution:

$$\frac{A^{\text{disp}}}{RT} = \frac{a_1}{kT} + \frac{a_2}{(kT)^2} \tag{2.8}$$

The integrals presented by a_1 and a_2 are approximated by power series expansions, rather than being solved analytically [52, 53]. The model constants introduced by these series were regressed by fitting the power series to pure n-alkane properties, namely saturated vapour pressure, and liquid, vapour, and supercritical volume data [52, 53].

Von Solms, et al. [45] proposed a simplified version of PC-SAFT (referred to here as sPC-SAFT). The simplification is based on the assumption that all segment diameters in the mixture are the same, i.e. that an average diameter adequately describes mixture properties [45].

This results in two modifications: the first modification reduces the complexity of the radial distribution function, g^{hs}, while the second modification reduces the complexity of A^{hs}. The modifications therefore reduce the complexity of PC-SAFT and subsequently reduces computing time, without altering the fundamental nature of the EoS or losing accuracy [45].

The association contribution to Eq. 1.5 is given by Eq. 2.9, where X_{A_i} is the fraction of molecules of component i not bonded to site A (Eq. 2.10):

$$\frac{A^{\text{assoc}}}{RT} = \sum_i n_i \sum_{A_i} \left[\ln X_{A_i} - \frac{X_{A_i}}{2} + \frac{1}{2} \right] \tag{2.9}$$

$$X_{A_i} = \left[1 + \frac{1}{V} \sum_j n_j \sum_{B_j} X_{B_j} \Delta^{A_i B_j} \right]^{-1} \tag{2.10}$$

The association strength, $\Delta^{A_i B_j}$, introduces an association integral, $I^{A_i B_j}$, which is determined when the RDF of the reference fluid, $g^{\text{hs}}(r)$, is evaluated over a range of separations around the distance of contact, σ, such that:

$$I^{A_i B_j} = g^{\text{hs}}(d_{ij}) K^{A_i B_j} \tag{2.11}$$

The association volume, $K^{A_i B_j}$, is determined by regression.

Association Schemes

X_{A_i} is approximated based on the association scheme assigned to a molecule. Wertheim's TPT1 constrains the association mechanism as follows [10, 16]:

1. The angle of association is not specified, therefore fluid properties are assumed to be independent of the angle between sites;
2. Bonding at one site on a molecule is independent of bonding at any other site on the same molecule, and;
3. Chainlike and tree-like associated clusters are allowed to form, but not ring-like structures.

The following steric hindrance approximations are made, with reference to Fig. 2.6: (a) A single bond exists only between 2 molecules, i and j, repulsing a third molecule, k, from the association point; (b) A single site on molecule i can only bond to one site on molecule j; (c) Double bonds between two molecules cannot exist.

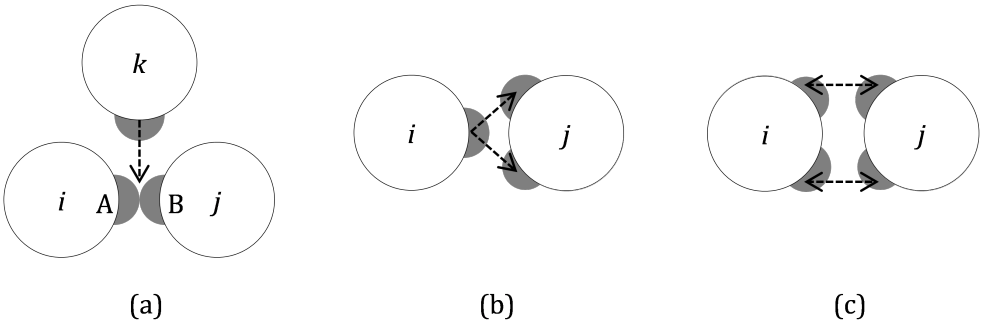

Figure 2.6: Schematic representation of steric hindrance approximations [16].

Different molecules associate differently, hence Eq. 2.10 depends on the association followed by the system molecules. Association schemes are used to represent or visualise how association occurs between molecules. The association schemes used throughout literature were originally proposed by Huang and Radosz [17].

The association schemes are simplified by realising that three types of association sites exist: positive electron acceptor sites, negative electron donor sites, and bipolar sites. Positive sites form hydrogen bonds with both negative and bipolar sites, negative sites form hydrogen bonds with both positive and bipolar sites, and bipolar sites form hydrogen bonds with all sites. The number of each type of site is shown along with the relevant association scheme in Table 2.1.

Alkanols are modelled successfully with both the 3B and the more rigorous 2B schemes. Depending on the mixture alkanols are found in, one or the other scheme seems to be more appropriate and a single, superior scheme to represent alkanols has yet to be identified. It is on this premise that de Villiers, et al. [67] developed the 2C scheme as a combination of the 2B and 3B schemes. The 2C scheme shows improvements over the 2B and 3B schemes for the modelling of phase equilibria of water + 1-alkanol systems when used with the sPC-SAFT EoS. In previous investigations alkanols were modelled with the 2B [17, 35, 54, 67], 2C [67], and 3B [67] schemes, while water has been modelled with the 2B [35, 54, 68], 3B [17, 68], and 4C [30, 67, 68] schemes. For water, the 4C-scheme has been proven to be superior to the other alternatives (2B and 3B), and is proposed as the scheme that should be used to model water [68–70].

In this investigation, water is modelled with the 4C scheme throughout, while for alkanols the performance of the 2B, 2C, and 3B schemes are compared with one another.

In sPC-SAFT, nonassociating components have 3 pure component parameters (σ, m, ε), while associating components have 5 pure component parameters (σ, m, ε, ε^{AB}, K^{AB}) that need to be determined by regression.

Table 2.1: Association schemes. B = bipolar site, N = negative electron donor site, P = positive electron acceptor site (adapted and redrawn from Huang and Radosz [47] and de Villiers [36]).

Species	Formula	Scheme	Sites	X_A Approximations
Water		2B	1N 1P	$X_A = X_B$
	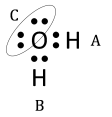	3B	2N 1P	$X_A = X_B$; $X_C = 2X_A - 1$
	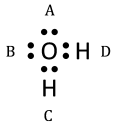	4C	2N 2P	$X_A = X_B = X_C = X_D$
Alkanol	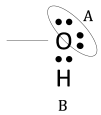	2B	1N 1P	$X_A = X_B$
	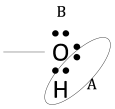	2C	1B 1N	$X_B = \sqrt{X_A}$
	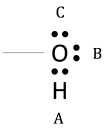	3B	2N 1P	$X_A = X_B$; $X_C = 2X_A - 1$

2.3.2 Combining Rules

All equations shown until this point are for mixtures. However, combining rules are required to represent mixtures. σ_{ij} is evaluated by:

$$\sigma_{ij} = \frac{\sigma_{ii} + \sigma_{jj}}{2} \tag{2.12}$$

The mixture segment number, m_{m}, is calculated through:

$$m_{\mathrm{m}} = \frac{1}{n_{\mathrm{t}}} \sum_i n_i m_i \tag{2.13}$$

The conventional Lorentz-Berthelot combing rule for ε_{ij} follows as:

$$\varepsilon_{ij} = (1 - l_{ij}) \sqrt{\varepsilon_{ii} \varepsilon_{jj}} \tag{2.14}$$

where l_{ij} is a binary interaction parameter. The combining rules for $\varepsilon^{A_iB_j}$ and $K^{A_iB_j}$ follow as [54]:

$$\varepsilon^{A_iB_j} = \frac{\varepsilon^{A_iB_i} + \varepsilon^{A_jB_j}}{2} \tag{2.15}$$

$$K^{A_iB_j} = \sqrt{K^{A_iB_i}K^{A_jB_j}} \tag{2.16}$$

2.3.3 Model Results

In the original PC-SAFT publication [53], pure component parameters were determined for 78 nonassociating and 18 associating species, ranging from small spherical molecules to complex chainlike polymers, by simultaneously correlating vapour pressure and saturated liquid densities. In a subsequent publication [54], pure component parameters were determined for associating molecules, including alkanols and amines. Several binary mixtures were also investigated (nonassociating/nonassociating [53], nonassociating/associating [54], and associating/associating [54]). Generally, satisfactory correlation of binary VLE data was achieved when a binary interaction parameter was included. Compared to SAFT-HR [17, 47] the performance of PC-SAFT is superior, resulting in better predictions of both pure fluid properties and binary VLE [53].

In turn, von Solms, et al. [45] compared the performance of sPC-SAFT to PC-SAFT by investigating its application to asymmetric and associating systems. Observed trends in model parameters allow for extrapolation to long-chain alkanes with adequate subsequent predictions obtained [45].

Von Solms, et al. [55] assessed the capabilities and limitations of sPC-SAFT. One major drawback of the EoS is its inability to predict the behaviour of aqueous systems accurately, especially water + alkanol systems. Furthermore, predictions of critical behaviour are still limited, since the model generally overpredicts the critical temperature and pressure [55]. The model struggles to describe polar interactions for molecules such as esters and ketones, especially in binary mixtures with alkanes [55].

2.4 SAFT-VR Mie

As stated in Section 2.1, the description of intermolecular forces is key in the development of an EoS. The original SAFT, SAFT-HR, and PC-SAFT use potential functions that are expressed in terms of σ and ε only, thereby assuming that all chemical species conform to the same corresponding state [48].

To address this limiting assumption, Gil-Villegas and co-workers [48, 49] introduced a SAFT variant for which the potential function incorporates a variable well-width parameter, λ, thereby giving the EoS its name, SAFT with Variable Range (SAFT-VR). λ is associated with the range over which attractive forces occur and allows the treatment of nonconformal fluid properties [48]. Thus, two components that have different λ-values do not obey corresponding states [48].

In the original work [48], three different hard-body intermolecular potential functions, namely the Sutherland, Yukawa, and square-well potentials were investigated, as well as the LJ soft-core potential. SAFT-VR was later extended for use with the soft-core Mie a-r potential function by Lafitte, et al. [41–43] to improve the description of repulsive interactions, with the specific aim of predicting both phase equilibria and second-order derivative properties simultaneously. The resulting EoS is called SAFT-VR Mie.

2.4.1 Derivation

SAFT-VR Mie, like the original SAFT [16, 21], considers perturbation to hard-sphere segments, such that molecules are formed according to the diagram in Fig. 2.2, and that A^r takes on the form of Eq. 2.2. The reference fluid used in SAFT-VR Mie is the generic Mie-potential [71], described as:

$$u_{ij}^{\text{Mie}}(r) = C_{ij}\varepsilon_{ij}\left[\left(\frac{\sigma_{ij}}{r}\right)^{\lambda_{ij}^{\text{r}}} - \left(\frac{\sigma_{ij}}{r}\right)^{\lambda_{ij}^{\text{a}}}\right] \tag{2.17}$$

$$C_{ij} = \frac{\lambda_{ij}^{\text{r}}}{\lambda_{ij}^{\text{r}} - \lambda_{ij}^{\text{a}}}\left(\frac{\lambda_{ij}^{\text{r}}}{\lambda_{ij}^{\text{a}}}\right)^{\frac{\lambda_{ij}^{\text{a}}}{\lambda_{ij}^{\text{r}} - \lambda_{ij}^{\text{a}}}} \tag{2.18}$$

The best known form of the Mie potential is the LJ 6-12 potential function. A schematic representation of three Mie-potentials, including the well-known LJ-potential, is shown in Fig. 2.7.

Generally the attractive range, λ^{a}, is set equal to 6, which corresponds to the quantum-mechanical description of fluctuating dipoles [42, 43] and is shown to be consistent with the theory of dispersion forces [72]. The repulsive range, λ^{r}, is left variable and determined through regression.

The original SAFT-VR formulation [48, 49] is derived from the second-order high temperature perturbation theory of Barker and Henderson [64–66]. For SAFT-VR Mie, Lafitte, et al. [73] extended this approach by including the third-order perturbation term, resulting in a third-order expansion of the dispersion contribution:

$$\frac{A^{\text{disp}}}{RT} = \frac{a_1}{kT} + \frac{a_2}{(kT)^2} + \frac{a_3}{(kT)^3} \tag{2.19}$$

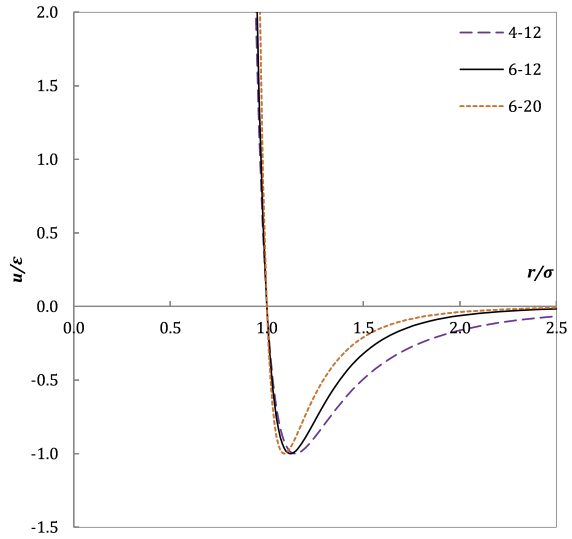

Figure 2.7: Schematic representation of three Mie a-r potentials.

For the chain contribution, the RDF as shown in Eq. 2.7 is expanded as a logarithm, and truncated to second-order, such that [42, 64–66]:

$$g_{ii}^{\text{Mie}}(\sigma_{ii}) = g_{ii}^{\text{hs}}(\sigma_{ii}) \exp\left[\frac{\varepsilon_{ii}}{kT}\frac{g_{1,ii}(\sigma_{ii})}{g_{ii}^{\text{hs}}(\sigma_{ii})} + \left(\frac{\varepsilon_{ii}}{kT}\right)^2 \frac{g_{2,ii}(\sigma_{ii})}{g_{ii}^{\text{hs}}(\sigma_{ii})}\right] \tag{2.20}$$

The association contribution in SAFT-VR Mie is defined identically to that of sPC-SAFT. However, instead of regressing the association volume, $K^{A_iB_j}$, it is obtained by the solution proposed by Jackson, et al. [19]. The association volume is now dependent on temperature, and introduces two new pure component parameters: $r^{\text{c}}_{A_iB_j}$ is the range of association, while $r^{\text{d}}_{A_iB_j}$ represents the distance at which a square-well association bonding site is placed from the segment centre. Following previous work [42, 74, 75] the bonding geometry is constrained to $r^{\text{d}}_{A_iB_j} = 0.4\sigma$, while $r^{\text{c}}_{A_iB_j}$ is regressed from pure component data. The same association schemes and association constraints as those used in the original SAFT formulation [16, 21], and subsequently in sPC-SAFT [45] are valid for SAFT-VR Mie.

In the original formulation of SAFT-VR Mie [42], the association integral was evaluated by approximating $g^{\text{Mie}}(r)$ as its hard-sphere counterpart, resulting in the same formulation presented in Eq. 2.11. In a subsequent paper by Dufal, et al. [75], the authors compared results for water, using three different reference fluids for the RDF in the association contribution, namely HS, LJ, and the generic Mie. However, despite the improved results obtained by the latter two methods, the HS approach [42] is followed in this work.

In SAFT-VR Mie, nonassociating components have 4 pure component parameters (σ, m, ε, λ^{r}), while associating components have 6 pure component parameters (σ, m, ε, λ^{r}, ε^{AB}, r^{c}_{AB}) that need to be determined by regression.

2.4.2 Combining Rules

For SAFT-VR Mie, σ_{ij} and m_{m} are evaluated by Eqs. 2.12 and 2.13, respectively. The unlike attractive and repulsive exponents are evaluated by:

$$\lambda^{\mathrm{p}}_{ij} - 3 = (1 - k_{ij})\sqrt{\left(\lambda^{\mathrm{p}}_{ii} - 3\right)\left(\lambda^{\mathrm{p}}_{jj} - 3\right)}\,; \quad \mathrm{p{=}a,r} \tag{2.21}$$

To satisfy Eq. 2.21 the following expression is used to obtain ε_{ij}:

$$\varepsilon_{ij} = (1 - l_{ij})\frac{\sqrt{\sigma^3_{ii}\sigma^3_{jj}}}{\sigma^3_{ij}}\sqrt{\varepsilon_{ii}\varepsilon_{jj}} \tag{2.22}$$

k_{ij} and l_{ij} are binary interaction parameters. A Berthelot-like combining rule is used to determine the association energy, $\varepsilon^{A_iB_j}$:

$$\varepsilon^{A_iB_j} = \sqrt{\varepsilon^{A_iB_i}\varepsilon^{A_jB_j}} \tag{2.23}$$

Lastly, simple combining rules are used for the size parameters, $r^{\mathrm{c}}_{A_iB_j}$ and $r^{\mathrm{d}}_{A_iB_j}$:

$$r^{\mathrm{p}}_{A_iB_j} = \frac{r^{\mathrm{p}}_{A_iB_i} + r^{\mathrm{p}}_{A_jB_j}}{2}\,; \quad \mathrm{p{=}c,d} \tag{2.24}$$

2.4.3 Model Results

In the original paper [42], the model was applied to selected pure compounds, including n-alkanes (C_1-C_{20}) and n-alkanols (C_1-C_4) to assess the prediction of associating molecules, and n-perfluoroalkanes (C_1-C_5) to assess the prediction of highly polarizable molecules [42]. Pure component parameters were regressed by including saturated vapour pressure, saturated liquid density, condensed liquid density (ρ^{liq}), and speed of sound (u^{liq}) data in the objective function [42].

In all cases, excellent results were obtained for the prediction of both first- (p^{sat}, ρ^{sat}, ρ^{liq}, h^{vap}) and second-order (u^{liq}, c_p) derivative properties [42]. A significant reduction in the overshoot of the near-critical region of pure component VLE is attained. This is attributed to the inclusion of the third-order perturbation term [42].

Comparison to predictions with SAFT-VR SW [48], soft-SAFT [50, 51], and PC-SAFT [52–54] emphasizes the fact that the variable repulsive exponent allows for simultaneous description

of both VLE and other thermodynamic properties [48]. This was not previously possible with fixed SW- or LJ-potentials.

In the original paper [42], the critical phase envelopes at high pressures for two binary systems, namely ethane + n-decane, and carbon dioxide + n-decane, were investigated. Predictions by SAFT-VR Mie are notably better than those obtained by SAFT-VR SW [42]. Further application of SAFT-VR Mie to mixture behaviour has been severely limited. Only one subsequent study by Dufal, et al. [76] was found, where binary aqueous mixtures of methanol, methane, carbon dioxide, and hydrogen sulphide were investigated.

2.5 Polar Contribution

From a molecular point of view, it is known that polar forces can significantly influence the behaviour of a molecule, and subsequently its thermodynamic properties [2]. The original formulations of SAFT and those presented in the preceding sections do not explicitly account for polar effects. In the most cases, behaviour caused by polar effects is accounted for implicitly in the dispersion term [35, 38], leading to a much larger pure component dispersion energy, ε_{ii}. However, since polar forces are inherently different from dispersion forces (see Section 2.1), implicitly accounting for polarity is not adequate in many cases [37]. Polar forces, which are physical forces, are also different in nature from association forces, which are chemical in nature [2], and the description of association schemes (Table 2.1) does not account for polarity.

Because of the additive nature of SAFT, additional terms describing interactions other than segment, chain, or association, have been developed and implemented successfully. Particularly noteworthy is the development of a term that explicitly accounts for polar interactions [37–39, 77–81]. A^{polar} has an additional pure component parameter describing the degree of polarity, but does not have a positional specifier.

Various polar terms have previously been developed, amongst others those of Jog and Chapman [37, 38], and Gross and Vrabec [39].

2.5.1 Jog and Chapman

Jog and Chapman [37, 38] derived a polar contribution from Wertheim's TPT1 [22–27]. Previous attempts to account for polarity followed an "effective molecular sphere approach" [82–84] (Fig. 2.8(a)). This approach approximates the dipolar molecule as a sphere with volume equal to the molecular volume, with an ideal dipole located at the centre of the sphere. This approach is limiting; as the molecule becomes larger the dipole effect becomes smaller due to the larger separation between dipoles. i.e. the nonsphericity of a molecule is not accounted

for. The molecular sphere approach also does not allow for multiple polar groups to be treated independently of one another [38].

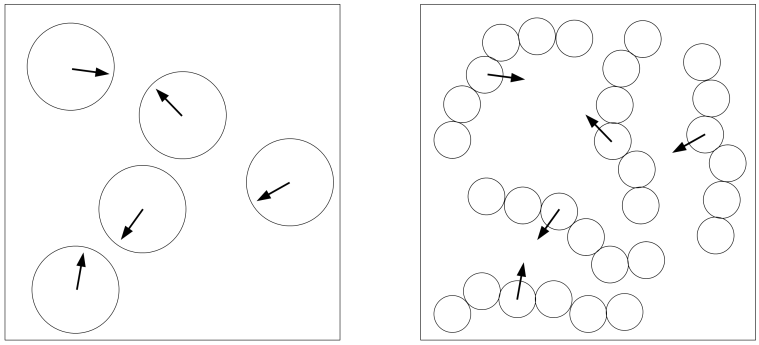

Figure 2.8: Graphic representation of the (a) molecular sphere approach; (b) segment approach [38].

In their derivation, Jog and Chapman attempted to address both these limitations. They applied a segment approach (Fig. 2.8(b)), where molecules are considered as chains of tangential segments, which accounts for molecular nonsphericity. Moreover, the number and magnitude of multiple dipoles on molecules can be characterised.

2.5.1.1 Derivation

Including the polar contribution to the residual Helmholtz energy results in [37]:

$$\frac{A^{\mathrm{r}}}{RT} = \frac{A^{\mathrm{hs}}}{RT} + \frac{A^{\mathrm{disp}}}{RT} + \frac{A^{\mathrm{chain}}}{RT} + \frac{A^{\mathrm{assoc}}}{RT} + \frac{A^{\mathrm{polar}}}{RT} \tag{2.25}$$

The polar contribution, A^{polar}, derived from the u-expansion, is an infinite series. The second- and third-order terms are explicitly calculated [85], while the higher-order terms are estimated through the Padé approximate of Rushbrooke, et al. [86], shown in Eq. 2.26:

$$A^{\mathrm{polar}} = \frac{A_2}{1 - (A_3/A_2)} \tag{2.26}$$

A_2 and A_3 are expressed in terms of the pure component dipole moment, μ_i, and are evaluated for a hard-sphere reference fluid. The two- and three body integrals introduce a new pure component parameter, $x_{\mathrm{p},i}$, which is the fraction of dipolar segments on molecule i and is treated as an adjustable parameter [38]. The two- and three body correlation functions are assumed to be independent of component at a given density, reducing the integrals to their pure component forms.

In the original work, Jog, et al. [38] intended their polar term to be used within the original SAFT framework [16, 21]. However, Tumakaka and Sadowski [87] showed that the JC polar term can easily be extended to any other form of SAFT without modification. Based on this argument, de Villiers [36] incorporated the JC polar term in the sPC-SAFT framework to bring about sPC-SAFT-JC.

In sPC-SAFT-JC, nonassociating components have 4 pure component parameters (σ, m, ε, x_{p}), while associating components have 6 pure component parameters (σ, m, ε, ε^{AB}, K^{AB}, x_{p}) that need to be determined by regression.

In SAFT-VR Mie-JC, nonassociating components have 5 pure component parameters (σ, m, ε, λ^{r}, x_{p}), while associating components have 7 pure component parameters (σ, m, ε, λ^{r}, ε^{AB}, r_{AB}^{c}, x_{p}) that need to be determined by regression.

2.5.1.2 Model Results

The polar SAFT, as presented by Jog and Chapman, was validated against molecular simulations [37], after which the model was extended to real fluids [38]. Here two very different mixtures were considered. The first were binary acetone + alkane mixtures [38]. This tested the model's ability to treat polar + nonpolar mixtures, as well as differences in molecular size. In comparison to the original SAFT, the polar SAFT provided better phase equilibrium predictions, with k_{ij} systematically smaller than for the original SAFT. Moreover, polar SAFT accurately predicts azeotropic compositions and pressures of the systems investigated [38].

The second were binary alkane + polar copolymer mixtures, where both the alkane and the concentration of the polar copolymer were varied [38]. These systems were chosen to evaluate whether the model could predict the phase behaviour of systems containing molecules with multiple dipoles. These systems proved difficult to model with the original SAFT, while polar SAFT delivered results that were in close agreement with experimental data [38].

2.5.2 Gross and Vrabec

Gross and co-workers conducted extensive work to describe the contribution of dipolar- [39], quadrupolar- [77], dipole-quadrupole [79], and induced polar [78] interactions to the reduced Helmholtz free energy. For this work only the dipolar contribution is considered.

2.5.2.1 Derivation

Gross and Vrabec derived their polar term from third-order perturbation theory, using a two-centre Lennard-Jones (2CLJ) plus pointdipole fluid as a reference [39]. Rather than accounting

for the number of segments in a molecule, the distance between two segment centres are accounted for by the molecular elongation, L. Gross and Vrabec specifically developed their polar term to be used with PC-SAFT and it was therefore necessary to reconcile the different reference fluids by relating m to L. The reader is referred to Gross and Vrabec [39] for an in-depth discussion on how the conversion was achieved.

Similar to Jog and Chapman, the polar contribution is presented with a third order Padé approximate, shown in Eq. 2.26. The second- and third-order expansions introduce a new model parameter, $n_{\mathrm{p},i}$, which is the number of dipolar segments. The two- and three body integrals are approximated as power series. The model constants required for the power series were fitted to molecular simulation data for the LJ plus pointdipole reference fluid, including saturated liquid and vapour density, saturated vapour pressure, and virial coefficient data in the regression procedure [39].

In the original work [39], the number of dipolar segments, $n_{\mathrm{p},i}$, is set equal to 1 for low molecular weight components, and not left adjustable like the similarly defined dipole fraction, $x_{\mathrm{p},i}$, in Jog and Chapman's formulation. However, in accordance with the JC polar term, $n_{\mathrm{p},i}$ is left variable during regression in this investigation.

In sPC-SAFT-GV, nonassociating components have 4 pure component parameters (σ, m, ε, n_{p}), while associating components have 6 pure component parameters (σ, m, ε, ε^{AB}, K^{AB}, n_{p}), that need to be determined by regression.

In SAFT-VR Mie-GV, nonassociating components have 5 pure component parameters (σ, m, ε, λ^{r}, n_{p}), while associating components have 7 pure component parameters (σ, m, ε, λ^{r}, ε^{AB}, r^{c}_{AB}, n_{p}), that need to be determined by regression.

2.5.2.2 Model Results

PC-SAFT-GV was initially compared to molecular simulations [39]. The results were in good agreement with the simulations, without the use of interaction parameters. This reflects the functionality of the second- and third-order terms in the Padé approximate [39].

The model was also tested against real fluid data [39]. In the pure component case, substantial improvement was observed in the phase behaviour predictions of high dipole moment molecules, while only a slight improvement was observed for weak dipoles [39]. In the case of binary mixtures, PC-SAFT-GV showed both an improvement in phase behaviour predictions and a systematic reduction in interaction parameter magnitude in comparison to nonpolar PC-SAFT [39].

2.5.3 Application

Al-Saifi, et al. [35] investigated both the JC and GV polar terms along with the Economou-term [80, 81] and found the JC and GV terms to be superior to the Economou-term. De Villiers [88, 89] extended the sPC-SAFT EoS with both polar terms and found that the two models yield similar results when predicting nP/P-nHB, P-nHB/P-nHB, nP/P-HB, P-HB/P-HB behaviour (nP=nonpolar, P-nHB=polar-nonassociating, P-HB=polar-associating), and that neither of the two models was superior. Cripwell [40] also used the sPC-SAFT-JC and sPC-SAFT-GV models to evaluate whether the models can account for structural isomerism in binary alkane + ketone mixtures, and found sPC-SAFT-GV to be superior to sPC-SAFT-JC.

2.6 Application of SAFT to Water + Alkanol Mixtures

The SAFT family of equations have been used to model various different systems since their development. A summary of the most notable applications to binary water + alkanol mixtures relevant to the scope of this project is given in Table 2.2. The scope of this search was restricted to include only the following models: PC-SAFT, sPC-SAFT, SAFT-VR, and SAFT-VR Mie, with and without the use of the polar contributions described in Section 2.5.

In many modelling cases, a binary interaction parameter is required to obtain a good model fit to experimental data. The models also struggle to predict both VLE and LLE of the same mixture using the same binary interaction parameter [30, 33]. Moreover, the investigations have also largely been aimed at aqueous mixtures of primary alkanols and have not exclusively focused on the modelling of water + secondary alkanol mixtures.

Table 2.2: Previous application of PC-SAFT, sPC-SAFT, SAFT-VR, and SAFT-VR Mie to the water + alkanol systems investigated in this study.

Model	Reference	alkanols
PC-SAFT	Gross and Sadowski, 2002 [54]	1-pentanol
	Voutsas, et al., 2007 [90]	methanol
	Shi and Liang, 2011 [91]	1-pentanol
	Bender, et al., 2013 [92]	1-pentanol
	Mejbri, et al., 2015 [32]	methanol, ethanol, 1-propanol, 2-propanol, 1-butanol, 1-pentanol
PC-SAFT-JC	Al-Saifi, et al., 2008 [35]	methanol, ethanol, 2-propanol
PC-SAFT-GV	Al-Saifi, et al., 2008 [35]	methanol, ethanol, 2-propanol
sPC-SAFT	Grenner, et al., 2007 [30]	ethanol, 1-propanol, 2-propanol, 1-butanol, 1-pentanol, 2-pentanol
	Grenner, et al., 2008 [93]	methanol, ethanol, 2-propanol
	Tsivintzelis, et al., 2008 [33]	1-butanol, 1-pentanol
	de Villiers, et al., 2011 [67]	methanol, ethanol, 1-propanol, 1-butanol, 1-pentanol
	Liang, et al., 2014 [69]	methanol, ethanol, 1-propanol, 1-butanol, 1-pentanol
sPC-SAFT-JC	de Villiers, et al., 2014 [89]	methanol, ethanol, 1-propanol, 1-butanol, 1-pentanol
sPC-SAFT-GV	de Villiers, et al., 2014 [89]	methanol, ethanol, 1-propanol, 1-butanol, 1-pentanol
SAFT-VR	Paragand, et al., 2010 [34]	ethanol
	Cristino, et al., 2013 [94]	ethanol
	Cristino, et al., 2013 [95]	1-propanol
SAFT-VR Mie	Dufal, et al., 2015 [75]	methanol

Chapter 3

Low Pressure Phase Equilibria

The phase behaviour of fluid mixtures has been studied extensively over the past century for two main reasons:

1. The properties of pure substances are relatively simple to investigate. One can attempt to predict mixture phase behaviour based on the phase behaviour observed in the constituent pure components. However, mixture phase behaviour is more often than not more complex than the assumption that (A-B) interactions are merely the average of (A-A) and (B-B) interactions [96]. The degree to which interactions between A and B occur is mainly observed through experimental work.

2. Mixtures of components add degrees of freedom to the system which lead to interesting phenomena not observed in pure component systems. Investigating mixtures gives insight to unique multiphase behaviour [96].

In this chapter, the most prominent phase behaviour observed in binary systems at low pressures are highlighted, whereafter experimental techniques used to observe phase behaviour are discussed. After experiments are conducted, the accuracy of the data is evaluated by conducting thermodynamic consistency tests, two of which are discussed. Finally, a summary of available data for the systems investigated in this study is given.

3.1 Low Pressure Phase Behaviour

Low pressure phase equilibrium behaviour can roughly be grouped according to the following descriptions: systems exhibiting only vapour-liquid equilibrium, with the components being completely miscible in the liquid state, and systems exhibiting liquid-liquid equilibrium, with no vapour-liquid behaviour at elevated temperatures. Where the vapour-liquid and liquid-liquid equilibria of the same mixture intersect, vapour-liquid-liquid equilibrium is observed.

Solid-liquid equilibrium also occurs, but falls beyond the scope of this project and will not be discussed.

At the point of thermodynamic equilibrium, the total Gibbs energy of a system is at a minimum, such that [3]:

$$\left(\mathrm{d}G^{\mathrm{t}}\right)_{T,p} \leq 0 \tag{3.1}$$

Eq. 3.1 leads directly to the equality of chemical potential for each component in each of the coexisting phases α, β, and π:

$$\mu_i^{\alpha} = \mu_i^{\beta} = \ldots = \mu_i^{\pi} \tag{3.2}$$

3.1.1 Vapour-Liquid Equilibrium

Vapour-liquid equilibrium (VLE) describes the coexistence of vapour and liquid phases and is most commonly expressed in terms of the composition of the coexisting phases. Generally the compositions of the coexisting liquid and vapour phases differ, with the vapour phase richer in the more volatile component [3].

The point at which the coexisting vapour and liquid phases have identical compositions is referred to as an azeotrope [3, 96]. Azeotropes are of interest to industry, since this condition determines the maximum purity that can be achieved through distillation without the addition of alternative separating media. Azeotropy typically occurs in systems where the intermolecular forces between *like* molecules and those between *unlike* molecules differ appreciably [3]. Furthermore, azeotropy is more likely to occur in a binary system where the boiling points of the constituent components under isobaric conditions, or vapour pressure under isothermal conditions, are close to one another [96].

Two types of azeotropes are observed in VLE, depicted in Fig. 3.1. The more common positive azeotrope is one that has a maximum vapour pressure and minimum boiling point, while a negative azeotrope displays a minimum vapour pressure and maximum boiling point [96]. Positive azeotropes occur in systems where the interactions between *like* molecules are stronger than those between *unlike* molecules. This results in solvation, or self-association, allowing more molecules to escape to the vapour phase and subsequently results in a pressure higher than the ideal case [3, 44]. Conversely, a negative azeotrope occurs when *unlike* interactions are stronger than *like* interactions, causing less molecules to escape to the vapour phase and a pressure which is lower than the ideal case [3, 44].

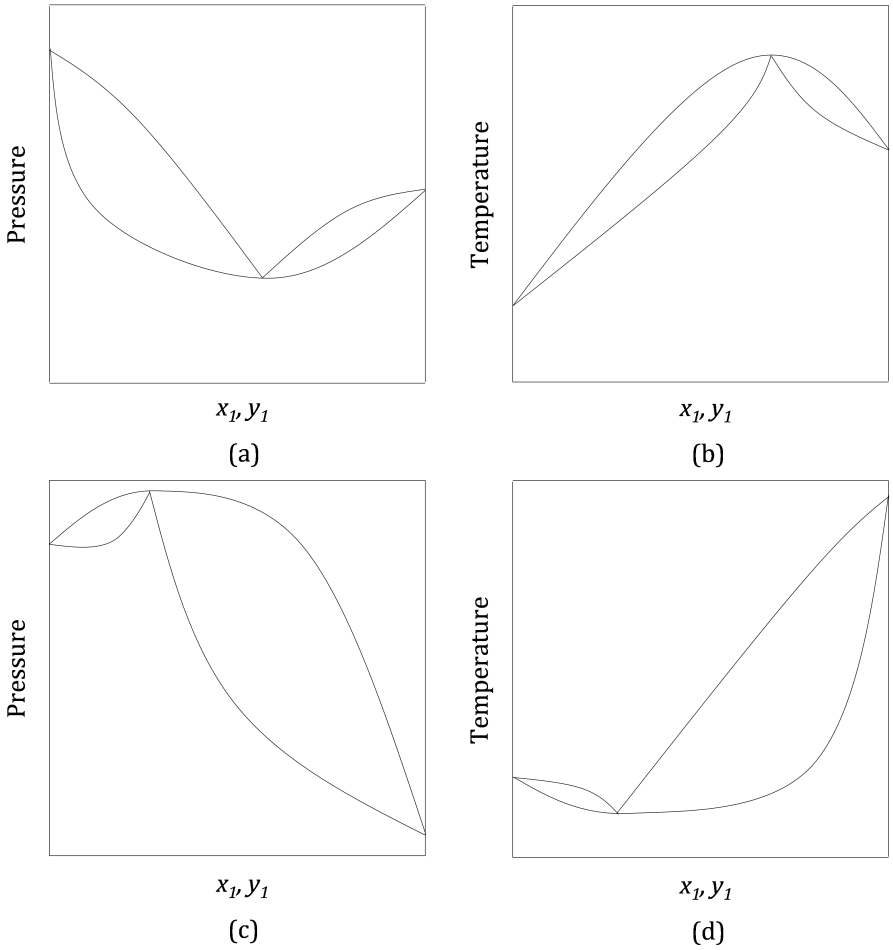

Figure 3.1: *P-xy* and *T-xy* diagrams illustrating azeotropy: (a) and (b) display a negative azeotrope; (c) and (d) display a positive azeotrope [3].

3.1.2 Liquid-Liquid Equilibrium

Liquid-liquid equilibrium (LLE) describes the coexistence of two immiscible liquid phases. LLE is strongly influenced by temperature, while pressure does not affect equilibrium significantly.

Eq. 3.1 states that any irreversible process at constant T and p proceeds in the direction which decreases the total Gibbs energy of the system, G^{t} [3]. Therefore a mixing process occurring at constant T and p will result in a total Gibbs energy which is lower than the unmixed state.

To illustrate this, consider Fig. 3.2: For system **I**, a single, homogeneous phase forms at all compositions. For system **II** at compositions $x_1^{\mathrm{A}} < x_1 < x_1^{\mathrm{B}}$, a lower total Gibbs energy, represented by the straight dashed line connecting A and B, is achieved when two heterogeneous phases (phases A and B), rather than a single homogeneous phase, form.

Four different types of binary liquid-liquid behaviour are shown in Fig. 3.3. Fig. 3.3(a) shows

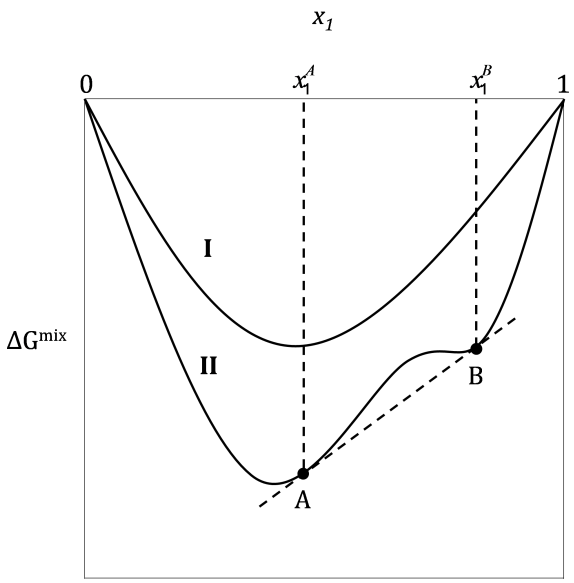

Figure 3.2: Change in Gibbs energy due to mixing [3, 96].

an island system. The curve *UAL* shows the composition of the phase rich in x_2, while *UBL* shows the composition of the x_1-rich phase. T_{L} indicates the lower critical solution temperature, or LCST. The upper critical solution temperature, UCST, is indicated by T_{U}. LLE exists for temperatures $T_{\mathrm{L}} < T < T_{\mathrm{U}}$. For temperatures outside of this range a single liquid phase exists [3].

The phase behaviour illustrated in Fig. 3.3(a) is rarely observed. When the solid-liquid equilibrium intersects with LLE curve, there is no LCST and the behaviour shown in Fig. 3.3(b) occurs. When the LLE region intersects the VLE curve, no UCST exists and results in Fig. 3.3(c). When neither LCST or UCST exist, the LLE phase behaviour is represented by a diagram similar to Fig. 3.3(d) [3, 97].

3.1.3 Vapour-Liquid-Liquid Equilibrium

When binary VLE and LLE intersect, a phenomenon know as vapour-liquid-liquid equilibrium (VLLE) results. At the point of intersection, there are three phases, namely two liquid phases and one vapour phase. By the phase rule, a binary system existing in three phases, has one degree of freedom. For a given pressure, the temperature and phase compositions at the three phase point are therefore unique.

The foour types of VLLE behaviour observed are shown in Fig. 3.4: (a) A heterogeneous azeotrope forming at the VLLE temperature, T^*, the lowest temperature at which a vapour can exist; (b) A positive homogeneous azeotrope, which lies outside the L_1+L_2 region; (c) T^* lying

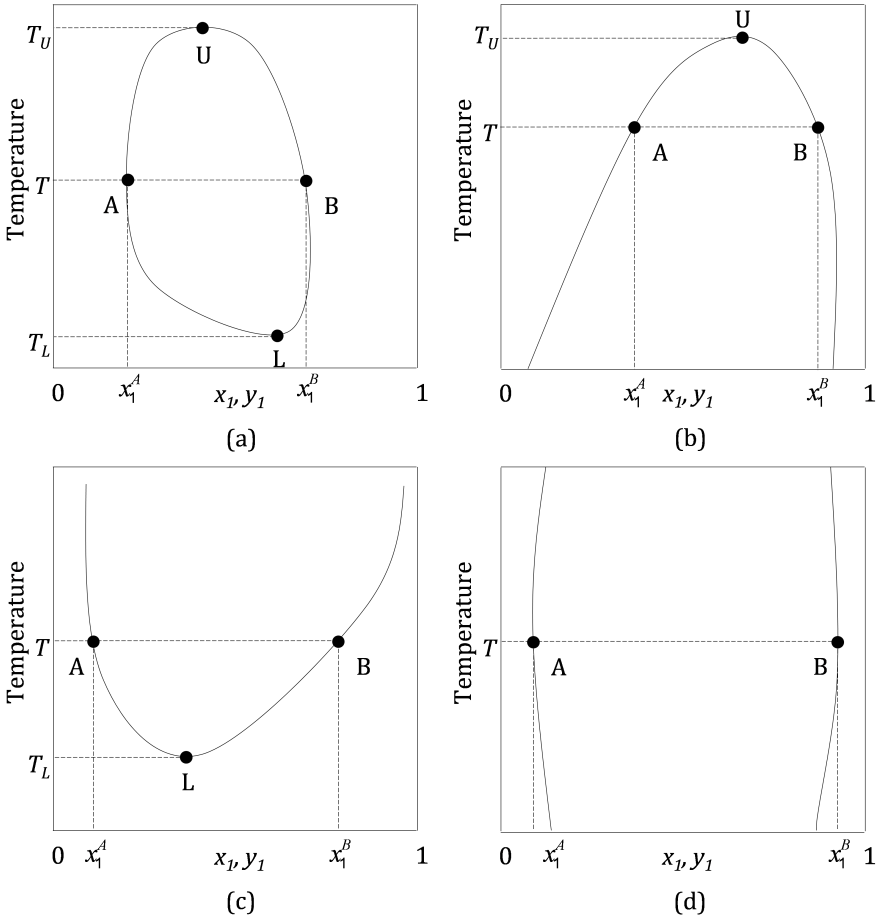

Figure 3.3: $T - xy$ diagrams illustrating different types of binary liquid-liquid behaviour [3, 97].

between the boiling temperatures of both the pure components, with no azeotrope forming; (d) A negative homogeneous azeotrope [96].

Fig. 3.4(a) is most commonly observed. It is found in systems where two components with similar boiling points are partially miscible. Examples of these systems are water + 1-butanol, methanol + cyclohexane, and water + aniline. Close to the UCST these systems adopt the form shown in Fig. 3.4(b), unless the azeotropic composition coincides with the UCST composition. Systems of the form shown in Fig. 3.4(b) occur for few systems, amongst others water + methyl-ethyl-ketone, and water + phenol. Fig. 3.4(c) is found in systems of immiscible liquids that have boiling points far from one another, for example n-pentane + nitrobenzene, propylene oxide + water, and benzene + sulphur. Fig. 3.4(d) is rare. Examples are aqueous mixtures of hydrogen bromide and hydrogen chloride [96].

The systems investigated in this project exhibit VLLE behaviour; however, only VLE measurements are conducted.

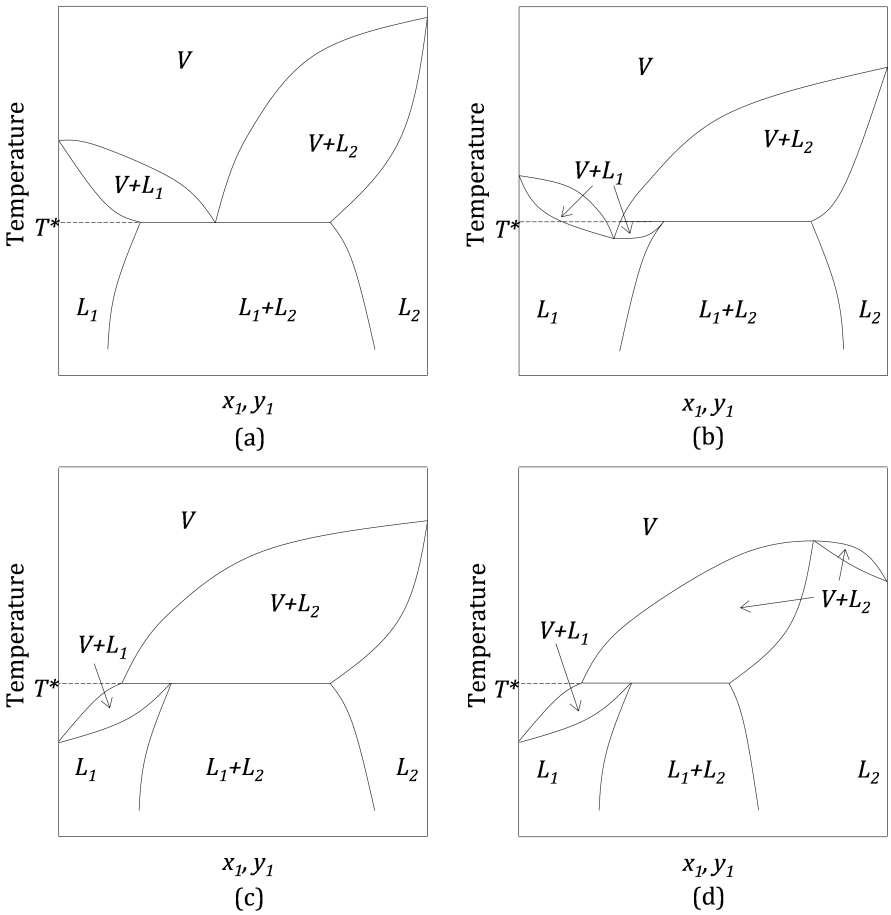

Figure 3.4: Four different types of VLLE behaviour at constant pressure [96].

3.2 Equilibrium Measurements

The various measurement techniques used to gather VLE data can be grouped into five categories. An in-depth discussion on these techniques is given in Raal and Mühlbauer [98], but are briefly described here.

Dynamic, or circulations methods

Dynamic methods typically make use of a boiling chamber, from whence the vapour phase only, or both the liquid and vapour phases move to a receiver, condenses and returns to the boiling chamber [99]. The compositions of the phases change over time until steady values are reached, after which it is assumed that equilibrium has been reached. Pressure is held constant and the equilibrium temperature recorded.

Static methods

For static methods, an equilibrium cell is charged with a liquid mixture and placed in a thermostated bath. Stirring the mixture brings about the equilibrium of the liquid and vapour phases and the system pressure is recorded [99]. Samples are withdrawn from each phase in order to determine the composition of the coexisting phases.

Dew/bubble point measurements

A mixture of known composition is introduced to a piston-cylinder setup in which the temperature is controlled and the phase transition pressure determined. This measurement technique is mainly used for high pressure VLE measurements [99].

Measurement of infinitely dilute activity coefficients

The nonidealities of a mixture is determined in the very dilute region. This is crucial for industrial purposes, since it is in the dilute region that separation becomes difficult. Infinitely dilute activity coefficients are determined by a number of techniques, amongst others inert gas stripping, ebulliometry, and gas chromatography [98]. However, this measurement technique does not provide information regarding phase equilibrium over the entire composition range.

Semimicro techniques

To conduct VLE measurements, high purity components are required. In the very dilute region, any impurity in the component of high concentration may influence the behaviour of the component present at low concentrations. Therefore, components need to be purified to high levels, and for many components this is a difficult, and/or expensive process. A semimicro technique is one where a much smaller inventory (ca. 2 mL) is used to determine the equilibrium phase behaviour of mixtures [98].

The most common measurements techniques used for low pressure VLE are the static and dynamic methods, and are conducted under isothermal and isobaric conditions respectively. The most distillation processes are conducted isobarically [3] in industry, therefore isobaric equilibrium data are of more value than their isothermal counterpart. In addition, due to the availability of a dynamic still, the measurements in this project will be conducted isobarically. The development of this method is discussed in the following sections.

3.2.1 Othmer Still

The Othmer still was one of the first dynamic VLE stills developed. A schematic representation of this still is shown in Fig. 3.5. Here the vapour phase is recirculated while the liquid phase remains in the boiling chamber. Condensed vapour is sampled from the condensate receiver, while the liquid phase is sampled from the boiling chamber.

The Othmer still's construction raises a few concerns with regards to the accuracy of its equilibrium data [98]:

- The large boiling chamber might cause vapour to condense on the chamber walls, inherently affecting the system's equilibrium. This can be overcome by placing a heating jacket around the boiling chamber. However, if the jacket becomes superheated, any liquid droplets that splash on the walls will vaporise, once again altering the equilibrium state.
- The vapour condensate receiver is too large and it is questioned whether a vapour sample taken from the sampling point is in equilibrium with the liquid in the boiling chamber.
- The contents of the boiling chamber are not stirred. It is therefore possible that temperature gradients develop and that the vapour flashes when re-entering the chamber.
- The temperature probe needs contact with both the liquid and vapour phases for an accurate temperature reading. The Othmer still measures only the vapour phase temperature.

Since the design of the Othmer still results in unreliable data, it is no longer used. It has been proposed that circulating both phases will result in a more accurate representation of equilibrium. Such a design is embodied in the form of the Gillespie still.

3.2.2 Gillespie Still

Circulation of both equilibrium phases was achieved by introducing a Cottrell tube [101] to the equipment setup and was first introduced by Lee [102]. This tube draws up a liquid containing vapour slugs from the boiling chamber. The thermometer probe is in direct contact with this fluid mixture and records the accurate equilibrium temperature. The flow of the fluid mixture through the Cottrell tube ensures sufficient time for mass transfer to occur between the respective phases such that equilibrium concentrations are achieved at the point of thermometer contact.

Gillespie [103] improved Lee's design by separating the liquid and entrained vapour phases from one another, as shown in Fig. 3.6. In this design, the boiling mixture moves through the Cottrell tube and comes into contact with the thermometer probe at the point where the two phases are separated. The liquid phase returns to the boiling chamber, while the vapour phase

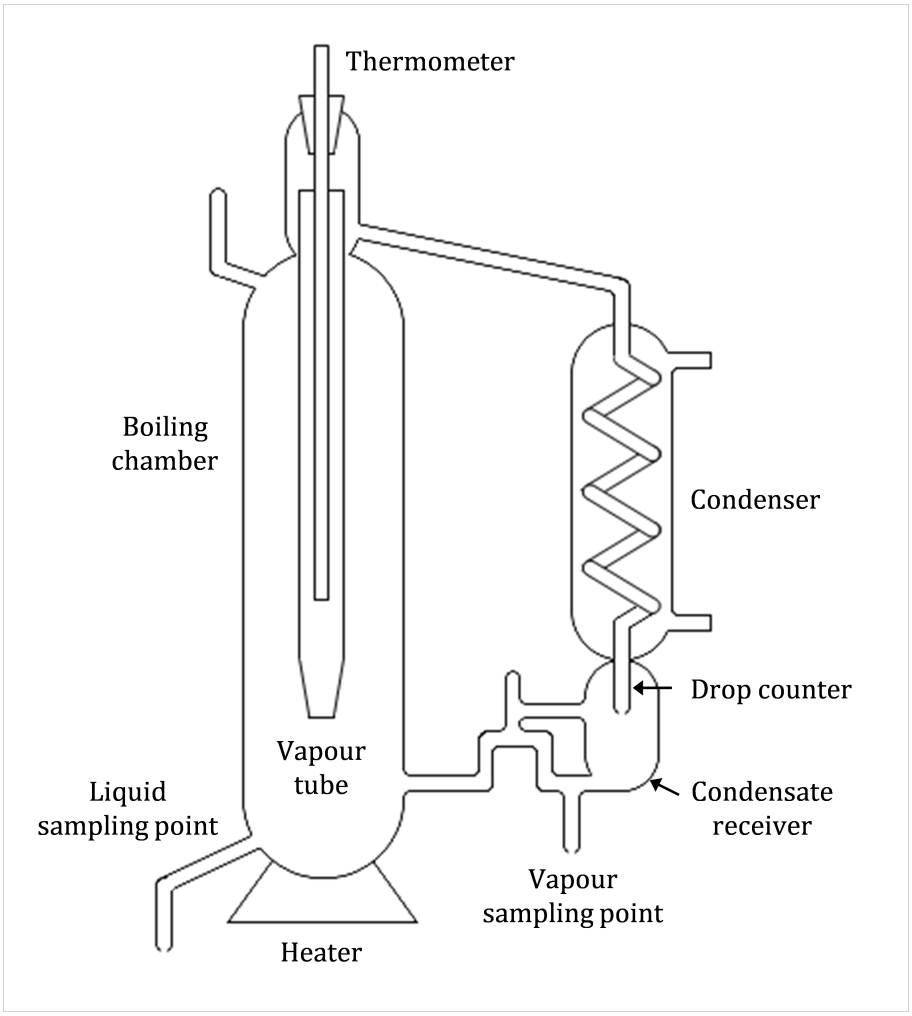

Figure 3.5: Othmer dynamic VLE still [100].

is cooled by condensers before returning to the boiling chamber. Vapour is sampled from the condensate receiver, while liquid is sampled from the boiling chamber.

The Gillespie design still had some flaws [98]:

- The liquid sample, which is drawn from the boiling chamber, is not in equilibrium with the vapour sampled from the condensate receiver.
- Partial condensation of vapour in the separation chamber must be prevented.
- The proposed sampling procedure disturbs the equilibrium attained in the still and subsequently affects equilibrium measurements.

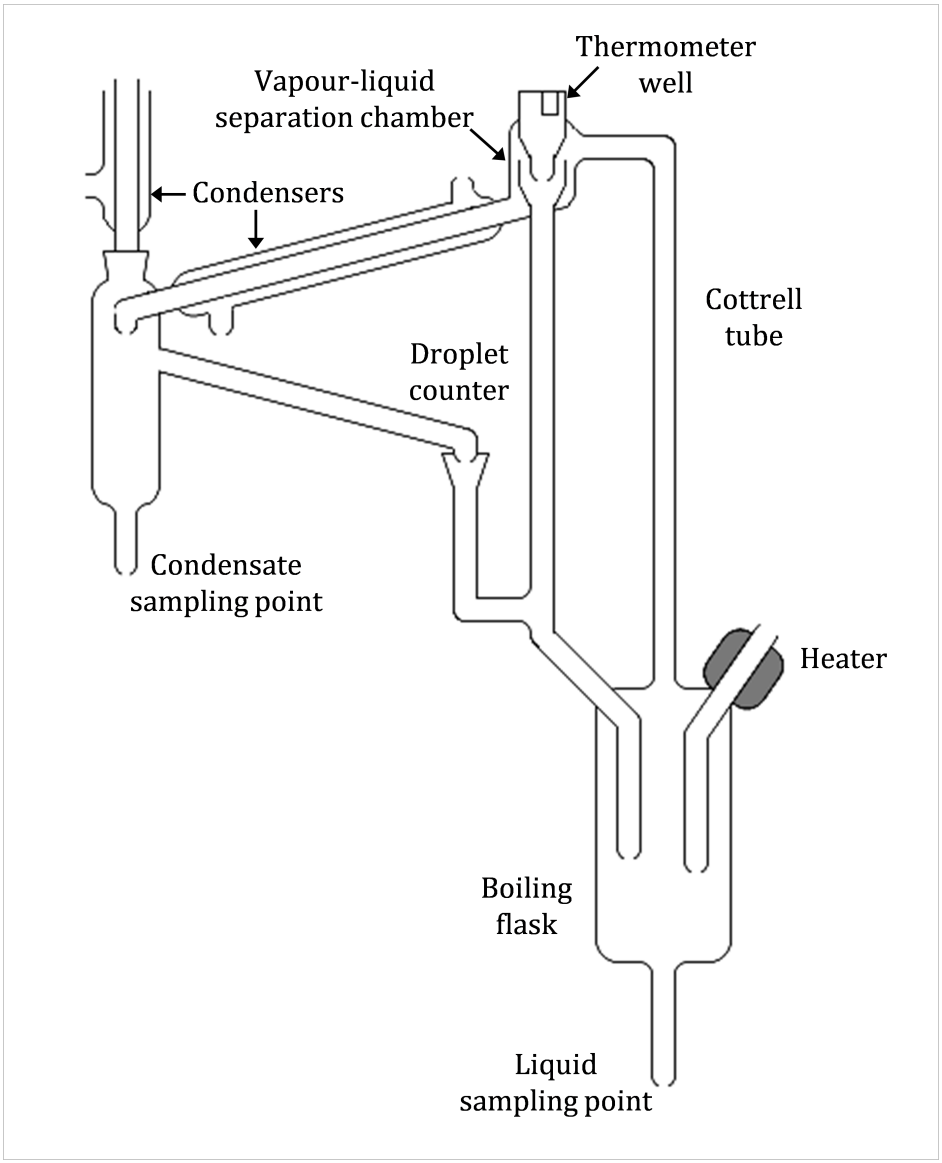

Figure 3.6: Gillespie dynamic VLE still [103].

Many authors have since improved the design of the Gillespie still to address the above-mentioned design flaws. Most notable are the following modifications: insulating still components to prevent condensation or flash heating; introduction of mechanical stirring in the boiling chamber to prevent the occurrence of temperature gradients; the addition of a liquid sampling port following the separation chamber; decreasing the size of the condensate receiver and adding an equivalent liquid receiver, thus allowing continual operation of the still while taking samples. For a more detailed description on the development of the equilibrium still, the reader is referred to the works of Raal and Mühlbauer [98] and Malanowski [104].

In this work, a modified Gillespie-type dynamic VLE still is used to conduct experimental

work. This still has been used in previous investigations [105, 106] and is shown to provide reliable phase equilibrium data.

3.3 Thermodynamic Consistency Testing

It is necessary to determine whether the experimental method used to generate phase equilibrium data delivers accurate and reliable data. Thermodynamic consistency testing validates experimental phase equilibrium data by testing whether it conforms to thermodynamic principles. The derivation of the Gibbs-Duhem equation for any extensive thermodynamic property, M, leads to a relation whereby thermodynamic consistency can be determined [3]:

$$\left(\frac{\partial M}{\partial p}\right)_{T,x} \mathrm{d}p + \left(\frac{\partial M}{\partial T}\right)_{p,x} \mathrm{d}T + \sum_i x_i \mathrm{d}\bar{M}_i = 0 \tag{3.3}$$

The Gibbs-Duhem equation shows that the partial properties of species in solution are dependent on the composition of the solution. The Gibbs-Duhem relationship provides a necessary, but not sufficient, test of data accuracy.

Applying Eq. 3.3 to the excess Gibbs energy we find:

$$\frac{V^{\mathrm{E}}}{RT}\mathrm{d}p - \frac{h^{\mathrm{E}}}{RT^2}\mathrm{d}T - \sum_i x_i \mathrm{d}\left(\ln \gamma_i\right) = 0 \tag{3.4}$$

For the case of constant temperature and pressure Eq. 3.4 reduces to:

$$\sum_i x_i \mathrm{d}\left(\ln \gamma_i\right) = 0 \tag{3.5}$$

A thermodynamic consistency test can now be derived from Eq. 3.5. There are two types of thermodynamic consistency tests: a point-to-point consistency test that evaluates the deviation of points relative to one another, such as the McDermott-Ellis test [107], and a test that aims to minimise the total deviation of all points form the Gibbs-Duhem relationship, also known as an area test. Such a test is embodied in the form of the Wisniak L/W test [108].

3.3.1 McDermott-Ellis Consistency Test

The McDermott-Ellis consistency test is obtained through integration of Eq. 3.5 by the trapezoidal rule [107]:

$$\sum_i \left(x_{ia} + x_{ib}\right)\left(\ln \gamma_{ib} - \ln \gamma_{ia}\right) = D \tag{3.6}$$

The summation is over all species at two experimental points, a and b. This test is used on a point-to-point basis, making it possible to identify an inconsistent data point by comparison to consecutive points [107].

For a thermodynamically consistent system $D = 0$. However, due to experimental error and measurement uncertainty it is expected that Eq. 3.6 will not hold exactly. Wisniak and Tamir [109] noted that the maximum allowable deviation, $D_{\max}$, should be a function of the parameter uncertainties:

$$D_{\max} = \sum_i (x_{ia} + x_{ib}) \left(\frac{1}{x_{ia}} + \frac{1}{x_{ib}} + \frac{1}{y_{ia}} + \frac{1}{y_{ib}} \right) \Delta x + 2 \sum_i |\ln \gamma_{ib} - \ln \gamma_{ia}| \Delta x + \sum_i (x_{ia} + x_{ib}) \frac{\Delta p}{p} + \sum_i (x_{ia} + x_{ib}) B_i \left(\frac{1}{|t_a + C_i|^2} + \frac{1}{|t_b + C_i|^2} \right) \Delta t \tag{3.7}$$

Data is considered to be thermodynamically consistent if $D < D_{\max}$. The Δ-terms in Eq. 3.7 are the measurement uncertainties of the respective variables, and temperature, t, is measured in degrees Celsius. B_i and C_i are the Antoine constants for component i, where the Antoine equation is defined as [109]:

$$\log(p_i^{\text{sat}}/\text{mmHg}) = A_i - \frac{B_i}{t/^{\circ}\text{C} + C_i} \tag{3.8}$$

3.3.2 Wisniak L/W Consistency Test

Wisniak developed a means by which the excess Gibbs energy (Eq. 3.9) can be determined from the mixture boiling point [108].

$$G^E = RT \sum_i x_i \ln \gamma_i \tag{3.9}$$

Wisniak made three assumptions [108]:

- All mixture nonidealities are concentrated in the liquid phase;
- The heat of vaporisation for each mixture component is constant over the temperature range of the phase envelope, and;
- Compared to the vapour molar volume, the liquid molar volume can be neglected.

Through lengthy derivation, a thermodynamic consistency test is found which can be applied to each pair of VLE points, j [108]:

$$L_j = \sum_i T_i^{\text{vap}} x_i \frac{\Delta S_i^{\text{vap}}}{\Delta S} - T = \frac{G^E}{\Delta S} - \frac{RTw}{\Delta S} = W_j \tag{3.10}$$

T_i^{vap} and ΔS_i^{vap} are the boiling point and entropy of vaporisation of species i at the system pressure, and $w = \sum_i x_i \ln(y_i/x_i)$. Integrating each side of Eq. 3.10 in terms of x_1 over the whole composition range, we find L and W:

$$L = \int_0^1 L_j \mathrm{d}x_1 = \int_0^1 W_j \mathrm{d}x_1 = W \tag{3.11}$$

For data that is thermodynamically consistent, the integrals L and W should be the same. However, due to experimental errors and the assumptions made to formulate the equation, deviation from this constraint will arise. Wisniak defined a deviation parameter (Eq. 3.12) and proposed that $D < 5$ for thermodynamically consistent data.

$$D = 100 \times \frac{|L - W|}{L + W} \tag{3.12}$$

The Wisniak L/W consistency test acts as both an area test as well as an alternative point-to-point test. Calculation of the deviation, D, incorporates the area test since evaluation of data over the whole composition range is required for its calculation. The point-to-point test is manifested in Eq. 3.11 which has to be satisfied at every experimental point, j. The Wisniak L/W test indicates if data are inconsistent, but since it is not derived directly from the Gibbs-Duhem relation it should be supplemented with another test, such as the McDermott-Ellis consistency test.

3.4 Existing Binary Water + Alkanol VLE data

From the literature it is clear that extensive research and subsequent measurements have been conducted for binary aqueous mixtures of methanol [110–114], ethanol [110, 111, 115–117], 1-propanol [116, 118–120], and 2-propanol [113, 114, 116, 121], to mention but a few. Binary systems containing the butanol isomers (1-butanol, 2-butanol, 2-methyl-1-propanol, 2-methyl-2-propanol) have also been studied extensively, both the VLE and LLE. However, the amount of available data drop off rapidly as the chain length of the alkanol increases.

The VLE data available for linear C_4- and C_5-linear alkanols in literature are summarised in Table 3.1.

3.5 Experimental Rationale

In this investigation, binary water + primary and secondary alkanol mixtures will be studied systematically to (1) observe the effect that a shifting functional group has on mixture phase behaviour, and (2) to identify any trends between mixtures containing alkanols with varying carbon chain length. It was decided to only consider primary and secondary linear alkanols to single out only the effect of a shifting hydroxyl group.

Four sets of experimental data will be generated:

- water + 1-butanol: This mixture serves as a reference by which verification of the experimental equipment and procedure will be conducted. The data available in literature are in good agreement (Fig. 3.7).

Table 3.1: Available vapour-liquid equilibrium data for (water + X) systems.

X	T/K	p/MPa	Reference
1-butanol	298.15		Butler, et al., 1933 [122]
	298.15 - 363.15		Pierotti, et al., 1959 [123]
	383.15		Kharin, et al., 1969 [124]
	333.15		Schreiber, et al., 1971 [125]
	308.15		Lyzlova, et al., 1979 [126]
	323.00		Fischer and Gmehling, 1994 [127]
	283.20 - 298.20		Freitag, et al., 2015 [128]
		0.1013	Stockhardt and Hull, 1931 [129]
		0.1013	Bushmakin, et al., 1936 [130]
		0.1013	Smith and Bonner, 1949 [131]
		0.1013	Boublík, 1960 [132]
		0.1013	Ellis and Garbett, 1960 [133]
		0.1013	Orr and Coates, 1960 [134]
		0.1013 - 0.4920	Hessel and Geiseler, 1965 [135]
		0.1010	Raju, et al., 1965 [136]
		0.1013	Kato, et al., 1970 [137]
		0.1013	Zong, et al., 1983 [138]
		0.1013	Ochi and Kojima, 1987 [139]
		0.1250 - 3.8210	Shakhverdiev, et al., 1994 [140]
		0.1013	Iwakabe and Kosuge, 2001 [141]
		0.1013	Gu, et al., 2002 [142]
		0.1013	Lladosa, et al., 2008 [143]
2-butanol	333.15 - 353.15		Altsybeeva, et al., 1964 [144]
	298.14		Otsuki, et al., 1973 [145]
	298.15		Gaube, et al., 1987 [146]
	323.00		Fischer and Gmehling, 1994 [127]
	318.19 - 353.45		Escobedo-Alvarado and Sandler, 1999 [147]
		0.1013	Boeke and Hanewald, 1942 [148]
		0.1013	Yamamoto and Maruyama, 1959 [149]
		0.0267 - 0.1013	Altsybeeva, et al., 1965 [144]
		0.1013	Iwakabe and Kosuge, 2001 [141]
1-pentanol		0.1013	Jasper, et al., 1944 [150]
		0.1013	Beregovykh, et al., 1971 [151]
		0.1013	Cho, et al., 1984 [152]
2-pentanol	343.15 - 363.15		Zou and Prausnitz, 1987 [153]

- water + 1-pentanol: To the author's knowledge there are only three sets of data for this system in literature, as shown in Table 3.1. The agreement between these sets is not good (Fig. 3.8), therefore it was decided to generate an additional data set for this system.

- water + 2-pentanol: To the author's knowledge, there is only one set of isothermal data for this system in literature. For comparison to the other mixtures that were measured isobarically, an isobaric data set needs to be generated.

- water + 3-pentanol: To the author's knowledge, no VLE data for this system is available in literature, therefore data needs to be generated.

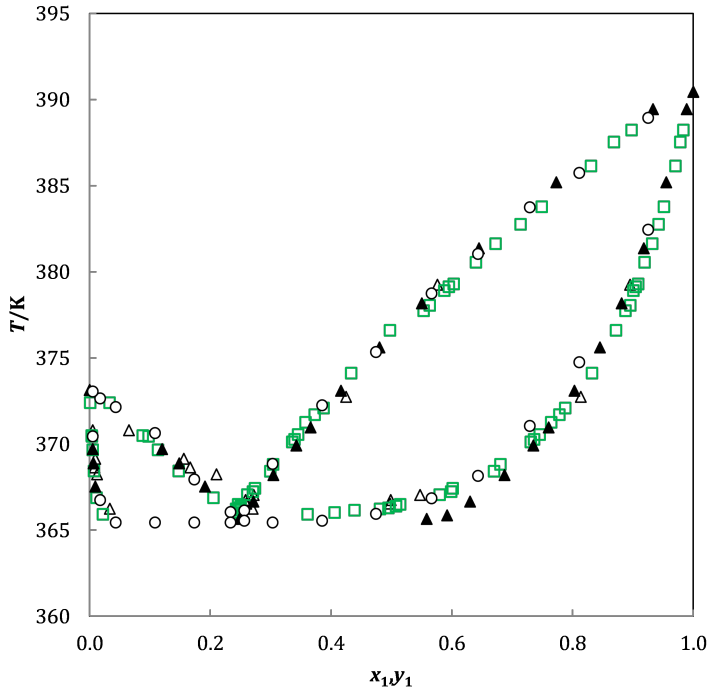

Figure 3.7: Literature data for 1-butanol (1) + water (2) (△ Gu, et al. [142]; □ Iwakabe and Kosuge [141]; ○ Kato, et al. [137] ; ▲ Lladosa, et al. [143]).

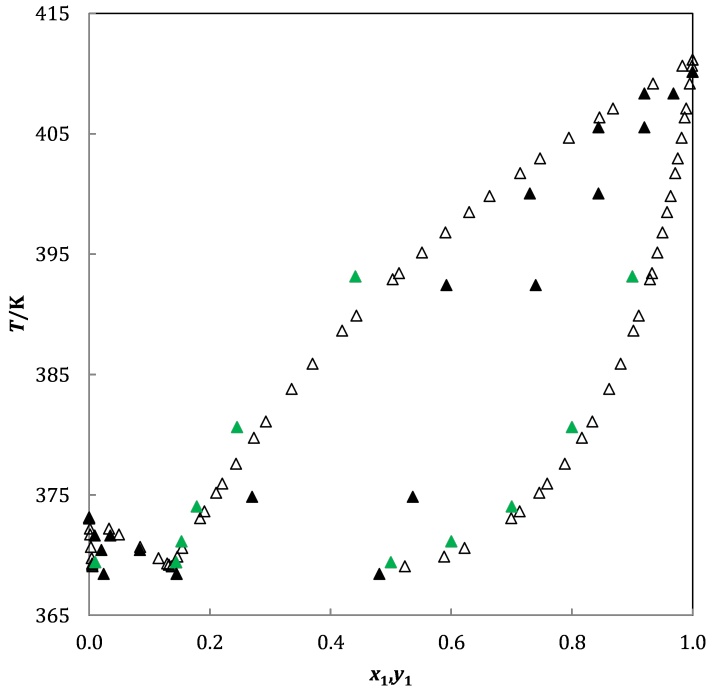

Figure 3.8: Literature data for 1-pentanol (1) + water (2) (▲ Beregovykh, et al. [151]; △ Cho, et al. [152]; ▲ Jasper, et al. [150]).

Chapter 4

Experimental Method

The materials and method used in the experimental work are presented in this chapter.

4.1 Materials

Details regarding the chemicals used in this work are shown in Table 4.1. The purities indicated in Table 4.1 are those indicated by the supplier. Analysis by gas chromatography showed no significant impurities in any of the chemicals. Karl-Fischer titrations were also conducted and showed that the chemicals contained negligible amounts of water. Hence, the chemicals were used as purchased without further purification.

Table 4.1: Information pertaining to the chemicals used in this work.

Component	Supplier	CAS Number	Purity (wt%)
1-butanol	Sigma-Aldrich	71-36-3	99.9
2-butanol	Sigma-Aldrich	78-92-2	99.5
1-pentanol	Sigma-Aldrich	71-41-0	99.0
2-pentanol	Sigma-Aldrich	6032-29-7	98.0
3-pentanol	Merck	584-02-1	98.0
2-ethyl-1-hexanol	Aldrich	104-76-7	99.6
methanol	Sigma-Aldrich	67-56-1	99.9

Millipore water with a resistivity of 18 megohm was used. Technical grade nitrogen, supplied by Afrox, was used for overpressure control in the still. Technical grade air and ultra high purity helium, both supplied by Afrox, were used to operate the gas chromatograph.

4.2 Experimental Setup and Equipment

Reference is made to the schematic representation of the experimental setup in Fig. 4.1.

The liquid mixture present in the flow heater (1.4) is partially evaporated by heat supplied by the immersion heater rod (9). The heated mixture passes through a spiral Cottrell tube (1.3), allowing concentrated phase change to occur. From here the mixture enters a separation chamber, specifically designed to prevent liquid drops from entraining in the vapour phase, and the vapour phase from condensing. The thermometer (7a) is in contact with the two-phase mixture, ensuring that the equilibrium temperature is measured. The liquid and vapour phases separate, condense, and return to the mixing chamber (1.2). The mixture is continuously stirred with a stirring magnet (4), controlled by a magnetic stirrer (3). From the mixing chamber the mixture returns to the immersion heater, completing the circulation loop.

In a previous study [154], the still was modified by addition of a Sartorius Labsonic® P ultrasonic homogeniser (14) with the purpose of aiding ternary VLLE-experiments. Ultrasound emulsifies the two equilibrium liquid phases, which improves mixing in the boiling flask and ensures adequate recirculation of these phases [155]. The mixtures investigated in this study exhibit VLLE behaviour, therefore ultrasound was used at all times to ensure that adequate mixing occurs in the mixing chamber.

The still is housed in an extraction cabinet to ensure that hazardous vapours are extracted. The still can be operated at pressures ranging from 2.5×10^{-4} to 0.3 MPa, and to a maximum temperature of 523 K. Temperature is measured by a Pt-100 probe which is connected to a digital Hart Scientific thermometer. The probe was calibrated by a SANAS (South African National Accreditation System) approved laboratory. The probe exhibited a maximum deviation of 0.10 K at temperatures between 303 K and 413 K. Pressure is measured by a Wika UT-10 unit which has a maximum operating pressure of 0.16 MPa absolute. The pressure transmitter has an uncertainty of 1.6×10^{-4} MPa.

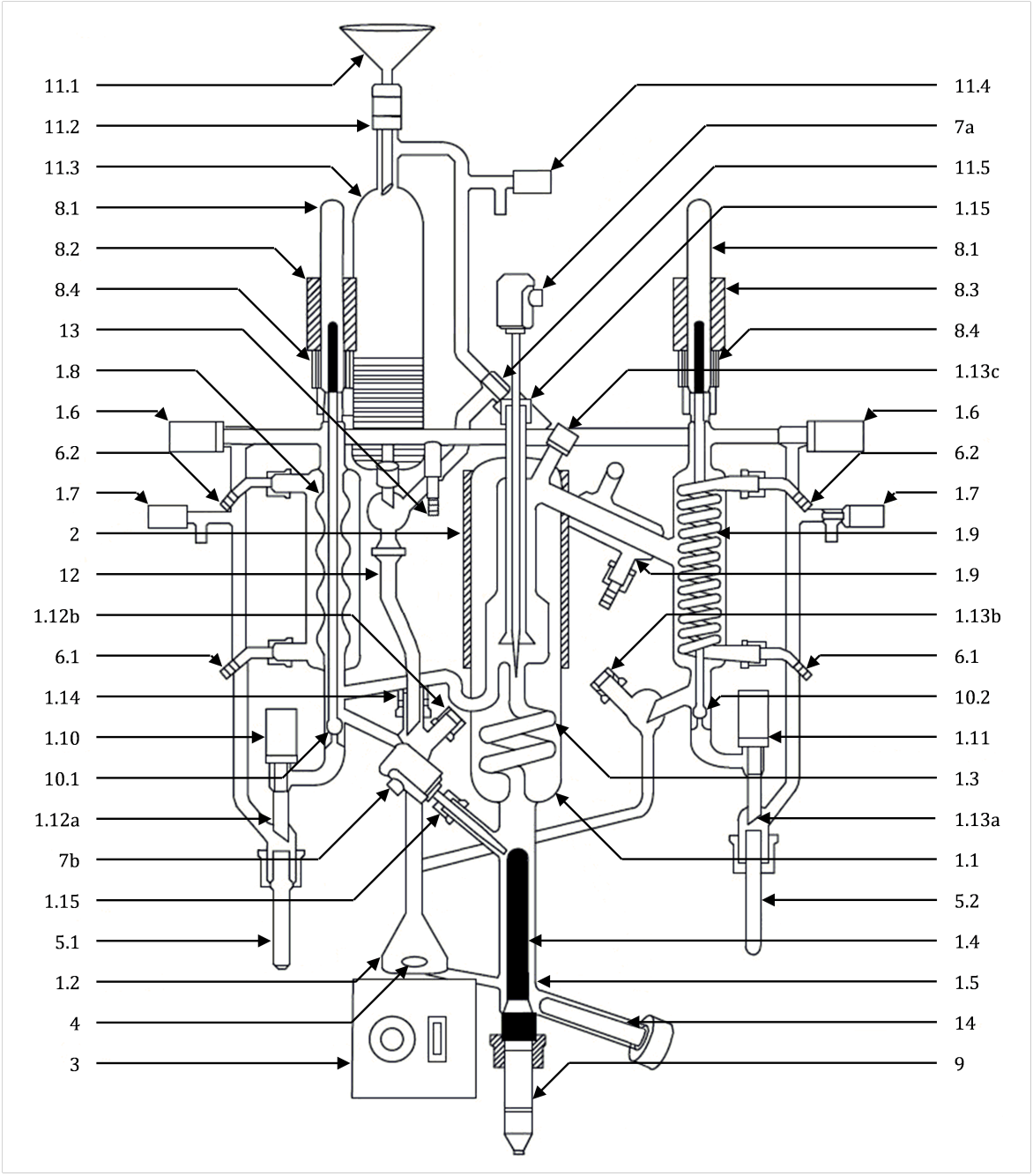

Figure 4.1: Schematic representation of the dynamic still. Figure reprinted with permission [154].

4.3 Experimental Procedure

For a more detailed procedure the reader is referred to Appendix A.

4.3.1 Still Preparation

Before operation starts, the operator must ensure that the still is dry to prevent contamination from previous experimental runs. Compressed air can be passed through the still to ensure that it is completely dried. For overpressure operation the nitrogen feed is opened. Water is fed to the cooling coils and the condensers (1.9) by a small pump housed in a water bath. The still can now be switched on, and the software opened.

The mode of operation (vacuum or overpressure) is selected on the hydraulic box and within the software. The homogeniser (14) is placed into its position and secured. The discharge valve (1.5) is closed before the mixture is fed to the mixing chamber (1.2). Approximately 100 mL of the first component is fed to the mixing chamber (1.2) via the feed burette (11.1). This amount is variable, based on the mixture volatility and the operating pressure; however, the mixture must completely submerge the immersion heater (9). The magnetic stirrer is switched on. This ensures that the mixture is thoroughly mixed and that no temperature and composition gradients occur.

Within the software, the operating pressure, mantle temperature, vapour return line temperature, and heater power need to be specified. These variables are dependent on the intended operating conditions, as well as the composition and volatility of the mixture. The heater setting is of importance: if it is too low, no vaporisation will occur, and if it is too high, there will be no liquid return. For the systems investigated in this study, the heating jacket (2) is set at a temperature approximately 10 K higher than the equilibrium temperature to ensure that no vapour condenses before reaching the sampling needle.

The measurement and control of the system pressure is conducted independently of the computer software. For overpressure conditions the system pressure is maintained by balancing the amount of nitrogen that enters the system with the nitrogen that leaves the system through the aeration valves (1.7). The manual nature of pressure control resulted in pressure fluctuations not larger than 2×10^{-4} MPa. The effect of pressure fluctuations on the experimental results is discussed in Section 4.4.1.

4.3.2 Obtaining Measurements

Once the still is prepared for operation, the apparatus is switched on through the software. If the power setting is appropriate, liquid return should appear within 5 minutes of operation.

Depending on the feed temperature and the mixture boiling temperature one can expect vapour return to appear after ca. 20 minutes of operation.

A constant vapour temperature reading indicates equilibrium and is reached approximately within an hour of starting operation. In addition to this, both the liquid and vapour returns should be steady to ensure accurate sampling.

As the vapour and liquid phases return to the mixing chamber, they are cooled down. The composition of these phases can fall within the LLE composition range, causing each returning stream to split into two, immiscible phases. Either one of these phases preferentially adheres to the walls of the return lines and lie within the sampling well. If sampling is conducted through the solenoid valves, this residue inherently contaminates the sample. Therefore, samples were not withdrawn through the solenoid valves (10.1 and 10.2), but rather extracted by means of syringes through the sampling ports 1.13c (vapour) and 1.12b (liquid). Hamilton 5 mL gas tight syringes were used for this purpose, each fitted with a SGE gas and liquid tight push-button syringe valve. Two syringes, one for vapour and one for liquid, were preloaded with approximately 100 μL and 400 μL respectively of methanol, which was used as solvent during analysis (see Section 4.3.4). The sampling needle was placed in the sampling port and the sample was extracted. Upon entering the syringe, the sample dissolved into the methanol to form a homogeneous sample. While sampling, the equilibrium temperature was recorded. The largest fluctuation in temperature measurement was 0.05 K.

After taking the respective samples, the experimental run is concluded. The operation of the still is stopped through the software. Between experimental runs the still is brought back to atmospheric pressure by slowly closing the overpressure throttling valve. Additional feed, approximately 5 mL of the second component, is added to the still via the feed burette (11.3) to resubmerge the immersion heater (9), as well as to shift the overall mixture composition along the composition spectrum. Once the additional feed is added to the system the next experimental run can commence.

4.3.3 Draining and Cleaning

The still contents may be left in the still overnight if experiments on the same feed composition is continued the next day. However, if a new feed composition is required, the still is drained and cleaned in order to ensure that no contamination occurs.

The mixture, the heating jacket, and the immersion heater must return to ambient temperature before the still contents are drained through the discharge valve (1.5). Approximately 110 mL acetone is fed to the still. The still is run for half an hour at atmospheric pressure. The solenoid valves are flushed a few times to ensure that the sampling wells are cleaned. After the

cleaning procedure, the still and its contents must cool down before draining the acetone from the still. The still is left overnight to dry. If necessary, pressurised air can be passed through the still to evaporate any residual acetone.

4.3.4 Analysis

Experimental samples were analysed through gas chromatography, using a Varian CP-3380 GC with a flame ionisation detector, connected to a desktop computer using DELTA 5.0 software. A ZB Wax capillary column with dimensions 30 m x 0.32 mm x 1 μm was operated at 523 K to quantify the amount of alkanol in each sample. For all systems 2-ethyl-1-hexanol was used as internal standard. Analysis samples were prepared as follows, by weighing each of the following additions:

- 10 μL of internal standard was added to each vial.
- Between 20 μL and 40 μL of experimental sample was added to the vial (mass A).
- The vial was filled with approximately 1.2 mL of solvent, i.e. methanol.

For each experimental run, a sample is withdrawn from the liquid and the vapour phases. Two analysis samples were prepared for each phase and the average of the two results were reported as the equilibrium value.

Calibration curves were used to quantify the amount of alkanol in each analytical sample. Given that each component produces a unique peak area on a chromatogram, and that the ratio of peak areas corresponds to the ratio of the respective component masses, a calibration curve can be set up using the following equation:

$$\frac{Area_{std}}{Area_{alk}} = R_f \frac{mass_{std}}{mass_{alk}} \tag{4.1}$$

Five samples of known mass, containing alkanol (1-butanol, 1-pentanol, 2-pentanol, or 3-pentanol) and internal standard, and varying the ratio between alkanol and internal standard, were prepared. Each sample was analysed by GC five times, and the average of analyses were used to determine the response factor, R_f, for each system. The response factor, and known mass of internal standard added to each analysis sample, is used to determine the mass of alkanol in each experimental sample (mass B). The mass of water in each sample is merely the difference between mass A and mass B.

An analysis of the compositional error is discussed in the following section.

4.4 Accuracy of Measurements

The accuracy of the results is due to experimental conditions and the analysis method, as explained in the sections below.

4.4.1 Experimental Effects

System inputs invariably have an effect on system outputs. In the case of this experimental procedure, the operation of the still and subsequent analyses are inputs to the mixture system, while the composition of the coexisting phases are the outputs. The operation of the still depends on two inputs, namely the pressure regulation and heater setting. Pressure needs to be regulated throughout experimentation, therefore its contribution to compositional error is not negligible. The heater setting is not changed during operation, therefore its effect on compositional error can be disregarded.

As stated in Section 4.3.1, the maximum deviations in pressure were 2×10^{-4} MPa. It will be shown in Chapter 6 that the sPC-SAFT-GV-2C model accurately predicts the VLE of water + 1-butanol. Therefore we can use this model to predict the phase behaviour at pressures $2{\times}10^{-4}$ MPa lower and higher than 0.1013 MPa, as shown in Fig. 4.2. At a specific temperature the deviation in the "true" equilibrium composition due to pressure fluctuations can then be determined. The worst deviation observed in Fig. 4.2 is 0.0029 mole fraction.

Temperature fluctuations of $\pm$0.05 K were apparent prior to sampling. Phase envelopes that pass through the same sample composition at temperatures 0.05 K higher and lower than the original sample temperature are plotted. These phase envelopes each correspond to a system pressure which gives an idea of the true fluctuations in pressure during sampling. As is apparent in Fig. 4.3, the temperature fluctuations are accompanied by pressure fluctuations of ca. 7×10^{-4} MPa, which are larger than the pressure fluctuations observed experimentally. However, the error in composition is also 0.0029 mole fraction.

The analysis presented here is for the liquid phase on the alkanol-rich side of the azeotrope. At this point the gradient of the T-xy diagram is not that steep, indicating that a small deviation in temperature has a more significant effect on the composition that in other regions of the phase diagram. Similar results are obtained in the vapour phase and at other compositions.

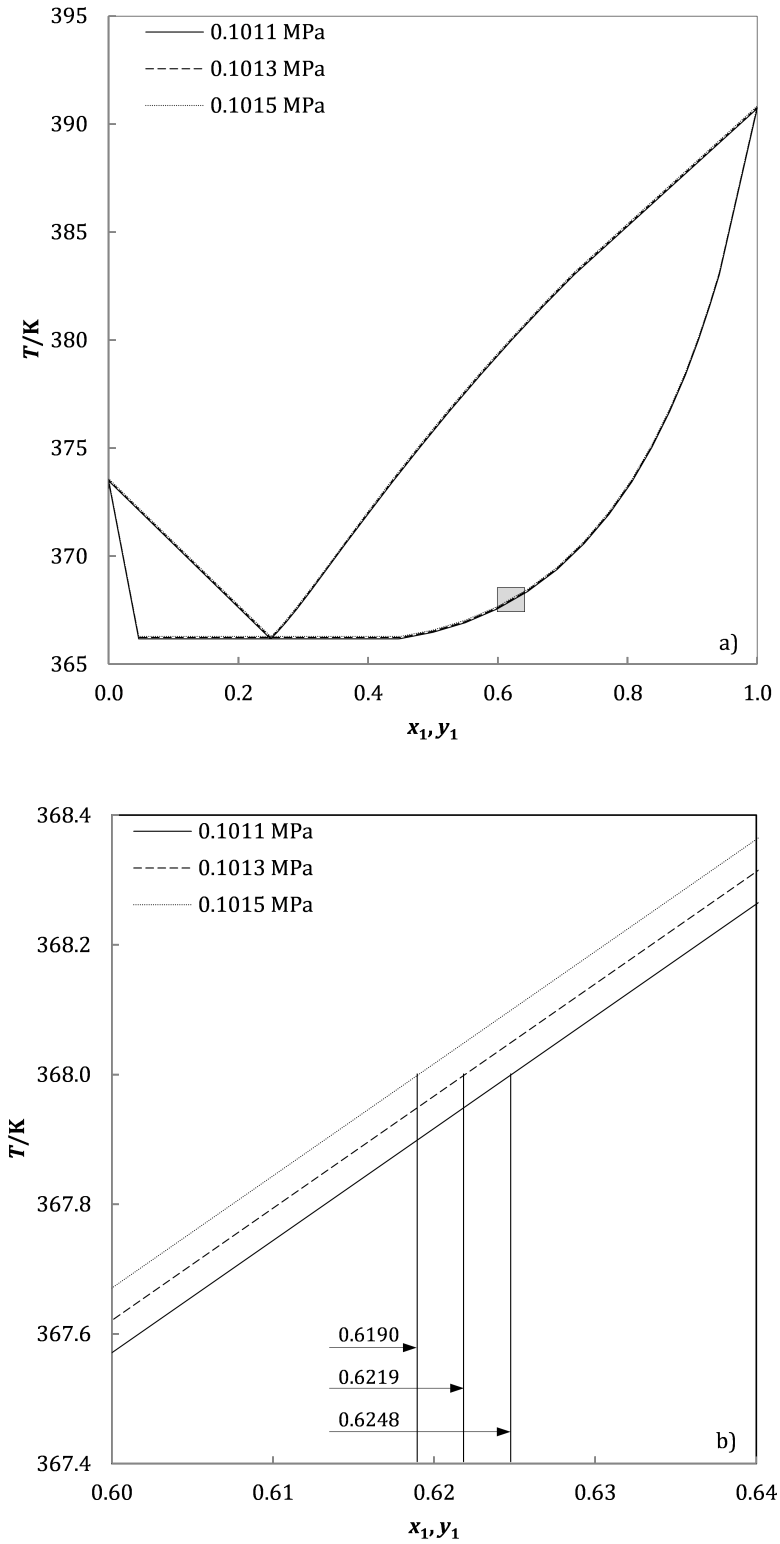

Figure 4.2: sPC-SAFT-GV-2C predictions for maximum pressure deviations for 1-butanol (1) + water (2) for (a) the whole composition range; (b) magnifying the greyed area in (a).

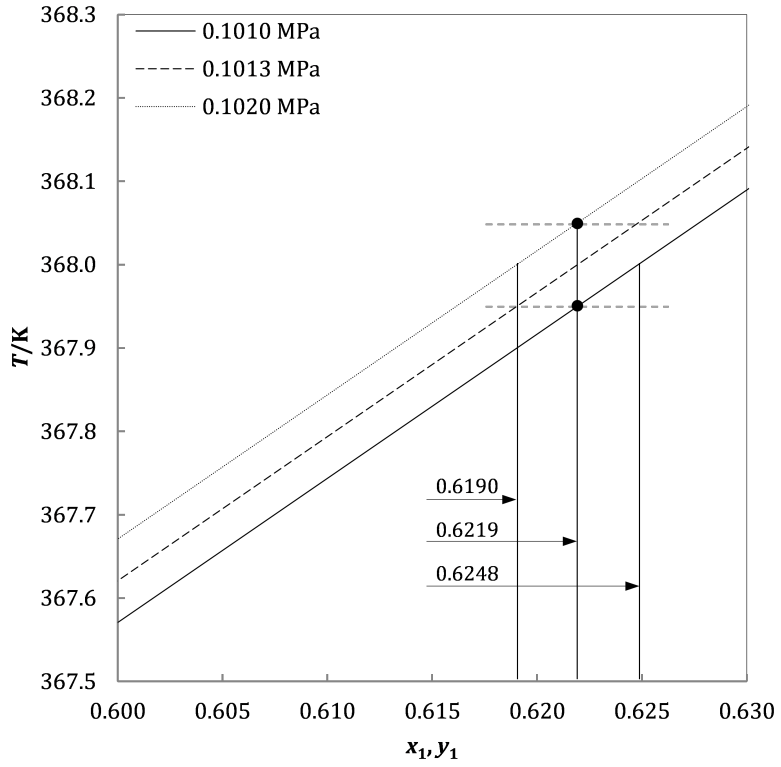

Figure 4.3: sPC-SAFT-GV-2C predictions for maximum temperature deviations for 1-butanol (1) + water (2).

4.4.2 Analysis Effects

The preparation and analysis of experimental samples also contribute to compositional error. Calibration curves are used to determine the alkanol content in an experimental sample. However, due to general wear and tear of the GC, and the fact that water is introduced to the column, which is undesirable, these curves drift over time, therefore it is important to determine the reproducibility and reliability of the GC results.

To do this, samples, of which the composition is known, were prepared after the analysis of a specific binary system was completed and analysed by GC, using the same calibration curves used to analyse the whole system. By doing this, the difference in predicted composition from the known composition could be determined, which gives an indication of the drift in the GC's operation. This was done for each binary system. The maximum analytical error was 0.02 mole fraction.

4.4.3 Total Accuracy

Taking into account both the experimental and the analytical error, since the latter is dependent on the former, and assuming that the respective errors are additive, the total compositional error reported for this work is 0.023 mole fraction. This error is approximately an order of magnitude larger than those reported in literature; however, it is believed that the error reported here includes the errors introduced by both the experimental and analytical effects, presenting a true reflection of the total uncertainty of the analysis.

Chapter 5

Experimental Results

The materials and methods presented in Chapter 4 were used to generate experimental data. Verification of the experimental method was conducted before new data was generated in order to provide confidence in the experimental data. The thermodynamic consistency of the generated data was tested, using the methods described in Chapter 3. The phase behaviour observed in binary aqueous mixtures of (C_2 - C_5) alkanols is discussed, with specific attention given to structural isomerism. This chapter therefore addresses **Objective 1** of this investigation. Methanol is left out of this discussion, since it does not exhibit azeotropic behaviour in water.

5.1 Verification

A reference system, water + 1-butanol at p = 0.1013 MPa, was reproduced in order to verify that the experimental equipment, and especially the sampling method used in this study, delivered reliable equilibrium results. For the reference system, there are a number of VLE data sets available in literature (see Table 3.1). The data measured in this work are plotted against two literature data sets in Fig. 5.1. Generally the difference between the literature data and that measured in this work is below the composition uncertainty of 0.023 mole fraction. The largest difference (0.04 mole fraction) is observed in the 1-butanol-rich liquid phase.

The data sets plotted in Fig. 5.1 were all found to be thermodynamically consistent, passing both the McDermott-Ellis and Wisniak L/W (D = 2.247, this work; D = 0.984 [141]; D = 0.982 [156]) tests. Given the good comparison of the measured data to literature data and the thermodynamic consistency of the measured data, the equipment and sampling method were deemed acceptable for further experimental work.

As an additional verification, the saturated vapour pressure of each component was measured over a range of temperatures to test the accuracy of temperature measurements. The saturated

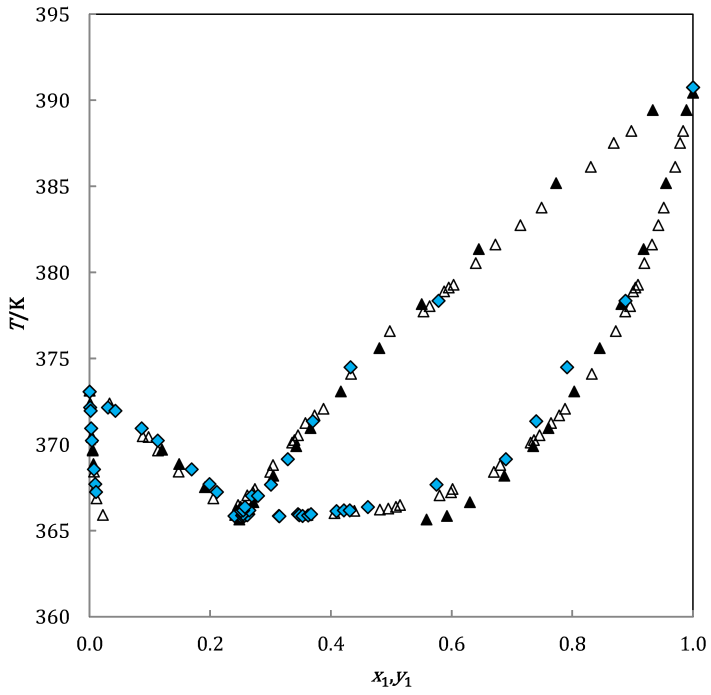

Figure 5.1: Binary *T-xy* diagram for the verification system, 1-butanol (1) + water (2) at p = 0.1013 MPa (◆ experimental data; △ Iwakabe and Kosuge [141]; ▲ Lladosa, et al. [156]).

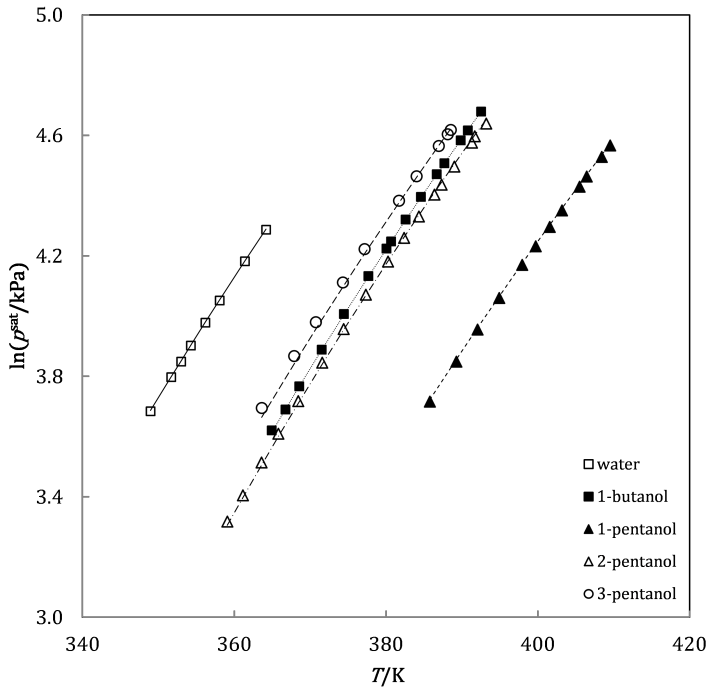

Figure 5.2: Saturated vapour pressures. DIPPR [157] correlations indicated by lines; experimental data indicated by markers.

vapour pressures measured in this investigation are plotted against DIPPR[†] [157] correlations in Fig. 5.2. This procedure also reinforces confidence in the purity of the chemicals as determined through GC analysis and Karl-Fischer titrations.

5.2 Results

The experimental data and thermodynamic consistency results are presented in Appendix B.

The VLE data for the system water + 1-pentanol are presented in Fig. 5.3 alongside three literature data sets. The data from this work compare well to that of Beregovykh, et al. [151] and Cho, et al. [152]. Jasper, et al. [150] conducted experiments in a single stage batch distillation apparatus and drew liquid samples directly from the boiling chamber. It is questionable whether these samples constitute "equilibrium samples" and can possibly explain the discrepancy between their data and those measured in this study, the data of Beregovykh, et al. [151], and Cho, et al. [152].

The VLE data for the systems water + 2-pentanol and water + 3-pentanol are shown in Figs. 5.4 and 5.5, respectively. At the experimental conditions (p = 0.1013 MPa) all four mixtures (water + 1-butanol, + 1-pentanol, + 2-pentanol, + 3-pentanol) have a positive, heterogeneous azeotrope. The discrepancy and scatter observed in the alkanol-rich composition range in both the 2-pentanol and 3-pentanol systems are discussed in Section 5.4.

[†] *Design Institute for Physical Properties*

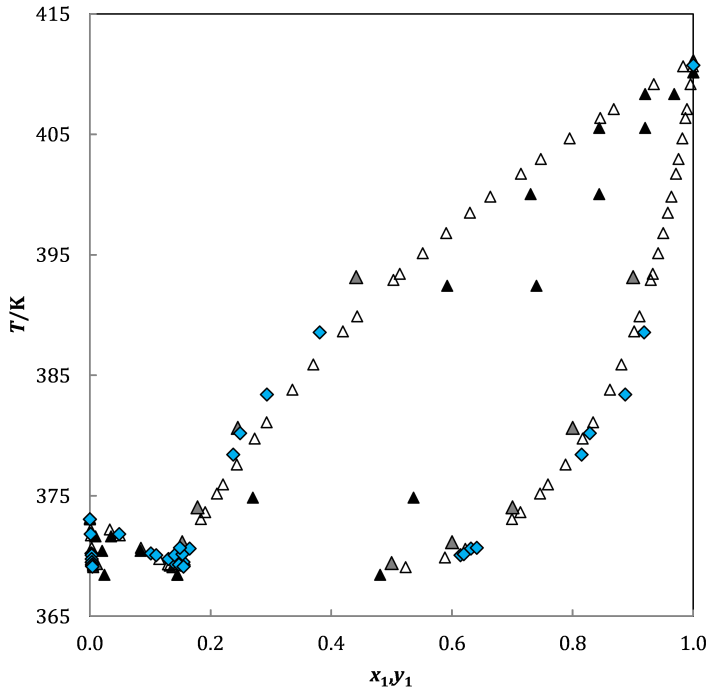

Figure 5.3: Binary T-xy diagram for 1-pentanol (1) + water (2) at p = 0.1013 MPa (◆ experimental data; ▲ Beregovykh, et al. [151]; △ Cho, et al. [152]; ▲ Jasper, et al. [150]).

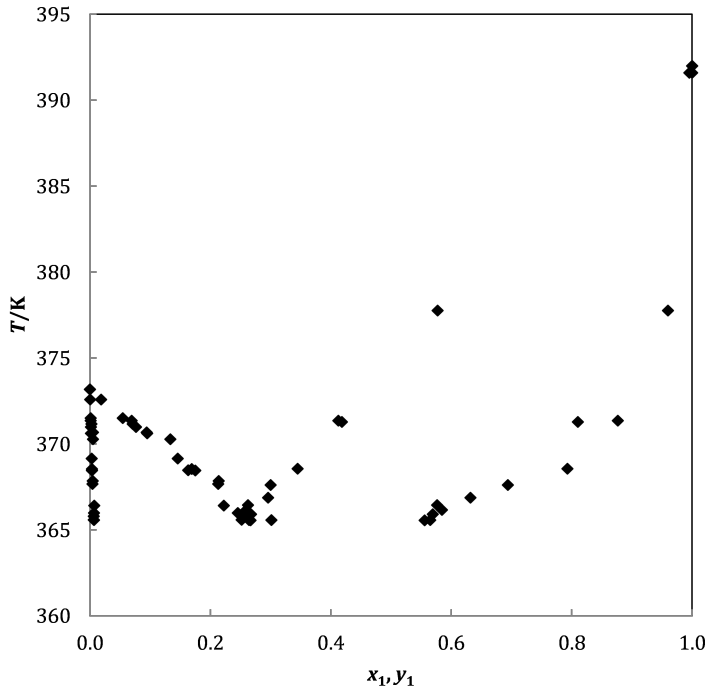

Figure 5.4: Binary T-xy diagram for 2-pentanol (1) + water (2) at p = 0.1013 MPa.

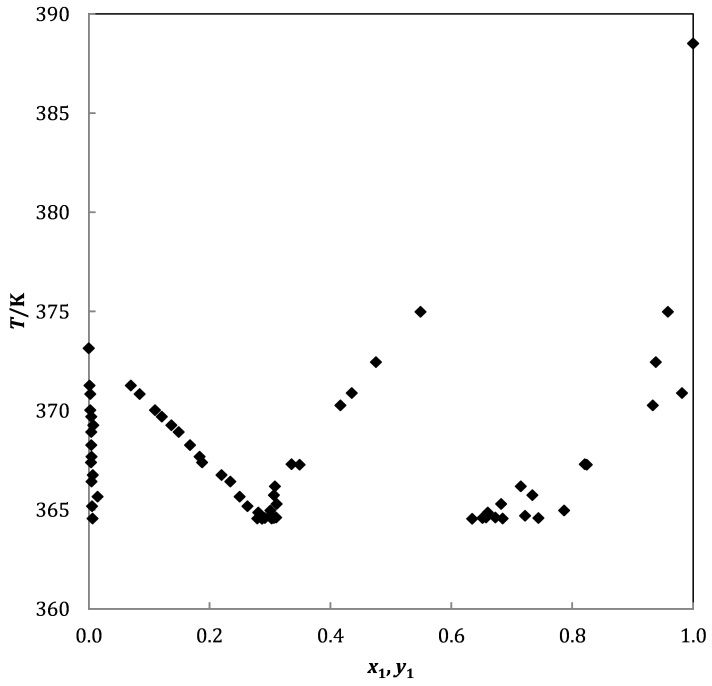

Figure 5.5: Binary T-xy diagram for 3-pentanol (1) + water (2) at p = 0.1013 MPa.

5.3 Discussion

The water + (C_2–C_5) linear alkanol mixtures form part of a homologous azeotropic series [158], with water being the azeotropic agent.

To interpret the phase envelopes for each of these binary systems, the pure component saturated vapour pressure, p^{sat}, for the primary and secondary (C_2–C_5) alkanols, including 2-hexanol, were compared in Fig. 5.6. p^{sat} increases as the length of the carbon chain decreases (e.g. from 1-propanol to ethanol), which is the expected behaviour. Comparison of structural isomers indicates that the position of the functional group influences p^{sat}. Steric hindrance effects brought about by shifting the hydroxyl group toward the centre of the carbon backbone (e.g. from 1-butanol to 2-butanol) dampens polar and associating behaviour. This molecular phenomenon is manifested in the macroscopic behaviour, resulting in higher vapour pressures.

The p^{sat} curves for the following alkanol pairs are quantitatively similar: ethanol and 2-propanol, 1-propanol and 2-butanol, 1-butanol and 2-pentanol, and 1-pentanol and 2-hexanol. These pairs are comprised of a primary C_x-alkanol and a secondary $C_{(x+1)}$-alkanol; in other words, a secondary alkanol "formed" by addition of a methyl group to the 1-carbon of a primary alkanol (Fig. 5.7).

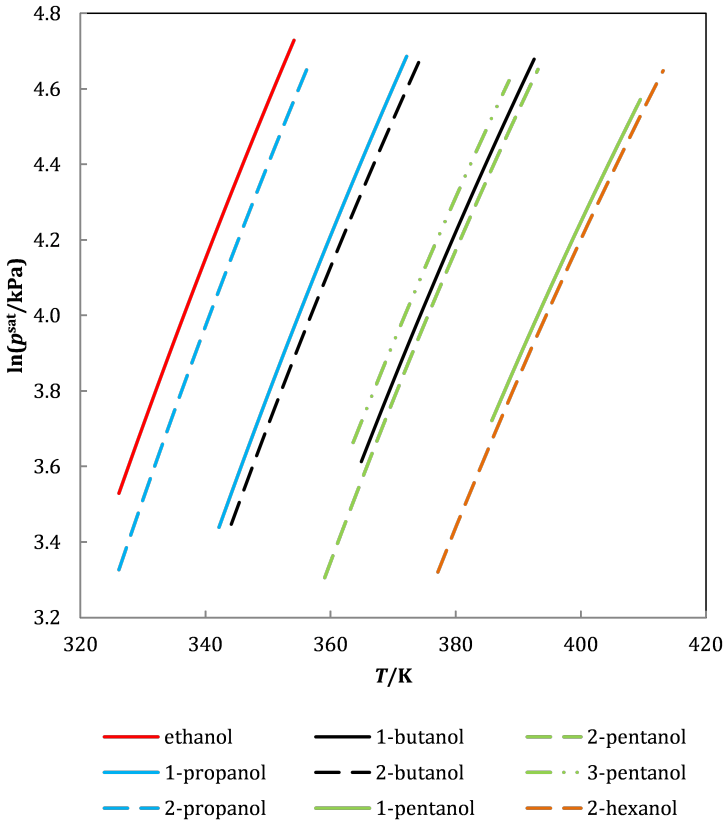

Figure 5.6: Vapour pressure curves for nine primary and secondary (C_2–C_6) alkanols (DIPPR [157] correlations).

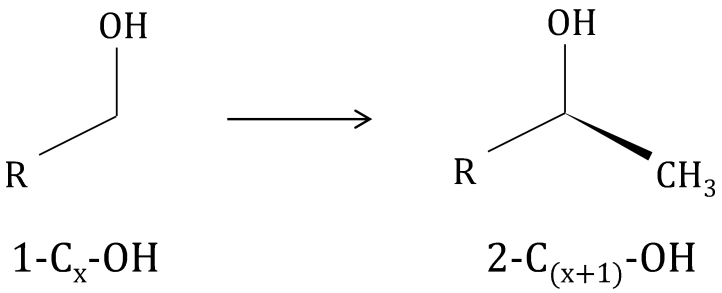

Figure 5.7: Addition of a methyl group to a primary alkanol (1-C_x-OH) to form a secondary alkanol (2-$C_{(x+1)}$-OH).

It is expected that the heavier molecule, i.e. the secondary alkanol, would have a higher vapour pressure than the primary alkanol. However, it would seem that, relative to association effects, the additional methyl group does not have a large energy contribution in the formation described here, resulting in similar vapour pressure behaviour between the pairs of alkanols.

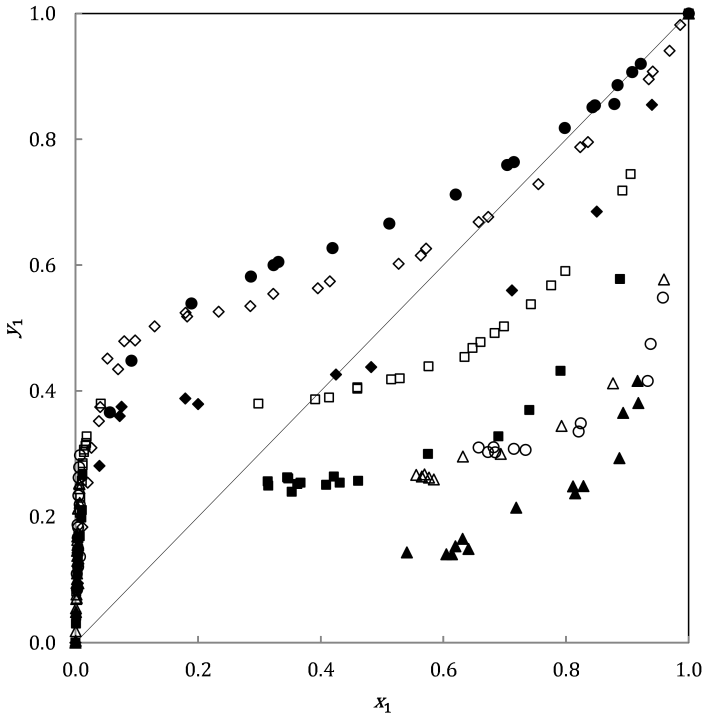

Figure 5.8: x-y plot of binary water (2) + alkanol (1) mixtures at p = 0.1013 MPa (● ethanol [110]; ◆ 1-propanol [120]; ◇ 2-propanol [159]; ■ 1-butanol; □ 2-butanol [141]; ▲ 1-pentanol, △ 2-pentanol, ○ 3-pentanol).

x-y data for the homologous azeotropic series are plotted in Fig. 5.8. The similarity in vapour pressure observed between the alkanol pairs is manifested in the binary phase equilibrium behaviour with water, since these pairs have similar phase equilibrium behaviour as well. Fig. 5.8 also highlights how the position of the functional group amongst structural isomers influences the shape of the phase envelope, as well as the azeotropic composition. Shifting the hydroxyl group away from the terminal methyl group causes a lower azeotropic temperature, and also shifts the azeotropic composition toward the alkanol-rich composition range. For instance, the azeotropic composition for water + 2-pentanol is richer in alkanol than the azeotropic composition of water + 1-pentanol. Once again similar azeotropic compositions are observed for the alkanol pairs comprising a primary C_x-alkanol and a secondary $C_{(x+1)}$-alkanol (Fig. 5.8).

The azeotropic points for eight water + alkanol systems are summarised in Table 5.1 and are arranged according to the normal boiling temperature, T_n, of the alkanol. The first three systems each exhibit a homogeneous azeotrope, meaning that the vapour and liquid compositions at the azeotrope are identical. The last four systems each exhibit a heterogeneous azeotrope, meaning that the azeotropic vapour composition falls between the compositions of the coexisting liquid phases. The water + 2-butanol system exhibits a homogeneous azeotrope at 0.1013 MPa,

Table 5.1: Azeotropic temperatures, T_{az}, and compositions for binary alkanol (1) + water (2) systems at p = 0.1013 MPa. T_n is the normal boiling temperature of the alkanol. y is the vapour composition. x is the liquid composition. Subscript w refers to the water-rich phase; subscript a refers to the alkanol-rich phase.

	T_n/K	T_{az}/K	y_1	$x_{1,w}$	$x_{1,a}$
ethanol (1) + water (2) [110]	351.52	351.33	0.9070	-	-
2-propanol (1) + water (2) [159]	355.75	353.38	0.6768	-	-
1-propanol (1) + water (2) [120]	370.15	360.65	0.4250	-	-
2-butanol (1) + water (2) [141]	371.15	360.47	0.3799	0.0410	0.2982
3-pentanol (1) + water (2)	388.30	364.60	0.3040	0.0075	0.6573
1-butanol (1) + water (2)	390.77	365.89	0.2615	0.0110	0.3144
2-pentanol (1) + water (2)	392.00	365.59	0.2591	0.0062	0.5558
1-pentanol (1) + water (2)	410.75	369.28	0.1491	0.0042	0.5406

meaning that the azeotropic vapour composition lies outside of the LLE composition range at T^*.

As T_n increases, the azeotropic composition becomes richer in water and the azeotropic temperature, T_{az}, and in the case of heterogeneous azeotropes $T_{az} = T^*$, increases. Here the similarity between the alkanol pairs is also apparent: the azeotropic temperature of water + primary C_x-alkanol, and that of water + secondary $C_{(x+1)}$-alkanol is within 1 K of one another, while the azeotropic vapour composition of these two systems differs by ca. 0.045 mole fraction. The exception is water + ethanol and water + 2-propanol; however, ethanol and 2-propanol differ much more from one another in size and saturated vapour pressure behaviour (see Fig. 5.6) than the following pairs of alkanols, which might explain why the observed trends deviate for these two alkanols.

Lastly, the water-rich region of the T-xy diagram is magnified in Fig. 5.9. It would seem that the shape of the phase envelope in the water-rich region is not influenced by the identity of the alkanol. In the water-rich region steric hindrance does not influence the degree to which association occurs. The abundance of smaller sized water molecules is not restricted by steric hindrance since they can access alkanol association sites irrespective of their position.

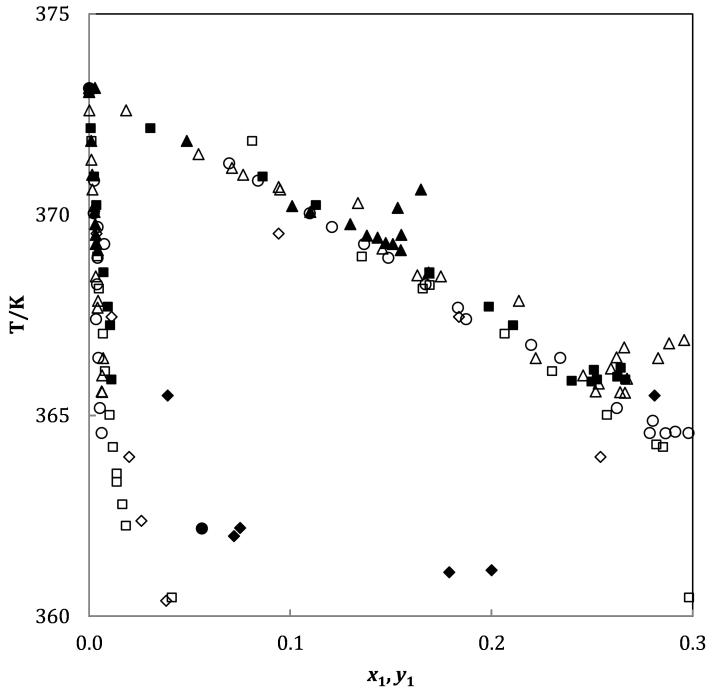

Figure 5.9: *T-xy* plot of binary alkanol (1) + water (2) mixtures at p = 0.1013 MPa (● ethanol [110]; ◆ 1-propanol [120]; ◇ 2-propanol [159]; ■ 1-butanol; □ 2-butanol [141]; ▲ 1-pentanol, △ 2-pentanol, ○ 3-pentanol).

5.4 Experimental Difficulties

For all the mixtures, very limited results were obtained for vapours corresponding to alkanol-rich liquid phases. In this composition region, the vapour boil-up into the sampling port (1.13c in Fig. 4.1) was low and the vapour samples that were extracted were not large enough for analysis.

The experimental method was verified in Section 5.1 with the water + 1-butanol system. Moreover, measurement of the water + 1-pentanol system was also successful. Using the same experimental and analysis procedures, the water + 2-pentanol and water + 3-pentanol systems were measured. These two systems proved to be very difficult to measure, compared to the water + 1-butanol and water + 1-pentanol systems. After repeated experiments, the inconsistency in the alkanol-rich composition region of both the water + 2-pentanol and water + 3-pentanol systems could not be consolidated. All data presented were shown to be thermodynamically consistent using the two tests presented in Section 3.3. However, the data presented in Figs. 5.4 and 5.5 are clearly not correct in its entirety, pointing toward a discrepancy in results obtained from the thermodynamic consistency tests.

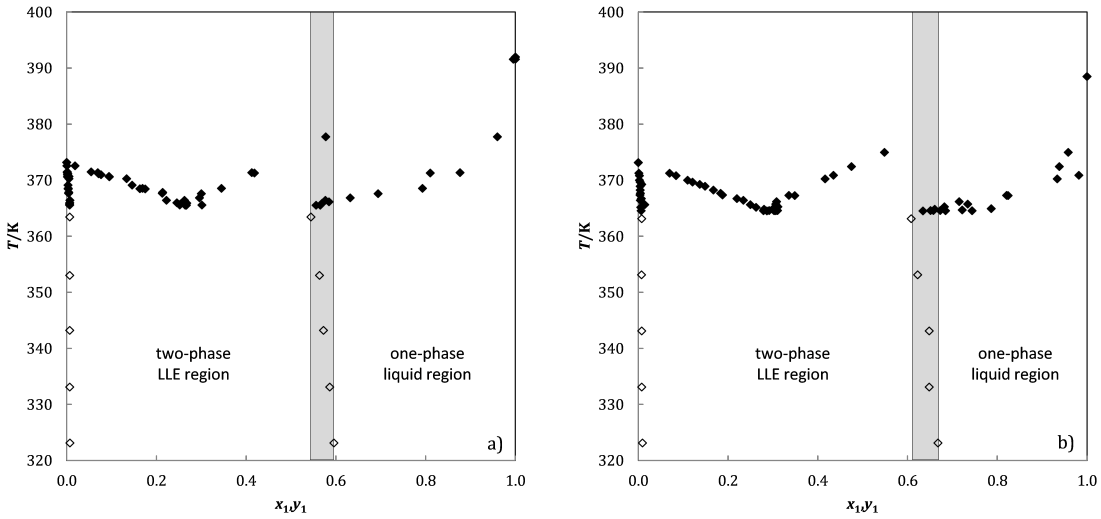

Figure 5.10: Diagram to illustrate the probable region of heterogeneous liquid samples at p = 0.1013 MPa for (a) 2-pentanol (1) + water (2); (b) 3-pentanol (1) + water (2).

During experimentation it was observed that the liquid phase returns to the mixing chamber as a heterogeneous mixture. Fig. 5.10 shows a greyed composition region for both the water + 2-pentanol and water + 3-pentanol systems. This region borders the alkanol-rich azeotropic liquid composition. Within this region it is conceivable that the exact equilibrium composition will be difficult to sample, since cooling of the liquid return can result in a sample where the composition falls within the LLE region. Fig. 5.10 shows that inconsistent data was repeatedly measured for both systems outside of this LLE region.

An alternative explanation arises: While a mixture, of which the overall composition falls in the two-phase LLE region, is heating up, the denser of the two coexisting phases will deposit in the sampling well. If this deposition is not completely flushed away during the experimental run, it will contaminate a sample drawn through the solenoid valve (1.12a in Fig. 4.1).

In an attempt to overcome the apparent liquid split, a heating line was placed around the liquid return line in the case that a small amount of energy was required to improve mixing. This resulted in a homogeneous liquid return, but the resulting data was even more scattered. The time between two samples was also increased to 2 hours to allow the system a longer time to reach equilibrium, but this was also unsuccessful.

The experimental difficulties could not be resolved and the data presented in this chapter are used as is. Further experimental work falls beyond the scope of this study.

5.5 Summary

In this chapter the experimental VLE results were presented and analysed alongside other water + (C_2–C_5) linear alkanol systems not measured in this work. Pure component behaviour of the respective alkanols sheds light on the effects of molecular structure: firstly, the effect that a shift in functional group on the carbon backbone has on phase behaviour, and secondly, the similarities between primary C_x- and secondary $C_{(x+1)}$-alkanols. It was observed that these similarities are translated into binary water + alkanol phase behaviour. Scattered data for the water + 2-pentanol and water + 3-pentanol mixtures stem from experimental difficulties that could not be overcome. These mixtures appear to be difficult to measure and might be the reason for the lack of literature data for these mixtures.

In the following chapter, the differences in phase behaviour observed for water + (C_2–C_5) linear alkanols will be used to test the predictive capability of the sPC-SAFT and SAFT-VR Mie model frameworks.

Chapter 6

Thermodynamic Modelling Results

The sPC-SAFT and SAFT-VR Mie equations of state were introduced in Chapter 2, as well as the Gross and Vrabec (GV), and Jog and Chapman (JC) polar terms. Each of these terms are included into the two parent model frameworks, such that the 6 EoS models are evaluated in this investigation: sPC-SAFT, sPC-SAFT-GV, sPC-SAFT-JC, SAFT-VR Mie, SAFT-VR Mie-GV, and SAFT-VR Mie-JC.

In this chapter, **Objectives 2, 3, and 4** are addressed. The importance of a suitable regression procedure is discussed, whereafter the pure component parameters are presented. These parameter sets are evaluated by assessing their applicability to pure component properties. The models and parameter sets are further evaluated by, firstly, assessing the description of VLE behaviour, and secondly, evaluating whether the models can be extended to other thermodynamic properties.

6.1 Parameter Regression

During regression of pure component parameters a few things, amongst others, need to be considered: the relationship that holds between thermodynamic properties and their mathematical description, the data that is included during regression of model parameters, and how the number of regression parameters influence the parameter space.

6.1.1 Relationship between Thermodynamic Properties and the State Function

Thermodynamic properties can be expressed mathematically in terms of the state function, $F = A^{\mathrm{r}}/RT$. The reader is referred to the monograph of Michelsen and Mollerup [46] for a review of the most notable first- and second-order properties of the EoS. Fig. 6.1 is a schematic representation of the relationships between thermodynamic properties and the reduced residual

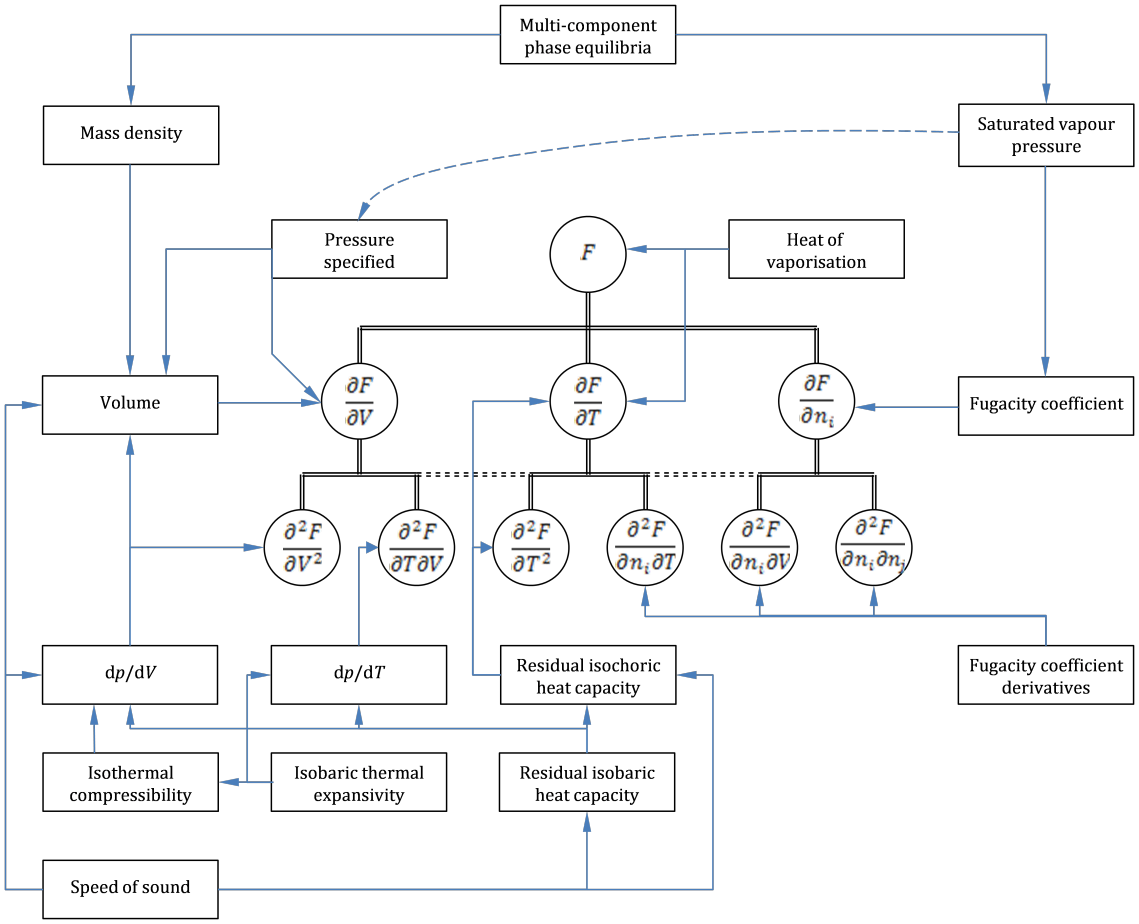

Figure 6.1: Diagram to illustrate the relationship between thermodynamic properties and $F = A^{\mathrm{r}}/RT$ (adapted and redrawn from de Villiers [36]).

Helmholtz energy state function, F. The partial derivatives of F are enclosed in circles, while the thermodynamic properties are in blocks. An arrow between a block and a circle indicates that the property can be described in terms of the partial derivative. Similarly, an arrow between two blocks indicates that the properties can be expressed in terms of one another.

6.1.2 Data Used in Regression Procedures

Knowledge of the relationships depicted in Fig. 6.1 allows tuning of pure component parameters to "align" the EoS to the thermodynamic behaviour of the component by minimising an objective function of the following form:

$$\mathrm{OF} = \sum_{X} \left[\frac{\omega_X}{N_X} \sum_{i=1}^{N_X} \left(\frac{X_i^{\mathrm{calc}} - X_i^{\mathrm{exp}}}{X_i^{\mathrm{exp}}} \right)^2 \right] \tag{6.1}$$

Here ω_X is a regression weight assigned to property X, N_X is the number of data points for property X, and i is a specific data point. Minimisation is conducted by using the Levenberg-

Marquardt [160, 161] algorithm. The quality of the model fit to experimental data can be evaluated by the percentage absolute average deviation, or %AAD, expressed as:

$$\%\text{AAD} = \frac{100}{N_X} \sum_{i=1}^{N_X} \left| \frac{X_i^{\text{calc}} - X_i^{\text{exp}}}{X_i^{\text{exp}}} \right| \tag{6.2}$$

The first consideration when choosing data to include in Eq. 6.1 is which derivatives of the state function will be represented in the regression procedure. Traditionally saturated vapour pressure, p^{sat}, and saturated liquid density, ρ^{sat}, data are included in the regression procedure with equal regression weights given to both properties. Saturated vapour pressure can be calculated from the fugacity coefficient, which in turn is dependent on the first-order compositional derivative of the EoS. Saturated liquid density requires accurate description of the system volume, which is dependent on the first-order volume derivative of the EoS. Extending the EoS to multicomponent phase equilibrium follows naturally from these regressions, since phase equilibrium is primarily dependent on p^{sat} and ρ^{sat} (see Fig. 6.1).

Including p^{sat} and ρ^{sat} data during regression provides information regarding the first-order compositional and volume derivatives. However, no information about the first-order temperature derivative or any of the second-order derivatives is included. Temperature can be accounted for indirectly by considering data over a large temperature range, generally $0.5 < T_{\text{r}} < 0.9$. However, this only provides a better description of the temperature behaviour of $\partial F/\partial n_i$ and $\partial F/\partial V$, and not necessarily the temperature behaviour of the entire state function. Parameters determined from only p^{sat} and ρ^{sat} generally give a very good description of mixture VLE, since phase equilibrium is primarily dependent on accurate description of pure component p^{sat} and ρ^{sat}. However, these parameters tend to give poor description of other thermodynamic properties, such as second-order derivative properties and mixture excess properties [36].

Secondly, the combination of properties used in the OF also needs to be considered. To illustrate this argument, consider Fig. 6.2. Including only p^{sat} and ρ^{sat} data in the regression procedure is likely to yield a parameter set (indicated by the square) that gives excellent prediction of these two properties, but which is unable to predict some of the other pure component properties. There should be a universal optimum parameter set (indicated by the star) that can accurately predict all thermodynamic properties of both pure components and their multicomponent mixtures and a corresponding regression procedure to obtain this set. However, this is still subject to the fundamental limitations introduced during the development of the EoS.

Different workers have extended the traditional OF by including additional pure component properties in the regression procedure with the specific aim to predict thermodynamic properties other than p^{sat} and ρ^{sat} accurately. To improve the prediction of isothermal compressibility,

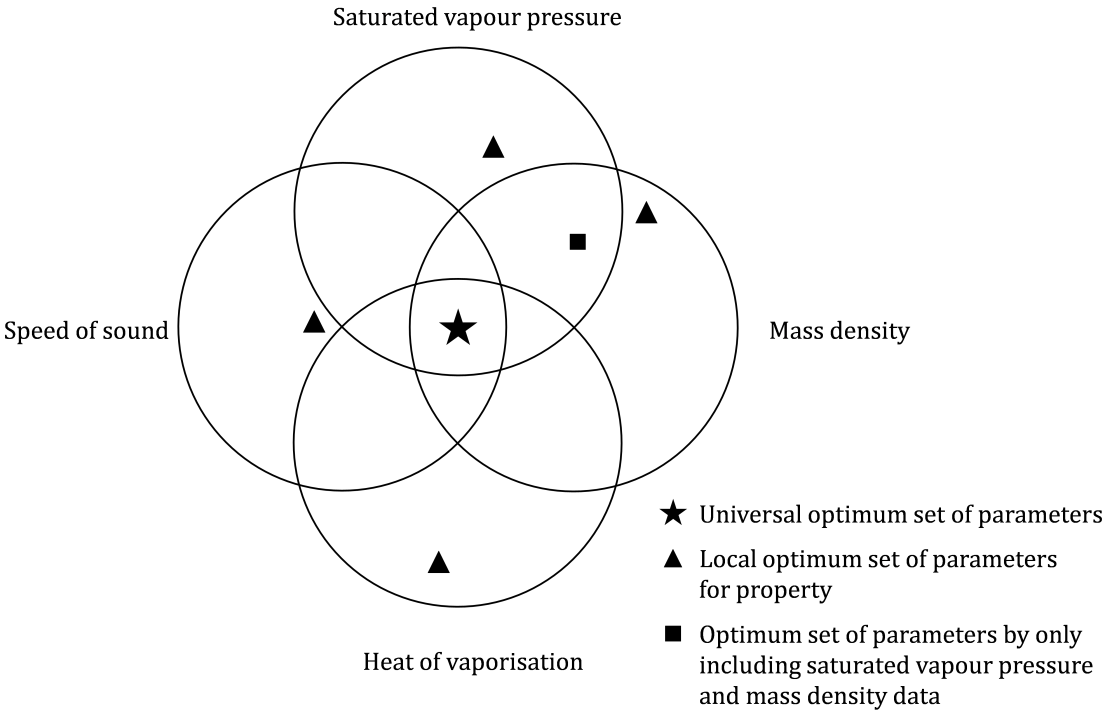

Figure 6.2: Diagram to illustrate parameter sets that can be obtained by including specific pure component data in the regression algorithm (adapted and redrawn from de Villiers [36]).

Lafitte, et al. [41] included condensed phase liquid properties (speed of sound, $u^{\text{liq}\dagger}$, and compressed liquid density, ρ^{comp}) in their OF for SAFT-VR Mie, using different weight factors, ω_X. The authors found that inclusion of u^{liq} data had a significant effect on the value of λ^{r} in SAFT-VR Mie, leading to more physically relevant values for this parameter [42]. Moreover, not only was the prediction of u^{liq} improved, but the EoS still retained accurate description of VLE properties. The authors also showed that the set of pure component properties obtained using their OF were transferable, since derivative properties not included in the regression procedure were also predicted successfully. Adding u^{liq} data to the regression procedure has another advantage; information regarding the first- and second-order temperature derivatives is now included.

For associating components it is often difficult to estimate the ratio between the dispersion and association contributions accurately [43]. To obtain physically realistic values for the association parameters, h^{vap} data is included in the regression procedure since h^{vap} is governed by association effects [43, 162].

†speed of sound, u^{liq}, is related to isothermal compressibility, β_{T}, through: $u^{\text{liq}} = \sqrt{(c_{\text{p}}V)/(c_{\text{V}}\beta_{\text{T}}M_{\text{W}})}$

6.1.3 The Parameter Space

The objective functions used to estimate EoS parameters almost always have multiple minima. In most cases, a nonlinear optimisation method, for instance a gradient-based quasi-Newton type method, is used; however, these optimisers tend to get "trapped" in local minima, especially when the starting values are inappropriate [163]. Introducing additional parameters that need to be regressed increases the possibility of degeneracy in the parameter space since multiple parameter sets are often obtained. These parameter sets provide equally good predictions of pure component properties [68, 76] but do not necessarily give equally good predictions of multicomponent phase properties. It is questionable whether the local minimum obtained by Eq. 6.1 is the same as the global minimum that would give the best description of all properties within the EoS being considered.

Furthermore, the danger with additional regression parameters is that blind manipulation of said parameters could arise, driving the EoS away from its foundation in physics and making it a pure correlative tool [76, 164]. The parameter set that provides the best mathematical fit is not necessarily the best physical model [76]. One would expect that the model containing more adjustable parameters in the regression procedure would perform better, therefore it is imperative to ensure that the values obtained for these parameters have physical significance.

The parameter space can be reduced by measuring the values of certain parameters, instead of regressing them. The fraction of unbonded molecules, X_A, can be determined by infrared and Raman spectroscopy [164–166]. An interesting alternative is to use X-ray diffraction and neutron scattering to investigate the radial distribution function [167].

Another regression alternative is the so-called grid-method used by Clark, et al. [68], dos Ramos, et al. [168], and later by Dufal, et al. [76]. The idea is to reduce the multidimensionality of the optimisation problem by fixing two pure component parameters in a grid-like fashion and regressing the remaining parameters. This allows one to observe the valleys in the OF and the relationship that holds between the different parameters.

6.1.4 Regression Procedure

The preceding sections attest to the complex relationship between the parameter space, the data used to determine values for these parameters, and the predictive capability of the models using the resulting parameter sets. An extensive study into different regression procedures can be conducted; however, the larger focus of this study is on the description of VLE, therefore regression procedures that have been shown to produce good VLE centric parameter sets are used in this investigation. For each model only a single regression procedure is considered.

sPC-SAFT

In two previous studies [36, 40], the following regression procedures proved to deliver good parameter sets for sPC-SAFT models, and were therefore also used in this study: For sPC-SAFT p^{sat}, ρ^{sat}, and h^{vap} data were included in the OF, with regression weights of 4:2:1. For the polar variants, p^{sat}, ρ^{sat}, and h^{vap} data, and additional binary VLE data with alkanes were included in the OF, using regression weights of 10:8:4:1.

SAFT-VR Mie

For SAFT-VR Mie a similar regression procedure to that of the original paper [42] was used: p^{sat}, ρ^{sat}, and u^{liq} data were included in the OF, using regression weights 4:4:1. For the polar variants, p^{sat}, ρ^{sat}, and u^{liq} data, and additional binary VLE data with alkanes were included in the OF, using regression weights of 10:8:4:1.

VLE data is included in the regression of parameter sets for the polar models in order to identify the correct ratio between polar and dispersive forces [36, 169].

6.2 Regressed Parameters

Information regarding the pure component data used during regression is summarised in Table 6.1. The references to c_p data in Table 6.1 are the data used to evaluate %AAD of the model fits to c_p in Tables 6.2 to 6.6. For p^{sat}, ρ^{sat}, and h^{vap} DIPPR [157] correlations were used to generate 30 data points in the temperature range $0.5 < T_{\text{r}} < 0.9$, since this range generally encompasses the two phase vapour-liquid region.

Table 6.1: Conditions and references of literature data used for regression purposes.

	M_w	μ [157]	u^{liq}			c_p			alkane VLE		
	g·mol^{-1}	D	T/K	p/MPa	Ref.	T/K	p/MPa	Ref	alkane	T/K	Ref.
meth	32.04	1.70	303	0.1 - 275	[170]	256 - 460	30	[171]	*n*-hexane	343	[172]
eth	46.07	1.70	313	0.1 - 30	[173]	326 - 471	6.4	[174]	*n*-heptane	333	[175]
1-prop	60.09	1.68	293 - 318	46	[176]	326 - 501	6.4	[174]	*n*-heptane	333	[175]
2-prop	60.09	1.70	273	0.1 - 30	[177]	253 - 323	0.1	[178]	*n*-heptane	323	[179]
1-but	74.12	1.67	323	0.1 - 96	[180]	326 - 521	6.4	[174]	*n*-nonane	323	[181]
2-but	74.12	1.66	273	0.1 - 30	[177]	188 - 345	0.1	[182]	*n*-hexane	323	[183]
1-pent	88.14	1.70	303	0.1 - 101	[184]	200 - 389	0.1	[185]	*n*-heptane	358	[186]
2-pent	88.14	1.67	283 - 313	0.1	[187]	307 - 367	0.1	[188]	*n*-heptane	358	[189]
3-pent	88.14	1.64	303	0.1 - 100	[190]	308 - 367	0.1	[188]	*n*-heptane	358	[191]
water	18.01	1.85	319	0.1 - 90	[192]	300 - 370	0.1	[193]	–		

Tables 6.2 to 6.6 provide the regressed parameters for water and the nine C_1-C_5 linear alkanols, with the relevant deviations from pure component data. Generally an increase in carbon chain length is accompanied by an increase in σ, m, ε, and ε^{AB}. For SAFT-VR Mie and SAFT-VR Mie-GV, λ^r increases as the carbon chain length increases. Both K^{AB} and r^c/σ decrease as the carbon chain length increases. Secondary alkanols typically have smaller K^{AB} and r^c/σ values than their corresponding primary alkanols. This corresponds to the decreased association strength witnessed in pure component saturated vapour pressure (see Section 5.3).

The procedure used to regressed parameters for SAFT-VR Mie-JC was unsuccessful. x_p was driven to zero for each component's parameter set, regardless of the initial guess or the choice of regression weights. For 2-propanol and 3-pentanol, no parameters could be determined for sPC-SAFT-JC. The molecular symmetry in these two molecules reduces the strength of the polar force and the model ultimately regards these molecules as being nonpolar.

To regress parameters for water, a similar strategy to that of Grenner, et al. [195] was followed, which was based on the following physical arguments: (a) the segment number, m, should be close to unity, (b) ε/k should be between 47 and 160 K [197], and (c) ε^{AB}/k should be close to 1813 K [198]. No VLE data were included during regression of polar model parameters for water.

In the original SAFT-VR Mie paper [42], the hard-sphere potential function is used to describe the RDF in A^{assoc} (see Eq. 2.11). In a subsequent study, Dufal, et al. [75] considered the LJ- and Mie-potential functions in addition to the original formulation, and determined parameter sets for water for each of these models. As is expected, the Mie-potential model has the best performance of the three models [75]. In each regression, the segment number, m, was fixed at 1. In this investigation, however, the original HS-formulation is used. New parameters are regressed, allowing m to vary as well. The new SAFT-VR Mie parameters for water are shown in Table 6.5 and perform as well as the parameters presented by Dufal, et al. [75], when pure component behaviour is considered. To verify the new parameters, a reference system, water + methanol, is shown in Fig. 6.3. Although the prediction by the 2B association scheme does not perform as well as the 2B-prediction by Dufal, et al. (c.f. Fig. 24 in Dufal, et al. [76]), it is reassuring to observe that the 2C scheme gives as good a prediction.

Table 6.2: sPC-SAFT pure component parameters.

	σ Å	m	(ε/k) K	$\left(\varepsilon^{AB}/k\right)$ K	K^{AB}	%AAD p^{sat}	ρ^{sat}	h^{vap}	u^{liq}	c_p
				2B						
meth[a]	2.5763	2.8770	164.91	2304.11	0.36080	0.96	1.16	1.86	6.95	3.58
eth[b]	3.2031	2.3697	215.70	2497.80	0.05000	0.39	0.70	0.26	7.63	4.65
1-prop[b]	3.1234	3.2802	214.45	2230.20	0.06260	0.37	0.14	1.35	2.58	3.37
2-prop	3.0110	3.6846	200.25	2077.88	0.05470	0.26	0.23	1.13	8.74	17.25
1-but[b]	3.3761	3.2691	243.22	2349.91	0.01860	0.31	0.64	1.19	2.06	2.62
2-but	3.3375	3.3702	234.02	2281.60	0.01039	0.16	0.27	1.10	1.17	23.46
1-pent[b]	3.5499	3.3580	254.01	2344.73	0.01810	0.86	0.17	0.79	4.07	8.07
2-pent[b]	3.7985	2.7822	260.16	2697.81	0.01241	0.46	0.27	1.88	6.19	5.24
3-pent	4.2277	2.0539	294.61	2876.76	0.00389	0.42	0.95	2.49	11.60	14.42
				2C						
meth	2.8031	2.3402	189.23	2449.03	0.11367	0.49	0.08	0.32	8.50	4.52
eth[c]	3.1895	2.3609	207.56	2695.69	0.03270	0.18	0.21	1.64	2.62	5.46
1-prop[c]	3.2473	2.9537	226.36	2448.02	0.02280	0.32	0.25	1.15	1.43	3.20
2-prop	3.0370	3.5876	201.84	2225.59	0.02831	0.26	0.23	1.12	7.39	17.83
1-but[c]	3.5065	2.9614	253.29	2601.00	0.00740	0.21	0.33	1.22	2.02	2.41
2-but	3.3382	3.3627	234.63	2394.08	0.00534	1.68	0.28	1.07	1.04	25.74
1-pent[c]	3.6350	3.1488	261.96	2555.34	0.00750	0.71	0.11	0.72	5.08	8.23
2-pent	3.9140	2.5611	273.02	2944.75	0.00213	0.21	0.32	0.15	7.09	3.84
3-pent	4.2731	1.9894	299.48	3040.09	0.00186	0.44	0.99	2.50	12.20	14.07
				3B						
meth[c]	2.8050	2.4573	198.80	2009.10	0.08880	0.54	2.38	6.39	21.90	1.56
eth[c]	2.7310	3.6829	180.17	1831.14	0.14580	0.12	0.07	0.71	16.70	4.08
1-prop[c]	3.1243	3.3294	220.03	1891.02	0.03880	0.20	0.24	1.29	6.59	2.54
2-prop	2.9448	3.9460	197.07	1728.10	0.04780	0.23	0.20	1.11	12.48	14.57
1-but[c]	3.3876	3.2765	242.37	2084.03	0.01507	0.19	0.21	1.20	2.40	1.97
2-but	3.3090	3.4635	230.66	1994.58	0.00982	0.16	0.18	1.12	2.29	16.60
1-pent[c]	3.5707	3.3261	255.03	2094.73	0.01393	0.09	0.16	0.82	3.39	3.14
2-pent	3.7465	2.9046	257.05	2381.81	0.00522	0.27	0.28	1.49	3.80	4.85
3-pent	4.0044	2.3964	273.98	2435.08	0.00495	0.38	0.69	2.41	9.46	15.61
water[d]	2.6273	1.5000	180.30	1804.22	0.18000	0.89	2.96	4.17	18.93	19.78
				alkanes						
n-pent[e]	3.7729	2.6896	231.20	–	–	0.25	1.29	1.60	13.91	2.27
n-hex[e]	3.7983	3.0576	236.77	–	–	0.64	0.62	1.99	12.82	2.46
n-hept[e]	3.8049	3.4831	238.40	–	–	0.25	0.87	1.41	14.05	0.93
n-oct[e]	3.8213	3.8468	241.87	–	–	0.14	0.60	1.09	13.17	0.48
n-non[e]	3.8282	4.2533	243.05	–	–	0.19	0.53	0.84	14.54	0.74

[a] Tybjerg, et al. [194]
[b] Grenner, et al. [30]
[c] de Villiers, et al. [67]
[d] Grenner and Schmelzer [195]
[e] Gross and Sadowski [53]

Table 6.3: sPC-SAFT-GV pure component parameters.

	σ Å	m	(ε/k) K	$\left(\varepsilon^{AB}/k\right)$ K	K^{AB}	n_{p}	%AAD p^{sat}	ρ^{sat}	h^{vap}	u^{liq}	c_p
					2B						
meth[a]	2.7164	2.5541	177.84	2296.30	0.23514	0.4534	0.45	0.17	0.92	9.39	3.40
eth[a]	3.0954	2.5766	194.85	2474.30	0.07586	0.9684	0.07	0.10	0.89	4.62	4.85
1-prop[a]	3.3093	2.8182	225.43	2342.90	0.03578	1.6270	0.18	0.25	1.24	1.56	3.00
2-prop	3.1970	3.1377	204.45	2224.23	0.03005	2.3228	0.23	0.24	0.94	6.11	14.60
1-but[a]	3.4800	3.0287	244.83	2413.66	0.01595	2.1267	0.19	0.19	1.14	1.93	2.40
2-but	3.5682	2.8257	238.68	2452.87	0.00754	2.9596	0.93	0.68	1.26	2.59	12.73
1-pent[a]	3.6846	3.0395	258.33	2443.40	0.01390	2.8121	0.05	0.16	0.79	5.30	5.31
2-pent	3.9570	2.4914	267.05	2812.76	0.00378	2.9533	0.31	0.28	1.24	6.90	4.03
3-pent	4.0528	2.3043	265.73	2727.70	0.00515	3.5917	0.63	0.41	1.81	11.00	12.83
					2C						
meth[a]	3.1616	1.7023	197.42	2627.80	0.05194	0.8712	0.64	0.48	0.71	5.28	2.72
eth[a]	3.2558	2.2361	202.27	2695.10	0.03035	1.1933	0.09	0.12	1.74	1.54	5.09
1-prop[a]	3.3108	2.8017	223.67	2466.70	0.02063	1.6800	0.22	0.14	1.11	0.55	3.20
2-prop	3.2670	2.9502	207.34	2407.32	0.01317	2.5364	0.21	0.24	0.83	4.44	14.68
1-but[a]	3.5584	2.8439	249.86	2609.82	0.00703	2.4012	0.14	0.22	1.16	2.24	2.64
2-but	3.5452	2.8668	236.41	2547.94	0.00412	3.1369	1.04	0.59	1.18	2.76	15.78
1-pent[a]	3.7459	2.9050	261.98	2622.20	0.00661	3.0296	0.15	0.18	0.86	6.25	5.36
2-pent	3.9922	2.4269	269.38	2974.17	0.00176	3.1542	0.28	0.28	1.15	7.66	3.84
3-pent	4.0878	2.2454	267.86	2885.16	0.00244	3.7708	0.63	0.41	1.76	11.56	12.61
					3B						
meth[a]	2.7169	2.6253	184.07	2073.10	0.11135	0.0994	1.01	1.21	5.05	14.03	5.91
eth	3.0004	2.8899	196.68	1967.75	0.06220	1.3022	1.94	0.59	0.86	14.97	3.39
1-prop[a]	3.2899	2.9001	230.11	2039.70	0.02419	1.1578	0.14	0.46	1.44	4.69	2.30
2-prop	3.0748	3.5196	203.83	1846.10	0.02993	1.4231	0.39	0.29	1.01	10.76	13.10
1-but[a]	3.4585	3.0982	244.98	2132.91	0.01347	1.4525	0.15	0.25	1.30	2.04	1.67
2-but	3.5766	2.8290	240.40	2182.27	0.00698	2.4521	1.05	0.86	1.61	1.83	4.06
1-pent[a]	3.6411	3.1551	256.69	2134.14	0.01268	2.0854	0.10	0.18	0.87	4.07	2.22
2-pent	3.8310	2.7346	258.81	2421.59	0.00442	2.3618	0.37	0.33	1.37	4.56	5.12
3-pent	3.9455	2.4940	260.54	2360.41	0.00557	2.9401	0.56	0.43	1.94	9.27	14.24
water[a]	2.6204	1.5052	149.96	1816.00	0.20245	0.3161	1.12	2.20	3.37	13.27	20.64

[a] de Villiers, et al. [89]

Table 6.4: sPC-SAFT-JC pure component parameters.

	σ Å	m	(ε/k) K	$\left(\varepsilon^{AB}/k\right)$ K	K^{AB}	x_{p}	%AAD p^{sat}	ρ^{sat}	h^{vap}	u^{liq}	c_p
					2B						
meth[a]	2.7721	2.5391	176.67	2318.30	0.23930	0.0695	0.45	0.19	0.45	8.85	3.81
eth[a]	3.1053	2.5570	192.25	2483.80	0.08310	0.1610	0.09	0.07	1.15	4.08	5.45
1-prop[a]	3.2424	2.9841	219.17	2263.70	0.05209	0.1708	0.27	0.25	1.38	2.16	3.26
2-prop	–	–	–	–	–	–	–	–	–	–	–
1-but[a]	3.4649	3.0771	243.92	2340.60	0.01972	0.2189	0.25	0.22	1.34	2.17	2.66
2-but	3.8476	2.3186	263.36	2568.38	0.00585	0.4448	1.01	1.12	2.04	4.01	13.04
1-pent[a]	3.7011	3.0186	260.37	2381.36	0.01620	0.3000	0.08	0.13	1.02	4.70	8.40
2-pent	3.9833	2.4539	275.45	2809.08	0.00393	0.2852	0.31	0.34	1.52	6.49	3.76
3-pent	–	–	–	–	–	–	–	–	–	–	–
					2C						
meth[a]	3.1718	1.6887	192.36	2621.30	0.06390	0.2960	0.57	0.52	2.00	4.00	4.33
eth[a]	3.2876	2.1752	198.25	2734.20	0.03440	0.2525	0.07	0.09	2.56	1.09	6.24
1-prop[a]	3.2777	2.8852	218.69	2416.10	0.02910	0.2030	1.13	0.16	1.25	0.51	3.54
2-prop	–	–	–	–	–	–	–	–	–	–	–
1-but[a]	3.4803	3.0346	244.10	2452.01	0.01097	0.2508	0.60	0.26	1.48	2.09	2.83
2-but	3.8430	2.3221	262.27	2670.81	0.00320	0.4748	0.98	1.11	2.02	4.07	16.17
1-pent[a]	3.7262	2.9606	262.16	2508.93	0.00828	0.3344	0.10	0.16	1.01	5.08	9.78
2-pent	4.0191	2.3910	278.53	2957.43	0.00191	0.3297	0.31	0.38	1.53	7.14	3.43
3-pent	–	–	–	–	–	–	–	–	–	–	–
					3B						
meth[a]	2.6231	2.7184	183.94	2072.60	0.11125	0.0238	1.02	1.22	5.06	14.09	5.73
eth[a]	2.9784	2.9434	199.29	2023.40	0.06206	0.0483	0.20	0.78	1.24	14.66	4.55
1-prop[a]	3.1338	3.3026	218.64	1891.30	0.04085	0.0713	0.16	0.27	1.42	6.30	2.60
2-prop	–	–	–	–	–	–	–	–	–	–	–
1-but[a]	3.4512	3.1233	244.23	2099.54	0.01497	0.1513	0.16	0.26	1.44	2.55	1.82
2-but	3.7359	2.5253	254.39	2237.92	0.00614	0.3329	1.27	1.01	2.20	1.83	5.52
1-pent[a]	3.6367	3.1755	256.38	2085.27	0.01432	0.2145	0.07	0.12	1.00	3.54	3.72
2-pent	3.8382	2.7261	262.90	2418.74	0.00451	0.1993	0.34	0.27	1.51	4.21	4.94
3-pent	–	–	–	–	–	–	–	–	–	–	–
water[a]	2.6179	1.5000	144.82	1838.90	0.20936	0.1250	1.09	1.94	3.25	11.54	19.74

[a] de Villiers, et al. [89]

Table 6.5: SAFT-VR Mie pure component parameters.

	σ Å	m	(ε/k) K	λ^{r}	$\left(\varepsilon^{AB}/k\right)$ K	$r_{AB}^{\mathrm{c}}/\sigma$	%AAD p^{sat}	ρ^{sat}	h^{vap}	u^{liq}	c_p
					2B						
meth	3.1208	1.7930	158.57	8.467	2754.06	0.44283	0.79	0.08	0.74	1.93	3.84
eth	3.4379	1.9548	206.62	10.635	2852.14	0.39795	0.29	0.07	1.47	1.07	5.68
1-prop[a]	3.5612	2.3356	227.66	10.179	2746.20	0.35377	0.83	0.25	1.48	0.19	2.51
2-prop	3.4405	2.5794	208.00	10.274	2690.76	0.35194	0.40	0.24	1.68	1.42	6.80
1-but[a]	3.7856	2.4377	278.92	11.660	2728.10	0.32449	0.70	0.63	1.48	3.49	1.86
2-but	3.6438	2.6900	250.14	11.163	2594.80	0.31639	0.38	0.29	1.91	1.57	12.15
1-pent	4.0140	2.4568	308.76	12.633	2632.72	0.34107	0.28	0.17	1.63	1.06	2.58
2-pent	4.1195	2.2813	306.92	12.885	2843.36	0.30111	0.15	0.25	2.22	1.06	5.17
3-pent	4.1647	2.2035	335.96	14.881	2542.45	0.32849	0.92	0.20	2.50	1.51	11.47
					2C						
meth	3.2028	1.6626	173.76	8.965	2871.61	0.39922	0.77	0.09	1.67	1.74	1.62
eth	3.5592	1.7728	224.50	11.319	3018.05	0.35465	0.39	0.10	2.46	0.96	5.75
1-prop	3.6008	2.2513	253.45	11.960	2794.88	0.34806	0.06	0.08	1.46	1.80	2.89
2-prop	3.4662	2.5156	213.91	10.617	2845.76	0.32060	0.29	0.19	1.48	1.05	9.28
1-but	3.7704	2.4614	266.49	11.338	2910.05	0.30421	0.15	0.23	1.93	1.59	2.18
2-but	3.6422	2.6879	251.07	11.212	2743.47	0.28710	0.32	0.26	1.90	1.23	15.54
1-pent	4.0186	2.4451	311.17	12.741	2774.96	0.31030	0.22	0.14	1.61	1.01	3.50
2-pent	4.1216	2.2740	308.55	12.966	3001.89	0.27574	0.14	0.22	2.20	0.86	4.63
3-pent	4.2516	2.0902	354.83	15.748	2694.37	0.29689	0.95	0.19	2.48	1.33	11.18
					3B						
meth	2.8985	2.2728	166.57	6.787	2521.48	0.38022	0.90	0.10	4.41	2.67	6.86
eth	3.2701	2.3168	160.57	8.072	2576.39	0.34371	0.67	0.27	1.21	1.80	2.81
1-prop	3.4694	2.5276	224.61	10.367	2380.01	0.34970	0.45	0.32	1.97	2.82	3.44
2-prop	3.3723	2.7527	199.80	9.862	2391.85	0.33093	0.78	0.41	1.92	3.88	0.46
1-but	3.7265	2.5631	259.55	11.107	2462.61	0.32202	0.50	0.37	2.01	2.54	1.35
2-but	3.8733	2.3059	239.24	9.718	2743.47	0.26369	1.08	0.60	1.72	4.17	1.83
1-pent	3.9842	2.5178	303.39	12.517	2346.36	0.33150	0.44	0.25	1.66	1.51	4.51
2-pent	4.0936	2.3271	287.90	11.822	2680.41	0.28156	0.63	0.38	1.94	1.27	6.44
3-pent	4.0943	2.3086	317.11	14.287	2245.33	0.33342	0.39	0.29	3.18	1.68	15.15
water	2.4539	1.7311	110.85	8.308	1991.07	0.56241	0.39	0.71	1.58	0.64	13.40
					alkanes						
n-pent[a]	4.2928	1.9606	321.94	15.847	–	–	1.06	0.40	2.51	2.53	2.74
n-hex[b]	4.5763	1.9371	382.57	18.647	–	–	0.42	0.18	2.60	1.96	0.94
n-hept[b]	4.4811	2.3185	369.30	17.589	–	–	0.23	0.09	2.191	1.00	3.29
n-oct[b]	4.4816	2.5944	371.00	17.299	–	–	0.34	0.10	1.72	0.58	3.70
n-non[b]	4.5672	2.4899	394.83	18.645	–	–	0.45	0.12	1.43	0.76	2.48

[a] Lafitte, et al. [42]
[b] Cripwell [196]

Table 6.6: SAFT-VR Mie-GV pure component parameters.

	σ Å	m	(ε/k) K	λ^{r}	$\left(\varepsilon^{AB}/k\right)$ K	$r_{AB}^{\mathrm{c}}/\sigma$	n_{p}	%AAD p^{sat}	ρ^{sat}	h^{vap}	u^{liq}	c_p
					2B							
meth	3.1559	1.7195	169.76	9.237	2777.34	0.45021	0.1279	0.83	0.07	1.18	1.73	5.50
eth	3.4462	1.9436	204.32	10.485	2857.92	0.39539	0.2764	0.29	0.08	1.46	1.02	5.58
1-prop	–	–	–	–	–	–	–	–	–	–	–	–
2-prop	–	–	–	–	–	–	–	–	–	–	–	–
1-but	–	–	–	–	–	–	–	–	–	–	–	–
2-but	3.6990	2.5839	241.04	10.652	2679.49	0.30634	1.5680	0.46	0.34	1.83	0.98	9.90
1-pent	4.0621	2.3796	307.13	12.554	2661.86	0.33623	1.8315	0.29	0.18	1.57	1.02	2.67
2-pent	4.1989	2.1683	306.19	12.793	2899.69	0.29288	2.1358	0.19	0.27	2.02	0.94	5.15
3-pent	4.3882	1.9226	352.33	15.843	2620.99	0.31961	2.9158	0.53	0.23	2.75	1.34	13.72
					2C							
meth	3.3277	1.4774	188.61	10.296	2903.87	0.40732	0.4760	0.73	0.06	3.98	1.58	3.50
eth	3.3978	2.0100	201.59	10.733	2815.52	0.38639	0.9106	1.97	0.53	2.91	1.30	5.79
1-prop	3.6280	2.2048	245.63	11.456	2855.32	0.33858	0.7454	0.07	0.11	1.40	0.10	2.89
2-prop	3.4795	2.4902	212.87	10.525	2865.19	0.31779	0.3016	0.30	0.19	1.48	0.92	9.11
1-but	–	–	–	–	–	–	–	–	–	–	–	–
2-but	3.7261	2.5296	244.94	10.855	2837.87	0.27661	1.9736	0.38	0.30	1.76	1.00	12.90
1-pent	4.1003	2.3180	312.39	12.784	2821.07	0.30333	2.2526	0.25	0.16	1.50	0.98	2.98
2-pent	4.2047	2.1563	309.65	13.001	3048.35	0.27021	2.1507	0.14	0.24	2.07	0.95	4.81
3-pent	4.4353	1.8689	366.06	16.451	2754.78	0.29571	2.3909	0.52	0.26	3.03	1.24	13.79
					3B							
meth	2.9774	1.9975	163.63	9.940	2588.15	0.42020	0.2614	1.88	0.19	3.49	2.34	13.19
eth	3.3224	2.1810	197.36	10.357	2549.46	0.37168	0.2605	1.11	0.42	1.71	4.88	7.10
1-prop	–	–	–	–	–	–	–	–	–	–	–	–
2-prop	–	–	–	–	–	–	–	–	–	–	–	–
1-but	–	–	–	–	–	–	–	–	–	–	–	–
2-but	3.6453	2.6996	241.63	10.787	2372.02	0.30370	0.7918	0.63	0.40	1.92	1.28	3.07
1-pent	3.9703	2.5387	295.90	12.168	2372.04	0.32994	0.4639	0.46	0.28	1.67	1.14	4.87
2-pent	4.0651	2.3718	293.57	12.424	2560.67	0.29498	0.6474	0.33	0.37	2.24	1.29	7.17
3-pent	–	–	–	–	–	–	–	–	–	–	–	–
water	3.0172	1.2410	63.500	6.544	1758.71	0.44421	1.0822	0.16	0.30	1.76	0.37	5.83

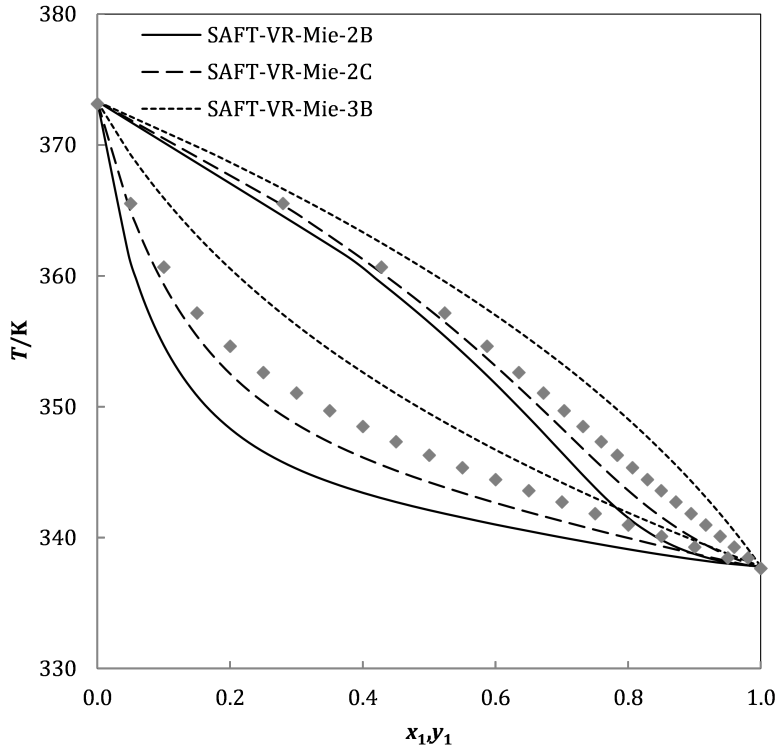

Figure 6.3: VLE of methanol (1) + water (2) at p = 0.1013 MPa. Data taken from Kojima, et al. [112].

6.3 Pure Component Properties

With the discussion in Section 6.1.2 in mind, it is expected that sPC-SAFT models will be biased toward p^{sat}, ρ^{sat}, and h^{vap}, while SAFT-VR Mie models will be biased toward p^{sat}, ρ^{sat}, and u^{liq}, since these respective combinations of data were included during regression. The analysis in this section is devoted toward evaluating whether the parameter sets are transferable, i.e. whether other pure component properties are predicted with the same accuracy as those properties included during regression.

The most important property to consider is the VLE of pure components and their mixtures. Second-order derivative properties, such as speed of sound, u^{liq}, and isobaric heat capacity, c_p, truly test the underlying physics of an EoS, because an EoS should not depend on specific thermodynamic properties, but rather consider microscopic contributions and provide holistic predictions [41, 199, 200].

6.3.1 Saturated Vapour Pressure, Saturated Liquid Density, and Heat of Vaporisation

In most cases, p^{sat}, ρ^{sat}, and h^{vap} predictions obtained by all models are comparable. sPC-SAFT and sPC-SAFT-GV perform equally well, and are both better than sPC-SAFT-JC, while SAFT-VR Mie is generally superior to SAFT-VR Mie-GV.

SAFT-VR Mie is built upon improved density description [42]. However, based on %AAD values, sPC-SAFT and SAFT-VR Mie models give similar results for ρ^{sat} (see Tables 6.2 to 6.6). SAFT-VR Mie does not lose accuracy in h^{vap} predictions, despite h^{vap} data not being included in the regression procedure for SAFT-VR Mie. In other words, the significant improvement in u^{liq} predictions gained by the regression procedure for the SAFT-VR Mie models does not come at the expense of h^{vap} description.

For all molecules, except methanol, it was found that all three association schemes give equally good description of p^{sat}, ρ^{sat}, and h^{vap}. From Fig. 6.4 it is evident that the 3B association scheme is not adequate to describe the associating behaviour of methanol.

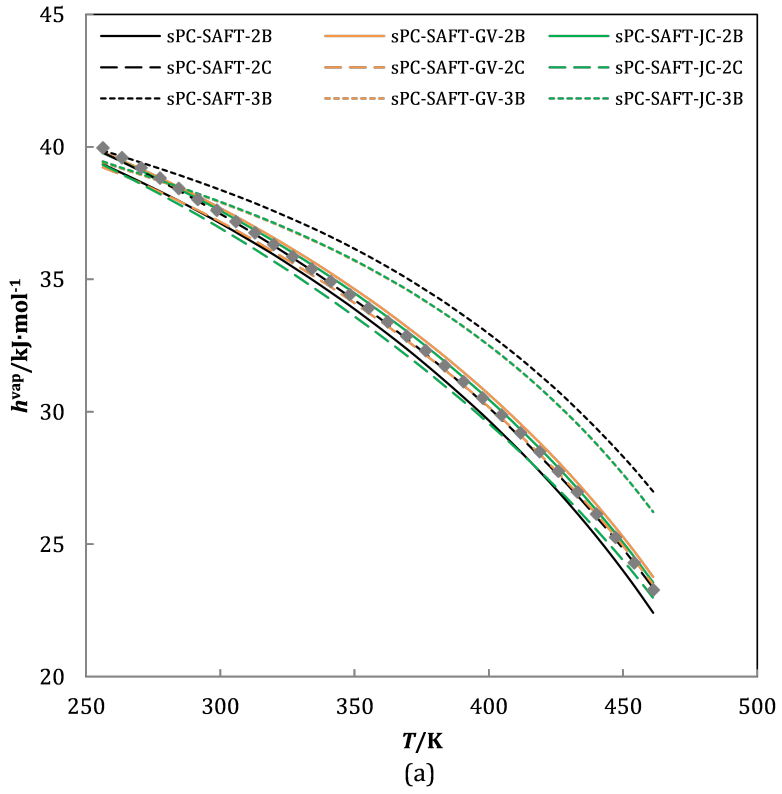

(a)

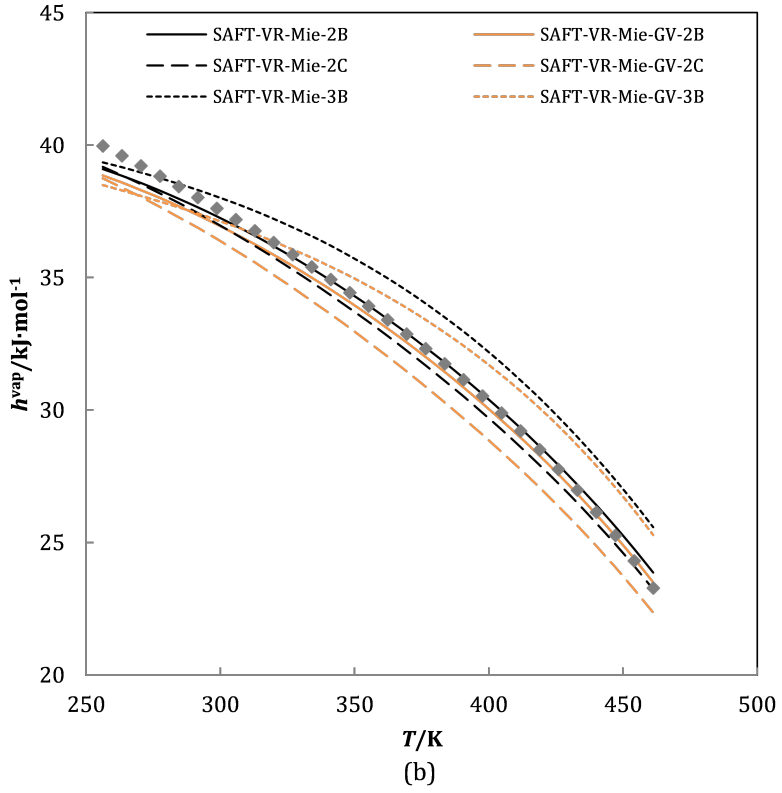

(b)

Figure 6.4: Heat of vaporisation of methanol predicted by (a) sPC-SAFT; (b) SAFT-VR Mie. Data calculated from DIPPR correlations [157].

6.3.2 Isobaric Heat Capacity

The isobaric heat capacity, c_p, is described mathematically [46]:

$$\frac{c_p}{R} = \frac{c_p^{\mathrm{r}}}{R} + \frac{c_p^{\mathrm{ig}}}{R} \tag{6.3}$$

$$\frac{c_p^{\mathrm{r}}}{R} = -\frac{T}{R}\frac{\left(\frac{\partial p}{\partial T}\right)_{V,n}^2}{\left(\frac{\partial p}{\partial V}\right)_{T,n}} - n - T^2\left(\frac{\partial^2 F}{\partial T^2}\right)_{V,n} - 2T\left(\frac{\partial F}{\partial T}\right)_{V,n} \tag{6.4}$$

$$\left(\frac{\partial p}{\partial T}\right)_{V,n} = -RT\left(\frac{\partial^2 F}{\partial T \partial V}\right)_{V,n} + \frac{p}{T} \tag{6.5}$$

$$\left(\frac{\partial p}{\partial V}\right) = -RT\left(\frac{\partial^2 F}{\partial V^2}\right)_{V,n} - \frac{nRT}{V^2} \tag{6.6}$$

c_p is therefore a function of both the first- and second-order temperature derivatives of the state function. Given the mathematical complexity of this property, it serves as a severe test of an EoS's performance, especially with respect to temperature description. Furthermore, it has been shown that c_p is strongly influenced by association phenomena [201, 202], making it an essential part of this particular study. Bearing in mind that no c_p data was included during regression, predictions obtained for this property are purely predictive.

c_p is better described by SAFT-VR Mie than sPC-SAFT. Both models use the Barker and Henderson perturbation theory [64–66]; sPC-SAFT is truncated to the second-order perturbation term [53], while SAFT-VR Mie includes the third-order term as well [42]. Therefore it is expected that SAFT-VR Mie should have a better description of the property's temperature dependence than sPC-SAFT, evidenced in predictions of pure component c_p.

%AAD values (see Tables 6.2 to 6.6) can be misleading as to how good the fit to experimental data is. sPC-SAFT generally struggles to capture the curvature of c_p (Fig. 6.5(a)). On the other hand, SAFT-VR Mie already gives improved results, with the description of the gradient almost always on par (Fig. 6.5(b)). Curvature predictions by the sPC-SAFT models become worse as the chain length of the alkanol increases. The sPC-SAFT models fail to describe the c_p for 1-butanol (Fig. 6.6). Here SAFT-VR Mie provides an improved description of the curvature at lower temperatures, but deviates from the experimental data at higher temperatures (Fig. 6.6).

The association schemes provide similar qualitative descriptions of c_p, regardless of the model (Fig. 6.7) and in most cases the qualitative description achieved by the 3B association scheme is most accurate. The fact that association scheme, rather than polar term, improves the qualitative prediction of c_p, indicates that polar interactions have a smaller contribution to c_p compared to association behaviour.

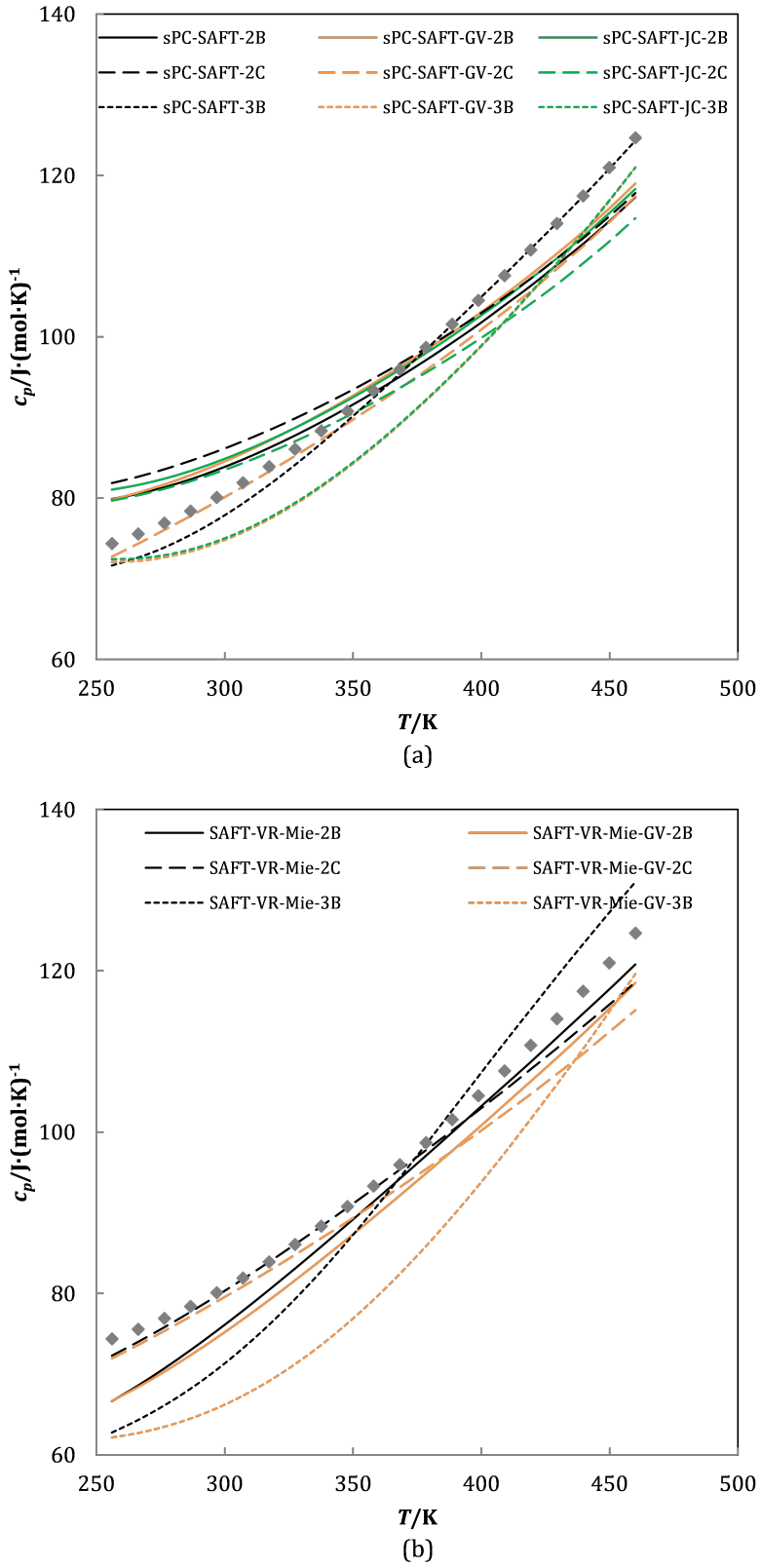

Figure 6.5: Isobaric heat capacity of methanol at p = 30 MPa predicted by (a) sPC-SAFT; (b) SAFT-VR Mie. Data taken from NIST [171].

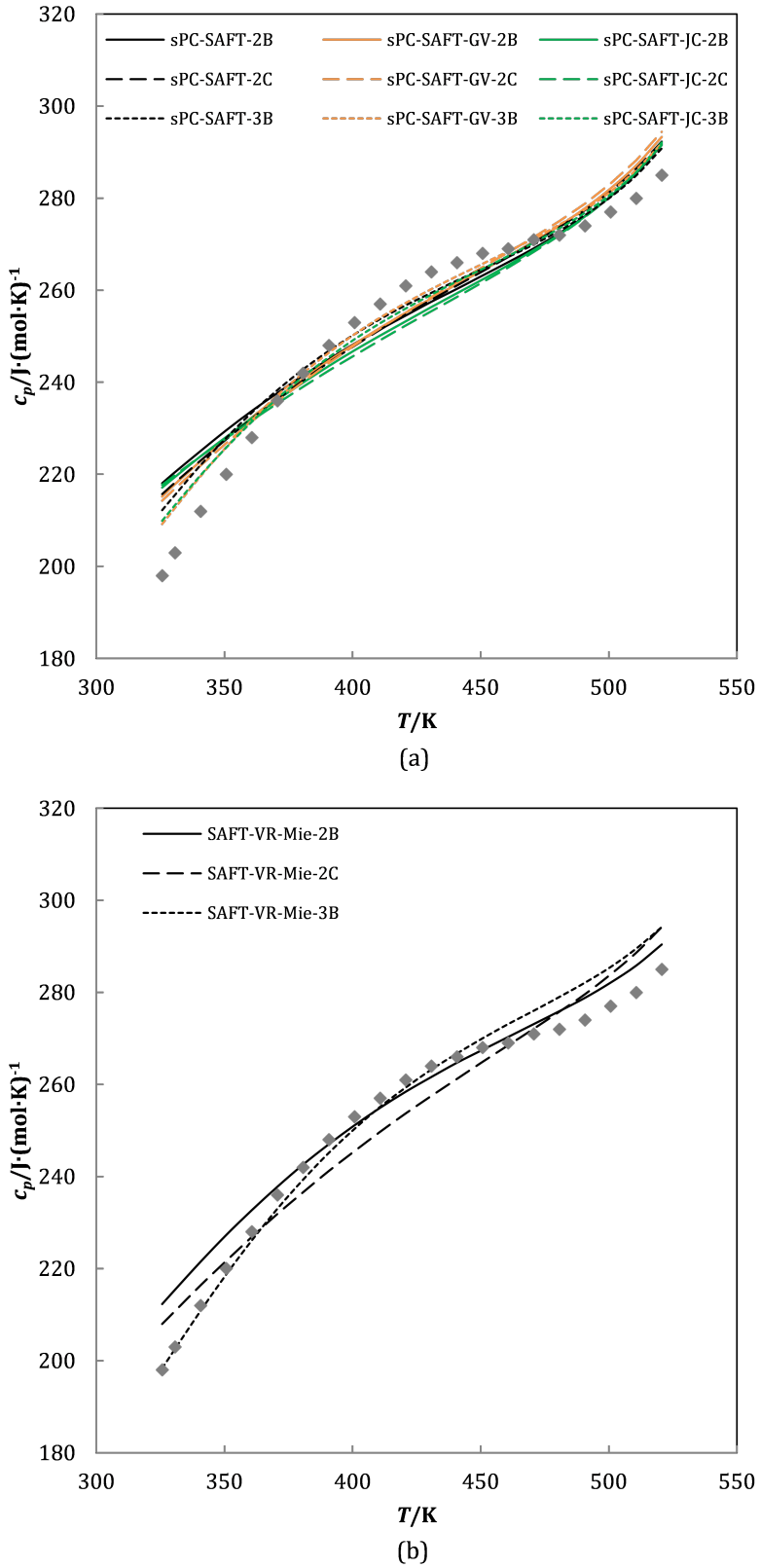

Figure 6.6: Isobaric heat capacity of 1-butanol at p = 6.4 MPa predicted by (a) sPC-SAFT; (b) SAFT-VR Mie. Data taken from Fulem, et al. [174].

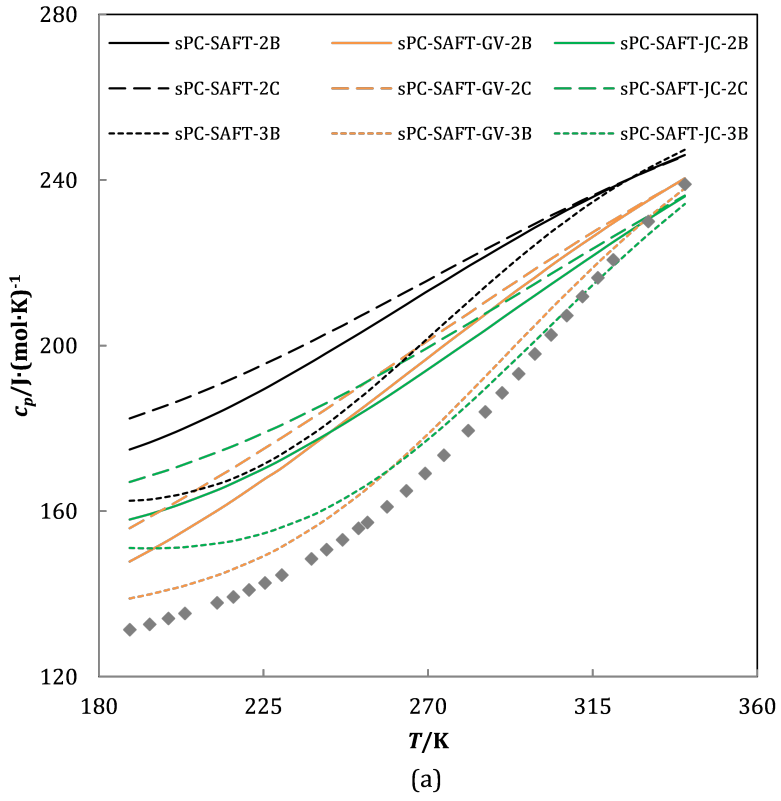

(a)

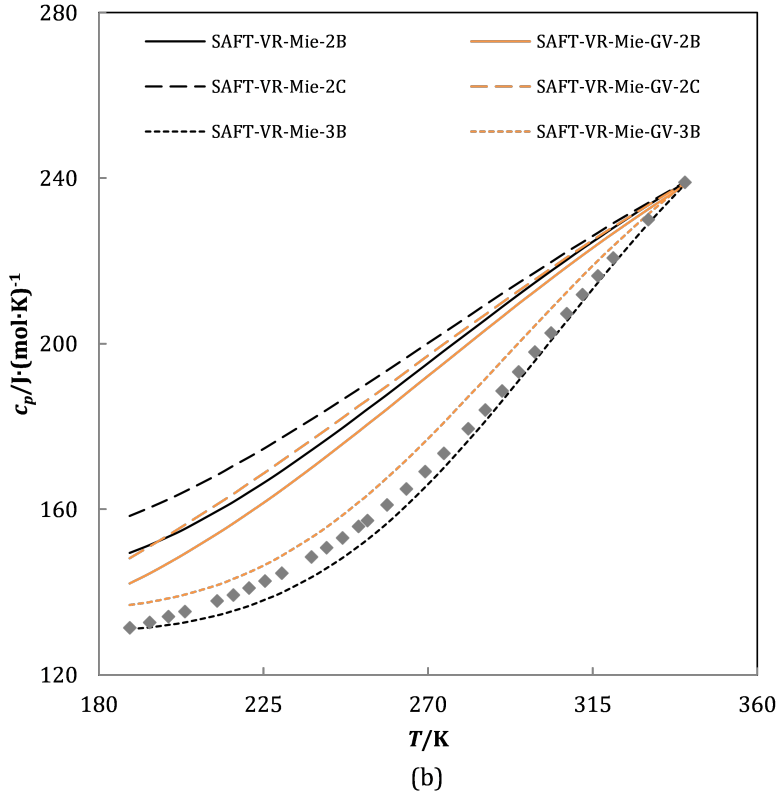

(b)

Figure 6.7: Isobaric heat capacity of 2-butanol at p = 0.1013 MPa predicted by (a) sPC-SAFT; (b) SAFT-VR Mie. Data taken from Andon, et al. [182].

6.3.3 Speed of Sound

Speed of sound is described mathematically:

$$u^{\text{liq}} = \sqrt{\frac{c_{\text{p}} V}{c_{\text{V}} \beta_T M_W}} \tag{6.7}$$

Accurate description of u^{liq} is dependent on accurate description of $c_p V/(c_V \beta_T)$. Given that ρ_i^{sat} is accurately predicted by all models, it is expected that volume predictions should be of similar accuracy. u^{liq} is therefore dependent on $c_p/(c_V \beta_T)$; bearing in mind that accurate prediction of this *ratio* does not necessarily imply that the respective properties are accurately described.

Since u^{liq} data were included during regression for SAFT-VR Mie, this model provides superior results to those obtained with the sPC-SAFT models. This property's curvature is well described by both the sPC-SAFT and SAFT-VR Mie models.

For the short chain alkanols, sPC-SAFT-GV and sPC-SAFT-JC provide similar predictions of u^{liq} which are better than sPC-SAFT (Fig. 6.8(a)). As the chain length increases however, worse predictions for u^{liq} are obtained when including a polar term to sPC-SAFT (Fig. 6.9(a)). Although SAFT-VR Mie-GV provides slightly better u^{liq} predictions than SAFT-VR Mie, the improvement is not very significant (Fig. 6.8(b) and Fig. 6.9(b)).

The 2C association scheme provides the best description of u^{liq} for most alkanols investigated in all model variants.

Water is a notoriously difficult molecule to model. sPC-SAFT describes the first-order thermodynamic properties of water well, but prediction of the second-order properties are unsatisfactory (see %AAD values in Tables 6.2 to 6.6). On the other hand, SAFT-VR Mie gives an excellent prediction of u^{liq} for water (Fig. 6.10).

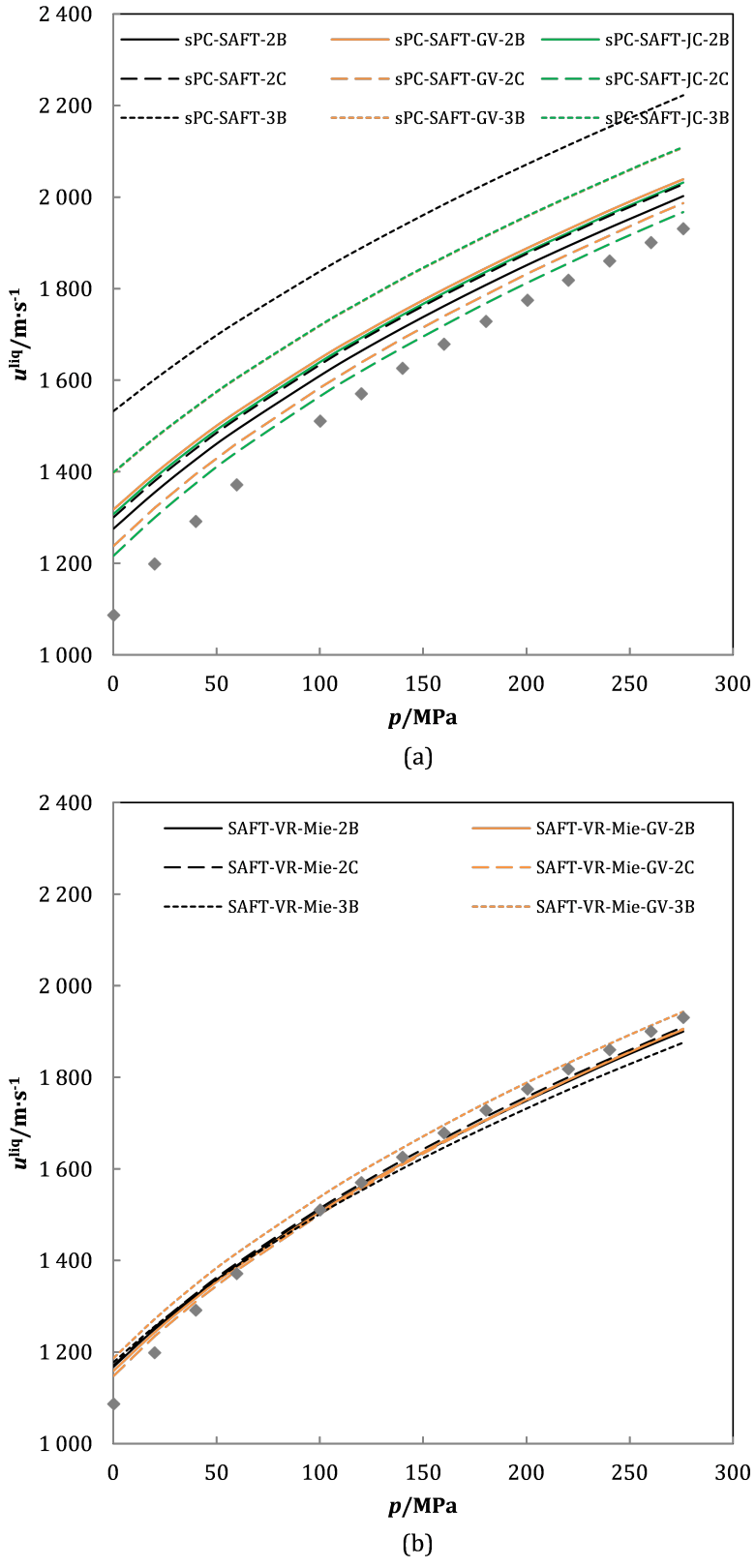

Figure 6.8: Speed of sound of methanol at T = 303.15 K predicted by (a) sPC-SAFT; (b) SAFT-VR Mie. Data taken from Sun, et al. [170].

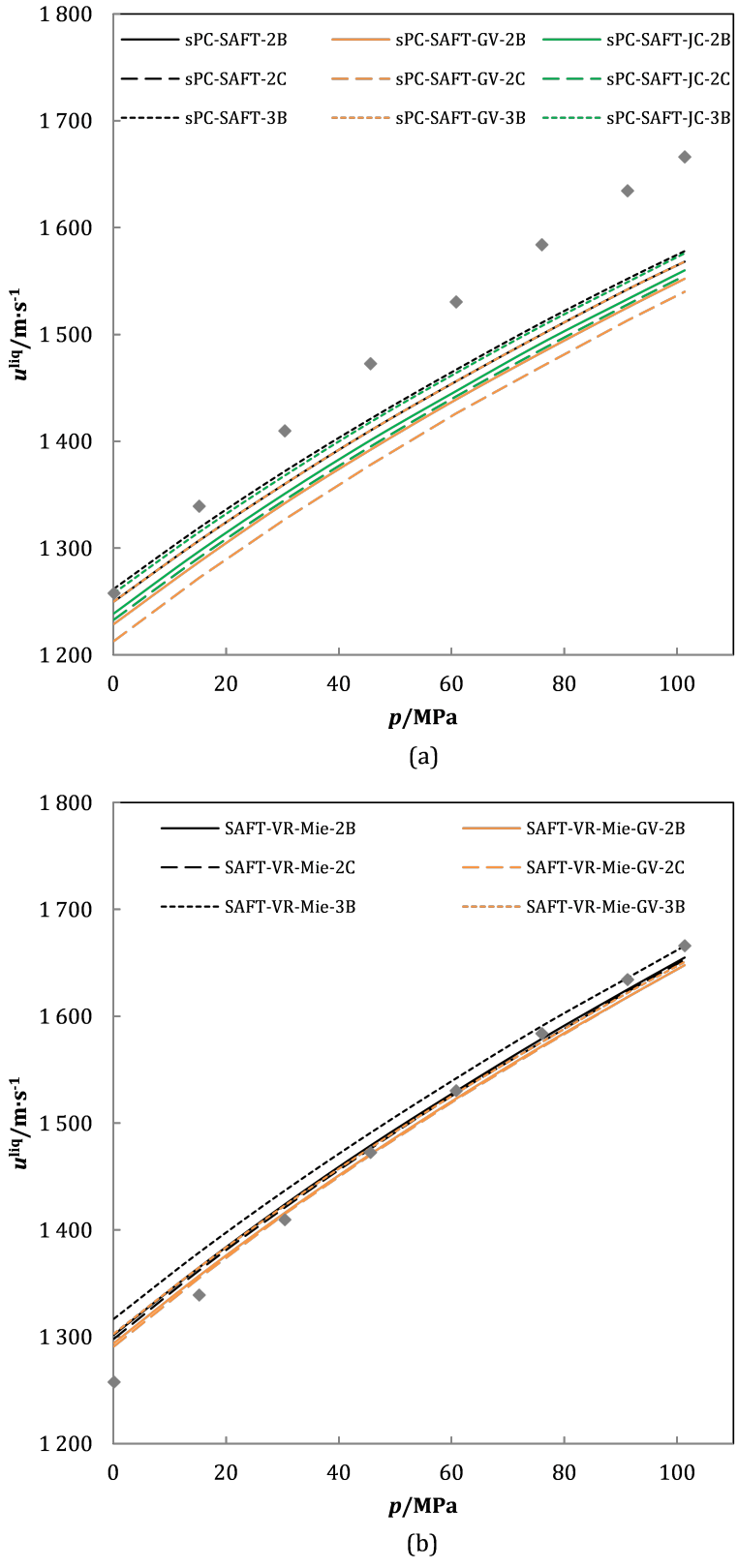

Figure 6.9: Speed of sound of 1-pentanol at T = 303.1 K predicted by (a) sPC-SAFT; (b) SAFT-VR Mie. Data taken from Dzida [184].

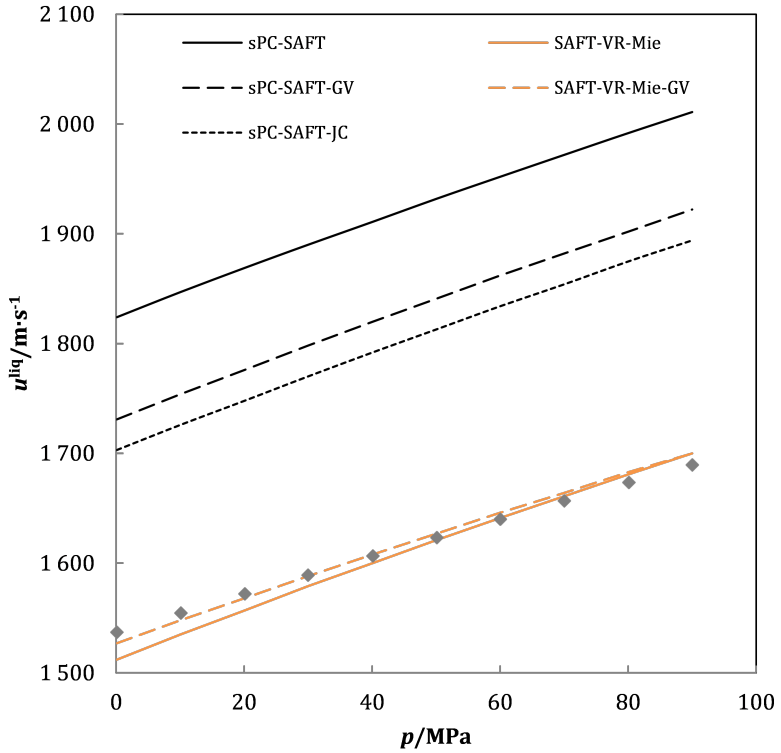

Figure 6.10: Speed of sound of water at T = 319 K predicted by sPC-SAFT and SAFT-VR Mie. Data taken from Benedetto, et al. [192].

6.3.4 Section Highlights

sPC-SAFT, sPC-SAFT-GV, SAFT-VR Mie, and SAFT-VR Mie-GV perform equally well when predicting pure component properties. sPC-SAFT-JC is outperformed when predicting first-order thermodynamic properties (p^{sat}, ρ^{sat}, and h^{vap}), but delivers similar results to those of sPC-SAFT-GV for the second-order thermodynamic properties (c_p and u^{liq}).

However, inclusion of a polar term does not provide significantly improved results, especially for SAFT-VR Mie. It is valuable to note that the polar predictions of pure component properties do not deteriorate, bearing in mind that alkane VLE data was including during regression of parameters for these models.

While the three association schemes provide similar results in most predictions, the 2C association scheme tends to be slightly better than 2B and 3B. Primary and secondary alkanol properties are predicted equally well.

6.4 Binary Alkane + Alkanol Mixtures

The focus now shifts to mixtures, where the interactions between *unlike* molecules are considered. This is important, since EoSs are almost always applied to determine mixture properties, therefore these models need to be able to describe *unlike* interactions as well as *like* interactions (pure component predictions). Moreover, only pure component data were included in the regression procedures for sPC-SAFT and SAFT-VR Mie, therefore it is necessary to determine whether the pure component parameters are transferable to mixture properties. For the polar models, binary VLE data with alkanes were included during regression of alkanol parameters in order to obtain more realistic polar parameter values. However, this also inherently causes the polar models to be biased toward the prediction of binary alkane + alkanol VLE.

The regression procedures used to determine pure component parameters are designed to produce good mixture VLE predictions. However, the accurate prediction of excess properties is not guaranteed, since no excess property data were included during regression. It is desired to have a single parameter set that is able to predict mixture VLE and excess properties simultaneously, therefore excess properties are also investigated.

Binary alkane + alkanol mixtures are investigated to observe how well the SAFT framework is able to describe association and polar effects in a "neutral" background; i.e. as part of a mixture where the second component, here alkanes, does not have any functionality over and above the usual dispersion forces. This approach also evaluates the treatment of self-association, because alkanes do not associate at all.

For this investigation, the use of binary interaction parameters are not considered and the focus is therefore on pure predictions.

6.4.1 Vapour-Liquid Equilibria

The results for the VLE of alkane + alkanol mixtures investigated in this study are summarised in Tables 6.7 to 6.11.

For most of the systems investigated, sPC-SAFT provides a good qualitative description of the binary alkane + alkanol VLE, but in many cases accurate description of the azeotrope is lacking (Figs. 6.11 and 6.12). These poor predictions are generally consolidated with the inclusion of a polar term, in which case excellent prediction of the azeotropic conditions (composition and T/p) are obtained (Figs. 6.11(a) and 6.12(a)). This suggests that, in these mixtures, polar interactions are not accounted for accurately in the nonpolar sPC-SAFT framework. The predictions for sPC-SAFT-GV and sPC-SAFT-JC are also almost identical, therefore the more suitable polar term for the sPC-SAFT framework is not apparent.

Table 6.7: VLE predictions of alkane + alkanol mixtures with sPC-SAFT.

mixture	T/p	2B $\Delta p^{a}/\Delta T^{b}$	2B Δy^{b}	2C $\Delta p^{a}/\Delta T^{b}$	2C Δy^{b}	3B $\Delta p^{a}/\Delta T^{b}$	3B Δy^{b}
methanol + *n*-hexane [172]	343.15 K	1.01	1.06	7.88	3.49	2.91	2.01
methanol + *n*-hexane [203]	303.15 K	2.32	1.38	6.77	2.49	4.09	2.25
methanol + *n*-octane [204]	0.1013 MPa	0.52	0.41	2.44	1.43	1.18	0.86
ethanol + *n*-heptane [175]	333.15 K	5.93	2.66	7.53	3.39	6.14	3.42
ethanol + *n*-heptane [205]	0.1013 MPa	3.31	6.07	3.67	6.53	1.17	2.43
ethanol + *n*-octane [206]	318.15 K	6.59	2.16	8.48	2.70	8.11	2.80
1-propanol + *n*-heptane [175]	333.15 K	3.62	1.94	5.82	3.11	2.42	1.75
1-propanol + *n*-octane [207]	358.15 K	6.72	2.28	9.30	3.30	5.01	2.01
2-propanol + *n*-hexane [179]	323.15 K	5.71	2.76	6.97	3.37	2.70	1.67
1-butanol + *n*-nonane [181]	323.15 K	7.30	1.97	9.40	2.87	4.03	0.90
1-butanol + *n*-heptane [208]	333.15 K	7.74	1.96	9.33	2.49	5.05	1.29
1-butanol + *n*-heptane [208]	363.15 K	7.32	3.02	7.59	3.42	6.66	2.43
2-butanol + *n*-hexane [183]	323.15 K	15.07	1.12	15.75	1.23	13.18	0.94
2-butanol + *n*-heptane [209]	348.15 K	8.93	3.96	9.46	4.15	7.56	3.61
1-pentanol + *n*-heptane [186]	358.15 K	6.28	2.84	6.87	3.11	4.88	2.19
1-pentanol + *n*-hexane [210]	323.15 K	7.81	1.45	9.47	1.76	4.33	0.86
2-pentanol + *n*-heptane [189]	348.15 K	6.29	2.16	7.02	2.50	4.75	1.43
2-pentanol + *n*-heptane [189]	358.15 K	5.30	1.64	5.93	1.96	4.02	1.04
3-pentanol + *n*-heptane [191]	348.15 K	0.48	0.38	0.62	0.44	0.55	0.50
3-pentanol + *n*-heptane [191]	358.15 K	0.50	0.61	0.30	0.57	0.63	0.67

[a] Deviations in %AAD.
[b] $\Delta z = \sum_i^{np} |z_i^{\text{calc}} - z_i^{\text{exp}}|$ where z represents T or y and np is the number of data points.

Table 6.8: VLE predictions of alkane + alkanol mixtures with sPC-SAFT-GV.

mixture	T/p	2B $\Delta p^{a}/\Delta T^{b}$	2B Δy^{b}	2C $\Delta p^{a}/\Delta T^{b}$	2C Δy^{b}	3B $\Delta p^{a}/\Delta T^{b}$	3B Δy^{b}
methanol + *n*-hexane [172]	343.15 K	1.63	1.43	1.14	1.14	2.78	1.61
methanol + *n*-hexane [203]	303.15 K	3.32	1.95	3.52	2.00	4.33	2.14
methanol + *n*-octane [204]	0.1013 MPa	0.77	0.49	0.61	0.49	0.89	0.81
ethanol + *n*-heptane [175]	333.15 K	0.66	0.63	0.81	0.76	9.17	3.74
ethanol + *n*-heptane [205]	0.1013 MPa	1.30	2.93	1.31	2.92	1.57	2.77
ethanol + *n*-octane [206]	318.15 K	1.81	0.68	2.00	0.79	12.85	3.33
1-propanol + *n*-heptane [175]	333.15 K	1.23	1.06	1.16	1.02	1.82	1.54
1-propanol + *n*-octane [207]	358.15 K	3.03	0.98	3.05	0.94	3.34	1.37
2-propanol + *n*-hexane [179]	323.15 K	3.46	1.98	3.55	1.85	2.72	1.83
1-butanol + *n*-nonane [181]	323.15 K	0.61	0.74	0.71	0.75	0.68	0.83
1-butanol + *n*-heptane [208]	333.15 K	2.06	0.75	1.66	0.62	2.24	0.82
1-butanol + *n*-heptane [208]	363.15 K	5.30	1.46	4.95	1.22	5.63	1.57
2-butanol + *n*-hexane [183]	323.15 K	5.29	2.03	5.37	1.99	5.18	2.18
2-butanol + *n*-heptane [209]	348.15 K	0.89	1.19	0.87	1.15	1.04	1.36
1-pentanol + *n*-heptane [186]	358.15 K	1.75	1.04	1.44	0.94	2.12	1.13
1-pentanol + *n*-hexane [210]	323.15 K	3.50	0.09	3.15	0.12	3.73	0.12
2-pentanol + *n*-heptane [189]	348.15 K	2.01	1.16	2.19	1.20	1.17	0.92
2-pentanol + *n*-heptane [189]	358.15 K	2.23	1.42	2.44	1.49	1.41	1.12
3-pentanol + *n*-heptane [191]	348.15 K	6.90	3.36	7.10	3.41	5.50	2.85
3-pentanol + *n*-heptane [191]	358.15 K	6.68	3.24	6.90	3.32	5.23	2.70

[a] Deviations in %AAD.
[b] $\Delta z = \sum_i^{np} |z_i^{\text{calc}} - z_i^{\text{exp}}|$ where z represents T or y and np is the number of data points.

Table 6.9: VLE predictions of alkane + alkanol mixtures with sPC-SAFT-JC.

mixture	T/p	2B $\Delta p^{a}/\Delta T^{b}$	2B Δy^{b}	2C $\Delta p^{a}/\Delta T^{b}$	2C Δy^{b}	3B $\Delta p^{a}/\Delta T^{b}$	3B Δy^{b}
methanol + *n*-hexane [172]	343.15 K	1.81	1.28	1.37	1.37	2.89	1.65
methanol + *n*-hexane [203]	303.15 K	2.05	1.46	4.09	2.25	4.52	2.22
methanol + *n*-octane [204]	0.1013 MPa	0.61	0.32	0.63	0.45	0.92	0.83
ethanol + *n*-heptane [175]	333.15 K	0.71	0.62	0.87	0.75	1.19	0.83
ethanol + *n*-heptane [205]	0.1013 MPa	1.21	2.80	1.27	2.81	1.35	3.01
ethanol + *n*-octane [206]	318.15 K	2.20	0.73	2.24	0.81	2.27	0.82
1-propanol + *n*-heptane [175]	333.15 K	1.33	1.11	1.38	0.98	2.20	1.79
1-propanol + *n*-octane [207]	358.15 K	3.54	1.17	3.07	1.23	3.78	1.59
1-butanol + *n*-nonane [181]	323.15 K	0.68	0.74	0.66	0.83	0.62	0.81
1-butanol + *n*-heptane [208]	333.15 K	2.56	0.89	2.48	0.84	2.39	0.85
1-butanol + *n*-heptane [208]	363.15 K	5.65	1.67	5.48	1.44	5.74	1.62
2-butanol + *n*-hexane [183]	323.15 K	5.44	2.02	5.44	2.01	5.32	2.15
2-butanol + *n*-heptane [209]	348.15 K	0.92	1.23	0.90	1.21	1.08	1.34
1-pentanol + *n*-heptane [186]	358.15 K	2.11	1.11	2.08	1.10	2.27	1.14
1-pentanol + *n*-hexane [210]	323.15 K	4.24	0.23	4.25	0.23	4.39	0.24
2-pentanol + *n*-heptane [189]	348.15 K	2.64	0.67	2.72	0.72	2.15	0.46
2-pentanol + *n*-heptane [189]	358.15 K	1.99	0.30	2.03	0.33	1.67	0.29

[a] Deviations in %AAD.
[b] $\Delta z = \sum_i^{np} |z_i^{\text{calc}} - z_i^{\text{exp}}|$ where z represents T or y and np is the number of data points.

Table 6.10: VLE predictions of alkane + alkanol mixtures with SAFT-VR Mie.

mixture	T/p	2B $\Delta p^{a}/\Delta T^{b}$	2B Δy^{b}	2C $\Delta p^{a}/\Delta T^{b}$	2C Δy^{b}	3B $\Delta p^{a}/\Delta T^{b}$	3B Δy^{b}
methanol + *n*-hexane [172]	343.15 K	7.40	3.41	1.40	1.26	49.06	13.94
methanol + *n*-hexane [203]	303.15 K	10.96	4.65	3.41	1.98	67.56	15.98
methanol + *n*-octane [204]	0.1013 MPa	1.86	1.43	0.43	0.29	10.36	7.23
ethanol + *n*-heptane [175]	333.15 K	1.73	1.10	4.48	2.02	19.25	8.26
ethanol + *n*-heptane [205]	0.1013 MPa	1.05	2.64	2.26	4.39	4.18	5.60
ethanol + *n*-octane [206]	318.15 K	2.18	0.92	5.32	1.65	26.30	7.17
1-propanol + *n*-heptane [175]	333.15 K	2.17	1.42	2.43	1.29	6.34	3.41
1-propanol + *n*-octane [207]	358.15 K	0.61	0.59	4.89	1.47	4.37	2.06
2-propanol + *n*-hexane [179]	323.15 K	2.74	1.42	0.64	0.53	9.02	4.38
1-butanol + *n*-nonane [181]	323.15 K	1.19	0.83	0.65	0.63	7.81	3.02
1-butanol + *n*-heptane [208]	333.15 K	2.13	0.69	2.46	0.57	3.70	1.42
1-butanol + *n*-heptane [208]	363.15 K	4.98	1.35	4.31	1.04	6.82	1.13
2-butanol + *n*-hexane [183]	323.15 K	6.63	1.90	7.66	1.65	2.98	3.05
2-butanol + *n*-heptane [209]	348.15 K	1.94	1.46	2.56	1.64	3.10	1.47
1-pentanol + *n*-heptane [186]	358.15 K	3.37	1.68	4.12	1.98	1.45	0.97
1-pentanol + *n*-hexane [210]	323.15 K	2.36	0.60	4.02	0.83	3.43	0.09
2-pentanol + *n*-heptane [189]	348.15 K	4.54	1.46	5.44	1.86	0.92	0.37
2-pentanol + *n*-heptane [189]	358.15 K	3.49	0.96	4.29	1.32	0.36	0.53
3-pentanol + *n*-heptane [191]	348.15 K	2.04	0.93	2.86	1.37	0.44	0.44
3-pentanol + *n*-heptane [191]	358.15 K	1.68	0.65	2.45	1.02	0.56	0.64

[a] Deviations in %AAD.
[b] $\Delta z = \sum_i^{np} |z_i^{\text{calc}} - z_i^{\text{exp}}|$ where z represents T or y and np is the number of data points.

Table 6.11: VLE predictions of alkane + alkanol mixtures with SAFT-VR Mie-GV.

mixture	T/p	2B $\Delta p^{a}/\Delta T^{b}$	2B Δy^{b}	2C $\Delta p^{a}/\Delta T^{b}$	2C Δy^{b}	3B $\Delta p^{a}/\Delta T^{b}$	3B Δy^{b}
methanol + *n*-hexane [172]	343.15 K	3.01	1.81	0.65	1.42	10.92	4.71
methanol + *n*-hexane [203]	303.15 K	5.13	2.62	14.62	9.61	12.37	5.11
methanol + *n*-octane [204]	0.1013 MPa	0.68	0.74	0.35	0.33	2.76	2.24
ethanol + *n*-heptane [175]	333.15 K	1.15	1.01	4.50	2.16	5.57	3.34
ethanol + *n*-heptane [205]	0.1013 MPa	0.81	2.23	0.79	1.07	1.34	1.79
ethanol + *n*-octane [206]	318.15 K	2.41	0.99	7.96	2.18	8.64	2.84
1-propanol + *n*-heptane [175]	333.15 K	–	–	1.00	0.91	–	–
1-propanol + *n*-octane [207]	358.15 K	–	–	2.59	0.61	–	–
2-propanol + *n*-hexane [179]	323.15 K	–	–	0.82	0.54	–	–
2-butanol + *n*-hexane [183]	323.15 K	3.37	2.98	3.28	2.96	3.64	3.09
2-butanol + *n*-heptane [209]	348.15 K	2.59	1.43	2.73	1.40	2.32	1.61
1-pentanol + *n*-heptane [186]	358.15 K	1.11	0.84	1.03	0.83	1.11	0.77
1-pentanol + *n*-hexane [210]	323.15 K	3.98	0.16	3.83	0.13	4.50	0.23
2-pentanol + *n*-heptane [189]	348.15 K	0.81	0.46	1.03	0.40	0.98	0.38
2-pentanol + *n*-heptane [189]	358.15 K	0.78	0.84	0.35	0.60	0.39	0.65
3-pentanol + *n*-heptane [191]	348.15 K	2.95	1.57	1.09	0.65	–	–
3-pentanol + *n*-heptane [191]	358.15 K	3.12	1.70	1.33	0.93	–	–

[a] Deviations in %AAD.
[b] $\Delta z = \sum_i^{np} |z_i^{\text{calc}} - z_i^{\text{exp}}|$ where z represents T or y and np is the number of data points.

SAFT-VR Mie predictions are more accurate than those of sPC-SAFT, as shown by example in Fig. 6.11. The treatment of dispersion forces in light of strong association seems to have a better balance in the SAFT-VR Mie framework than it does in the sPC-SAFT framework. The inclusion of a polar term to the SAFT-VR Mie framework provides the slight improvement required to give an excellent prediction of the phase equilibrium behaviour, as shown in Fig. 6.12(b). In both the sPC-SAFT and SAFT-VR Mie frameworks, polar interactions need to be accounted for explicitly to obtain improved predictions of binary alkane + alkanol VLE, although the magnitude of the improvement is relatively small.

The exception is observed for 3-pentanol (Fig. 6.13), where excellent description of VLE behaviour in alkanes is obtained with the nonpolar models, while the addition of a polar term gives worse results. This is the case for both sPC-SAFT and SAFT-VR Mie and attests to the reduced polar contribution for 3-pentanol.

The choice of association scheme yields different predictions for both sPC-SAFT and SAFT-VR Mie for the short-chain alkanols (Fig. 6.14). However, the difference between the three schemes' predictions becomes smaller as the chain length of the alkanol increases (see Fig. 6.12). This indicates that, as the length of the carbon chain increases, the longer alkyl chain dilutes the association effect, causing the association contribution to become less significant.

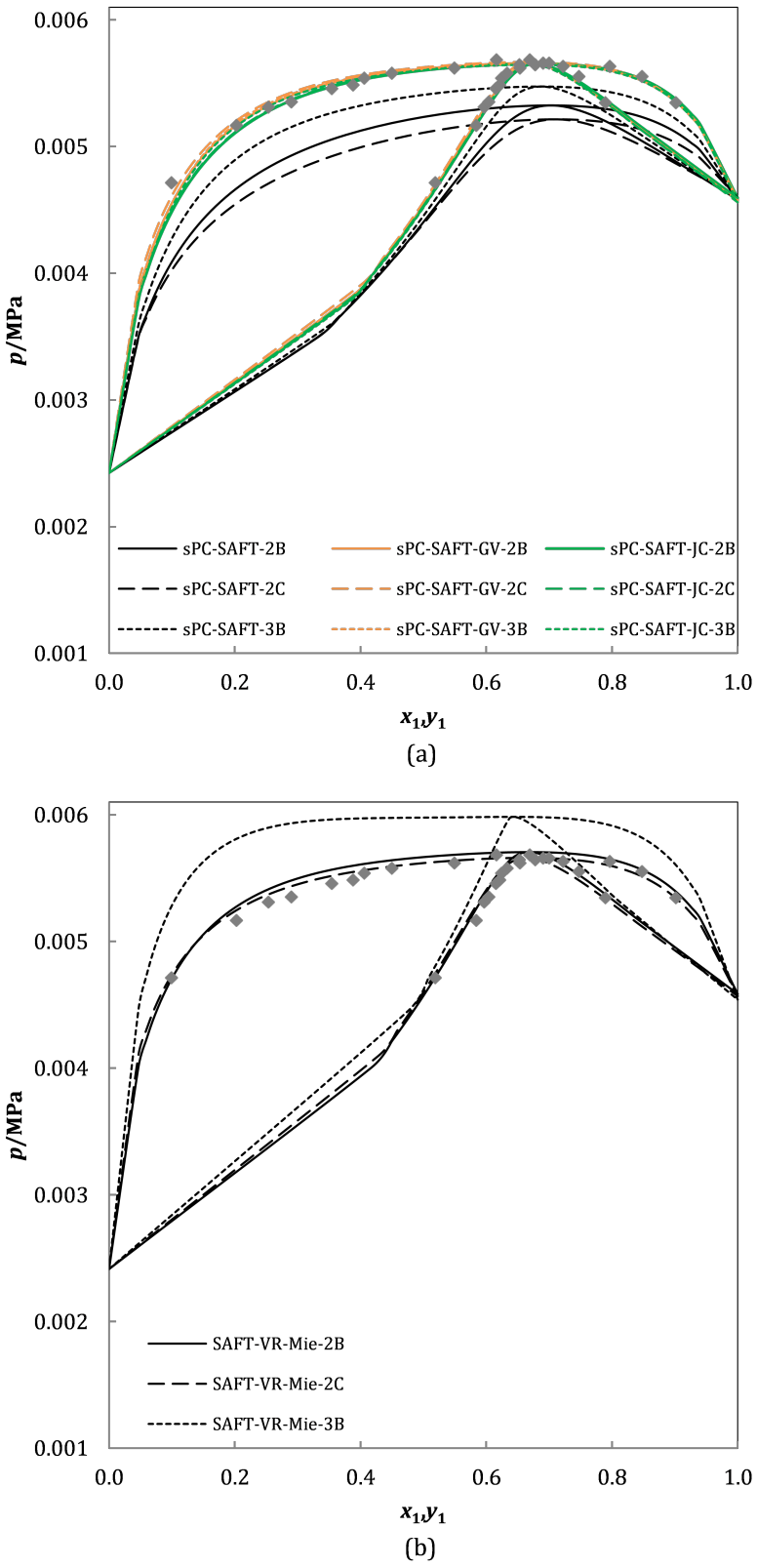

Figure 6.11: VLE of 1-butanol (1) + *n*-nonane (2) at T = 323.15 K predicted by (a) sPC-SAFT; (b) SAFT-VR Mie. Data taken from Heintz, et al. [181].

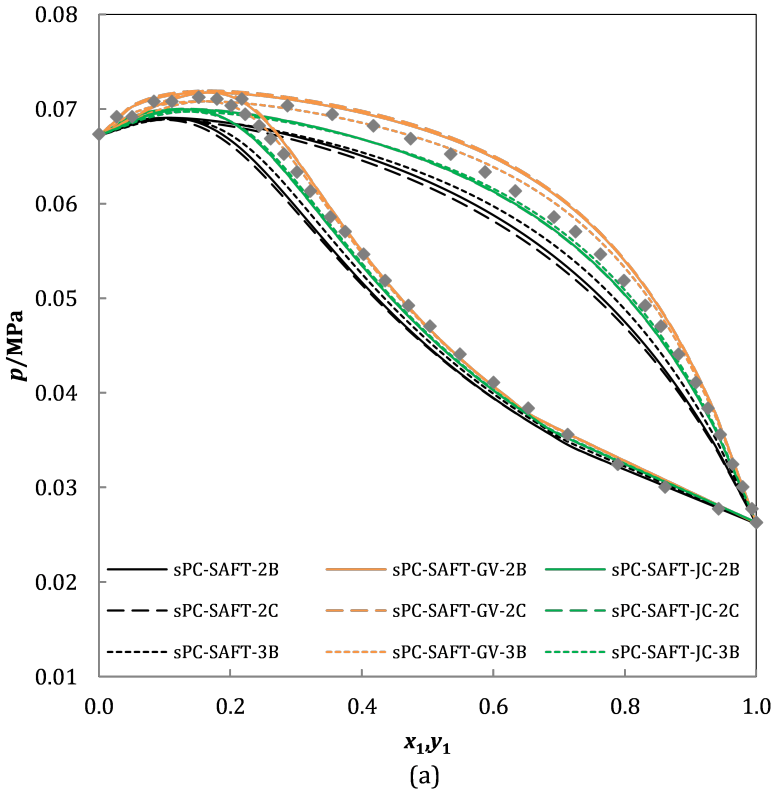

(a)

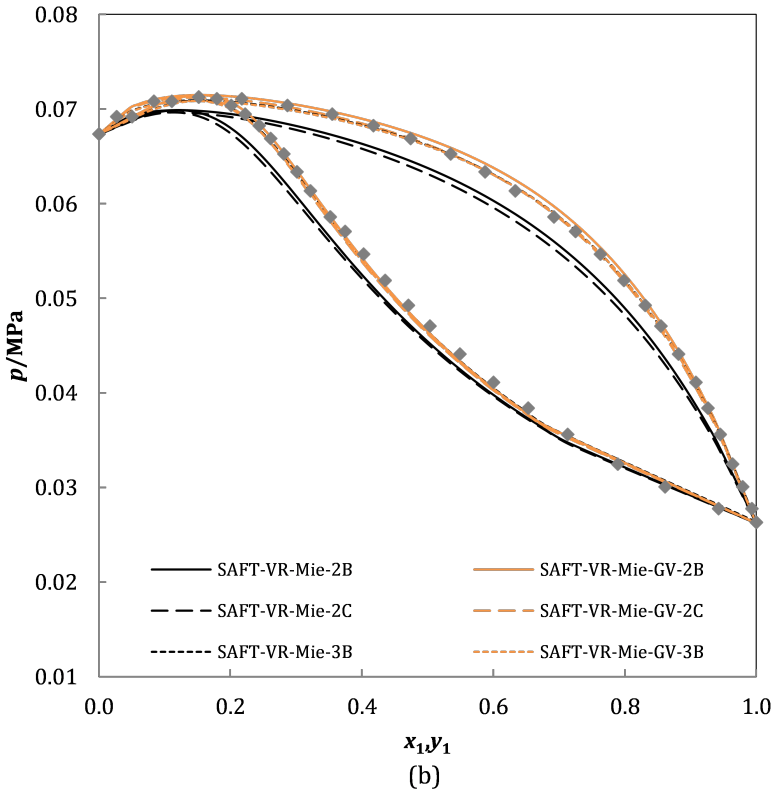

(b)

Figure 6.12: VLE of 2-pentanol (1) + n-heptane (2) at T = 358.15 K predicted by (a) sPC-SAFT; (b) SAFT-VR Mie. Data taken from Wolfova, et al. [189].

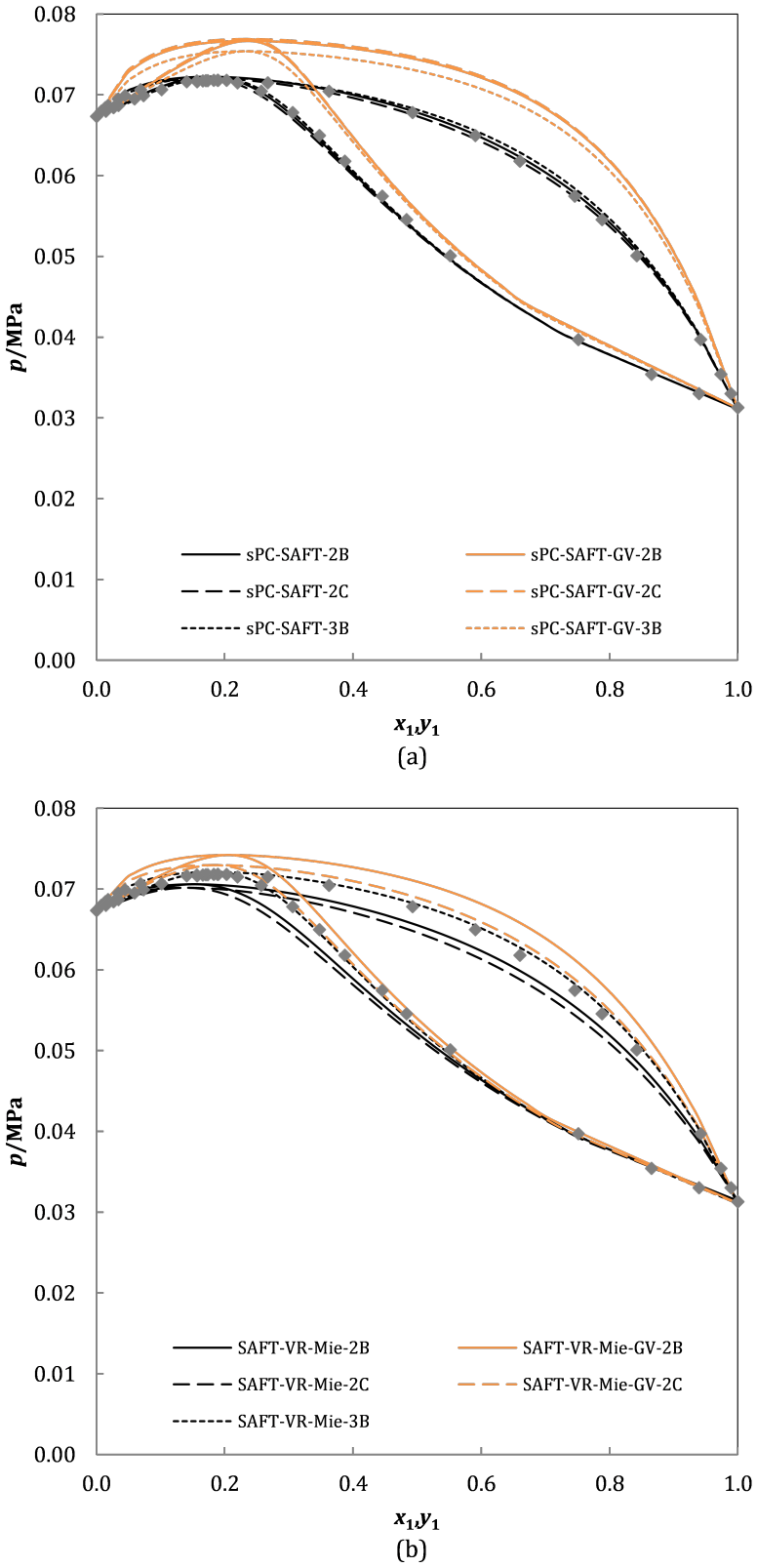

Figure 6.13: VLE of 3-pentanol (1) + n-heptane (2) at T = 358.15 K predicted by (a) sPC-SAFT; (b) SAFT-VR Mie. Data taken from Wolfova, et al. [191].

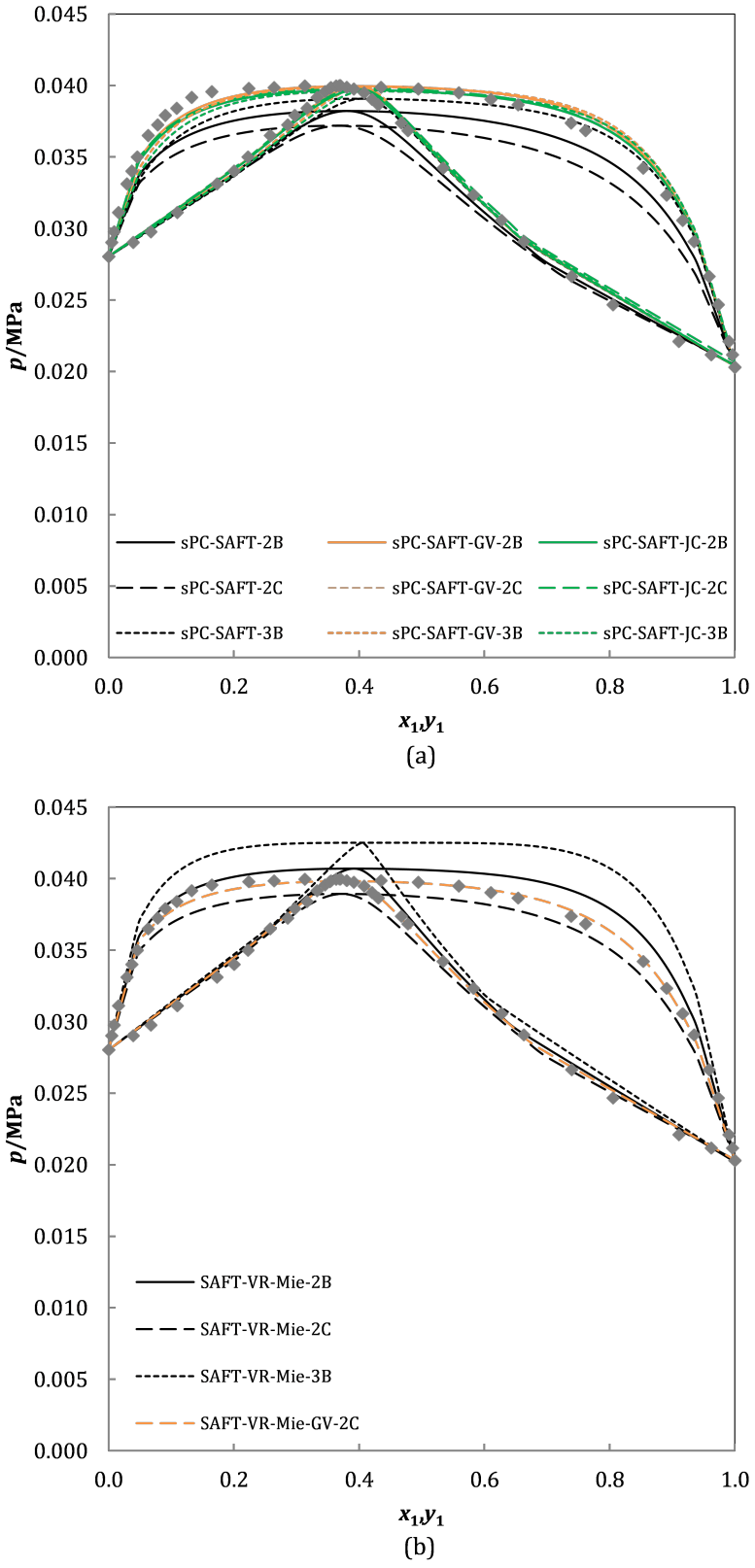

Figure 6.14: VLE of 1-propanol (1) + *n*-heptane (2) at T = 333.15 MPa predicted by (a) sPC-SAFT; (b) SAFT-VR Mie. Data taken from Pena and Cheda [175].

The choice of association scheme becomes almost irrelevant for the polar models, since predictions with each of the three schemes are almost indistinguishable. This indicates that the association contribution predicted by each of the schemes becomes similar when polarity is accounted for explicitly, rendering the choice of association scheme arbitrary.

It is reassuring to note that the description of secondary alkanols in alkane mixtures (e.g. Figs. 6.12 and 6.13) is similar to those of primary alkanols in alkane mixtures (e.g. Figs. 6.11 and 6.14), over all the EoS variants considered in this investigation. This provides confidence that the SAFT framework can distinguish between structural isomers of linear alkanols.

6.4.2 Excess Thermodynamic Properties

Although the description of excess properties is not the main focus of this investigation, the application of both the sPC-SAFT and SAFT-VR Mie models to these properties is investigated. The aim of this analysis is to evaluate the holistic predictive capability of the EoSs and whether the model parameters presented in Section 6.2 can be extended to modelling excess properties as well. Three excess properties, namely excess enthalpy, h^{E}, excess volume, V^{E}, and excess isobaric heat capacity, c_p^{E}, are discussed.

Information regarding excess properties that were evaluated in this discussion is summarised in Table 6.12. Where no reference is given, no data were found for the property in question.

Table 6.12: References for the available excess property literature data.

	alkanes			water		
	h^{E}	V^{E}	c_p^{E}	h^{E}	V^{E}	c_p^{E}
methanol	*n*-pentane [211]	*n*-pentane [212]	*n*-heptane [213]	[214]	[215]	[216]
ethanol	*n*-heptane [217]	*n*-heptane [218]	*n*-heptane [219]	[220]	[221]	[216]
1-propanol	*n*-heptane [222]	*n*-heptane [218]	*n*-heptane [219]	[223]	[224]	[216]
2-propanol	*n*-heptane [225]	*n*-octane [226]	*n*-heptane [227]	[214]	[224]	–
1-butanol	*n*-hexane [228]	*n*-heptane [218]	*n*-heptane [213]	[229]	[224]	[230]
2-butanol	–	*n*-heptane [227]	*n*-heptane [227]	[229]	[224]	–
1-pentanol	*n*-heptane [231]	*n*-heptane [232]	*n*-heptane [213]	[229]	–	–
2-pentanol	*n*-heptane [233]	*n*-heptane [227]	*n*-heptane [227]	[229]	–	–
3-pentanol	–	*n*-heptane [227]	*n*-heptane [227]	–	–	–

6.4.2.1 Excess Enthalpy

Excess enthalpy, which is equal to heat of mixing, remains an important property in process design, deeming accurate description of this property essential. Excess enthalpy gives an indication of the molecular interactions involved during a mixing process. During mixing of components, interactions between *like* molecules are disrupted by the attraction formed between *unlike* molecules [3, 44]. If *like* interactions are stronger than *unlike* interactions, energy is required to break *like* interactions, and subsequently the mixing process is endothermic, resulting in a positive excess enthalpy. Conversely, if *unlike* interactions are stronger than *like* interactions, the mixing process occurs exothermically and the excess enthalpy is negative [3, 44].

Mathematically, excess enthalpy is expressed as [46]:

$$h^{\mathrm{E}} = h^{\mathrm{r}}(T,p,n) - \sum_i x_i h_i^{\mathrm{r}}(T,p,n_i) \tag{6.8}$$

$$h_i^{\mathrm{r}}(T,p,n_i) = -RT^2\left(\frac{\partial F}{\partial T}\right)_{V,n} + pV - nRT \tag{6.9}$$

From Eq. 6.9 it is evident that adequate description of h^{E} is dependent on accurate description of the first-order temperature derivative of the state function.

Generally the qualitative description of h^{E} is good for all models considered; however, most of the models' predictions overshoot the experimental data (Figs. 6.15 and 6.16). For most systems, SAFT-VR Mie predictions are equal to, or better than sPC-SAFT predictions, providing quantitative results that are closer to experimental values (Fig. 6.15(b)). This might be a result of a slightly better temperature description brought about by the third-order perturbation term included in SAFT-VR Mie, as opposed to the second-order expansion used in sPC-SAFT.

Polar predictions are almost always worse than their nonpolar counterparts (Figs. 6.15 and 6.16). This indicates that excess enthalpy, much like enthalpy of vaporisation, is governed by association effects [43, 162], rather than polar effects.

When considering the association schemes, the 2C scheme generally provides the closest representation of experimental data (Fig. 6.15). The excess enthalpy of several systems were investigated (see Table 6.12) and it is concluded that the good fit obtained by sPC-SAFT-3B in Fig. 6.16(a) is merely coincidental.

The qualitatively good predictions for excess enthalpy of alkane + alkanol mixtures are obtained with parameter sets geared to predict VLE behaviour, therefore these fits are largely coincidental.

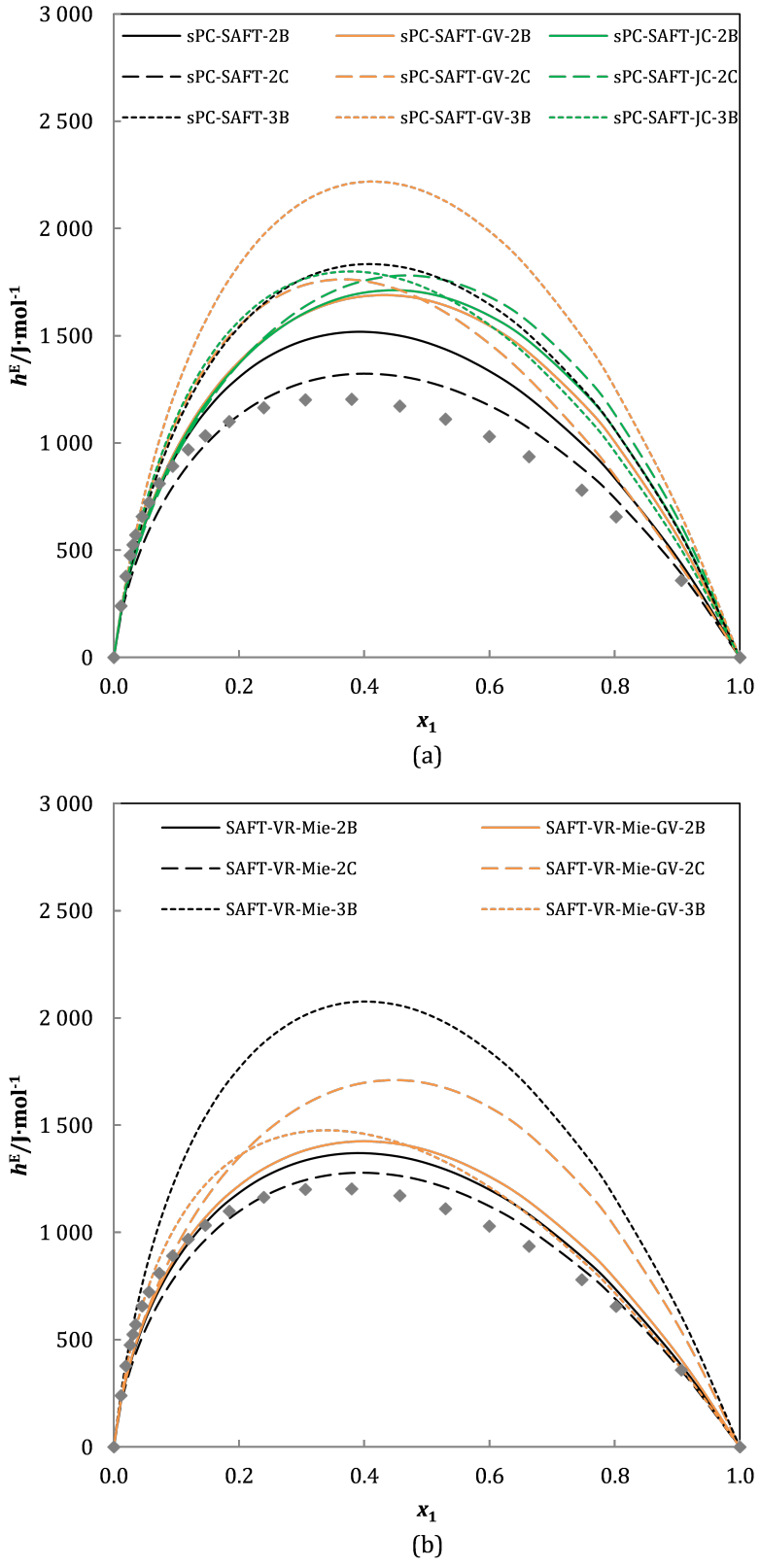

Figure 6.15: Excess enthalpy of ethanol (1) + n-heptane (2) at T = 333.15 K and p = 0.1013 MPa predicted by (a) sPC-SAFT; (b) SAFT-VR Mie. Data taken from van Ness, et al. [217].

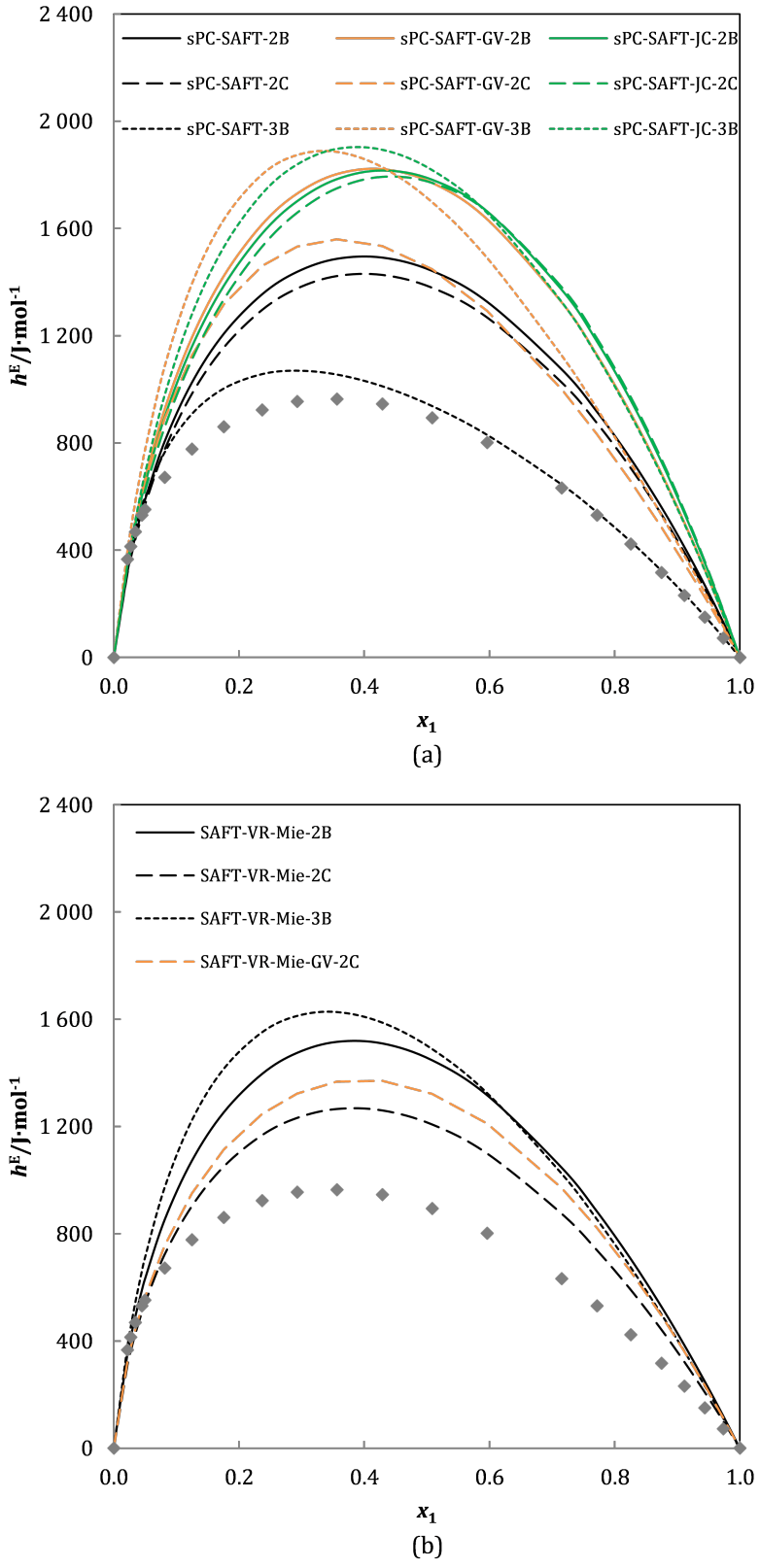

Figure 6.16: Excess enthalpy of 1-propanol (1) + n-heptane (2) at T = 318.15 K and p = 0.1013 MPa predicted (a) by sPC-SAFT; (b) SAFT-VR Mie. Data taken from Savini, et al. [222].

6.4.2.2 Excess Volume

Excess volume describes how the volume of a mixture changes due to the manner in which molecules pack together when different components are mixed. A negative excess volume indicates that the *unlike* interactions "pull" the mixture species closer together, therefore molecules are more closely packed in mixture than they are as pure components [44]. Mathematically the excess volume is described as [46]:

$$V^{\mathrm{E}} = V^{\mathrm{r}}(T, p, n) - \sum_i x_i V_i^{\mathrm{r}}(T, p, n_i) \tag{6.10}$$

From Eq. 6.10 it is apparent that excess volume is strongly dependent on the first-order volume derivative of the state function (see Fig. 6.1). For accurate V^{E} description, the pure component and mixture volume derivatives of the state function need to be accurate. Given that the description of ρ_i^{sat}, and therefore pure component volume derivative, is very good for all the models (see Section 6.3), prediction of V^{E} evaluates the mixture volume derivative.

V^{E} of both primary and secondary alkanol mixtures is poorly described by all models (Figs. 6.17 and 6.18). Generally the property is parabolic in shape; however, as the chain length increases, predictions quickly become sinusoidal, indicating that the behaviour observed during experimentation is not captured by any of the EoSs. The sPC-SAFT and SAFT-VR Mie frameworks therefore struggle to describe the first-order volume derivative of the mixture. Moreover, the prediction quality is not dependent on the choice of association scheme.

It is stressed that only pure component data, and in the case of the polar models, binary VLE data, were used to determine pure component parameter sets, therefore the prediction of excess properties is not guaranteed.

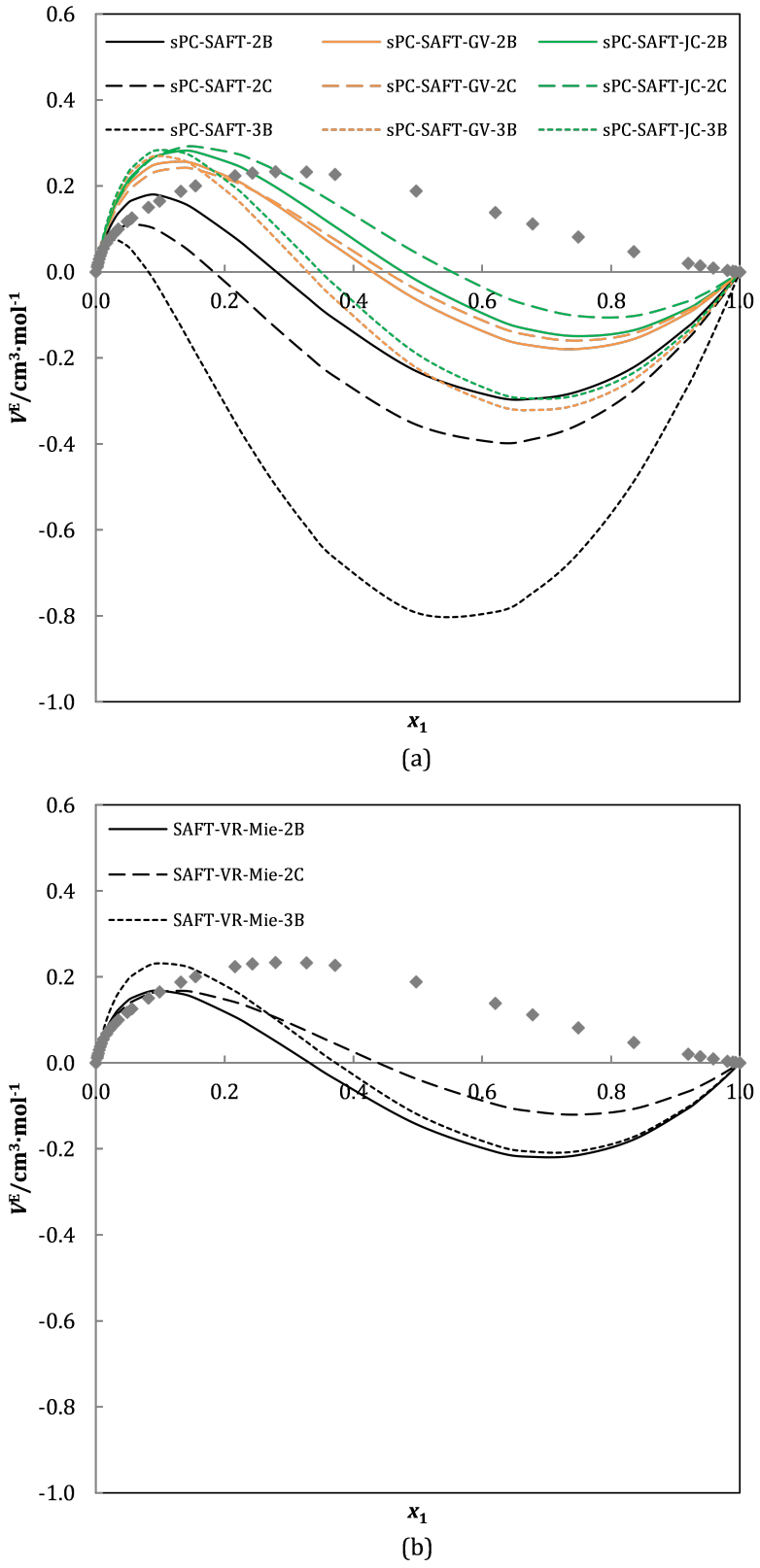

Figure 6.17: Excess volume of 1-butanol (1) + n-heptane (2) at T = 298 K and p = 0.1013 MPa predicted by (a) sPC-SAFT; (b) SAFT-VR Mie. Data taken from Treszczanowicz and Benson [218].

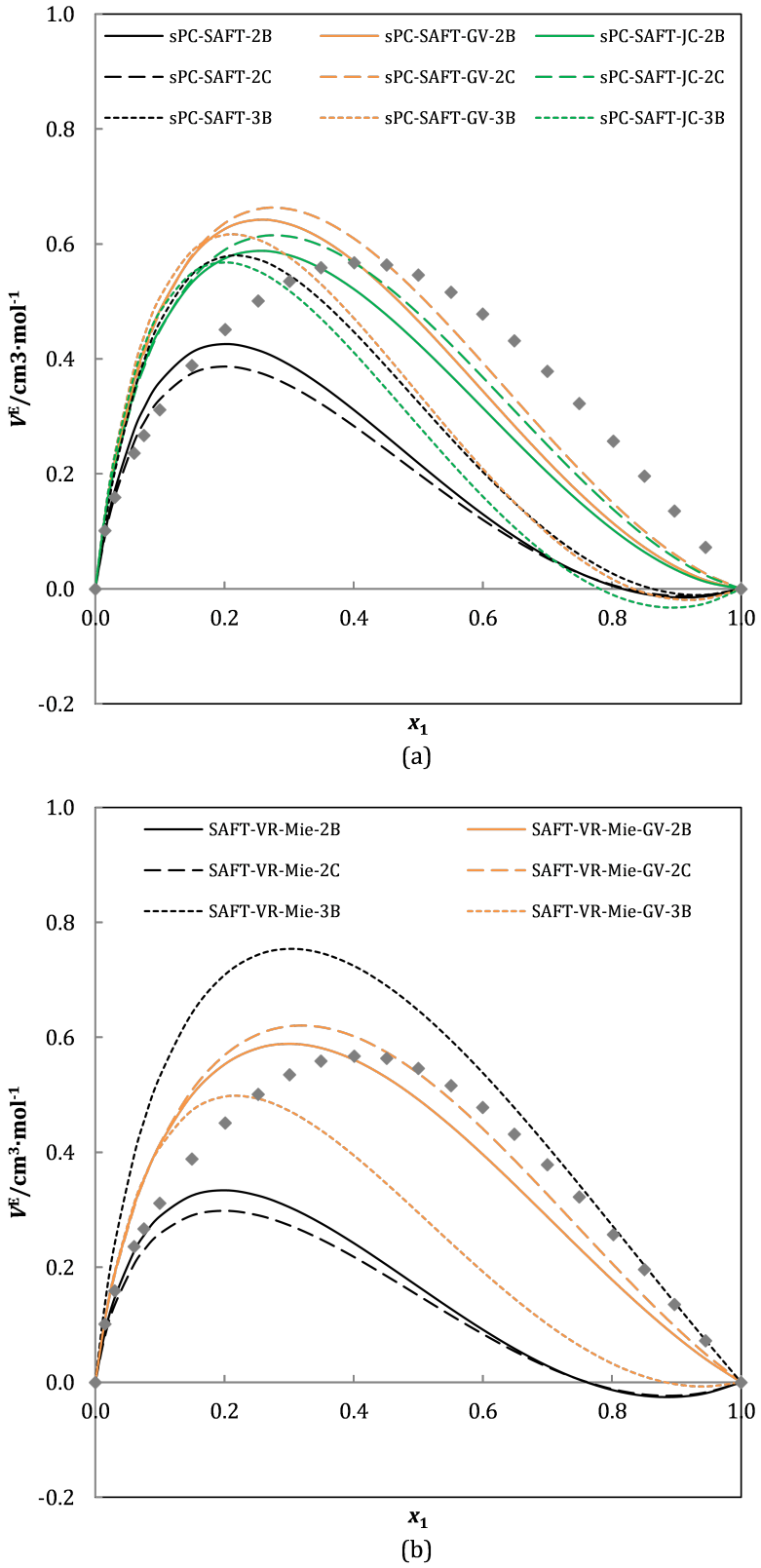

Figure 6.18: Excess volume of 2-butanol (1) and n-heptane (2) at T = 298.15 K and p = 0.1013 MPa predicted by (a) sPC-SAFT; (b) SAFT-VR Mie. Data taken from Tanaka and Toyama [227].

6.4.2.3 Excess Isobaric Heat Capacity

The excess isobaric heat capacity is expressed analogous to its excess enthalpy and excess volume counterparts:

$$c_p^{\mathrm{E}} = c_p^{\mathrm{r}}(T,p,n) - \sum_i x_i c_{p,i}^{\mathrm{r}}(T,p,n_i) \tag{6.11}$$

$c_{p,i}^{\mathrm{r}}$ is determined by Eqs. 6.4 to 6.6, reprinted here for ease of reference:

$$\frac{c_p^{\mathrm{r}}}{R} = -\frac{T}{R}\frac{\left(\frac{\partial p}{\partial T}\right)_{V,n}^2}{\left(\frac{\partial p}{\partial V}\right)_{T,n}} - n - T^2\left(\frac{\partial^2 F}{\partial T^2}\right)_{V,n} - 2T\left(\frac{\partial F}{\partial T}\right)_{V,n} \tag{6.4}$$

$$\left(\frac{\partial p}{\partial T}\right)_{V,n} = -RT\left(\frac{\partial^2 F}{\partial T \partial V}\right)_{V,n} + \frac{p}{T} \tag{6.5}$$

$$\left(\frac{\partial p}{\partial V}\right) = -RT\left(\frac{\partial^2 F}{\partial V^2}\right)_{V,n} - \frac{nRT}{V^2} \tag{6.6}$$

Investigating the prediction of c_p^{E} therefore provides a stringent evaluation of an EoS's ability to describe the second-order temperature derivatives of pure components and their mixtures.

For alkane + alkanol mixtures, the shape of c_p^{E} is parabolic for the C_1-C_3 alkanol mixtures (Fig. 6.19), and becomes "m"-shaped as the chain length of the alkanol increases (Fig. 6.20). However, the model predictions for all mixtures are parabolic, therefore the models are all able to capture the qualitative behaviour of c_p^{E} for the C_1-C_3 alkanol mixtures (e.g. Fig. 6.19), but are unable to describe the interactions between alkane and alkanol molecules observed in the c_p^{E} for C_4 and C_5 alkanol mixtures (e.g. Fig. 6.20).

It is evident from Figs. 6.19 and 6.20 that all model predictions with the 3B association scheme overshoots experimental data. This indicates that the 3B scheme overestimates the degree of association that occurs between the alkanol molecules. The excess isobaric heat capacity of several alkane + alkanol mixtures were investigated, and it is concluded that the good fit obtained by sPC-SAFT-3B in Fig. 6.19 is coincidental. In all of the mixtures investigated, the 2B and 2C schemes provide similar predictions for each of the models, indicating that the description of association obtained by the 2B and 2C association schemes is very similar for this property.

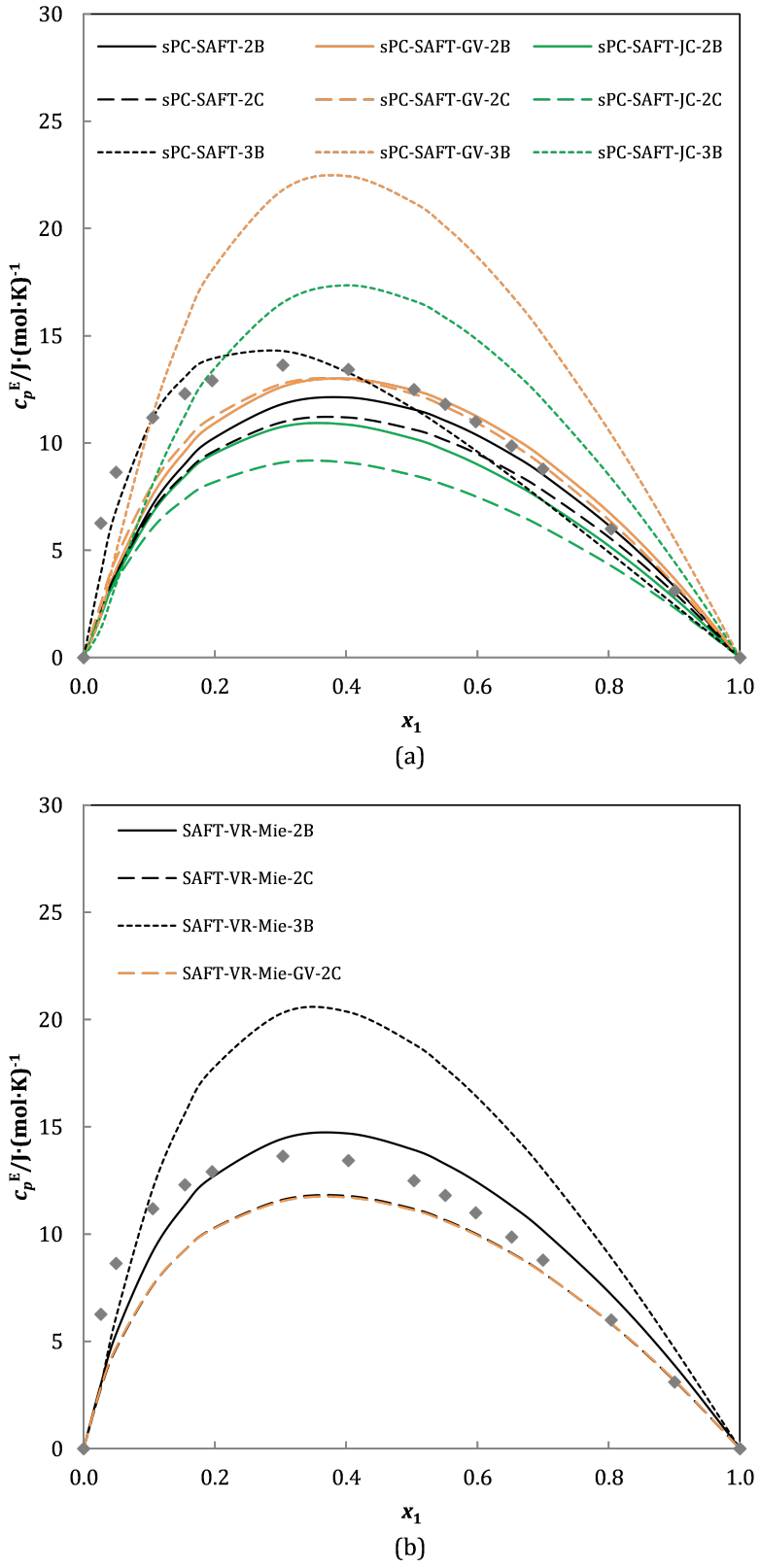

Figure 6.19: Excess isobaric heat capacity of 1-propanol (1) + n-heptane (2) at T = 298 K and p = 0.1013 MPa predicted by (a) sPC-SAFT; (b) SAFT-VR Mie. Data taken from Fortier and Benson [219].

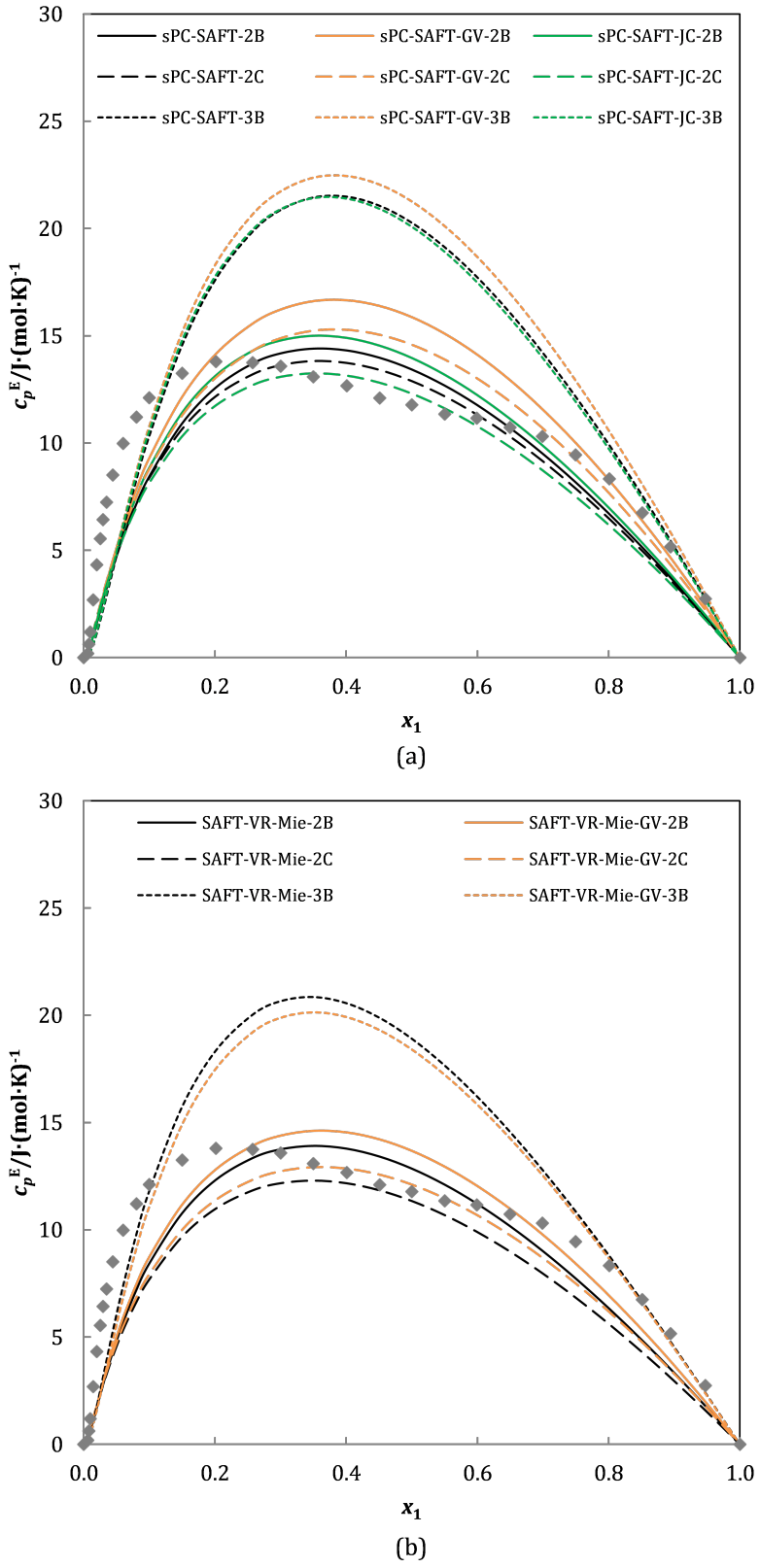

Figure 6.20: Excess isobaric heat capacity of 2-pentanol (1) + n-heptane (2) at T = 298 K and p = 0.1013 MPa predicted by (a) sPC-SAFT; (b) SAFT-VR Mie. Data taken from Tanaka and Toyama [227].

6.4.3 Section Highlights

sPC-SAFT and SAFT-VR Mie give equally good qualitative description of alkane + alkanol VLE behaviour. SAFT-VR Mie predictions, however, are quantitatively more accurate than those obtained by sPC-SAFT. sPC-SAFT-GV and sPC-SAFT-JC provide significantly improved predictions for alkane + alkanol VLE compared to sPC-SAFT. Similarly, the results obtained by SAFT-VR Mie-GV are slightly better than their SAFT-VR Mie counterparts. This indicates that the contribution of polar effects to the phase equilibrium behaviour in alkane + alkanol mixtures is significant enough that it needs to be accounted for explicitly in both the sPC-SAFT and SAFT-VR Mie frameworks.

It is emphasised that the results obtained for the excess properties are by-products of parameters geared at predicting VLE behaviour. The predictions that are obtained give a holistic view of the predictive capability of the sPC-SAFT and SAFT-VR Mie model frameworks, using VLE centric parameter sets. The qualitative description of h^{E} and c_p^{E} obtained by each of the models is generally very good. However, accuracy is lacking in most cases. Moreover, the predictions of V^{E} are very poor. These description flaws indicate that both sPC-SAFT and SAFT-VR Mie require further refinement before accurate description of thermodynamic properties other than phase equilibrium can be achieved.

6.5 Binary Water + Alkanol Mixtures

The focus now shifts to mixtures in which association occurs between both *like* molecules and *unlike* molecules, termed self-association and cross-association, respectively. The description of this type of phase interaction remains a challenging task for any EoS [33]. Furthermore, it is also necessary to evaluate whether polar effects have a significant contribution to the mixture energy which need to be accounted for explicitly. The prediction of mixture properties is investigated, with the knowledge that only pure component property data was included during regression of sPC-SAFT and SAFT-VR Mie parameters, and binary VLE data with alkanes was included during regression of sPC-SAFT-GV, sPC-SAFT-JC, and SAFT-VR Mie-GV parameters.

The 4C association scheme is used for water throughout this investigation. The legends in Figs. 6.21 to 6.34 refer to the association scheme of the alkanol.

No binary interaction parameters are considered, therefore the analysis is based on pure predictions.

Table 6.13: VLE predictions of water + alkanol mixtures with sPC-SAFT, sPC-SAFT-GV, and sPC-SAFT-JC.

mixture	T/p	2B $\Delta p^{a}/\Delta T^{b}$	2B Δy^{b}	2C $\Delta p^{a}/\Delta T^{b}$	2C Δy^{b}	3B $\Delta p^{a}/\Delta T^{b}$	3B Δy^{b}
sPC-SAFT							
methanol + water [111]	333.15 K	17.39	3.37	3.43	0.66	11.21	3.62
methanol + water [112]	0.1013 MPa	2.80	3.15	0.25	0.56	2.47	3.23
ethanol + water [111]	333.15 K	8.41	2.71	0.38	0.99	8.51	3.61
ethanol + water [115]	0.1013 MPa	2.59	3.74	0.45	0.68	2.67	4.36
1-propanol + water [118]	333.15 K	7.00	1.79	1.47	1.65	8.18	4.08
1-propanol + water [119]	0.1013 MPa	1.07	2.23	0.98	1.80	2.28	4.38
2-propanol + water [121]	0.1013 MPa	3.61	6.11	1.65	3.04	0.80	0.94
1-butanol + water	0.1013 MPa	1.96	2.35	0.93	2.83	1.39	3.31
2-butanol + water [141]	0.1013 MPa	4.14	7.28	1.95	3.49	1.53	2.49
1-pentanol + water	0.1013 MPa	2.40	2.99	1.62	4.75	2.05	5.89
2-pentanol + water	0.1013 MPa	2.95	6.74	1.67	4.41	1.71	5.67
3-pentanol + water	0.1013 MPa	5.08	12.32	3.74	9.85	3.35	8.15
sPC-SAFT-GV							
methanol + water [111]	333.15 K	18.72	3.68	1.58	0.73	6.28	1.99
methanol + water [112]	0.1013 MPa	3.03	3.46	0.27	0.81	1.53	1.82
ethanol + water [111]	333.15 K	9.43	3.25	0.50	0.88	5.79	3.27
ethanol + water [115]	0.1013 MPa	2.90	4.40	0.40	0.56	2.07	3.98
1-propanol + water [118]	333.15 K	8.31	2.29	0.89	1.30	6.29	3.27
1-propanol + water [119]	0.1013 MPa	1.47	3.09	0.80	1.33	1.73	3.11
2-propanol + water [121]	0.1013 MPa	3.50	5.88	1.48	2.71	1.40	1.91
1-butanol + water	0.1013 MPa	2.20	1.90	1.09	2.56	0.82	2.74
2-butanol + water [141]	0.1013 MPa	4.38	8.12	1.89	3.79	0.92	1.37
1-pentanol + water	0.1013 MPa	2.55	2.31	1.61	4.04	1.53	4.87
2-pentanol + water	0.1013 MPa	3.90	9.09	2.16	5.54	1.46	4.74
3-pentanol + water	0.1013 MPa	5.02	11.73	3.33	9.19	2.79	7.39
sPC-SAFT-JC							
methanol + water [111]	333.15 K	19.05	3.70	1.61	0.85	7.26	2.35
methanol + water [112]	0.1013 MPa	3.08	3.48	0.28	0.95	1.74	2.14
ethanol + water [111]	333.15 K	9.17	3.10	0.34	1.07	4.42	2.23
ethanol + water [115]	0.1013 MPa	2.79	4.11	0.48	0.77	1.33	2.38
1-propanol + water [118]	333.15 K	9.15	2.45	1.03	1.17	3.08	2.08
1-propanol + water [119]	0.1013 MPa	1.56	3.19	0.65	1.35	1.13	2.06
1-butanol + water	0.1013 MPa	2.26	1.99	1.23	2.73	0.85	2.83
2-butanol + water [141]	0.1013 MPa	4.69	8.98	2.04	4.46	0.75	1.31
1-pentanol + water	0.1013 MPa	2.73	2.60	1.66	4.01	1.52	4.98
2-pentanol + water	0.1013 MPa	4.34	9.88	2.40	5.95	1.39	4.58

[a] Deviations in %AAD.
[b] $\Delta z = \sum_i^{np} |z_i^{\text{calc}} - z_i^{\text{exp}}|$ where z represents T or y and np is the number of data points.

Table 6.14: VLE predictions of water + alkanol mixtures with SAFT-VR Mie.

mixture	T/p	2B $\Delta p^{a}/\Delta T^{b}$	2B Δy^{b}	2C $\Delta p^{a}/\Delta T^{b}$	2C Δy^{b}	3B $\Delta p^{a}/\Delta T^{b}$	3B Δy^{b}
methanol + water [111]	333.15 K	21.94	4.09	10.56	2.03	13.65	4.20
methanol + water [112]	0.1013 MPa	3.55	3.87	1.45	1.34	2.84	3.71
ethanol + water [111]	333.15 K	17.60	5.68	8.84	2.84	11.64	5.00
ethanol + water [115]	0.1013 MPa	5.07	7.38	2.36	3.17	3.55	6.07
1-propanol + water [118]	333.15 K	9.93	2.90	3.79	1.07	13.10	5.81
1-propanol + water [119]	0.1013 MPa	1.82	3.66	0.62	1.54	3.06	5.91
2-propanol + water [121]	0.1013 MPa	3.81	6.30	1.41	2.56	1.06	2.50
1-butanol + water	0.1013 MPa	2.45	2.40	1.07	2.95	2.15	4.14
2-butanol + water [141]	0.1013 MPa	3.26	5.78	0.83	2.39	4.10	8.64
1-pentanol + water	0.1013 MPa	3.90	3.54	1.96	3.99	1.79	5.67
2-pentanol + water	0.1013 MPa	3.12	6.13	1.66	5.13	2.84	8.08
3-pentanol + water	0.1013 MPa	6.48	11.69	3.72	8.39	2.17	6.37

[a] Deviations in %AAD.
[b] $\Delta z = \sum_i^{np} |z_i^{\text{calc}} - z_i^{\text{exp}}|$ where z represents T or y and np is the number of data points.

6.5.1 Vapour-Liquid Equilibria

The results for the VLE of water + alkanol mixtures investigated in this study are summarised in Tables 6.13 and 6.14.

VLE predictions of aqueous alkanol mixtures are achieved with all models except SAFT-VR Mie-GV. Predictions obtained with SAFT-VR Mie-GV are unsatisfactory (see Fig. 6.21), therefore SAFT-VR Mie-GV is excluded from this discussion.

Shown in Figs. 6.22 to 6.24 are the VLE of three primary alkanols in water. Immediately apparent is that SAFT-VR Mie predictions are much less accurate than those obtained by the sPC-SAFT models. For the water + 1-butanol mixture (Fig. 6.23), SAFT-VR Mie-3B does not predict VLLE behaviour, and does therefore not capture the molecular interactions of this mixture. The SAFT-VR Mie predictions which are closest to experimental values are obtained with the 2C association scheme (Figs. 6.22 to 6.24).

In each of the models (sPC-SAFT, sPC-SAFT-GV, sPC-SAFT-JC, SAFT-VR Mie) the choice of association scheme delivers different predictions (Figs. 6.22 to 6.24), indicating that the phase behaviour is strongly dependent on association and how associative behaviour is described. sPC-SAFT-GV-XX and sPC-SAFT-JC-XX predictions are similar to sPC-SAFT-XX predictions, where XX is either the 2B or 2C association scheme (Figs. 6.22 to 6.24). This indicates that, compared to the association contribution, the polar contribution to the mixture energy is small. When using the 3B scheme the difference between the sPC-SAFT, sPC-SAFT-GV, and sPC-SAFT-JC predictions is more prominent (Figs. 6.22 to 6.24). This illustrates that, when a larger degree of association is described, as is achieved with the 3B association scheme, the polar contribution is significant enough to yield different predictions.

As stated previously, the polar contribution to the aqueous primary alkanol mixtures, modelled with the 2B or 2C association schemes, is small. However, based on %AAD values (see Table 6.13) the best predictions for the aqueous primary alkanol mixtures are obtained by sPC-SAFT-GV, followed closely by sPC-SAFT-JC. Having said that, the improvement gained by the polar models does not justify the inclusion of a polar term. In light of strong association, the contribution from polar interactions is small and does not necessarily need to be accounted for explicitly.

Based on %AAD values, the primary alkanol mixtures are best represented with the 2C association scheme in all models. This is also apparent from the model predictions shown in Figs. 6.22 to 6.24.

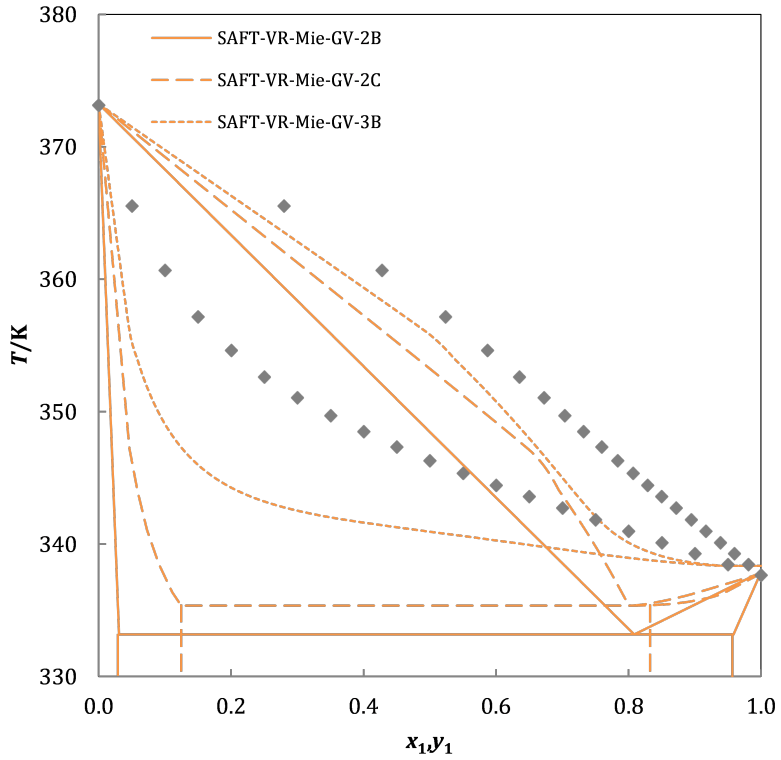

(a)

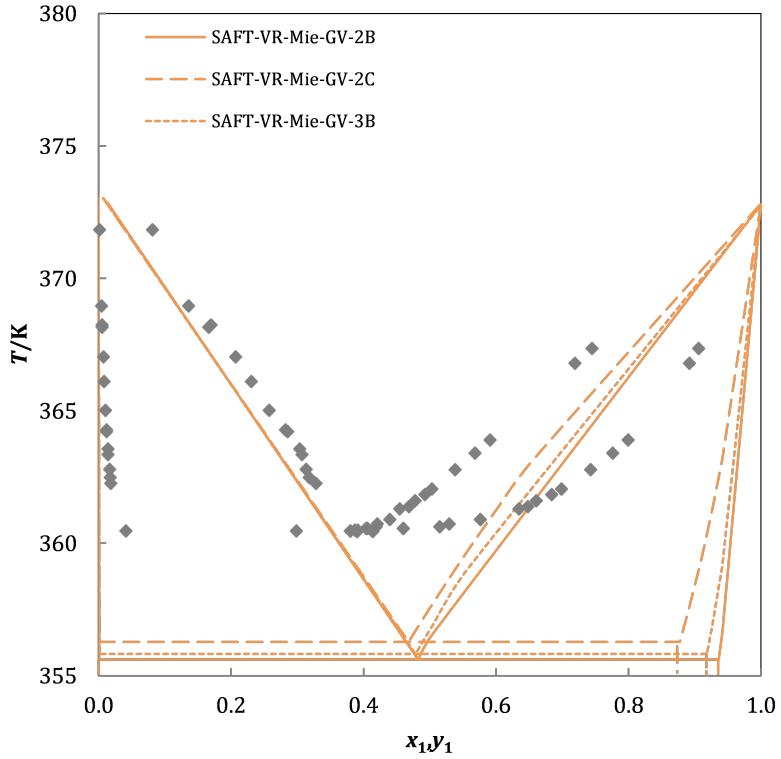

(b)

Figure 6.21: SAFT-VR Mie-GV predictions for VLE of (a) methanol (1) + water (2) at p = 0.1013 MPa. Data taken from Kojima, et al. [112]; (b) 2-butanol (1) + water (2) at p = 0.1013 MPa. Data taken from Iwakabe and Kosuge [141].

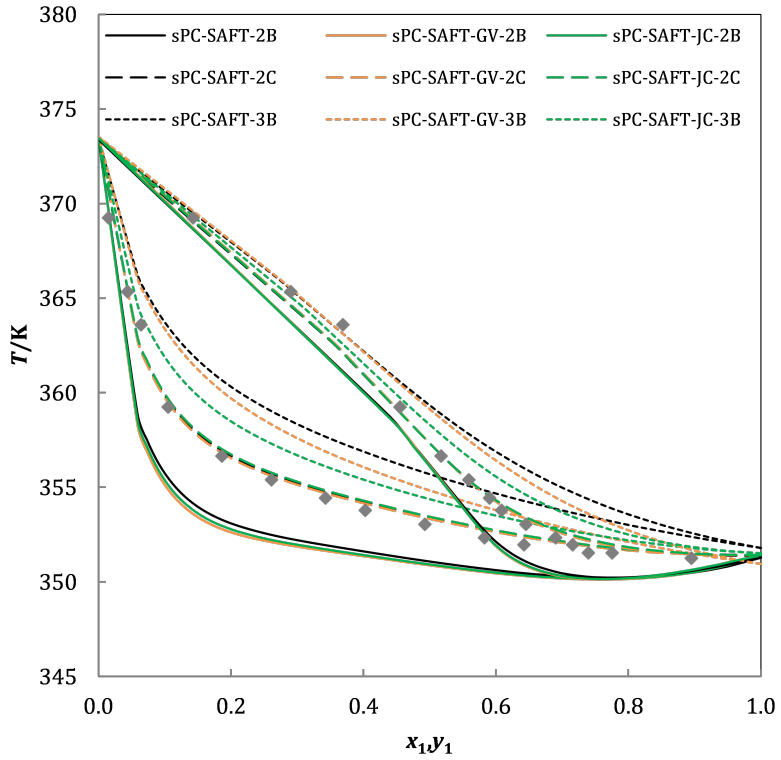

Figure 6.22: VLE of ethanol (1) + water (2) at p = 0.1013 MPa predicted by (a) sPC-SAFT; (b) SAFT-VR Mie. Data taken from Danner and Gess [115].

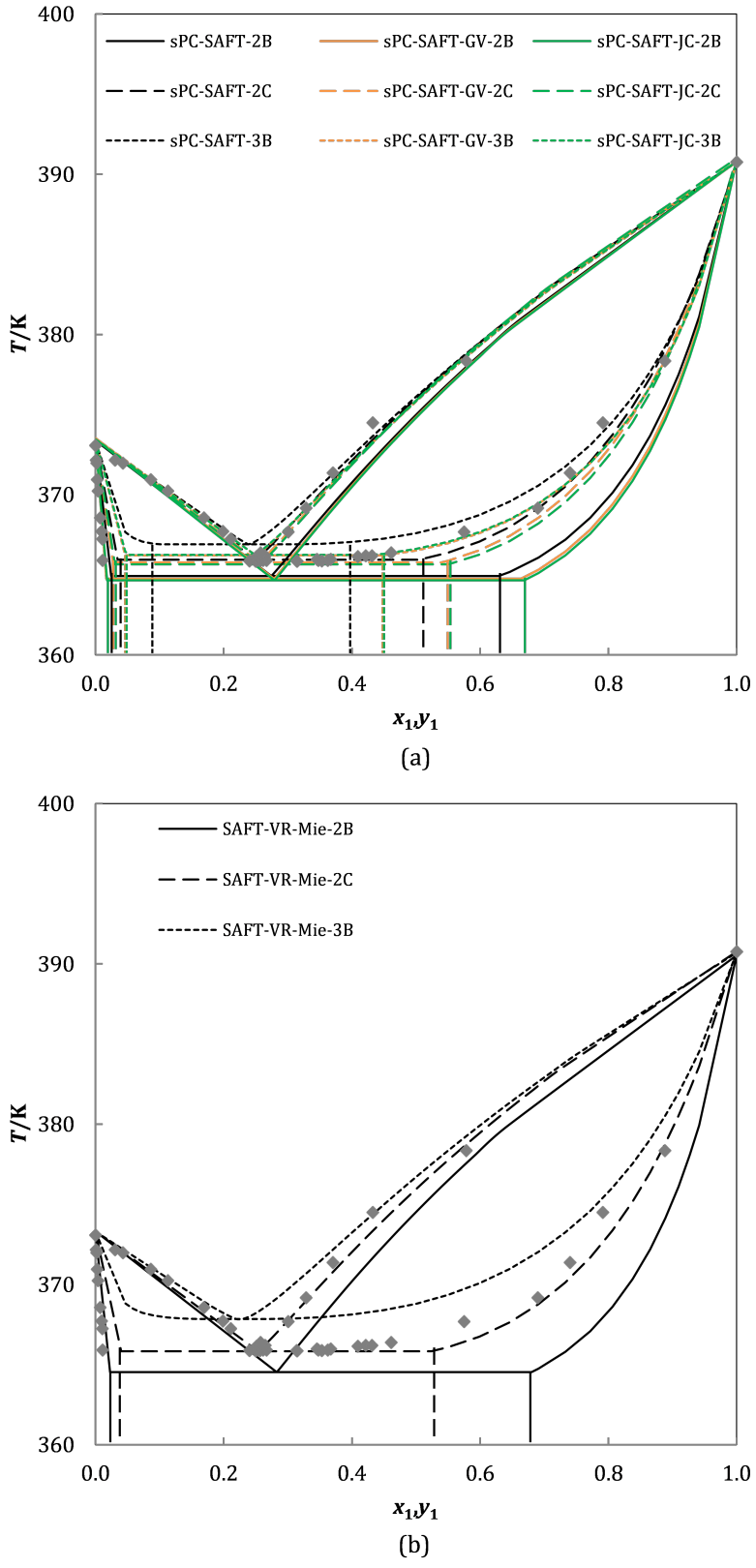

Figure 6.23: VLE of 1-butanol (1) + water (2) at p = 0.1013 MPa predicted by (a) sPC-SAFT; (b) SAFT-VR Mie. Experimental data from this work.

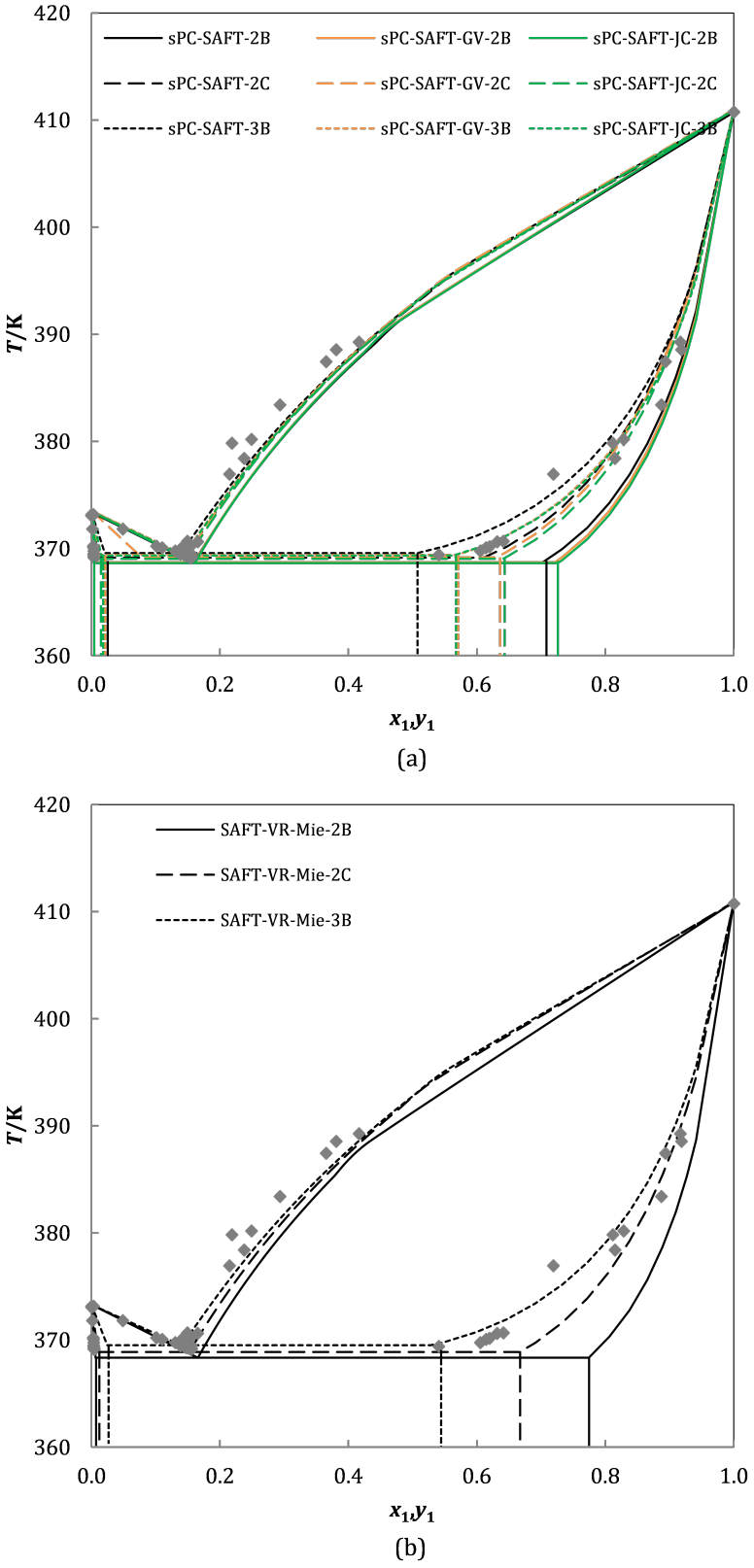

Figure 6.24: VLE of 1-pentanol (1) + water (2) at p = 0.1013 MPa predicted by (a) sPC-SAFT; (b) SAFT-VR Mie. Experimental data from this work.

The VLE of four water + secondary alkanol mixtures are shown in Figs. 6.25 to 6.28. In general, the observations are similar to those made for the primary alkanol mixtures. The 2B, 2C, and 3B association schemes yield different predictions in each model. sPC-SAFT-XX, sPC-SAFT-GV-XX, and sPC-SAFT-JC-XX deliver very similar results, where XX is the 2B or 2C association schemes, indicating that, compared to the association contribution, the polar effects do not contribute significantly toward the mixture energy. Once again the difference between sPC-SAFT-3B, sPC-SAFT-GV-3B, and sPC-SAFT-JC-3B predictions is larger, suggesting that the polar contribution to the system energy is significant enough to make a difference in prediction results when the alkanol is described with the 3B association scheme.

Based on %AAD values, the secondary alkanol mixtures are best represented with the 3B association scheme in the sPC-SAFT framework. This is apparent in Figs. 6.25 and 6.26. The scatter in the alkanol-rich liquid phase present in the water + 2-pentanol (Fig. 6.27) and water + 3-pentanol (Fig. 6.28) data makes it difficult to determine exactly how the association and polar interaction contribute toward the respective mixture energies. Subsequently, no concrete conclusion about the best association scheme can be made. However, in the sPC-SAFT framework, the 3B association gives the closest prediction of the azeotropic conditions in both the water + 2-pentanol (Fig. 6.27) and water + 3-pentanol (Fig. 6.28) systems. It would seem that, for the secondary alkanols, a larger degree of association needs to be accounted for, compared to the primary alkanols, which are best described by the 2C association scheme in aqueous mixtures.

The polar addition to the sPC-SAFT framework provides improved description for the aqueous mixtures of 2-butanol (Fig. 6.26), 2-pentanol (Fig. 6.27), and 3-pentanol (Fig. 6.28). Here sPC-SAFT-JC-3B yields the best description of the respective mixtures.

The water + 2-propanol system proves difficult to model (Fig. 6.25). With sPC-SAFT, sPC-SAFT-GV, and SAFT-VR Mie the 2B and 2C association schemes underestimate the degree of association that occurs between the molecules, therefore the models falsely predict VLLE behaviour. In all three models the 3B scheme provides the best qualitative description of the phase behaviour. The closest quantitative prediction is achieved with sPC-SAFT-3B.

Generally the SAFT-VR Mie predictions for the VLE of aqueous secondary alkanol mixtures are very poor in comparison to those obtained by the sPC-SAFT models. As with water + 1-butanol (see Fig. 6.23), SAFT-VR Mie-3B does not capture the behaviour of water + 2-butanol, since no VLLE is predicted by this model, as shown in Fig. 6.26.

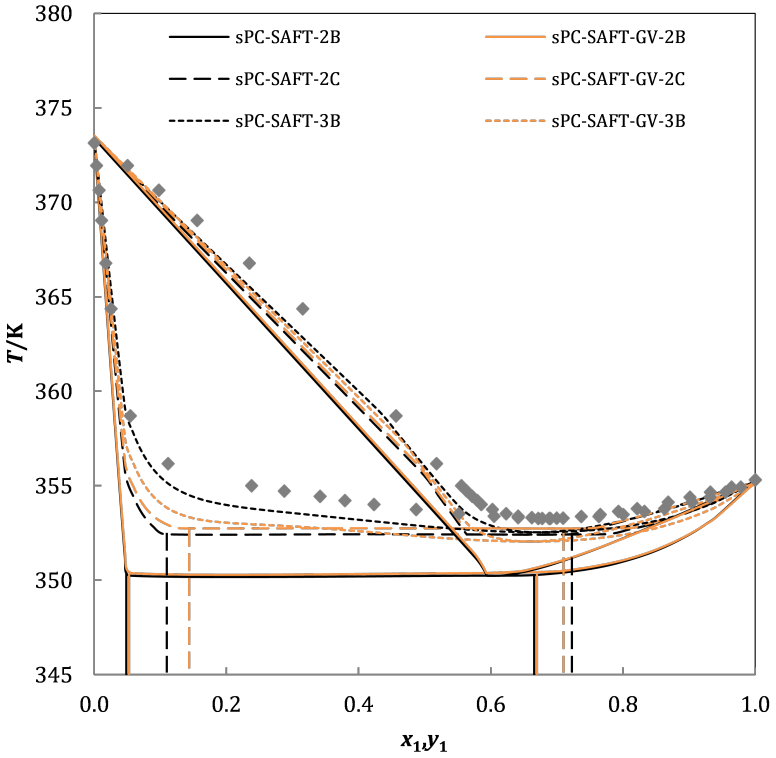

(a)

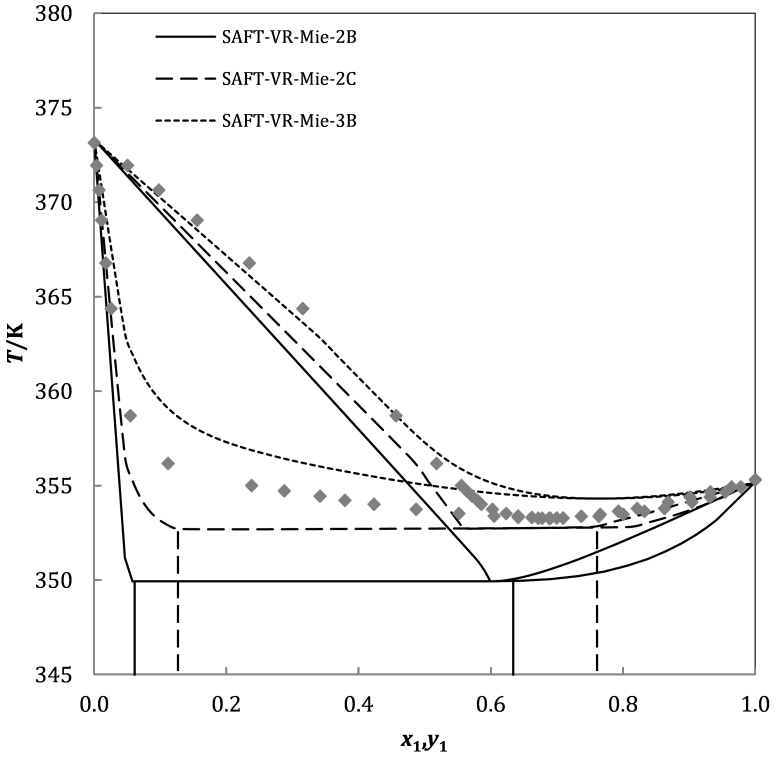

(b)

Figure 6.25: VLE of 2-propanol (1) + water (2) at p = 0.1013 MPa predicted by (a) sPC-SAFT; (b) SAFT-VR Mie. Data taken from Arce, et al. [121].

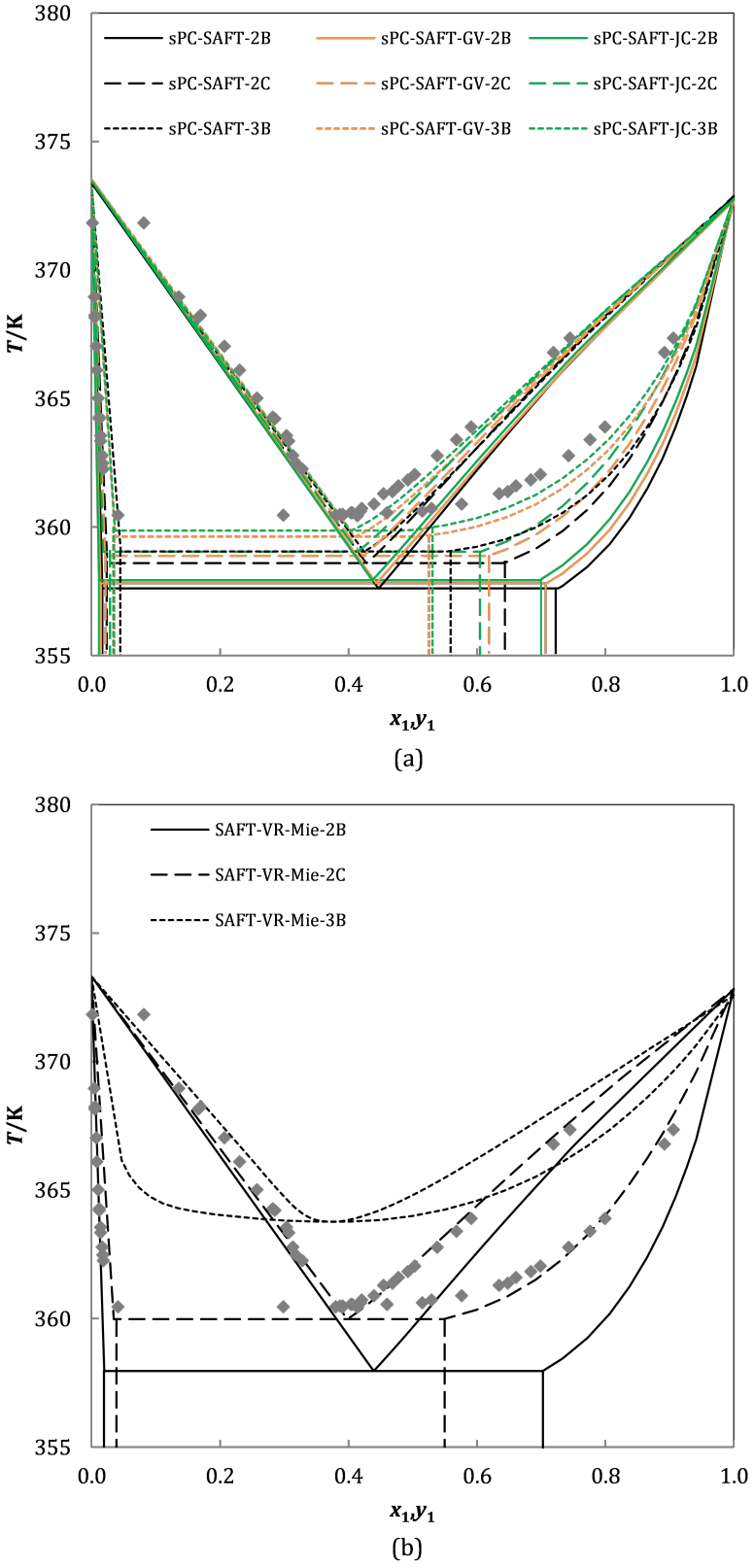

Figure 6.26: VLE of 2-butanol (1) + water (2) at p = 0.1013 MPa predicted by (a) sPC-SAFT; (b) SAFT-VR Mie. Data taken from Iwakabe and Kosuge [141].

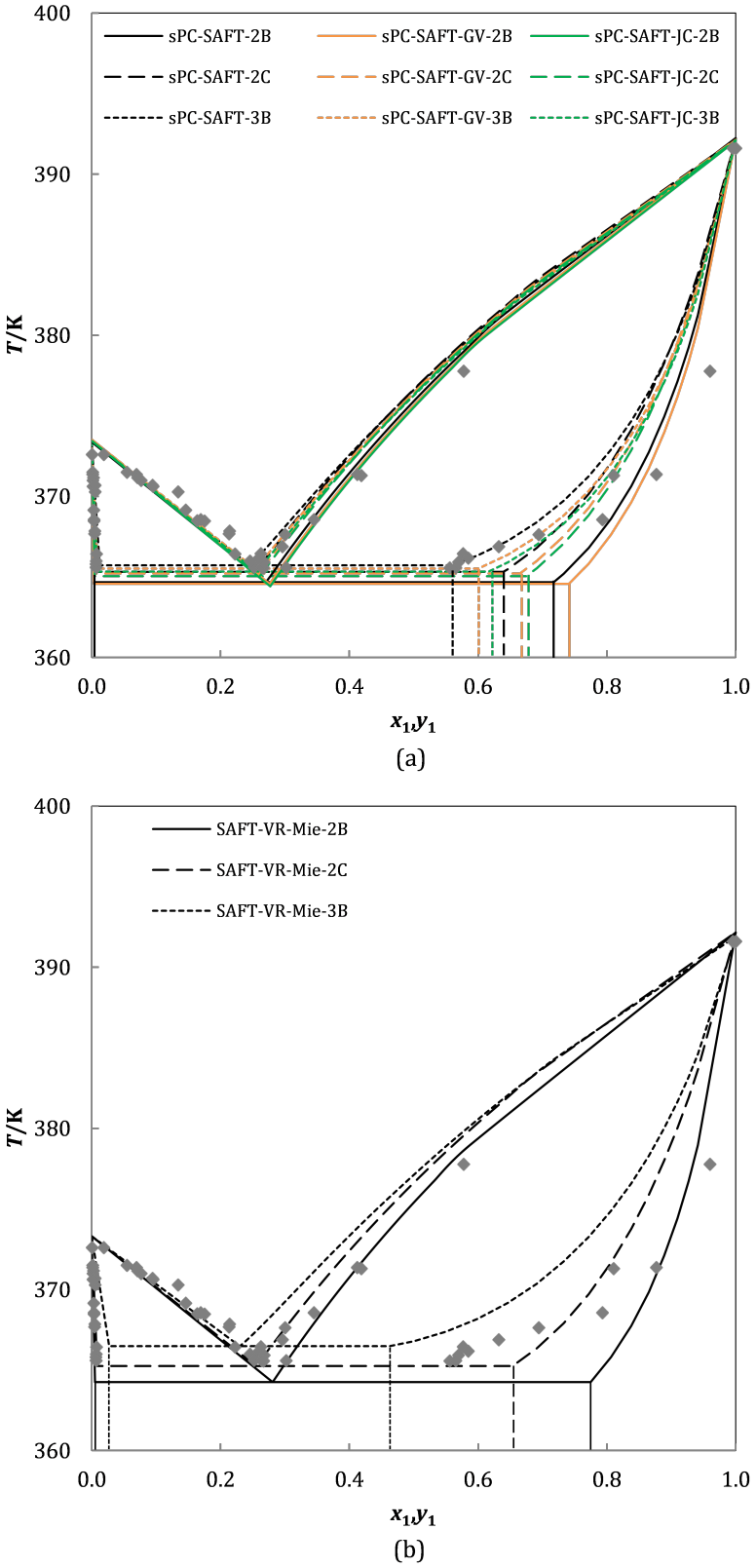

Figure 6.27: VLE of 2-pentanol (1) + water (2) at p = 0.1013 MPa predicted by (a) sPC-SAFT; (b) SAFT-VR Mie. Experimental data from this work.

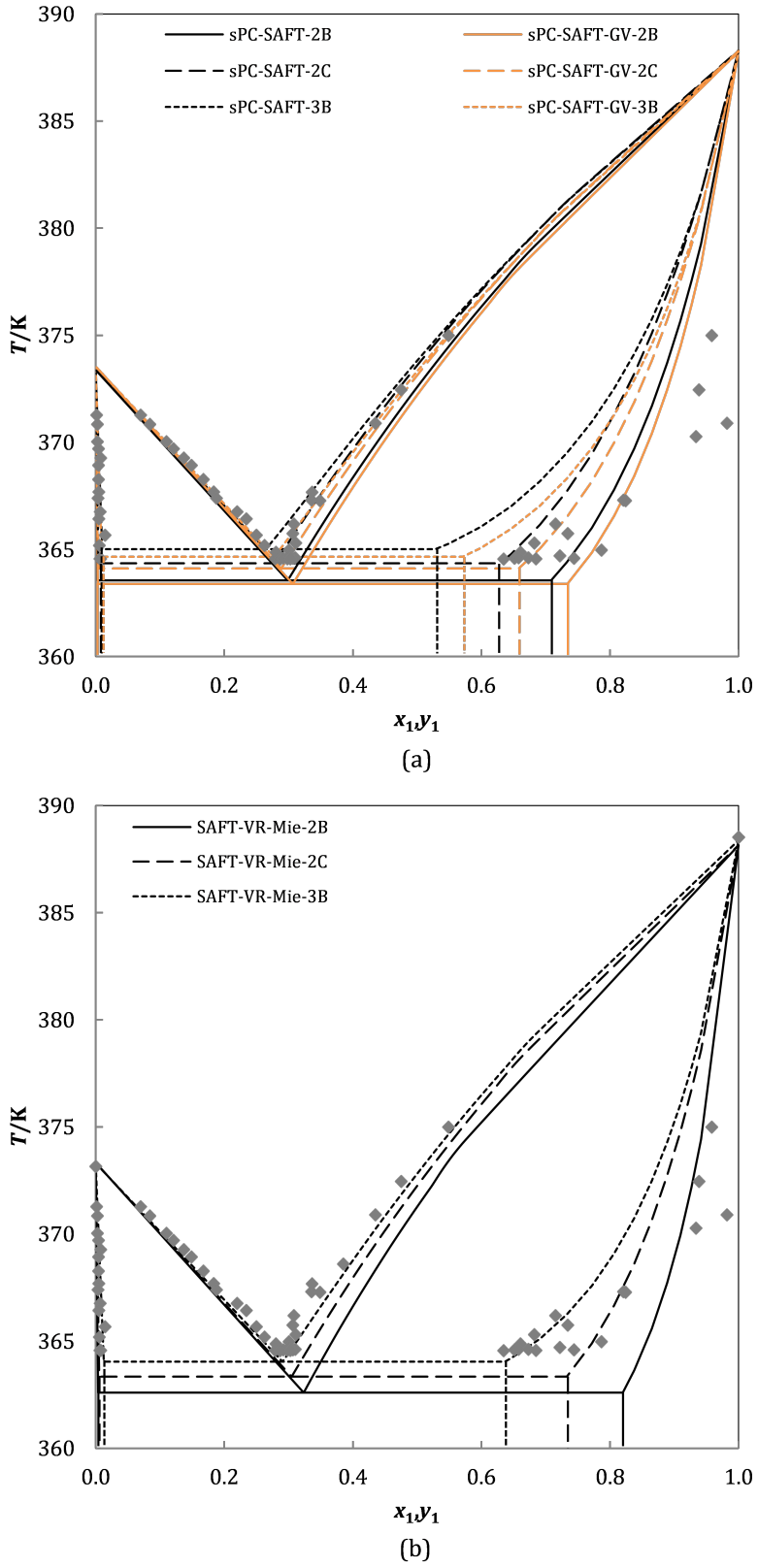

Figure 6.28: VLE of 3-pentanol (1) + water (2) at p = 0.1013 MPa predicted by (a) sPC-SAFT; (b) SAFT-VR Mie. Experimental data from this work.

6.5.2 Excess Thermodynamic Properties

Similarly to the alkane + alkanol mixtures, the excess enthalpy, h^{E}, excess volume, V^{E}, and excess isobaric heat capacity, c_p^{E}, of water + alkanol mixtures were investigated. This investigation evaluates whether the EoSs can be extended to model thermodynamic properties other than phase equilibrium.

Information regarding excess properties that were evaluated in this discussion is summarised in Table 6.12. Where no reference is given, no data were found for the property in question.

6.5.2.1 Excess Enthalpy

Excess enthalpy gives an idea of the interactions that occur between *unlike* molecules, relative to those between *like* molecules, when mixing of components occur [3, 44]. For water + alkanol mixtures, h^{E} is either highly asymmetric (Fig. 6.29), or sinusoidal (Fig. 6.30) in shape, indicating that the behaviour of these mixtures is extremely complex. For all the mixtures investigated, the 2B and 2C association schemes predict a negative quadratic function. In the sPC-SAFT framework, the 3B scheme predicts a positive quadratic function, which is the closest prediction for water + ethanol in Fig. 6.29; however, the models fail to describe the asymmetry observed in h^{E} of this system. Moreover, none of the models are able to capture the sinusoidal behaviour in mixtures such as the one presented in Fig. 6.30.

All in all it would seem that neither the sPC-SAFT, nor the SAFT-VR Mie frameworks are able to describe the complex interactions between water and alkanol molecules when h^{E} is predicted, using VLE centric parameter sets.

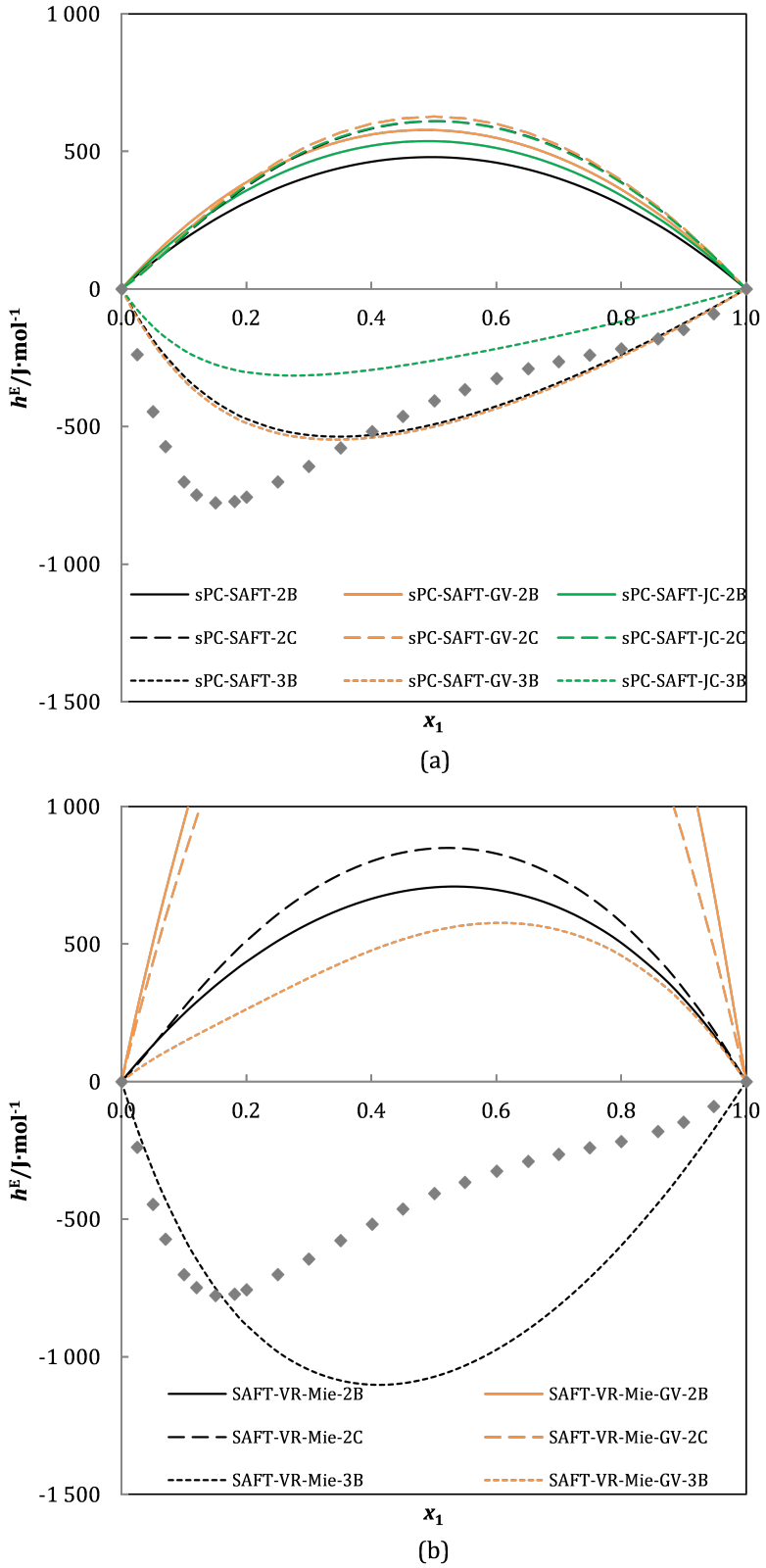

Figure 6.29: Excess enthalpy of ethanol (1) + water (2) at T = 298.15 K and p = 0.1013 MPa predicted by (a) sPC-SAFT; (b) SAFT-VR Mie. Data taken from Ott, et al. [220].

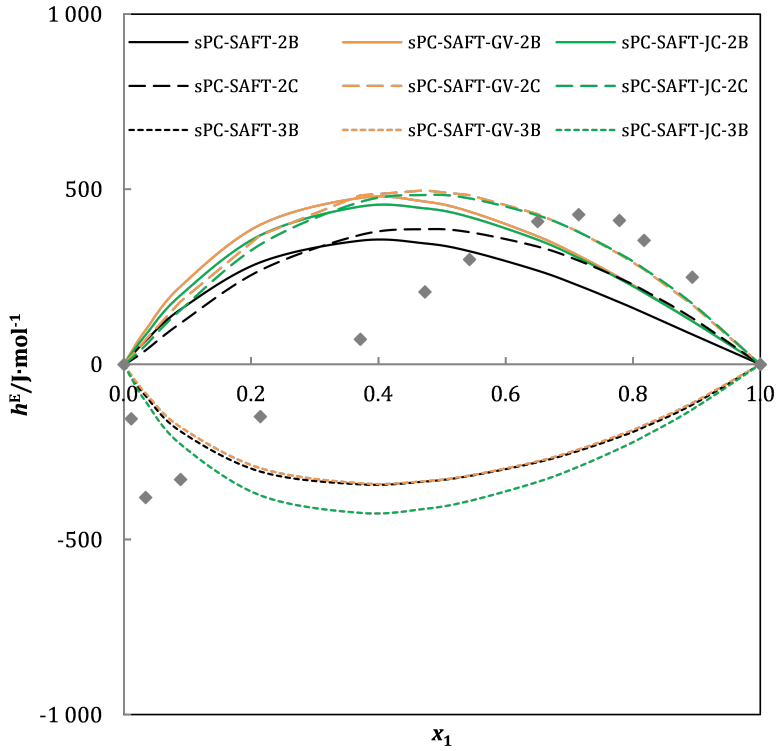

(a)

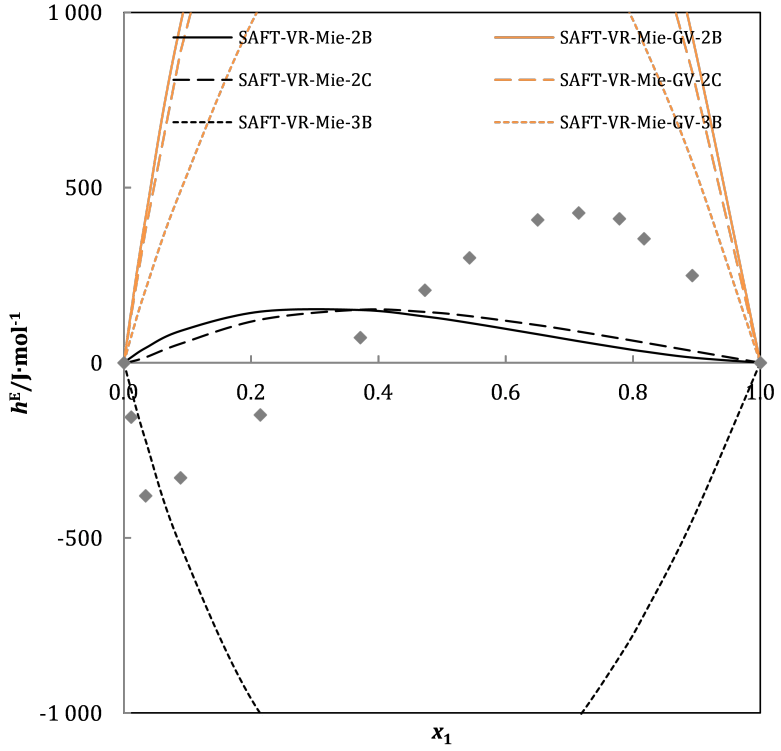

(b)

Figure 6.30: Excess enthalpy of 2-butanol (1) + water (2) at T = 298.15 K and p = 0.1013 MPa predicted by (a) sPC-SAFT; (b) SAFT-VR Mie. Data taken from Marongiu, et al. [229].

6.5.2.2 Excess Volume

For the water + alkanol mixtures investigated, V^{E} is a positive quadratic function, indicating that the attraction between the *unlike* molecules causes them to pack more tightly than when they are in their respective pure component states.

For water + methanol and water + ethanol, nonpolar and polar sPC-SAFT predictions are qualitatively correct since these models capture the curvature of V^{E}, but are not numerically accurate (Fig. 6.31). For the higher alkanols, the nonpolar predictions become sinusoidal while polar predictions become negative quadratic functions. However, V^{E} remains a positive quadratic function. SAFT-VR Mie performs better than the sPC-SAFT models since the predictions for all investigated mixtures remain qualitatively accurate, but are not necessarily quantitatively correct (Fig. 6.32). SAFT-VR Mie therefore provides a better description of the interactions between water and alkanol molecules and how these interactions affect the mixture volume. All SAFT-VR Mie-GV predictions are sinusoidal in shape and are therefore unable to capture the behaviour of this property.

It is stressed, however, that these predictions were achieved by using pure component parameters geared toward the prediction of VLE.

6.5.2.3 Excess Isobaric Heat Capacity

c_p^{E} data were only found for the aqueous mixtures of methanol, ethanol, 1-propanol, and 1-butanol, therefore the following discussion is inherently limited. This property is highly asymmetric, and skewed toward the water-rich composition range (Figs. 6.33 and 6.34), indicating the highly complex interactions occurring in aqueous alkanol mixtures. As shown by example in Figs. 6.33 and 6.34, none of the predictions capture the behaviour expressed in the experimental data, using VLE centric parameter sets.

However, from Figs. 6.33 and 6.34 it is apparent that the same association scheme delivers similar qualitative predictions in each of the models, with the exception of SAFT-VR Mie-GV. This shows that c_p^{E} is governed by association effects, rather than polar interactions.

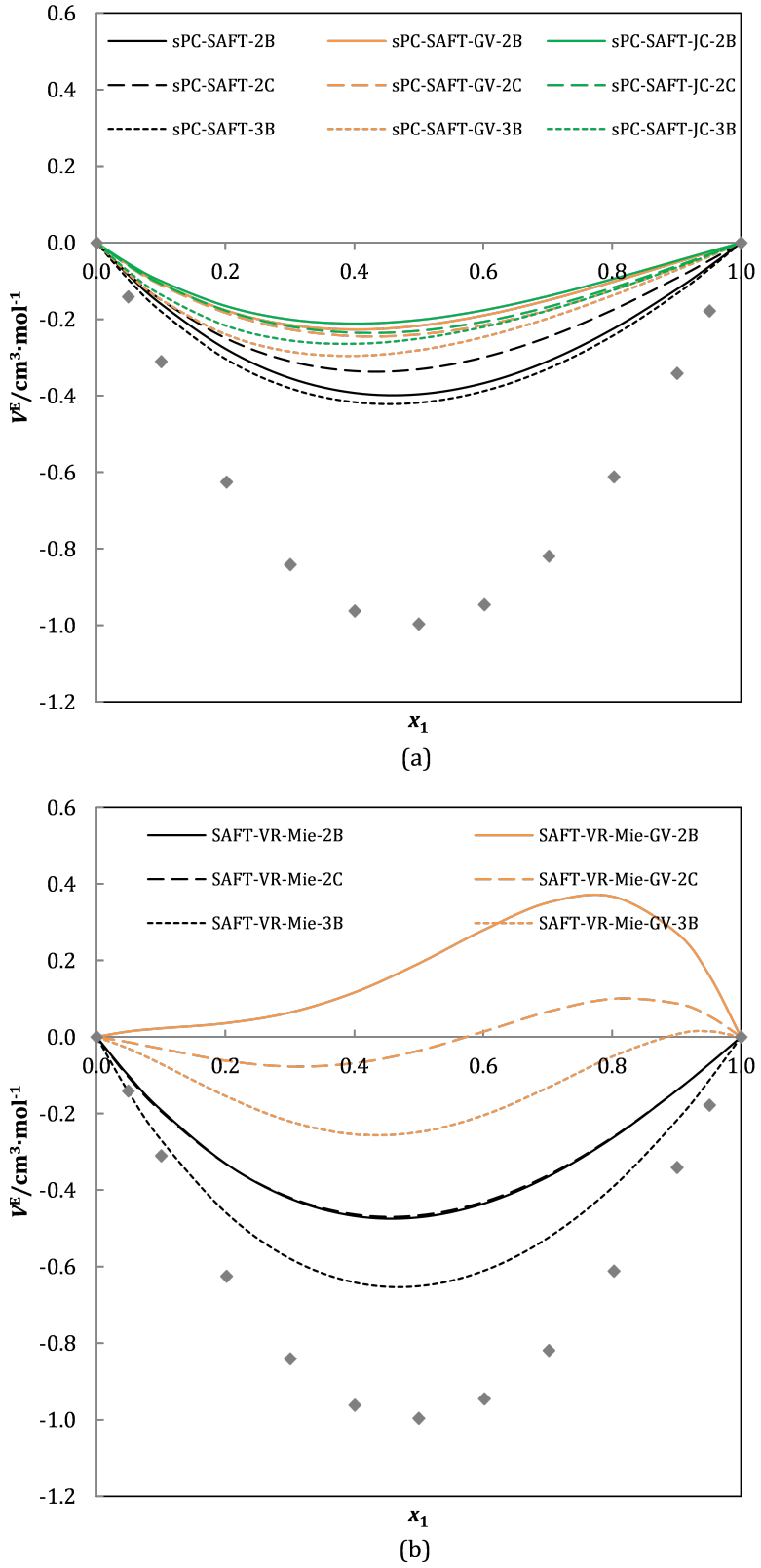

Figure 6.31: Excess volume of methanol (1) + water (2) at T = 298.15 K and p = 0.1013 MPa predicted by (a) sPC-SAFT; (b) SAFT-VR Mie. Data taken from González, et al. [215].

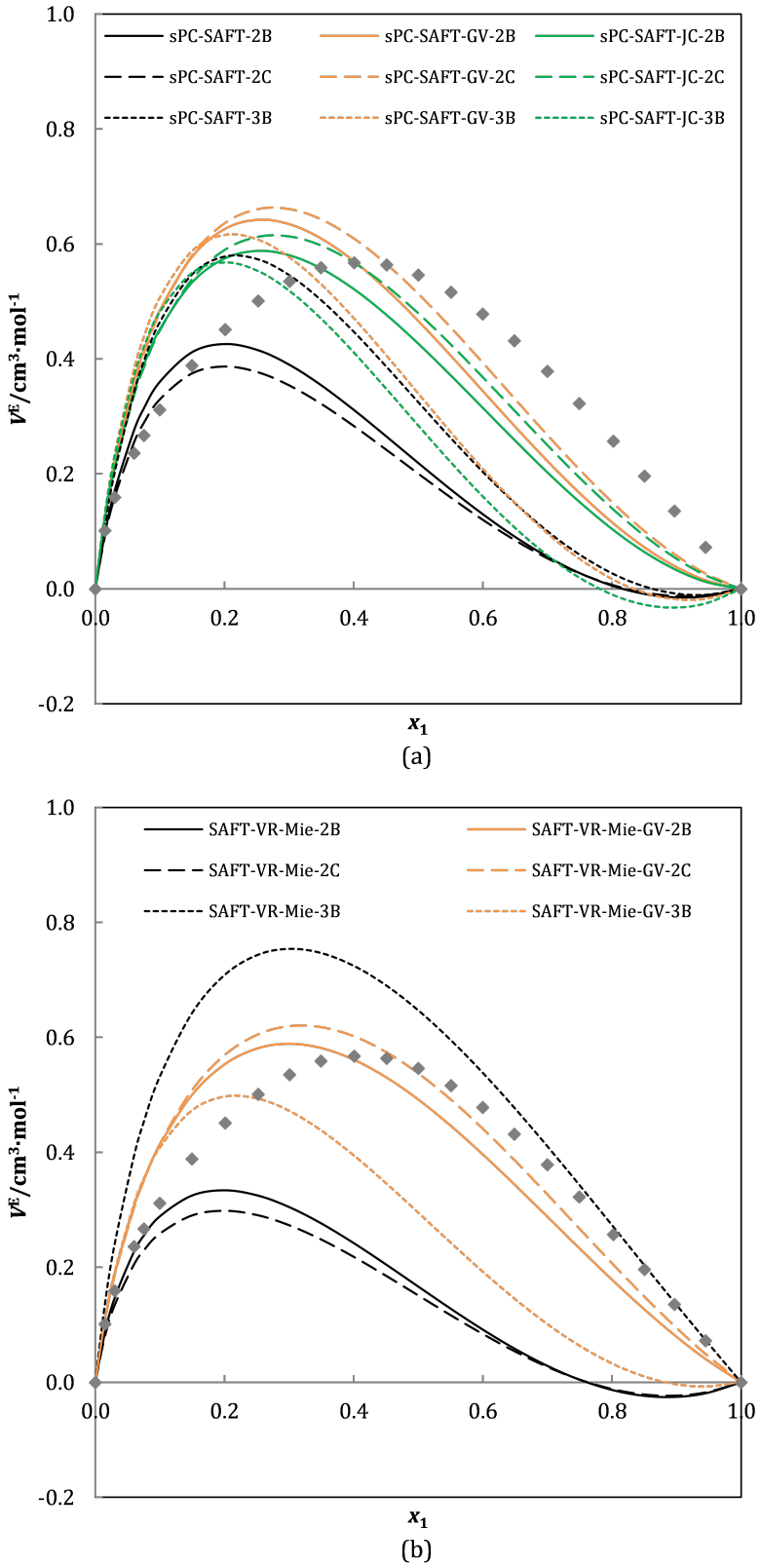

Figure 6.32: Excess volume of 2-butanol (1) + water (2) at T = 298.15 K and p = 0.1013 MPa predicted by (a) sPC-SAFT; (b) SAFT-VR Mie. Data taken from Herráez and Belda [224].

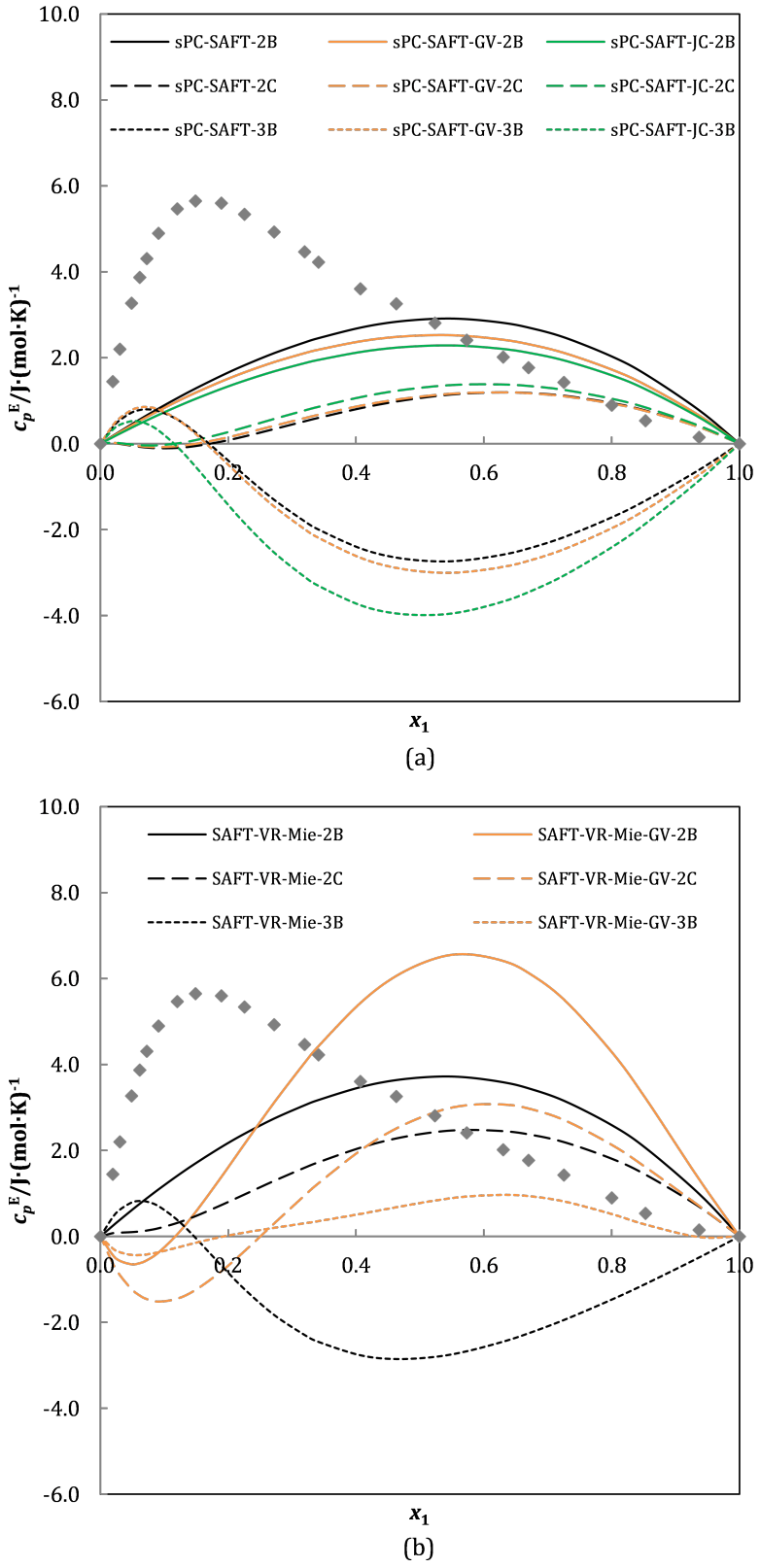

Figure 6.33: Excess isobaric heat capacity of methanol (1) + water (2) at T = 288.15 K and p = 0.1013 MPa predicted by (a) sPC-SAFT; (b) SAFT-VR Mie. Data taken from Benson and D'Arcy [216].

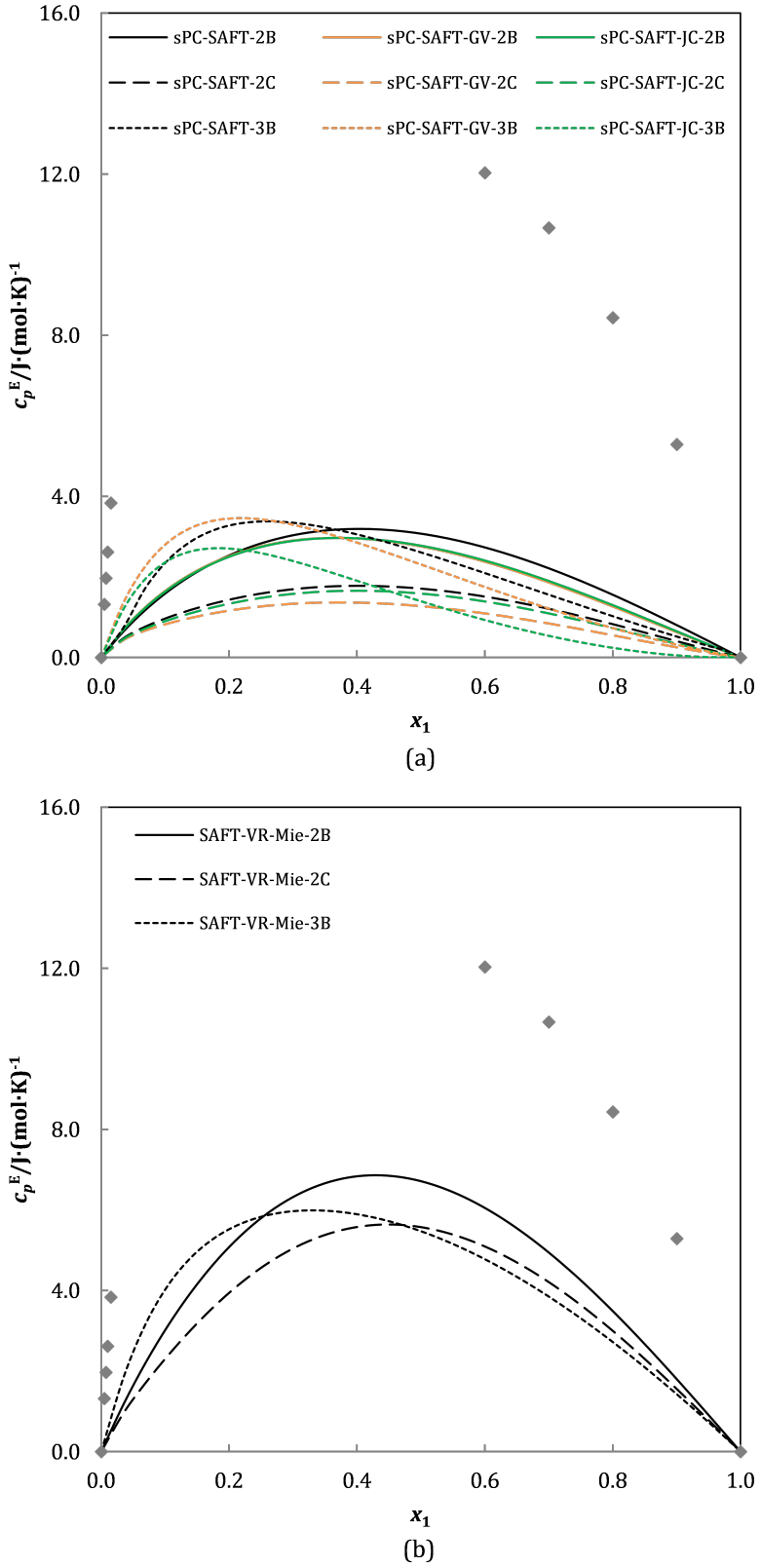

Figure 6.34: Excess isobaric heat capacity of 1-butanol (1) + water (2) at T = 298.15 K and p = 0.1013 MPa predicted by (a) sPC-SAFT; (b) SAFT-VR Mie. Data taken from Ogawa and Murakami [230].

6.5.3 Section Highlights

By comparison, SAFT-VR Mie does not perform as well as the sPC-SAFT models for the VLE prediction of aqueous alkanol mixtures, while similar predictions are obtained for the excess properties. The primary alkanols are best described by the 2C association scheme in mixtures containing water, while secondary alkanols are best described by the 3B association scheme in aqueous mixtures.

sPC-SAFT-GV provides the best description of the water + primary alkanol phase equilibria; however, the improvement gained by addition of the polar term is not significant, indicating that polar interactions are not significant compared to association interactions. sPC-SAFT-JC best describes the VLE behaviour of water + secondary alkanol mixtures, and provides better predictions than sPC-SAFT. It seems that, compared to the association contribution, polar contributions are more significant in the secondary alkanol mixtures.

It is emphasised that the results obtained for the excess properties are by-products of parameters geared at predicting VLE behaviour, and that these results give a holistic view of the predictive capability of the sPC-SAFT and SAFT-VR Mie model frameworks. Given the good qualitative results obtained for the excess thermodynamic properties of alkane + alkanol mixtures, the performance of all models is poor for the excess properties water + alkanol mixtures by comparison. None of the models are able to describe the excess thermodynamic properties even qualitatively, indicating that the treatment of cross-association, or the mixing rules for association parameters in the SAFT framework is potentially incorrect. However, this statement requires further investigation.

6.6 Summary

The models investigated deliver similar results for both primary and secondary alkanols, indicating that the models can distinguish between structural isomers of linear alkanols. The polar models provide significant improvement over the nonpolar models when modelling the VLE of alkane + alkanol mixtures. The excess thermodynamic properties of alkane + alkanol mixtures are not described well by the polar models, but this does not necessarily indicate that the polar addition is incorrect or unnecessary.

In aqueous mixtures of primary alkanols, the VLE is adequately described without the polar terms. In these mixtures it would seem that the association energy has a much larger influence on equilibrium phase behaviour than polar effects. On the other hand, the water + secondary alkanol mixtures are generally better predicted with sPC-SAFT-JC than the nonpolar models. The excess properties of water + alkanol mixtures are poorly described by all the models.

Generally the best association scheme for all alkanols is the 2C scheme, while the 3B scheme best describes the association behaviour of secondary alkanols in aqueous mixtures. In alkane + alkanol mixtures sPC-SAFT and SAFT-VR Mie perform equally well, while sPC-SAFT is the better of the two models for water + alkanol mixtures.

Similar discrepancies in predictions were obtained for both the sPC-SAFT and SAFT-VR Mie models, indicating that the problem in predicting thermodynamic properties does not lie with a single model. It would seem that the SAFT framework, or Wertheim's perturbation theory, has inherent flaws that need to be addressed before it can be attempted to improve thermodynamic modelling.

Chapter 7

Summary and Conclusions

7.1 Reviewing the Objectives

The overarching aim of this work was to determine what effect a shifting hydroxyl group has on the equilibrium phase behaviour in water + alkanol mixtures, and subsequently to evaluate the ability of sPC-SAFT, sPC-SAFT-GV, sPC-SAFT-JC, SAFT-VR Mie, SAFT-VR Mie-GV, and SAFT-VR Mie-JC to predict this phase behaviour. To this end, additional VLE data were generated for water + (C_1 - C_5) linear alkanol mixtures for which no data were found, namely 2-pentanol and 3-pentanol. Model parameters were determined for all components to asses the performance of each model. Thus, reviewing the objectives in Section 1.3:

1. Generate isobaric VLE data for binary water + alkanol mixtures

Isobaric VLE data were generated on a dynamic Gillespie-type still at p=0.1013 MPa. The accuracy of temperature and pressure measurements were 0.05 K and 2×10^{-4} MPa, respectively. Together with analytic errors this resulted in compositional measurements that were accurate within 0.023 mole fraction. The experimental equipment and sampling method were verified by conducting VLE measurements for the water + 1-butanol system. After verification, VLE data for water + 1-pentanol, + 2-pentanol, and + 3-pentanol were generated. All VLE data measured in this study were determined to be thermodynamically consistent by both the McDermott-Ellis and Wisniak L/W consistency tests.

Each of the four mixtures measured, namely binary aqueous mixtures of 1-butanol, 1-pentanol, 2-pentanol, and 3-pentanol, exhibit VLLE behaviour, with a minimum boiling heterogeneous azeotrope. Shifting the polar hydroxyl group away from the terminal methyl group results in higher saturated vapour pressure, as is expected. However, similar saturated vapour pressure behaviour was observed for primary C_x- and secondary $C_{(x+1)}$-alkanols, a similarity that is also observed in binary water + alkanol equilibrium phase behaviour.

The water + 2-pentanol and water + 3-pentanol mixtures were extremely difficult to measure and after repeated measurements the inconsistencies in the liquid phase data scatter could not be resolved.

2. Generate pure component parameters

Pure component parameter sets were regressed for sPC-SAFT, sPC-SAFT-GV, sPC-SAFT-JC, SAFT-VR Mie, and SAFT-VR Mie-JC, for each of the 9 (C_1 – C_5) linear alkanols and water. Only one regression method was considered for each of the models (sPC-SAFT: p^{sat}, ρ^{sat}, h^{vap}; sPC-SAFT-GV and sPC-SAFT-JC: p^{sat}, ρ^{sat}, h^{vap}, binary alkane VLE; SAFT-VR Mie: p^{sat}, ρ^{sat}, u^{liq}; SAFT-VR Mie-GV and SAFT-VR Mie-JC: p^{sat}, ρ^{sat}, u^{liq}, binary alkane VLE). No parameters could be determined for SAFT-VR Mie-JC, because the polar parameter was driven to zero in each regression, regardless of initial guess. Subsequently the performance of SAFT-VR Mie-JC could not be evaluated.

3.(a) The performance of sPC-SAFT compared to SAFT-VR Mie.

The five models (sPC-SAFT, sPC-SAFT-GV, sPC-SAFT-JC, SAFT-VR Mie, and SAFT-VR Mie-GV) give equally good description of pure component properties, with the SAFT-VR Mie models providing slightly better results for c_p and superior results for u^{liq} compared to the sPC-SAFT models.

Both model frameworks are able to describe VLE behaviour of alkane + alkanol mixtures equally well, while sPC-SAFT performs better than SAFT-VR Mie for the VLE of water + alkanol mixtures.

3.(b) Accounting for molecular polarity

For all pure component properties the inclusion of a polar term to both sPC-SAFT and SAFT-VR Mie does not provide significantly improved predictions. The polar models provide improved, and accurate, predictions for alkane + alkanol mixtures, indicating that polarity needs to be accounted for explicitly in these mixtures. Here sPC-SAFT-GV and sPC-SAFT-JC give similar predictions, therefore the more suitable polar term is not apparent. However, the polar models do not significantly improve the predictions for water + alkanol mixtures, supporting the idea that polar forces are insignificant in light of strong association.

3.(c) The choice of association scheme for alkanol molecules

For pure component properties the three association schemes deliver almost identical results for the alkanols. In alkane + alkanol mixtures, the 2C association scheme delivers the best results

for VLE when the nonpolar models are used. However, the polar model predictions of alkane + alkanol mixtures were unaffected by the choice of association scheme, rendering the choice of association scheme in the polar models arbitrary. In water + primary alkanol mixtures, VLE is best described with the 2C scheme, while aqueous mixtures of secondary alkanols are best described by the 3B scheme.

3.(d) The modelling of secondary alkanols compared to primary alkanols

The quality of modelling results for secondary alkanols is similar to those obtained for primary alkanols. The SAFT framework is therefore sufficiently versatile to accommodate structural isomers of alkanols.

4. Prediction of mixture excess properties

Predicting excess thermodynamic properties, especially those of water + alkanol mixtures, is troublesome in both model frameworks, indicating that the SAFT framework as a whole requires further refinement in order to simultaneously predict all thermodynamic properties accurately.

7.2 Recommendations

Based on the outcomes of this investigation, the following recommendations are made for future work:

- The experimental methodology for these complex mixtures should be revisited, giving particular attention to the sampling method. It is also necessary to investigate how to overcome the liquid phase split observed during experimentation.
- It might be worthwhile to investigate regression procedures other than the procedure used in this study, for SAFT-VR Mie, SAFT-VR Mie-GV, and SAFT-VR Mie-JC. Different combination of pure component data included in the regression procedure, as well as different regression weights should be considered, in the same fashion as the brief investigation conducted by de Villiers [36]. The use of homologous group correlations to determine polar parameters should also be investigated [36, 40, 169, 234].
- Since the parameter space for associating molecules is large in SAFT-VR Mie, SAFT-VR Mie-GV, and SAFT-VR Mie-JC, the grid-method used to determine parameters in studies by Clark, et al. [68], dos Ramos, et al. [168], and Dufal, et al. [75, 76], is suggested. Using this method, the relationship between different properties can be observed and the interrelationship between the pure component parameters is also highlighted. This

method will most probably indicate the global optimum parameter set, provided that the parameters that are fixed during the searching procedure include the global minimum.

- The current study is limiting since it only considers a few alkanols. An extended study considering larger alkanols, which also have more structural isomers, should be conducted.

References

[1] Kontogeorgis GM, Folas GK. Thermodynamic models for industrial applications: From classical and advanced mixing rules to association theories. United Kingdom: John Wiley & Sons; 2010.

[2] Prausnitz JM, Lichtenthaler RN, de Azevedo EG. Molecular thermodynamics of fluid-phase equilibria. 3rd ed. New Jersey: Pearson Education; 1999.

[3] Smith JM, Van Ness HC, Abbott MM. Introduction to chemical engineering thermodynamics. 7th ed. New York: McGraw-Hill; 2005.

[4] van der Waals JD. On the continuity of the gaseous and liquid states [Doctoral dissertation]. University of Leiden. Leiden; 1873.

[5] Valderrama JO. The state of the cubic equations of state. Industrial & Engineering Chemistry Research. 2003;42(8):1603–1618.

[6] Redlich O, Kwong JNS. On the thermodynamics of solutions. V. An equation of state. Fugacities of gaseous solutions. Chemical Reviews. 1949;44(1):233–244.

[7] Soave G. Equilibrium constants from a modified Redlich-Kwong equation of state. Chemical Engineering Science. 1972;27(6):1197–1203.

[8] Peng DY, Robinson DB. A new two-constant equation of state. Industrial & Engineering Chemistry Fundamentals. 1976;15(1):59–64.

[9] Kontogeorgis GM, Economou IG. Equations of state: From the ideas of van der Waals to association theories. The Journal of Supercritical Fluids. 2010;55(2):421–437.

[10] Müller EA, Gubbins KE. Molecular-based equations of state for associating fluids: A review of SAFT and related approaches. Industrial & Engineering Chemistry Research. 2001;40(10):2193–2211.

[11] Heidemann RA, Prausnitz JM. A van der Waals-type equation of state for fluids with associating molecules. Proceedings of the National Academy of Sciences. 1976;73(6):1773–1776.

[12] Ikonomou GD, Donohue MD. Extension of the associated perturbed anisotropic chain theory to mixtures with more than one associating component. Fluid Phase Equilibria. 1988;39(2):129–159.

[13] Anderko A. A simple equation of state incorporating association. Fluid Phase Equilibria. 1989;45(1):39–67.

[14] Anderko A. Extension of the AEOS model to systems containing any number of associating and inert components. Fluid Phase Equilibria. 1989;50(1):21–52.

[15] Panayiotou C, Sanchez IC. Hydrogen bonding in fluids: An equation-of-state approach. The Journal of Physical Chemistry. 1991;95(24):10090–10097.

[16] Chapman WG, Gubbins KE, Jackson G, Radosz M. New reference equation of state for associating liquids. Industrial & Engineering Chemistry Research. 1990;29(8):1709–1721.

[17] Huang SH, Radosz M. Equation of state for small, large, polydisperse, and associating molecules. Industrial & Engineering Chemistry Research. 1990;29(11):2284–2294.

[18] Kontogeorgis GM, Voutsas EC, Yakoumis IV, Tassios DP. An equation of state for associating fluids. Industrial & Engineering Chemistry Research. 1996;35(11):4310–4318.

[19] Jackson G, Chapman WG, Gubbins KE. Phase equilibria of associating fluids: Spherical molecules with multiple bonding sites. Molecular Physics. 1988;65(1):1–31.

[20] Chapman WG, Jackson G, Gubbins KE. Phase equilibria of associating fluids: Chain molecules with multiple bonding sites. Molecular Physics. 1988;65(5):1057–1079.

[21] Chapman WG, Gubbins KE, Jackson G, Radosz M. SAFT: Equation-of-state solution model for associating fluids. Fluid Phase Equilibria. 1989;52:31–38.

[22] Wertheim MS. Fluids with highly directional attractive forces. I. Statistical thermodynamics. Journal of Statistical Physics. 1984;35(1):19–34.

[23] Wertheim MS. Fluids with highly directional attractive forces. II. Thermodynamic perturbation theory and integral equations. Journal of Statistical Physics. 1984;35(1):35–47.

[24] Wertheim MS. Fluids with highly directional attractive forces. III. Multiple attraction sites. Journal of Statistical Physics. 1986;42(3):459–476.

[25] Wertheim MS. Fluids with highly directional attractive forces. IV. Equilibrium polymerization. Journal of Statistical Physics. 1986;42(3):477–492.

[26] Wertheim MS. Fluids of dimerizing hard spheres, and fluid mixtures of hard spheres and dispheres. The Journal of Chemical Physics. 1986;85(5):2929–2936.

[27] Wertheim MS. Thermodynamic perturbation theory of polymerization. The Journal of Chemical Physics. 1987;87(12):7323–7331.

[28] Sear RP, Jackson G. Thermodynamic perturbation theory for association with bond cooperativity. Journal of Chemical Physics. 1996;105(3):1113–1120.

[29] Yukhnevich GV. Hydrogen-bond cooperativity. Journal of Molecular Liquids. 1990;46:211–219.

[30] Grenner A, Kontogeorgis GM, von Solms N, Michelsen ML. Modeling phase equilibria of alkanols with the simplified PC-SAFT equation of state and generalized pure compound parameters. Fluid Phase Equilibria. 2007;258(1):83–94.

[31] Voutsas EC, Kontogeorgis GM, Yakoumis IV, Tassios DP. Correlation of liquid-liquid equilibria for alcohol/hydrocarbon mixtures using the CPA equation of state. Fluid Phase Equilibria. 1997;132(1):61–75.

[32] Mejbri K, Taieb A, Bellagi A. Phase equilibria calculation of binary and ternary mixtures of associating fluids applying PC-SAFT equation of state. The Journal of Supercritical Fluids. 2015;104:132–144.

[33] Tsivintzelis I, Grenner A, Economou IG, Kontogeorgis GM. Evaluation of the Nonrandom Hydrogen Bonding (NRHB) theory and the simplified Perturbed-Chain-Statistical Associating Fluid Theory (sPC-SAFT). 2. Liquid-liquid equilibria and prediction of monomer fraction in hydrogen bonding systems. Industrial & Engineering Chemistry Research. 2008;47(15):5651–5659.

[34] Paragand F, Feyzi F, Behzadi B. Application of the SAFT-VR equation of state to vapor-liquid equilibrium calculations for pure components and binary mixtures using the Sutherland potential. Fluid Phase Equilibria. 2010;290(1):181–194.

[35] Al-Saifi NM, Hamad EZ, Englezos P. Prediction of vapor-liquid equilibrium in water-alcohol-hydrocarbon systems with the dipolar Perturbed-Chain SAFT equation of state. Fluid Phase Equilibria. 2008;271(1):82–93.

[36] de Villiers AJ. Evaluation and improvement of the sPC-SAFT equation of state for complex mixtures. [Doctoral dissertation]. University of Stellenbosch. Stellenbosch; 2011.

[37] Jog PK, Chapman WG. Application of Wertheim's thermodynamic perturbation theory to dipolar hard sphere chains. Molecular Physics. 1999;97(3):307–319.

[38] Jog PK, Sauer SG, Blaesing J, Chapman WG. Application of dipolar chain theory to the phase behavior of polar fluids and mixtures. Industrial & Engineering Chemistry Research. 2001;40(21):4641–4648.

[39] Gross J, Vrabec J. An equation-of-state contribution for polar components: Dipolar molecules. AIChE Journal. 2006;52(3):1194–1204.

[40] Cripwell JT. Assessment of the capabilities of two polar sPC-SAFT terms through application to measured ketone-alkane phase equilibria data [Master's thesis]. University of Stellenbosch. Stellenbosch; 2014.

[41] Lafitte T, Bessieres D, Piñeiro MM, Daridon JL. Simultaneous estimation of phase behavior and second-derivative properties using the Statistical Associating Fluid Theory with variable range approach. The Journal of Chemical Physics. 2006;124(2):024509.

[42] Lafitte T, Apostolakou A, Avendaño C, Galindo A, Adjiman CS, Müller EA, et al. Accurate Statistical Associating Fluid Theory for chain molecules formed from Mie segments. The Journal of Chemical Physics. 2013;139(15):154504.

[43] Lafitte T, Piñeiro MM, Daridon JL, Bessières D. A comprehensive description of chemical association effects on second derivative properties of alcohols through a SAFT-VR approach. The Journal of Physical Chemistry B. 2007;111(13):3447–3461.

[44] Koretsky MD. Engineering and chemical thermodynamics. New Jersey: John Wiley & Sons; 2004.

[45] von Solms N, Michelsen ML, Kontogeorgis GM. Computational and physical performance of a modified PC-SAFT equation of state for highly asymmetric and associating mixtures. Industrial & Engineering Chemistry Research. 2003;42(5):1098–1105.

[46] Michelsen ML, Mollerup JM. Thermodynamic models: Fundamentals & computational aspects. 2nd ed. Copenhagen: Tie-Line Publications; 2007.

[47] Huang SH, Radosz M. Equation of state for small, large, polydisperse, and associating molecules: Extension to fluid mixtures. Industrial & Engineering Chemistry Research. 1991;30(8):1994–2005.

[48] Gil-Villegas A, Galindo A, Whitehead PJ, Mills SJ, Jackson G, Burgess AN. Statistical associating fluid theory for chain molecules with attractive potentials of variable range. The Journal of Chemical Physics. 1997;106(10):4168–4186.

[49] Galindo A, Davies LA, Gil-Villegas A, Jackson G. The thermodynamics of mixtures and the corresponding mixing rules in the SAFT-VR approach for potentials of variable range. Molecular Physics. 1998;93(2):241–252.

[50] Blas FJ, Vega LF. Thermodynamic behaviour of homonuclear and heteronuclear Lennard-Jones chains with association sites from simulation and theory. Molecular Physics. 1997;92(1):135–150.

[51] Blas FJ, Vega LF. Prediction of binary and ternary diagrams using the Statistical Associating Fluid Theory (SAFT) equation of state. Industrial & Engineering Chemistry Research. 1998;37(2):660–674.

[52] Gross J, Sadowski G. Application of perturbation theory to a hard-chain reference fluid: An equation of state for square-well chains. Fluid Phase Equilibria. 2000;168(2):183–199.

[53] Gross J, Sadowski G. Perturbed-Chain SAFT: An equation of state based on a perturbation theory for chain molecules. Industrial & Engineering Chemistry Research. 2001;40(4):1244–1260.

[54] Gross J, Sadowski G. Application of the Perturbed-Chain SAFT equation of state to associating systems. Industrial & Engineering Chemistry Research. 2002;41(22):5510–5515.

[55] von Solms N, Kouskoumvekaki IA, Michelsen ML, Kontogeorgis GM. Capabilities, limitations and challenges of a simplified PC-SAFT equation of state. Fluid Phase Equilibria. 2006;241(1):344–353.

[56] Wei YS, Sadus RJ. Equations of state for the calculation of fluid-phase equilibria. AIChE Journal. 2000;46(1):169–196.

[57] Economou IG. Statistical Associating Fluid Theory: A successful model for the calculation of thermodynamic and phase equilibrium properties of complex fluid mixtures. Industrial & Engineering Chemistry Research. 2002;41(5):953–962.

[58] Tan SP, Adidharma H, Radosz M. Recent advances and applications of Statistical Associating Fluid Theory. Industrial & Engineering Chemistry Research. 2008;47(21):8063–8082.

[59] Kontogeorgis GM. Association theories for complex thermodynamics. Chemical Engineering Research and Design. 2013;91(10):1840–1858.

[60] Chen SS, Kreglewski A. Applications of the augmented van der Waals Theory of fluids.: I. Pure fluids. Berichte der Bunsengesellschaft für physikalische Chemie. 1977;81(10):1048–1052.

[61] Boublík T. Hard-sphere equation of state. The Journal of Chemical Physics. 1970;53(1):471–472.

[62] Mansoori GA, Carnahan NF, Starling KE, Leland TW Jr. Equilibrium thermodynamic properties of the mixture of hard spheres. The Journal of Chemical Physics. 1971;54(4):1523–1525.

[63] Carnahan NF, Starling KE. Equation of state for nonattracting rigid spheres. The Journal of Chemical Physics. 1969;51(2):635–636.

[64] Barker JA, Henderson D. Perturbation theory and equation of state for fluids: the square-well potential. The Journal of Chemical Physics. 1967;47(8):2856–2861.

[65] Barker JA, Henderson D. Perturbation theory and equation of state for fluids. II. A successful theory of liquids. The Journal of Chemical Physics. 1967;47(11):4714–4721.

[66] Barker JA, Henderson D. What is "liquid"? Understanding the states of matter. Reviews of Modern Physics. 1976;48(4):587–671.

[67] de Villiers AJ, Schwarz CE, Burger AJ. New association scheme for 1-alcohols in alcohol/water mixtures with sPC-SAFT: The 2C association scheme. Industrial & Engineering Chemistry Research. 2011;50(14):8711–8725.

[68] Clark GNI, Haslam AJ, Galindo A, Jackson G. Developing optimal Wertheim-like models of water for use in Statistical Associating Fluid Theory (SAFT) and related approaches. Molecular Physics. 2006;104(22):3561–3581.

[69] Liang X, Tsivintzelis I, Kontogeorgis GM. Modeling water containing systems with the simplified PC-SAFT and CPA equations of state. Industrial & Engineering Chemistry Research. 2014;53(37):14493–14507.

[70] Kontogeorgis GM, Tsivintzelis I, von Solms N, Grenner A, Bøgh D, Frost M, et al. Use of monomer fraction data in the parametrization of association theories. Fluid Phase Equilibria. 2010;296(2):219–229.

[71] Mie G. Zur kinetischen Theorie der einatomigen Körper. Annalen der Physik. 1903;316(8):657–697.

[72] London F. The general theory of molecular forces. Transactions of the Faraday Society. 1937;33:8b–26.

[73] Lafitte T, Plantier F, Piñeiro MM, Daridon JL, Bessières D. Accurate global thermophysical characterization of hydrofluoroethers through a Statistical Associating Fluid Theory Variable Range approach, based on new experimental high-pressure volumetric and acoustic data. Industrial & Engineering Chemistry Research. 2007;46(21):6998–7007.

[74] Müller EA, Gubbins KE. An equation of state for water from a simplified intermolecular potential. Industrial & Engineering Chemistry Research. 1995;34(10):3662–3673.

[75] Dufal S, Lafitte T, Haslam AJ, Galindo A, Clark GNI, Vega C, et al. The A in SAFT: developing the contribution of association to the Helmholtz free energy within a Wertheim TPT1 treatment of generic Mie fluids. Molecular Physics. 2015;113(9):948–984.

[76] Dufal S, Lafitte T, Galindo A, Jackson G, Haslam AJ. Developing intermolecular-potential models for use with the SAFT-VR Mie equation of state. AIChE Journal. 2015;61(9):2891–2912.

[77] Gross J. An equation-of-state contribution for polar components: Quadrupolar molecules. AIChE Journal. 2005;51(9):2556–2568.

[78] Kleiner M, Gross J. An equation of state contribution for polar components: Polarizable dipoles. AIChE Journal. 2006;52(5):1951–1961.

[79] Vrabec J, Gross J. Vapor-liquid equilibria simulation and an equation of state contribution for dipole-quadrupole interactions. The Journal of Physical Chemistry B. 2008;112(1):51–60.

[80] Karakatsani EK, Spyriouni T, Economou IG. Extended Statistical Associating Fluid Theory (SAFT) equations of state for dipolar fluids. AIChE Journal. 2005;51(8):2328–2342.

[81] Karakatsani EK, Kontogeorgis GM, Economou IG. Evaluation of the Truncated Perturbed Chain-Polar Statistical Associating Fluid Theory for Complex Mixture Fluid Phase Equilibria. Industrial & Engineering Chemistry Research. 2006;45(17):6063–6074.

[82] Kraska T, Gubbins KE. Phase equilibria calculations with a modified SAFT equation of state. 1. Pure alkanes, alkanols, and water. Industrial & Engineering Chemistry Research. 1996;35(12):4727–4737.

[83] Kraska T, Gubbins KE. Phase equilibria calculations with a modified SAFT equation of state. 2. Binary mixtures of n-alkanes, 1-alkanols, and water. Industrial & Engineering Chemistry Research. 1996;35(12):4738–4746.

[84] Xu K, Li YG, Liu WB. Application of perturbation theory to chain and polar fluids: Pure alkanes, alkanols and water. Fluid Phase Equilibria. 1998;142(1):55–66.

[85] Gubbins KE, Twu CH. Thermodynamics of polyatomic fluid mixtures. I Theory. Chemical Engineering Science. 1978;33(7):863–878.

[86] Rushbrooke GS, Stell G, Høye JS. Theory of polar liquids. I. Dipolar hard spheres. Molecular Physics. 1973;26(5):1199–1215.

[87] Tumakaka F, Sadowski G. Application of the Perturbed-Chain SAFT equation of state to polar systems. Fluid Phase Equilibria. 2004;217(2):233–239.

[88] de Villiers AJ, Schwarz CE, Burger AJ. Improving vapour-liquid-equilibria predictions for mixtures with non-associating polar components using sPC-SAFT extended with two dipolar terms. Fluid Phase Equilibria. 2011;305(2):174–184.

[89] de Villiers AJ, Schwarz CE, Chobanov KG, Burger AJ. Application of sPC-SAFT-JC and sPC-SAFT-GV to phase equilibria predictions of alkane/alcohol, alcohol/alcohol, and water/alcohol binary systems. Industrial & Engineering Chemistry Research. 2014;53(14):6065–6075.

[90] Voutsas E, Perakis C, Pappa G, Tassios D. An evaluation of the performance of the Cubic-Plus-Association equation of state in mixtures of non-polar, polar and associating compounds: Towards a single model for non-polymeric systems. Fluid Phase Equilibria. 2007;261(1):343–350.

[91] Shi L, Liang X. An object-oriented approach for structure design of property calculation programs using equations of state. Industrial & Engineering Chemistry Research. 2011;50(10):6404–6412.

[92] Bender N, Staudt PB, Soares RP, Cardozo NSM. Performance of predictive models in phase equilibria of complex associating systems: PC-SAFT and CEoS/GE. Brazilian Journal of Chemical Engineering. 2013;30(1):75–82.

[93] Grenner A, Tsivintzelis I, Economou IG, Panayiotou C, Kontogeorgis GM. Evaluation of the Nonrandom Hydrogen Bonding (NRHB) Theory and the simplified Perturbed-Chain-Statistical Associating Fluid Theory (sPC-SAFT). 1. Vapor-liquid equilibria. Industrial & Engineering Chemistry Research. 2008;47(15):5636–5650.

[94] Cristino AF, Rosa S, Morgado P, Galindo A, Filipe EJM, Palavra AMF, et al. High-temperature vapour-liquid equilibrium for the water-alcohol systems and modeling with SAFT-VR: 1. Water-ethanol. Fluid Phase Equilibria. 2013;341:48–53.

[95] Cristino AF, Rosa S, Morgado P, Galindo A, Filipe EJM, Palavra AMF, et al. High-temperature vapour-liquid equilibrium for the (water+alcohol) systems and modelling with SAFT-VR: 2. Water-1-propanol. The Journal of Chemical Thermodynamics. 2013;60:15–18.

[96] Rowlinson JS. Liquids and liquid mixtures. 2nd ed. London: Butterworths; 1969.

[97] Sørensen JM, Magnussen T, Rasmussen P, Fredenslund A. Liquid-liquid equilibrium data: Their retrieval, correlation and prediction Part I: Retrieval. Fluid Phase Equilibria. 1979;2(4):297–309.

[98] Raal JD, Mühlbauer AL. Phase equilibria: Measurement and computation. Washington D.C.: Taylor and Francis; 1998.

[99] Abbott MM. Low-pressure phase equilibria: Measurement of VLE. Fluid Phase Equilibria. 1986;29:193–207.

[100] Othmer DF. Composition of vapors from boiling binary solutions. Industrial & Engineering Chemistry. 1928;20(7):743–746.

[101] Cottrell FG. On the determination of boiling points of solutions. Journal of the American Chemical Society. 1919;41(5):721–729.

[102] Lee SC. Partial pressure isotherms II. The Journal of Physical Chemistry. 1930;35(12):3558–3582.

[103] Gillespie DTC. Vapor-liquid equilibrium still for miscible liquids. Industrial & Engineering Chemistry Analytical Edition. 1946;18(9):575–577.

[104] Malanowski S. Experimental methods for vapour-liquid equilibria. Part I. Circulation methods. Fluid Phase Equilibria. 1982;8(2):197–219.

[105] Pienaar C, Schwarz CE, Knoetze JH, Burger AJ. Vapor-liquid-liquid equilibria measurements for the dehydration of ethanol, isopropanol, and *n*-propanol via azeotropic distillation using DIPE and isooctane as entrainers. Journal of Chemical & Engineering Data. 2013;58(3):537–550.

[106] Cripwell JT, Schwarz CE, Burger AJ. Vapor-liquid equilibria measurements for the nine *n*-alkane/ketone pairs comprising 2-, 3-, and 4-heptanone with *n*-octane, *n*-nonane, and *n*-decane. Journal of Chemical & Engineering Data. 2015;60:602–611.

[107] McDermott C, Ellis SRM. A multicomponent consistency test. Chemical Engineering Science. 1965;20(4):293–296.

[108] Wisniak J. A new test for the thermodynamic consistency of vapor-liquid equilibrium. Industrial & Engineering Chemistry Research. 1993;32(7):1531–1533.

[109] Wisniak J, Tamir A. Vapor-liquid equilibriums in the ternary systems water-formic acid-acetic acid and water-acetic acid-propionic acid. Journal of Chemical & Engineering Data. 1977;22(3):253–260.

[110] Kurihara K, Nakamichi M, Kojima K. Isobaric vapor-liquid equilibria for methanol + ethanol + water and the three constituent binary systems. Journal of Chemical & Engineering Data. 1993;38(3):446–449.

[111] Kurihara K, Minoura T, Takeda K, Kojima K. Isothermal vapor-liquid equilibria for methanol + ethanol + water, methanol + water, and ethanol + water. Journal of Chemical & Engineering Data. 1995;40(3):679–684.

[112] Kojima K, Tochigi K, Seki H, Watase K. Determination of vapor-liquid equilibrium from boiling point curve. Kagaku Kogaku. 1968;32(2):149–153.

[113] Khalfaoui B, Meniai AH, Borja R. Thermodynamic properties of water + normal alcohols and vapor-liquid equilibria for binary systems of methanol or 2-propanol with water. Fluid Phase Equilibria. 1997;127(1):181–190.

[114] Verhoeye L, de Schepper H. The vapourliquid equilibria of the binary, ternary and quaternary systems formed by acetone, methanol, propan-2-ol, and water. Journal of Applied Chemistry and Biotechnology. 1973;23(8):607–619.

[115] Danner RP, Gess MA. A data base standard for the evaluation of vapor-liquid-equilibrium models. Fluid Phase Equilibria. 1990;56:285–301.

[116] Tochigi K, Inoue H, Kojima K. Determination of azeotropes in binary systems at reduced pressures. Fluid Phase Equilibria. 1985;22(3):343–352.

[117] Kolbe B, Gmehling J. Thermodynamic properties of ethanol + water. I. Vapour-liquid equilibria measurements from 90 to 150 °C by the static method. Fluid Phase Equilibria. 1985;23(2):213–226.

[118] Woerpel U, Vohland P, Schuberth H. The effect of urea on the vapor-liquid equilibrium behavior of *n*-propanol/water at 60 °C. Zeitschrift für physikalische Chemie (Leipzig). 1977;258(5):905.

[119] Gabaldón C, Marzal P, Montón JB, Rodrigo MA. Isobaric vapor-liquid equilibria of the water + 1-propanol system at 30, 60, and 100 kPa. Journal of Chemical & Engineering Data. 1996;41(5):1176–1180.

[120] Murti P, van Winkle M. Vapor-liquid equilibria for binary systems of methanol, ethyl alcohol, 1-propanol, and 2-propanol with ethyl acetate and 1-propanol-water. Industrial & Engineering Chemistry Chemical & Engineering Data Series. 1958;3(1):72–81.

[121] Arce A, Arce A Jr, Martínez-Ageitos J, Rodil E, Soto A. (Vapour + liquid) equilibrium of (DIPE + IPA + water) at 101.32 kPa. The Journal of Chemical Thermodynamics. 2003;35(6):871–884.

[122] Butler JAV, Thomson DW, Maclennan WH. 173. The free energy of the normal aliphatic alcohols in aqueous solution. Part I. The partial vapour pressures of aqueous solutions of methyl, *n*-propyl, and *n*-butyl alcohols. Part II. The solubilities of some normal aliphatic alcohols in water. Part III. The theory of binary solutions, and its application to aqueous-alcoholic solutions. Journal of the Chemical Society (Resumed). 1933;p. 674–686.

[123] Pierotti GJ, Deal CH, Derr EL. Activity coefficients and molecular structure. Industrial & Engineering Chemistry. 1959;51(1):95–102.

[124] Kharin SE, Perelygin VM, Remizov GP. Liquid-vapor phase equilibrium in ethanol-*n*-butanol and water-*n*-butanol systems. Izv Vyssh Uchebn Zaved, Khim Khim Tekhnol. 1969;12:424–428.

[125] Schreiber E, Schuettau E, Rant D, Schuberth H. Extent to which a metal chloride can influence the behavior of isothermal phase equilibrium in *n*-propanol-water and *n*-butanol-water systems. Zeitschrift für Physikalische Chemie (Leipzig). 1971;247:23–40.

[126] Lyzlova RV, Zaiko LN, Susarev MP. Experimental study and calculation of equilibrium between liquid and vapor in the *n*-butyl alcohol-isobutyl alcohol-water ternary system at 35 °C. Russian Journal of Physical Chemistry (Leningrad). 1979;52(3):551–555.

[127] Fischer K, Gmehling J. *P-x* and γ^{∞} data for the different binary butanol-water systems at 50 °C. Journal of Chemical & Engineering Data. 1994;39(2):309–315.

[128] Freitag J, Kosuge H, Schmelzer JP, Kato S. VLE measurements using a static cell vapor phase manual sampling method accompanied with an empirical data consistency test. The Journal of Chemical Thermodynamics. 2015;80:92–101.

[129] Stockhardt JS, Hull CM. Vapor-liquid equilibria and boiling-point composition relations for systems *n*-butanol-water and isobutanol-water. Industrial & Engineering Chemistry. 1931;23(12):1438–1440.

[130] Bushmakin IN, Begetova AP, Kuchinskaya KI. The equilibrium between the liquid and vapor of the binary system butyl alcoholwater. Sintetichesmii Kauchuk. 1936;4:8–11.

[131] Smith TE, Bonner RF. Vapor-liquid equilibrium still for partially miscible liquids. Industrial & Engineering Chemistry. 1949;41(12):2867–2871.

[132] Boublík T. Gleichgewicht flüssigkeit-Dampf XX. Bestimmung des gleichgewichts flüssigkeit-Dampf in Systemen, deren Komponenten in flüssiger Phase beschränkt mischbar sind. Collection of Czechoslovak Chemical Communications. 1960;25(1):285–288.

[133] Ellis SRM, Garbett RD. A new equilibrium still for the study of partially miscible systems. Industrial & Engineering Chemistry. 1960;52(5):385–388.

[134] Orr V, Coates J. Versatile vapor-liquid equilibrium still. Industrial & Engineering Chemistry. 1960;52(1):27–30.

[135] Hessel D, Geiseler G. Über die druckabhängigkeit des heteroazeotropen systems *n*-butanol/wasser. Zeitschrift für Physikalische Chemie (Leipzig). 1965;229(3):199.

[136] Raju BN, Ranganathan R, Rao MN. Vapour-liquid equilibrium still for partially miscible systems. Indian Chemical Engineer. 1965;7:33–37.

[137] Kato M, Konishi H, Hirata M. New apparatus for isobaric dew and bubble point method. Methanol-water, ethyl acetate-ethanol, water-1-butanol, and ethyl acetate-water systems. Journal of Chemical & Engineering Data. 1970;15(3):435–439.

[138] Zong ZL, Yang XH, Zheng XY. determination and correlation of vapor-liquid equilibria of alcohol solutions. Journal of Chemical Engineering of Japan. 1983;16(1):1–6.

[139] Ochi K, Kojima K. A measurement of vapor-liquid equilibria at extreme dilution. Journal of Chemical Engineering of Japan. 1987;20(1):6–10.

[140] Shakhverdiev AN, Naziev YM, Safarov DT. Temperature dependence of the density of aqueous solutions of *n*-butyl alcohol. Russian Journal of Physical Chemistry. 1994;68(4):553–555.

[141] Iwakabe K, Kosuge H. Isobaric vapor-liquid-liquid equilibria with a newly developed still. Fluid Phase Equilibria. 2001;192(1):171–186.

[142] Gu F, Wang L, Wu Z. Vapor-liquid and liquid-liquid equilibrium for octane + maleic anhydride system. Journal of Chemical & Engineering Data. 2002;47(4):643–647.

[143] Lladosa E, Montón JB, Burguet MC, Muñoz R. Phase equilibrium for the esterification reaction of acetic acid + butan-1-ol at 101.3 kPa. Journal of Chemical & Engineering Data. 2008;53(1):108–115.

[144] Altsybeeva AI, Belousov VP, Ovtrakht NV, Morachevskii AG. Phase equilibria and the thermodynamic properties of the sec-butyl alcohol-water system. Russian Journal of Physical Chemistry. 1964;38(5):1242–1247.

[145] Otsuki H, Kurokawa Y, Yui N. Vapour-liquid equilibrium on sec-butanol-water and sec-butanol-water-uranyl nitrate hexahydrate systems at 25 ^{o}C. Technology Reports of the Tohoku University. 1973;38:197–206.

[146] Gaube J, Krenzer L, Olf G, Wendel R. Vapour-liquid equilibria measurements for some binary mixtures showing partial miscibility. Fluid Phase Equilibria. 1987;35(1):279–289.

[147] Escobedo-Alvarado GN, Sandler SI. Vapor-liquid equilibrium of two aqueous systems that exhibit liquid-liquid phase separation. Journal of Chemical & Engineering Data. 1999;44(2):319–322.

[148] Boeke J, Hanewald KH. Specific gravity-composition, boiling point-composition and vapour-liquid equilibria relations for the systems methyl ethyl ketone-water and sec-butanol-water. Recueil des Travaux Chimiques des Pays-Bas. 1942;61(12):881–887.

[149] Yamamoto Y, Maruyama T. Separating agents in azeotropic distillation of sec-butanol and water. Kagaku Kogaku Ronbunshu. 1959;23(10):635–640.

[150] Jasper JJ, Farrell LG, Madoff M. The partially miscible system water-normal amyl alcohol. Journal of Chemical Education. 1944;21(11):536–538.

[151] Beregovykh VV, Timofeev VS, Luk'yanova RN, Yakushev VM, Serafimov LA. Liquid-vapor equilibrium in systems formed by water and butyl acetate with homologs of monohydric C_1-C_5 saturated alcohols. Uch Zap Mosk Inst Tonkoi Khim Tekhnol. 1971;1(3):38–44.

[152] Cho TH, Ochi K, Kojima K. Isobaric vapor-liquid equilibria for binary systems with limited miscibility, water-normal-amyl alcohol and water-isoamyl alcohol. Kagaku Kogaku Ronbunshu. 1984;10(2):181–183.

[153] Zou M, Prausnitz JM. Vapor-liquid and liquid-liquid equilibria in binary aqueous systems. Journal of Chemical & Engineering Data. 1987;32(1):34–37.

[154] Pienaar C. Evaluation of entrainers for the dehydration of C_2 and C_3 alcohols via azeotropic distillation [Master's thesis]. University of Stellenbosch. Stellenbosch; 2012.

[155] Gomis V, Ruiz F, Asensi JC. The application of ultrasound in the determination of isobaric vapour-liquid-liquid equilibrium data. Fluid Phase Equilibria. 2000;172(2):245–259.

[156] Lladosa E, Cháfer A, Montón JB, Martínez NF. Liquid-liquid and vapor-liquid-liquid equilibrium of the 4-methyl-2-pentanone + 2-butanol + water system. Journal of Chemical & Engineering Data. 2011;56(5):1925–1932.

[157] DIPPR 801 Database, Design Institute for Physical Properties. *Sponsored by AICHe*;. Available from: http://www.aiche.org/dippr.

[158] Malesiński W. Azeotropy and Other Theoretical Problems. Canada: John Wiley & Sons; 1965.

[159] Gironi F, Lamberti L. Vapour-liquid equilibrium data for the water-2-propanol system in the presence of dissolved salts. Fluid Phase Equilibria. 1995;105(2):273–286.

[160] Levenberg K. A method for the solution of certain non-linear problems in least squares. Quarterly of Applied Mathematics. 1944;2(2):164–168.

[161] Marquardt DW. An algorithm for least-squares estimation of nonlinear parameters. Journal of the Society for Industrial and Applied Mathematics. 1963;11(2):431–441.

[162] Ungerer P, Tavitian B, Boutin A. Applications of molecular simulation in the oil and gas industry: Monte Carlo methods. Paris: Editions Technip; 2005.

[163] Behzadi B, Ghotbi C, Galindo A. Application of the simplex simulated annealing technique to nonlinear parameter optimization for the SAFT-VR equation of state. Chemical Engineering Science. 2005;60(23):6607–6621.

[164] von Solms N, Michelsen ML, Passos CP, Derawi SO, Kontogeorgis GM. Investigating models for associating fluids using spectroscopy. Industrial & Engineering Chemistry Research. 2006;45(15):5368–5374.

[165] Asprion N, Hasse H, Maurer G. FT-IR spectroscopic investigations of hydrogen bonding in alcohol-hydrocarbon solutions. Fluid Phase Equilibria. 2001;186(1):1–25.

[166] Martínez S. Methanol/*n*-hexane system. I. Infrared studies. Spectrochimica Acta Part A: Molecular Spectroscopy. 1986;42(4):531–536.

[167] Yamaguchi T, Hidaka K, Soper AK. The structure of liquid methanol revisited: a neutron diffraction experiment at -80 ^{o}C and +25 ^{o}C. Molecular Physics. 1999;96(8):1159–1168.

[168] dos Ramos MC, Docherty H, Blas FJ, Galindo A. Application of the generalised SAFT-VR approach for long-ranged square-well potentials to model the phase behaviour of real fluids. Fluid Phase Equilibria. 2009;276(2):116–126.

[169] Dominik A, Chapman WG, Kleiner M, Sadowski G. Modeling of polar systems with the Perturbed-Chain SAFT equation of state. Investigation of the performance of two polar terms. Industrial & Engineering Chemistry Research. 2005;44(17):6928–6938.

[170] Sun T, Biswas SN, Trappeniers NJ, Ten Seldam CA. Acoustic and thermodynamic properties of methanol from 273 to 333 K and at pressures to 280 MPa. Journal of Chemical & Engineering Data. 1988;33(4):395–398.

[171] NIST Chemistry WebBook;. Available from: http://webbook.nist.gov/chemistry/.

[172] Wolff H, Höppel HE. Deuteriumbrückenassoziation und konzentrationsabhängiger Dampfdruck-Isotopie-Effekt von Methanol in *n*-Hexan. Berichte der Bunsengesellschaft für physikalische Chemie. 1968;72(6):722–725.

[173] Wegge R, Richter M, Span R. Speed of sound measurements in ethanol and benzene over the temperature range from (253.2 to 353.2) K at pressures up to 30 MPa. Journal of Chemical & Engineering Data. 2015;60(5):1345–1353.

[174] Fulem M, Růžička K, Růžička V. Heat capacities of alkanols: Part I. Selected 1-alkanols C_2 to C_{10} at elevated temperatures and pressures. Thermochimica Acta. 2002;382(1):119–128.

[175] Pena MD, Cheda DR. Liquid-vapor equilibrium. III. Systems of *n*-propanol-*n*-hexane at 50 °C and *n*-propanol-*n*-heptane at 60 °C. Anales de Química. 1970;66:747–755.

[176] Dzida M, Ernst S. Speed of sound in propan-1-ol + heptane mixtures under elevated pressures. Journal of Chemical & Engineering Data. 2003;48(6):1453–1457.

[177] Dávila MJ, Gedanitz H, Span R. Speed of sound in saturated aliphatic alcohols (propan-2-ol, butan-2-ol, and 2-methylpropan-1-ol) and alkanediols (ethane-1,2-diol, propane-1,2- and -1,3-diol) at temperature between 253.15 K and 353.15 K and pressures up to 30 MPa. The Journal of Chemical Thermodynamics. 2016;101:199–206.

[178] Casás LM, Plantier F, Piñeiro MM, Legido JL, Bessières D. Calibration of a low temperature calorimeter and application in the determination of isobaric heat capacity of 2-propanol. Thermochimica Acta. 2010;507–508:123–126.

[179] Maciel MRW, Francesconi AZ. Excess Gibbs free energies of (*n*-hexane + propan-1-ol) at 338.15 and 348.15 K and of (*n*-hexane + propan-2-ol) at 323.15, 338.15, and 348.15 K. The Journal of Chemical Thermodynamics. 1988;20(5):539–544.

[180] Wilson W, Bradley D. Speed of sound in four primary alcohols as a function of temperature and pressure. The Journal of the Acoustical Society of America. 1964;36(2):333–337.

[181] Heintz A, Dolch E, Lichtenthaler RN. New experimental VLE-data for alkanol/alkane mixtures and their description by an extended real association (ERAS) model. Fluid Phase Equilibria. 1986;27:61–79.

[182] Andon RJL, Connett JE, Counsell JF, Lees EB, Martin JF. Thermodynamic properties of organic oxygen compounds. Part XXVII. (±)-Butan-2-ol and (+)-butan-2-ol. Journal of the Chemical Society A: Inorganic, Physical, Theoretical. 1971;p. 661–664.

[183] Araujo ME, Maciel MRW, Francesconi AZ. Excess Gibbs free energies of (hexane + butan-2-ol) and of (cyclohexane + butan-2-ol) at the temperatures (323.15, 338.15, and 348.15) K. The Journal of Chemical Thermodynamics. 1993;25(11):1295–1299.

[184] Dzida M. Study of the effects of temperature and pressure on the thermodynamic and acoustic properties of pentan-1-ol, 2-methyl-2-butanol, and cyclopentanol in the pressure range from (0.1 to 100) MPa and temperature from (293 to 318) K. Journal of Chemical & Engineering Data. 2009;54(3):1034–1040.

[185] Counsell JF, Lees EB, Martin JF. Thermodynamic properties of organic oxygen compounds. Part XIX. Low-temperature heat capacity and entropy of propan-1-ol, 2-methylpropan-1-ol, and pentan-1-ol. Journal of the Chemical Society A: Inorganic, Physical, Theoretical. 1968;p. 1819–1823.

[186] Máchová I, Linek J, Wichterle I. Vapour-liquid equilibria in the heptane - 1-pentanol and heptane - 3-methyl-1-butanol systems at 75, 85 and 95 °C. Fluid Phase Equilibria. 1988;41(3):257–267.

[187] Ribeiro AF, Langa E, Mainar AM, Pardo JI, Urieta JS. Excess molar enthalpy, density, and speed of sound for the mixtures β-pinene + 1- or 2-pentanol at (283.15, 298.15, and 313.15) K. Journal of Chemical & Engineering Data. 2006;51(5):1846–1851.

[188] Čenský M, Růžička K, Růžička V, Zábranský M. Heat capacities of alkanols: II. Some isomeric C_5 alkanols. Thermochimica Acta. 2003;408(1):45–53.

[189] Wolfová J, Linek J, Wichterle I. Vapour-liquid equilibria in the heptane-2-pentanol and heptane-2-methyl-1-butanol systems at 75, 85 and 95 °C. Fluid Phase Equilibria. 1991;64:281–289.

[190] González-Salgado D, Troncoso J, Plantier F, Daridon JL, Bessières D. Study of the volumetric properties of weakly associated alcohols by means of high-pressure speed of sound measurements. The Journal of Chemical Thermodynamics. 2006;38(7):893–899.

[191] Wolfová J, Linek J, Wichterle I. Vapour-liquid equilibria in the heptane-3-pentanol and heptane-2-methyl-2-butanol systems at constant temperature. Fluid Phase Equilibria. 1990;54:69–79.

[192] Benedetto G, Gavioso RM, Albo PAG, Lago S, Ripa DM, Spagnolo R. Speed of sound in pure water at temperatures between 274 and 394 K and at pressures up to 90 MPa. International Journal of Thermophysics. 2005;26(6):1667–1680.

[193] Lourenço MJV, Santos FJV, Ramires MLV, Nieto de Castro CA. Isobaric specific heat capacity of water and aqueous cesium chloride solutions for temperatures between 298 K and 370 K at $p = 0.1$ MPa. The Journal of Chemical Thermodynamics. 2006;38(8):970–974.

[194] Tybjerg PCV, Kontogeorgis GM, Michelsen ML, Stenby EH. Phase equilibria modeling of methanol-containing systems with the CPA and sPC-SAFT equations of state. Fluid Phase Equilibria. 2010;288(1):128–138.

[195] Grenner A, Schmelzer J, von Solms N, Kontogeorgis GM. Comparison of two association models (Elliott-Suresh-Donohue and simplified PC-SAFT) for complex phase equilibria of hydrocarbon-water and amine-containing mixtures. Industrial & Engineering Chemistry Research. 2006;45(24):8170–8179.

[196] Cripwell JT. Improvement of the thermodynamic description of polar molecules and their mixtures in the SAFT framework [Doctoral dissertation]. Stellenbosch University. Stellenbosch; 2017.

[197] Errington JR, Boulougouris GC, Economou IG, Panagiotopoulos AZ, Theodorou DN. Molecular simulation of phase equilibria for water-methane and water-ethane mixtures. The Journal of Physical Chemistry B. 1998;102(44):8865–8873.

[198] Koh CA, Tanaka H, Walsh JM, Gubbins KE, Zollweg JA. Thermodynamic and structural properties of methanol-water mixtures: Experiment, theory, and molecular simulation. Fluid Phase Equilibria. 1993;83:51–58.

[199] Llovell F, Peters CJ, Vega LF. Second-order thermodynamic derivative properties of selected mixtures by the soft-SAFT equation of state. Fluid Phase Equilibria. 2006;248(2):115–122.

[200] de Villiers AJ, Schwarz CE, Burger AJ, Kontogeorgis GM. Evaluation of the PC-SAFT, SAFT and CPA equations of state in predicting derivative properties of selected non-polar and hydrogen-bonding compounds. Fluid Phase Equilibria. 2013;338:1–15.

[201] Cerdeiriña CA, González-Salgado D, Romaní L, del Carmen Delgado M, Torres LA, Costas M. Towards an understanding of the heat capacity of liquids. A simple two-state model for molecular association. The Journal of Chemical Physics. 2004;120(14):6648–6659.

[202] Cerdeiriña CA, Troncoso J, González-Salgado D, García-Miaja G, Hernández-Segura GO, Bessières D, et al. Heat capacity of associated systems. Experimental data and application of a two-state model to pure liquids and mixtures. The Journal of Physical Chemistry B. 2007;111(5):1119–1128.

[203] Oracz P. Recommendations for VLE data on binary 1-alkanol + n-alkane systems. Fluid Phase Equilibria. 1993;89(1):103–172.

[204] Budantseva LS, Lesteva TM, Nemtsov MS. Liquid-vapor equilibrium in systems methanol-C_7-C_8 hydrocarbons of different classes. Russian Journal of Physical Chemistry. 1975;49:1844.

[205] Katz K, Newman M. Vapor-liquid equilibria for ethyl alcohol-n-heptane at low pressure. Industrial & Engineering Chemistry. 1956;48(1):137–141.

[206] Boublikova L, Lu BCY. Isothermal vapour-liquid equilibria for the ethanol-n-octane system. Journal of Chemical Technology and Biotechnology. 1969;19(3):89–92.

[207] Hiaki T, Takahashi K, Tsuji T, Hongo M, Kojima K. Vapor-liquid equilibria of ethanol + octane at 343.15 K and 1-propanol + octane at 358.15 K. Journal of Chemical & Engineering Data. 1995;40(1):271–273.

[208] Berro C, Péneloux A. Excess Gibbs energies and excess volumes of 1-butanol-n-heptane and 2-methyl-1-propanol-n-heptane binary systems. Journal of Chemical & Engineering Data. 1984;29(2):206–210.

[209] Kumar A, Katti S. Excess free-energies of binary mixtures of isomeric butanols with normal heptane. Indian Journal of Chemistry Section A. 1980;19(8):795–797.

[210] Ronc M, Ratcliff GR. Measurement of vapor-liquid equilibria using a semi-continuous total pressure static equilibrium still. The Canadian Journal of Chemical Engineering. 1976;54(4):326–332.

[211] Ott JB, Sipowska JT, Marchant BG. Excess enthalpies for (pentane + methanol) at the temperatures (283.15, 298.15, and 363.15) K and the pressures (0.4, 5, and 15) MPa. The Journal of Chemical Thermodynamics. 1994;26(7):717–725.

[212] Orge B, Iglesias M, Rodríguez A, Canosa JM, Tojo J. Mixing properties of (methanol, ethanol, or 1-propanol) with (n-pentane, n-hexane, n-heptane and n-octane) at 298.15 K. Fluid Phase Equilibria. 1997;133(1):213–227.

[213] Tanaka R, Toyama S, Murakami S. Heat capacities of $\{x\mathrm{C}_n\mathrm{H}_{2n+1}+(1\text{-}x)\mathrm{C}_7\mathrm{H}_{16}\}$ for $n =$ 1 to 6 at 298.15 K. The Journal of Chemical Thermodynamics. 1986;18(1):63–73.

[214] Lama RF, Lu BCY. Excess thermodynamic properties of aqueous alcohol solutions. Journal of Chemical & Engineering Data. 1965;10(3):216–219.

[215] González B, Calvar N, Gómez E, Domínguez A. Density, dynamic viscosity, and derived properties of binary mixtures of methanol or ethanol with water, ethyl acetate, and methyl acetate at T = (293.15, 298.15, and 303.15) K. The Journal of Chemical Thermodynamics. 2007;39(12):1578–1588.

[216] Benson GC, D'Arcy PJ. Excess isobaric heat capacities of water-n-alcohol mixtures. Journal of Chemical & Engineering Data. 1982;27(4):439–442.

[217] van Ness HC, Soczek CA, Kochar NK. Thermodynamic excess properties for ethanol-n-heptane. Journal of Chemical & Engineering Data. 1967;12(3):346–351.

[218] Treszczanowicz AJ, Benson GC. Excess volumes for n-alkanols + n-alkanes. I. Binary mixtures of methanol, ethanol, n-propanol, and n-butanol + n-heptane. The Journal of Chemical Thermodynamics. 1977;9(12):1189–1197.

[219] Fortier JL, Benson GC. Excess heat capacities of binary liquid mixtures determined with a Picker flow calorimeter. The Journal of Chemical Thermodynamics. 1976;8(5):411–423.

[220] Ott JB, Stouffer CE, Cornett GV, Woodfield BF, Wirthlin RC, Christensen JJ, et al. Excess enthalpies for (ethanol + water) at 298.15 K and pressures of 0.4, 5, 10, and 15 MPa. The Journal of Chemical Thermodynamics. 1986;18(1):1–12.

[221] Grolier JPE, Wilhelm E. Excess volumes and excess heat capacities of water + ethanol at 298.15 K. Fluid Phase Equilibria. 1981;6(3–4):283–287.

[222] Savini CG, Winterhalter DR, van Ness HC. Heats of mixing of some alcohol-hydrocarbon systems. Journal of Chemical and Engineering Data. 1965;10(2):168–171.

[223] Denda M, Touhara H, Nakanishi K. Excess molar enthalpies for (water + a fluoroalkanol). The Journal of Chemical Thermodynamics. 1987;19(5):539–542.

[224] Herráez JV, Belda R. Refractive indices, densities and excess molar volumes of monoalcohols + water. Journal of Solution Chemistry. 2006;35(9):1315–1328.

[225] van Ness HC, Soczek CA, Peloquin GL, Machado RL. Thermodynamic excess properties of three alcohol-hydrocarbon systems. Journal of Chemical & Engineering Data. 1967;12(2):217–224.

[226] González B, Dominguez A, Tojo J. Viscosities, densities and speeds of sound of the binary systems: 2-propanol with octane, or decane, or dodecane at T=(293.15, 298.15, and 303.15) K. The Journal of Chemical Thermodynamics. 2003;35(6):939–953.

[227] Tanaka R, Toyama S. Excess molar heat capacities and excess molar volumes of (propan-2-ol, or butan-2-ol, or pentan-2-ol, or pentan-3-ol, or 2-methylbutan-2-ol + n-heptane) at the temperature 298.15 K. The Journal of Chemical Thermodynamics. 1996;28(12):1403–1410.

[228] Kwaterski M, Rezanova EN, Lichtenthaler RN. Excess molar volumes and excess molar enthalpies of binary and ternary mixtures of (ethanol or 1-butanol), triethylamine and n-hexane. Fluid Phase Equilibria. 2005;237(1):170–185.

[229] Marongiu B, Ferino I, Monaci R, Solinas V, Torrazza S. Thermodynamic properties of aqueous non-electrolyte mixtures. Alkanols + water systems. Journal of Molecular Liquids. 1984;28(4):229–247.

[230] Ogawa H, Murakami S. Excess isobaric heat capacities for water + alkanol mixtures at 298.15 K. Thermochimica Acta. 1986;109(1):145–154.

[231] Hamam SEM, Kumaran MK, Benson GC. Excess enthalpies of some binary mixtures: (a C_5-alkanol + *n*-heptane) at 298.15 K. The Journal of Chemical Thermodynamics. 1984;16(11):1013–1017.

[232] Treszczanowicz AJ, Benson GC. Excess volumes for *n*-alkanols + *n*-alkanes. II. Binary mixtures of *n*-pentanol, *n*-hexanol, *n*-octanol, and *n*-decanol + *n*-heptane. The Journal of Chemical Thermodynamics. 1978;10(10):967–974.

[233] Young JC Jr, Binford JS Jr, Campbell SW. Excess enthalpies of five pentanol isomer + *n*-heptane systems measured at 303.15 K and a model describing the behavior. Fluid Phase Equilibria. 2003;209(2):255–264.

[234] Sauer SG, Chapman WG. A parametric study of dipolar chain theory with applications to ketone mixtures. Industrial & Engineering Chemistry Research. 2003;42(22):5687–5696.

Appendix A

Detailed Experimental Methodology

As stated in Chapter 4 the experimental procedure is divided into 4 main parts. Here each of the parts are described in more detail. The schematic representation of the still is reprinted in Fig. A.1 for ease of reference. The accompanying labels are given in Table A.1.

A.1 Still Preparation

1. Prior to starting a new experimental sequence the following aspects need to be checked:

   - Maintenance of the pump requires that the quality and quantity of the pump oil must be monitored. The oil level should lie in the midrange of the oil sight glass and the oil should be clear. If the oil level is low it should be topped up. If the oil is murky the pump manual should be consulted.
   - To prevent contamination from previous experimental runs, the still must be dry prior to adding fresh feed. The washing procedure is described in Section A.3. Compressed air can be passed through the apparatus to ensure that is dry.
   - Check that the pump supplying water to the condensers is completely submerged.
   - Open the nitrogen canister if operation is at overpressure conditions. Set the regulator to allow only a small flow of nitrogen to the equipment.

2. Start the still and the computer software.

3. Select the mode of pressure operation: Switch the three-way valve located on the hydraulic box to either vacuum or pressure. Make the same selection in the computer software. For operation at atmospheric conditions choose “ATM” in the software, while selecting either ‘Vacuum” or “Pressure” on the three-way valve.

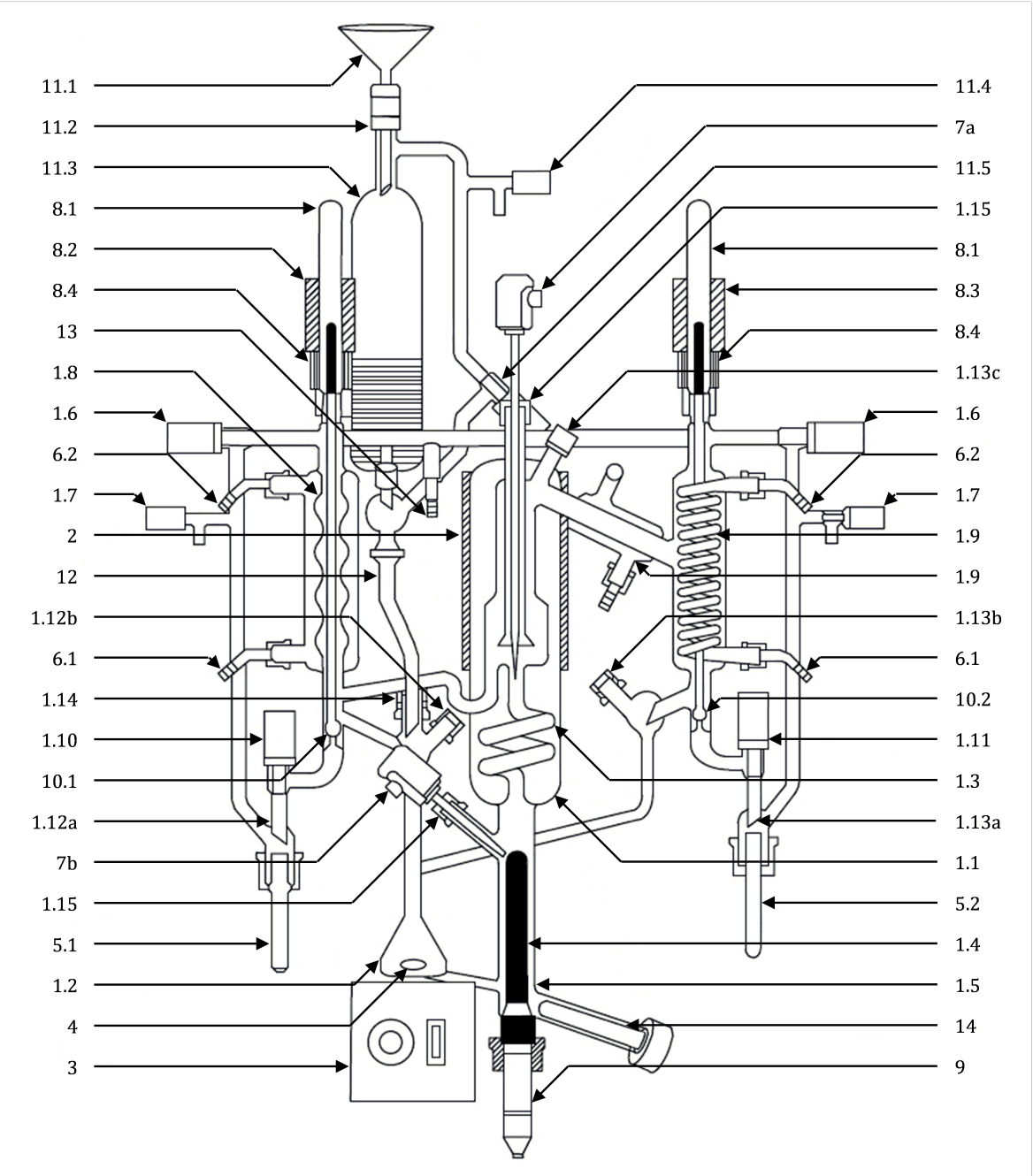

Figure A.1: Schematic representation of the dynamic still. Figure reprinted with permission [154].

4. Before adding feed to the still, secure the ultrasonic homogeniser (14), and close the discharge valve (1.5) and feed burette valve.

5. Add approximately 100 mL of fresh feed to the feed burette. For a binary A-B system the still is initially charged with pure A. The vapour pressure of the pure component is

measured for two reasons: (1) It is a data point in the composition range, and (2) It

Table A.1: Labels for experimental setup shown in Fig. A.1.

No.	Description	No.	Description	No.	Description
1.1	Glass body of phase equilibrium apparatus	1.14	Liquid phase filler nozzle	8.4	Spacer
1.2	Mixing chamber	1.15	Temperature probe nozzle	9	Immersion heater rod
1.3	Cottrell pump with silvered vacuum jacket	2	Heating jacket	10.1	Liquid phase valve rod
1.4	Flow heater	3	Magnetic stirrer	10.2	Vapour phase valve rod
1.5	Discharge valve	4	Stirring magnet	11.1	Funnel
1.6	Stop valve	5.1	Liquid phase glass receiver vial	11.2	Feed burette filler nozzle
1.7	Aeration valve	5.2	Vapour phase glass receiver vial	11.3	Feed burette
1.8	Liquid phase cooler	6.1	Hose connection olive - inlet	11.4	Feed burette aeration valve
1.9	Condenser	6.2	Hose connection olive - outlet	11.5	Feed burette stop valve
1.10	Liquid phase stop valve	7	Temperature sensor	12	Inlet line
1.11	Vapour phase stop valve	8.1	Valve cap	13	Glass connecting olive for pressure control
1.12	Liquid phase sampling nozzle	8.2	Liquid phase solenoid coil	14	Ultrasonic homogeniser
1.13	Vapour phase sampling nozzle	8.3	Vapour phase solenoid coil		

gives an indication of the reliability of the experimental data, since vapour pressures are typically available in literature. Vapour pressure can also indicate whether the still was in fact clean before charging, since any slight amount of contamination will influence the vapour pressure of the pure component.

6. Open the feed burette valve to allow the feed to enter the mixing chamber (1.2). The flow heater (1.4) should be completely submerged in liquid.

7. Once the still is charged, close the feed burette valve and switch on the magnetic stirrer.

8. Fit the glass receiver vials (5.1 and 5.2) and sampling nozzle caps (1.12b and 1.13b)

securely. Close the aeration valves (1.7) and feed burette stop valve (11.5). Open the stop valves (1.6) to ensure that the whole still is operated isobarically.

9. The power setting, pressure set point, mantle temperature, and vapour return line temperature are specified within the computer software:

   - The power setting is dependent on the volatility and heat capacity of the system components, as well as the operating pressure. The power setting should be high enough to produce a vapour, but not too much that only vapour is produced. For example, a power setting of 23 % is sufficient to produce both liquid and vapour returns for pure acetone (T_b = 329 K) at ~ 0.1 MPa, while a power setting of 65 % is necessary to produce the same conditions for pure water (T_b = 373 K) at ~ 0.1 MPa. A power setting of 65% was used throughout this work for all systems investigated.
   - The equipment pressure is controlled independently of the computer software. For both overpressure and vacuum conditions pressure is indicated by a Wika UT-10 unit. For overpressure operation the system pressure is maintained by balancing the amount of nitrogen that enters the system with the nitrogen that leaves the system through the aeration valves (1.7). However, for vacuum conditions it is necessary to specify a pressure set point within the computer software in order to operate the vacuum pump. The pressure set point is set to approximately 5×10^{-3} MPa below the desired value to ensure that the vacuum pump runs smoothly. Pressure control by the computer software was bypassed in a previous project [40] since this control caused large deviations from the set point. The amount of vacuum drawn from the system is manually throttled by the valve on the hydraulic box to achieve the desired pressure value.
   - Set the mantle (2) temperature to ~ 20 K above the equilibrium temperature to ensure that the vapour is completely in the vapour phase upon reaching the vapour sampling needle.
   - Switch on the vapour return line heater for experimental runs in the water-rich side of the composition range. The glass tube returning to the mixing chamber has a very small diameter. Water has a very high surface tension and subsequently blocks the entrance of the tube. Heating the condensed vapour receiver port (1.13b) and the vapour return line reduces the surface tension and the viscosity of water, allowing it to flow back to the mixing chamber.

A.2 Obtaining Measurements

1. Once the still has been prepared for operation, switch on the equipment by clicking on the "Start" button in the software. When operating at vacuum conditions the pump will start drawing vacuum. The system should be allowed to stabilise before altering the pressure by means of the throttling valve.

2. Liquid sampling:

   (a) Flush the liquid phase sampling well, which is controlled by the solenoid valve (10.1), periodically. A small volume of fluid collects in the well and should be removed in order to take samples representative of equilibrium conditions.

   (b) Open the solenoid valve (10.1) pressing the remote button situated on the floor of the extraction cabinet.

   (c) The flushed liquid is collected in the glass vial (5.1) by opening the stop valve (1.10).

   (d) Close the isolation valve (1.6) after the second flushing sequence to isolate the sampling arm from the rest of the system.

   (e) Open the aeration valve (1.7) to bring the sampling arm to atmospheric pressure.

   (f) Discard the liquid in the glass vial (5.1).

   (g) Wipe away any residual liquid drops still present on the sampling nozzle (1.12a) before fitting a clean glass vial to the still.

   (h) Close the aeration valve (1.7) and reopen the isolation valve (1.6).

   (i) Flushing is conducted twice, 15 and 30 minutes after adding additional component to the still, after which the still is left to run for an hour before sampling.

   (j) Sampling is conducted in the same way as flushing, but the liquid is kept for analysis.

3. Vapour sampling; Syringe preparation:

   (a) Preload a Hamilton 5 mL syringe, fitted with a needle valve, with approximately 100-200 μL of solvent using needle A.

   (b) Remove needle A, clean the valve fitting with compressed air, and fit clean needle B to the valve. This procedure is conducted to ensure that no solvent could potentially evaporate from the needle while it is housed in the vapour sampling nozzle (1.13c).

   (c) Place needle B, attached to the syringe, in position in the vapour sampling nozzle (1.13c) approximately one hour before sampling to ensure that the needle heats up and that negligible condensation occurs on the outside of the needle.

4. Vapour sampling; Sampling procedure:
   (a) Open the needle valve to draw a sample of the vapour phase.
   (b) Allow approximately 45 seconds for sampling to ensure the drawn sample is large enough for analysis.
   (c) Monitor both the temperature and pressure readings during the sampling period to ensure that no large deviations occur.
5. Terminate operation of the still in the computer software once samples are taken.
6. Open the feed burette stop valve (11.5) to bring the still to atmospheric pressure.
7. If the still was initially charged with pure component A add a small amount of component B to the mixing chamber after each run to move along the composition spectrum. The volume of B added should ensure submersion of the immersion heater. If the components are non-volatile and expand upon heating it might be necessary to drain a small amount of mixture from the discharge valve (1.5) to add a large enough quantity of component B.
8. Replace the septum in the valve cap on the vapour sampling nozzle (1.13c)after each run.
9. Switch on the equipment again to start the next run and repeat the procedure.

A.3 Draining and Cleaning

The still contents may be left in the still overnight if experiments on the same feed composition are continued the next day. If measurements from the other side of the composition spectrum are started, or if a new binary system is investigated, it is necessary to clean the still. The cleaning procedure is as follows:

1. Switch of the still in the computer software, close the nitrogen canister, and switch off the ultrasonic homogeniser (14).
2. Allow the still and its contents to cool down. Close the doors of the extraction cabinet to speed up this process.
3. Drain the mixture from the discharge valve (1.5). Leave the the stirring magnet (4) on in order to drain as much liquid as possible from the mixing chamber.
4. Carefully unfasten the ultrasonic homogeniser (14). Use a wad of tissue paper to absorb any residual liquid exiting the heating chamber.

5. Charge the feed burette (11.3) with approximately 110 mL of acetone and allow it to into the mixing chamber (1.2). To prevent any acetone from contacting the teflon seal connecting the feed burette (11.3) to the inlet line (12), open the feed burette stop valve (1.4) and remove the liquid phase sampling nozzle (1.12b) cap.

6. Run the still at atmospheric conditions by selecting "ATM" in the computer software.

7. Use a power setting of 30 % and a mantle temperature of 293 K.

8. Run the apparatus for approximately 30 minutes. Flush the solenoid valves (8.1) a few times to clean the sampling wells, and drain the flushed liquid from the glass receivers (5.1 and 5.2). This procedure also cleans the stop valve taps (1.10 and 1.11).

9. To "flood" the condensers, the pressure setting is set to "Vacuum" and the throttling valve is opened. This decreases the pressure of the system rapidly, causing an increase in both the liquid and vapour returns.

10. Once the washing procedure is completed, allow the still and its contents to cool down, and drain the acetone from the mixing chamber (1.2).

11. To ensure the acetone remaining in the still is evaporated, remove the temperature probe (7a) from the equilibrium chamber (1.1), and open all other valves.

A. DETAILED EXPERIMENTAL METHODOLOGY

Appendix B

Experimental Results

B.1 Thermodynamic Consistency Testing

The thermodynamic consistency of the experimental data was tested using the McDermott-Ellis and the Wisniak L/W consistency tests, as described in Section 3.3. The *PRO-VLE 2.0* software was used to calculate activity coefficients required for the McDermott-Ellis test, and the L_i and W_i values required for the Wisniak L/W test.

The following component specific values were used:

Table B.1: Pure component parameters used in thermodynamic testing.

	1-butanol	1-pentanol	2-pentanol	3-pentanol	water
Antoine A	7.15113	6.94073	7.03923	7.07968	7.39153
Antoine B	1185.47064	1163.37441	1143.58654	1155.96259	1277.16443
Antoine C	159.96527	148.80322	155.99669	160.09934	182.76958
T_c/K	563.1	588.2	560.4	559.6	647.1
p_c/atm	43.56	38.69	36.61	36.12	217.75
V_c/cm^3·mol^{-1}	273.00	326.00	329.00	325.00	55.95
T_b/K	390.77	410.76	392.20	388.45	373.15
ω	0.58828	0.57899	0.55498	0.51427	0.34486
V^L_{alkanol}/cm^3·mol^{-1}	102.9603	120.2944	120.7865	119.1496	*
V^L_{water}/cm^3·mol^{-1}	18.8805	19.0749	18.8908	18.8517	
Δh^{vap}/cal·mol^{-1}	10310.00	10799.96	10273.60	10099.92	9716.79
μ/Debye	1.66984	1.70000	1.66089	1.63991	1.84972

B.2 Water + 1-Butanol

Table B.2: Vapour-liquid equilibrium experimental results for the water (2) + 1-butanol (1) system at p = 0.1013 MPa (D=2.247).

T/K	x_{1a}	x_{1b}	Δx	y_{1a}	y_{1b}	Δy	$x_{1,\mathrm{avg}}$	$y_{1,\mathrm{avg}}$	γ_1	γ_2	L	W
373.08							0.0000	0.0000				
372.16	0.0007	0.0007	0.0000	0.0303	0.0304	0.0001	0.0007	0.0304	80.386	1.019	1.003	1.404
371.98	0.0014	0.0014	0.0000	0.0426	0.0427	0.0001	0.0014	0.0427	61.801	1.013	12.585	13.254
370.95	0.0024	0.0024	0.0000	0.0864	0.0861	0.0003	0.0024	0.0862	75.093	1.005	12.623	13.293
370.24	0.0035	0.0034	0.0001	0.1122	0.1131	0.0009	0.0035	0.1126	68.965	1.003	12.661	13.332
368.57	0.0070	0.0071	0.0000	0.1674	0.1707	0.0034	0.0070	0.1690	54.782	1.002	12.699	13.371
367.71	0.0093	0.0092	0.0001	0.1997	0.1976	0.0020	0.0093	0.1986	50.659	1.000	12.737	13.410
367.25	0.0102	0.0104	0.0002	0.2126	0.2088	0.0038	0.0103	0.2107	49.143	1.004	12.775	13.449
367.04	0.2693	0.2684	0.0009	0.2763	0.2810	0.0047	0.2688	0.2786	2.516	1.251	12.813	13.488
365.87	0.3161	0.3106	0.0054	0.2576	0.2554	0.0022	0.3133	0.2565	2.086	1.435	12.851	13.527
365.85	0.3139	0.3148	0.0008	0.2547	0.2447	0.0100	0.3144	0.2497	2.025	1.452	12.889	13.566
365.97	0.3485	0.3421	0.0064	0.2667	0.2585	0.0081	0.3453	0.2626	1.929	1.487	13.317	13.998
365.91	0.3452	0.3491	0.0039	0.2640	0.2580	0.0060	0.3472	0.2610	1.912	1.498	13.409	14.093
365.87	0.3504	0.3551	0.0047	0.2400	0.2398	0.0002	0.3528	0.2399	1.732	1.557	13.549	14.236
365.90	0.3543	0.3697	0.0153	0.2570	0.2478	0.0091	0.3619	0.2524	1.774	1.551	13.680	14.369
365.97	0.3619	0.3716	0.0097	0.2581	0.2504	0.0077	0.3667	0.2543	1.759	1.555	13.696	14.382
366.14	0.4238	0.3943	0.0295	0.2471	0.2548	0.0076	0.4088	0.2509	1.547	1.662	14.268	14.958
366.19	0.4156	0.4273	0.0117	0.2746	0.2542	0.0204	0.4214	0.2642	1.577	1.665	14.441	15.132
366.19	0.4353	0.4267	0.0086	0.2533	0.2553	0.0021	0.4310	0.2543	1.484	1.716	14.611	15.304
366.38	0.4567	0.4651	0.0084	0.2598	0.2543	0.0055	0.4608	0.2571	1.392	1.792	14.948	15.639
367.69	0.5885	0.5614	0.0271	0.3084	0.2922	0.0162	0.5748	0.3002	1.235	2.037	15.644	16.298
369.17	0.6887	0.6903	0.0016	0.3254	0.3307	0.0053	0.6895	0.3281	1.059	2.535	16.178	16.779
371.37	0.7411	0.7391	0.0020	0.3712	0.3685	0.0026	0.7401	0.3699	1.019	2.620	14.865	15.366
374.50	0.7988	0.7834	0.0153	0.4381	0.4260	0.0120	0.7910	0.4320	0.985	2.624	12.626	12.996
378.36	0.8848	0.8909	0.0061	0.5753	0.5811	0.0059	0.8878	0.5782	1.015	3.170	10.457	10.690
390.77							1.0000	1.0000				

B.3 Water + 1-Pentanol

Table B.3: Vapour-liquid equilibrium experimental results for the water (2) + 1-pentanol (1) system at p = 0.1013 MPa (D=1.816).

T/K	x_{1a}	x_{1b}	Δx	y_{1a}	y_{1b}	Δy	$x_{1,\mathrm{avg}}$	$y_{1,\mathrm{avg}}$	γ_1	γ_2	L	W
373.06							0.0000	0.0000				
371.84	0.0009	0.0009	0.0000	0.0477	0.0494	0.0017	0.0009	0.0485	224.680	1.012	1.344	1.753
370.22	0.0025	0.0025	0.0000	0.1028	0.0990	0.0039	0.0025	0.1009	180.949	1.016	3.024	3.477
370.07	0.0030	0.0023	0.0007	0.1108	0.1089	0.0019	0.0026	0.1099	186.298	1.012	3.180	3.637
369.48	0.0029	0.0028	0.0000	0.1355	0.1406	0.0051	0.0028	0.1380	223.201	1.001	3.778	4.252
369.77	0.0030	0.0030	0.0000	0.1279	0.1318	0.0039	0.0030	0.1298	198.211	1.000	3.493	3.959
369.29	0.0032	0.0031	0.0001	0.1542	0.1559	0.0017	0.0032	0.1551	225.522	0.989	3.981	4.461
369.18	0.0032	0.0032	0.0000	0.1581	0.1528	0.0053	0.0032	0.1554	225.219	0.992	4.092	4.575
369.27	0.0032	0.0033	0.0001	0.1577	0.1443	0.0134	0.0032	0.1509	216.866	0.994	4.003	4.483
369.50	0.0032	0.0033	0.0001	0.1563	0.1540	0.0022	0.0033	0.1551	218.484	0.981	3.774	4.248
369.30	0.0035	0.0035	0.0001	0.1471	0.1478	0.0007	0.0035	0.1474	195.297	0.998	3.983	4.463
369.12	0.0041	0.0043	0.0002	0.1544	0.1554	0.0010	0.0042	0.1549	171.490	0.996	4.190	4.676
370.07	0.5982	0.6300	0.0318	0.1419	0.1386	0.0033	0.6138	0.1402	1.023	2.523	26.250	27.190
370.17	0.6053	0.6341	0.0289	0.1514	0.1553	0.0038	0.6195	0.1533	1.104	2.512	26.364	27.301
370.63	0.6224	0.6406	0.0182	0.1633	0.1666	0.0033	0.6314	0.1649	1.142	2.516	26.353	27.269
370.69	0.6290	0.6535	0.0245	0.1495	0.1482	0.0013	0.6411	0.1489	1.013	2.627	26.654	27.573
378.42	0.9139	0.7311	0.1828	0.2361	0.2384	0.0023	0.8148	0.2372	0.921	3.466	25.428	25.975
380.20	0.8255	0.8313	0.0059	0.2433	0.2546	0.0113	0.8284	0.2488	0.885	3.465	24.157	24.617
383.42	0.8512	0.9254	0.0742	0.2924	0.2937	0.0012	0.8871	0.2931	0.858	4.448	23.131	23.453
388.58	0.9307	0.9057	0.0250	0.3876	0.3739	0.0137	0.9181	0.3807	0.886	4.533	19.126	19.265
410.75							1.0000	1.0000				

B.4 Water + 2-Pentanol

Table B.4: Vapour-liquid equilibrium experimental results for the water (2) + 2-pentanol (1) system at p = 0.1013 MPa (D=3.070).

T/K	x_{1a}	x_{1b}	Δx	y_{1a}	y_{1b}	Δy	$x_{1,\mathrm{avg}}$	$y_{1,\mathrm{avg}}$	γ_1	γ_2	L	W
373.19							0.0000	0.0000				
372.60	0.0001	0.0001	0.0000	0.0185	0.0182	0.0002	0.0001	0.0183	370.121	1.015	7.038	7.615
371.51	0.0009	0.0009	0.0000	0.0543	0.0544	0.0001	0.0009	0.0543	123.594	1.018	5.963	6.510
371.37	0.0011	0.0012	0.0000	0.0692	0.0691	0.0001	0.0011	0.0691	128.226	1.007	6.178	6.731
371.00	0.0014	0.0015	0.0000	0.0761	0.0769	0.0008	0.0015	0.0765	113.108	1.013	6.608	7.173
370.63	0.0016	0.0015	0.0001	0.0938	0.0961	0.0023	0.0015	0.0949	134.187	1.006	5.748	6.289
371.17	0.0023	0.0022	0.0001	0.0699	0.0719	0.0019	0.0023	0.0709	67.031	1.014	6.393	6.952
369.16	0.0026	0.0025	0.0001	0.1447	0.1469	0.0022	0.0026	0.1458	129.946	1.004	5.103	5.626
368.49	0.0030	0.0030	0.0000	0.1631	0.1632	0.0001	0.0030	0.1632	127.552	1.008	5.318	5.847
368.56	0.0031	0.0031	0.0000	0.1667	0.1708	0.0041	0.0031	0.1688	128.014	0.999	4.888	5.405
368.47	0.0033	0.0033	0.0000	0.1725	0.1771	0.0046	0.0033	0.1748	126.498	0.995	5.533	6.068
367.69	0.0042	0.0042	0.0000	0.2162	0.2094	0.0068	0.0042	0.2128	125.233	0.978	5.540	6.064
367.86	0.0044	0.0042	0.0002	0.2124	0.2147	0.0023	0.0043	0.2136	120.124	0.971	5.373	5.892
370.29	0.0047	0.0048	0.0001	0.1351	0.1321	0.0030	0.0047	0.1336	62.227	0.979	2.951	3.398
370.69	0.0049	0.0048	0.0001	0.0934	0.0949	0.0014	0.0048	0.0942	42.423	1.008	6.823	7.394
365.80	0.0061	0.0062	0.0000	0.2576	0.2491	0.0085	0.0061	0.2533	109.299	0.998	7.468	8.057
365.60	0.0061	0.0063	0.0002	0.2530	0.2506	0.0024	0.0062	0.2518	108.761	1.008	7.253	7.836
365.59	0.0064	0.0064	0.0000	0.2914	0.3117	0.0202	0.0064	0.3014	125.376	0.942	7.683	8.278
366.00	0.0066	0.0063	0.0002	0.2415	0.2496	0.0081	0.0065	0.2455	99.928	1.002	7.274	7.856
366.43	0.0070	0.0070	0.0000	0.2255	0.2185	0.0070	0.0070	0.2220	82.261	1.017	4.673	5.184
365.57	0.5616	0.5501	0.0115	0.2599	0.2731	0.0131	0.5558	0.2664	1.283	2.214	2.738	3.195
365.58	0.5658	0.5638	0.0020	0.2561	0.2719	0.0157	0.5648	0.2639	1.250	2.266	18.357	18.995
365.92	0.5645	0.5740	0.0095	0.2632	0.2715	0.0083	0.5692	0.2673	1.239	2.250	2.953	3.416
366.45	0.5652	0.5879	0.0226	0.2586	0.2658	0.0072	0.5764	0.2622	1.174	2.259	3.383	3.858
366.17	0.5817	0.5869	0.0052	0.2555	0.2634	0.0080	0.5843	0.2594	1.159	2.335	3.168	3.637
366.88	0.6256	0.6379	0.0122	0.2979	0.2937	0.0042	0.6317	0.2958	1.188	2.440	3.598	4.079
367.63	0.7277	0.6620	0.0657	0.2978	0.3023	0.0045	0.6937	0.3001	1.064	2.835	3.813	4.300
368.57	0.7867	0.7988	0.0121	0.3596	0.3304	0.0292	0.7927	0.3446	1.030	3.786	19.700	20.187
371.30	0.8176	0.8025	0.0151	0.3954	0.4430	0.0477	0.8100	0.4184	1.098	3.316	17.298	17.653
371.37	0.7760	0.9988	0.2228	0.3989	0.4259	0.0270	0.8766	0.4121	0.997	5.146	18.491	18.837
377.77	0.9995	0.9223	0.0772	0.5469	0.6102	0.0634	0.9597	0.5773	0.998	9.021	13.666	13.760
391.60	1.0541	1.0136	0.0405	1.0348	0.9577	0.0771	0.9999	0.9950	1.014	27.066	4.458	4.963
392.00							1.0000	1.0000				

B.5 Water + 3-Pentanol

Table B.5: Vapour-liquid equilibrium experimental results for the water (2) + 3-pentanol (1) system at p = 0.1013 MPa (D=1.632).

T/K	x_{1a}	x_{1b}	Δx	y_{1a}	y_{1b}	Δy	$x_{1,\mathrm{avg}}$	$y_{1,\mathrm{avg}}$	γ_1	γ_2	L	W
373.16							0.0000	0.0000				
371.28	0.0010	0.0010	0.0000	0.0691	0.0699	0.0008	0.0010	0.0695	129.247	1.010	1.885	2.307
370.04	0.0022	0.0022	0.0000	0.1108	0.1085	0.0023	0.0022	0.1096	96.775	1.012	3.144	3.598
370.85	0.0023	0.0023	0.0000	0.0832	0.0847	0.0016	0.0023	0.0839	68.112	1.011	2.335	2.768
367.40	0.0035	0.0034	0.0001	0.1880	0.1866	0.0014	0.0034	0.1873	117.679	1.020	5.802	6.336
368.27	0.0039	0.0038	0.0001	0.1670	0.1674	0.0005	0.0039	0.1672	89.708	1.013	4.939	5.445
368.93	0.0041	0.0042	0.0001	0.1472	0.1503	0.0031	0.0041	0.1487	72.605	1.010	4.284	4.769
369.70	0.0042	0.0041	0.0000	0.1199	0.1215	0.0016	0.0041	0.1207	56.976	1.014	3.514	3.977
367.69	0.0043	0.0044	0.0001	0.1845	0.1822	0.0022	0.0044	0.1834	89.115	1.015	5.527	6.051
366.44	0.0043	0.0046	0.0002	0.2293	0.2391	0.0098	0.0044	0.2341	117.325	0.998	6.778	7.343
365.19	0.0052	0.0052	0.0001	0.2633	0.2612	0.0020	0.0052	0.2622	117.753	1.009	8.040	8.650
364.57	0.0060	0.0062	0.0002	0.2805	0.2768	0.0038	0.0061	0.2787	109.154	1.011	8.674	9.307
366.76	0.0068	0.0066	0.0002	0.2165	0.2229	0.0064	0.0067	0.2197	72.233	1.007	6.493	7.046
369.27	0.0075	0.0073	0.0002	0.1371	0.1361	0.0010	0.0074	0.1366	36.725	1.015	3.994	4.468
365.67	0.0241	0.0050	0.0191	0.2223	0.2803	0.0579	0.0142	0.2496	40.317	1.017	7.699	8.289
364.56	0.6345	0.6337	0.0008	0.2890	0.2839	0.0052	0.6341	0.2864	1.086	2.717	18.337	18.869
364.60	0.6432	0.6596	0.0164	0.2788	0.3044	0.0256	0.6513	0.2913	1.074	2.827	18.561	19.089
364.62	0.6346	0.6812	0.0466	0.3016	0.3190	0.0174	0.6573	0.3101	1.132	2.798	18.633	19.160
364.87	0.7691	0.5723	0.1968	0.2839	0.2765	0.0075	0.6603	0.2802	1.007	2.917	18.429	18.940
364.62	0.6350	0.7139	0.0789	0.3097	0.2965	0.0132	0.6728	0.3030	1.080	2.961	18.871	19.395
365.30	0.6863	0.6777	0.0087	0.2959	0.3262	0.0303	0.6820	0.3107	1.063	2.936	18.333	18.819
364.57	0.6976	0.6720	0.0256	0.2955	0.3093	0.0138	0.6846	0.3023	1.061	3.081	19.104	19.628
366.19	0.7767	0.6599	0.1168	0.3088	0.3071	0.0017	0.7148	0.3079	0.970	3.177	17.948	18.380
364.71	0.7309	0.7127	0.0182	0.2879	0.3142	0.0263	0.7217	0.3008	0.996	3.481	19.535	20.046
365.75	0.6794	0.7952	0.1158	0.3054	0.3069	0.0016	0.7339	0.3061	0.956	3.472	18.683	19.135
364.59	0.7117	0.7779	0.0662	0.3072	0.3050	0.0022	0.7437	0.3061	0.988	3.768	19.993	20.508
364.97	0.7758	0.7971	0.0214	0.2967	0.3044	0.0077	0.7863	0.3005	0.904	4.490	20.269	20.755
367.31	0.6953	0.9839	0.2886	0.3366	0.3343	0.0023	0.8206	0.3355	0.880	4.649	18.456	18.810
367.28	0.8640	0.7868	0.0773	0.3467	0.3505	0.0039	0.8240	0.3486	0.912	4.652	18.540	18.895
370.28	0.9476	0.9193	0.0283	0.4350	0.3982	0.0368	0.9333	0.4161	0.855	9.837	17.222	17.409
372.46	0.8979	0.9809	0.0831	0.4578	0.4929	0.0351	0.9380	0.4749	0.893	8.788	15.114	15.211
375.00	0.9822	0.9347	0.0475	0.6069	0.4978	0.1091	0.9580	0.5486	0.918	10.187	12.883	12.887
388.53							1.0000	1.0000				